

measurement systems laboratory

massachusetts institute of technology, cambridge massachusetts 02139

N71-35444

PR-8

**STUDIES OF SPACE EXPERIMENTS TO MEASURE
GRAVITATIONAL CONSTANT VARIATIONS
AND THE EOTVOS RATIO**

L. S. Wilk, ed.

July 1971

PR-8

PROGRESS REPORT

STUDIES OF SPACE EXPERIMENTS TO MEASURE
GRAVITATIONAL CONSTANT VARIATIONS
AND THE EOTVOS RATIO

Progress to 1 April 1971
NASA Contract NAS9-8328

APPROVED: _____

W. Markley

Director
Measurement Systems Laboratory

TABLE OF CONTENTS

02-115139

I.	Introduction	1
II.	Measurement of Variations of the Gravitational Constant	3
	A. Gravitational Clock	6
	B. Beams' Balance	12
	C. Centrifugal Balance Sphere	18
	D. Synchronous Orbit Sphere	25
III.	Measurement of the Eotvos Ratio	37
IV.	Summary and Conclusions	59
Appendix A	An Elementary Analysis of the Adaptation of the Beams' Experimental Concept to a $\Delta G/G$ Detector to be Used in Space	A-1
Appendix B	Error Study of the Beams' Experimental Concept Used in a $\Delta G/G$ Detector	B-1
Appendix C	Digital Simulation of a Space Experiment to Measure the Newtonian Gravitational Constant	C-1
Appendix D	A Preliminary Analysis of the Effects of Using Non-Spherical Masses in a Beams-Type Measurement of G or $\Delta G/G$	D-1
Appendix E	Analysis of an Experiment to Determine the Gravitational Constant in an Orbiting Space Laboratory	E-1
Appendix F	Analysis of the Gravitational Field in Wilk's Sphere with Three Tunnels	F-1
Appendix G	A Study of Primary Masses for Gravitational Experiments	G-1

ACKNOWLEDGEMENTS

The basic conception of the experiments, (along with their instruments and primary analysis) contained in this report originated with the following individuals:

Gravitational Clock - Dr. Rainer Weiss
Associate Professor of Physics, M.I.T.

Adaptation of Beams Balance - Bernard E. Blood
formerly DSR Staff, M.I.T.

Centrifugal Balance Sphere - Leonard S. Wilk
DSR Staff, M.I.T.

Synchronous Orbit Sphere - Dr. Philip K. Chapman
Astronaut Office, M.S.C.

Measurement of the Eotvos Ratio - Dr. Philip K. Chapman
Astronaut Office, M.S.C. and

Andrew J. Hanson
Research Assistant, M.I.T.

This progress report was edited by Prof. Winston R. Markey, Principal Investigator; Dr. John Hovorka; and Leonard S. Wilk.

The Appendices have also appeared as separate reports issued by the Measurement Systems Laboratory during the reporting period of this progress report. Appendix G is included with the permission of Arthur D. Little, Inc., Cambridge, Mass. The authors of the Appendices are as follows:

Appendix A (RN-60) Bernard E. Blood
Appendix B (RN-63) Bernard E. Blood
Appendix C (RN-61) Harold L. Jones
Appendix D (RE-74) William N. Lee
Appendix E (RE-72) John P. Vinti
Appendix F (RE-73) John P. Vinti
Appendix G Arthur D. Little, Inc.

The work described in this progress report was performed under DSR Contract 71390, Sponsored by the National Aeronautics and Space Administration under Contract NAS 9-8328

The publication of this report does not constitute approval by the National Aeronautics and Space Administration of the findings contained herein. It is published for the exchange of information and the stimulation of ideas.

ABSTRACT

Space experiments for detecting variations of the Newtonian gravitational constant and for detecting the difference between inertial and passive gravitational mass have been examined. These variations are precluded by Einstein's theory of gravitation, the General Theory of Relativity, and the experiments pose strong tests of that theory.

Four designs are studied to detect gravitational constant variations. The one that has the best potential for achieving the required resolution, is a space-adapted approach of a technique devised by Prof. J.W. Beams (University of Virginia). An analysis of the major factors of this experiment uncover no prohibition from attaining a necessary measurement resolution of $\Delta G/G$ of 1 part in 10^{10} , although the instrument design requirements may prove difficult to achieve. This is the largest resolution permitted (reserving an order of magnitude for experimental confidence) to detect the maximum effect predicted by the Brans-Dicke theory, for a highly eccentric solar orbit.

An experiment is proposed to check the equivalence between inertial and gravitational mass to an accuracy of 1 part in 10^{14} . The proposed instrument design to achieve this experiment in earth orbit appears feasible.

An experiment with this accuracy will provide the first experimental test of the inertial-gravitational mass equivalence of the weak-interaction binding energy. Based upon our best estimate of the magnitude of the weak interaction binding energy, this experiment would test its mass equivalence to 1 part in 10^3 . The weak interaction (or part of it) has previously upset supposedly well-established assumptions in physics.

SECTION I

Introduction

The overall effort in this reporting period was to study several proposed experiments, to be conducted in space, involving the measurement of gravitational-inertial forces. One purpose of these experiments would be to investigate the nature of the gravitational attraction between objects (here called the G-Constancy Experiment). The specific question is whether the attractive force is simply proportional to the masses and inverse square of the separation, or whether the force is also related to the gravitational potential (i.e. whether Newton's "constant" G appearing in the force equation is not constant but itself varies with the gravitational potential). A second purpose is to investigate the equivalence of inertial and passive gravitational masses. The specific question here is whether the inertial-gravitational mass ratio of one material is identical to that of another. That is, is the Eotvos ratio equal to zero?

In particular, the study of the G-Constancy Experiment focused upon the evaluation of the experimental equipment wherein gravitational forces are counter-balanced by inertia reaction forces (in a D'Alembertian sense). These are described in Section II and the relevant appendices. The first method described in Section II is the Gravitational Clock, where a set of non-rotating attracting masses provides a gravitational potential well for the oscillation of a test body rotor, the relevant measurement being the frequency of oscillation of the rotor. This method was reported previously⁽¹⁾ and the description in Section II presents some new observations. In the next method, the Beams Balance, the attracting masses are rotated so that the test body rotor is subjected to a constant torque; the relevant measurement here is the angular acceleration of the rotor.

The third method described in Section II, the Centrifugal Balance Sphere, utilizes a homogeneous sphere to provide gravitational attraction for three test objects which are in tunnels internal to the sphere. This attractive force is counterbalanced by a centrifugal force due to the orbiting of the three test objects. Each test object is constrained by a suspension system to remain along a radius fixed to the rotating sphere. The relevant measurement in this case is that of the angular velocity of the sphere needed to keep the test

bodies radially motionless. The fourth method, the Synchronous-Orbit Sphere, is similar to the Centrifugal-Balance Sphere except that the (only) test body is not constrained by a suspension system. The relevant measurement is that of the angular velocity of the sphere needed to keep the test body from colliding with the tunnel sides. Approximately 85% of our effort was devoted to studies of these four methods.

The study of the Eotvos Experiment focused upon the evaluation of a new method to measure the Eotvos ratio. The method exploits the possibility of measuring small forces under near-weightless conditions. The essence of the method here would be to determine, not simply the existence or non-existence of a different gravitational pull on different materials, but specifically the differing pull, if any, on objects having different amounts of weak-interaction energy in their total makeup.* Section III contains a discussion of the detection of small differences in the force exerted by the earth on different orbiting test masses, in terms of the small orbital differences implied.

* If the experiment provides a non-null measurement, this result may be attributable to a small fractional anomaly in one of the larger contributors to atomic mass or a large fractional anomaly of the weak-interaction. The assumption made here is that latter effect prevails.

SECTION II

Measurement of Variations of the Gravitational Constant

The Einstein theory of general relativity is the currently accepted theory of gravity. It is a very beautiful and deductive theory founded on a shallow experimental base. It clearly gives Newtonian gravitation in the weak field, and low velocity limits and furthermore predicts non-Newtonian effects which comprise tests for the theory. There are to date four non-Newtonian predictions of the theory for which observations have been attempted. The gravitational red shift, the phenomenon in which clocks appear to run slower in a strong gravitational potential, has been measured by a terrestrial Mossbauer experiment⁽²⁾ to be within 1% of the value predicted by the Einstein theory. It is, however, not a decisive test of the theory since it can be interpreted as a result of energy conservation in a special relativistic formulation of Newtonian gravity. The deflection of star light by a gravitational field is poorly measured.⁽³⁾ The best that can be said at present is that there appears to be a deflection of star light by the sun of approximately the value predicted by the Einstein theory; however, there is an uncertainty of the order of one-half of the size of the effect. The apparent change in the velocity of light in a gravitational field has been measured by radar ranging of Venus near superior conjunction with the sun.⁽⁴⁾ The data as well as knowledge of the planetary dynamics of earth and Venus are sufficiently good to establish the Einstein value to 10%. Finally it was pointed out by Einstein that the anomalous perihelion advance of Mercury could be explained by the general theory. This offers a more stringent test of the theory than the other phenomena that have been mentioned. The perihelion advance is a cumulative effect that can be measured with sufficient accuracy to give information on second order non-Newtonian contributions in the theory. Dicke⁽⁵⁾ has cast some doubt on the validity of the Einstein explanation of the perihelion advance by suggesting that a solar mass quadrupole moment may contribute part of it. Attempts to explain the entire perihelion advance by a solar oblateness or a non-spherical distribution of mass within the orbit of Mercury were made in the 19th century. However, this would cause other changes in the orbital parameters of Mercury such as a regression of the nodes

of the orbit which have not been observed. At present, however, it is not possible to reject Dicke's suggestion that as much as 10% of the perihelion advance might be due to a solar mass oblateness.

Besides the explicit effects predicted by the theory, there are tests of a different nature that tend to result in null experiments, but are nevertheless important. A fundamental axiom of the Einstein theory is the principle of equivalence, which has several interpretations. As first used by Einstein, it states that it is impossible to distinguish a gravitational field from an acceleration, in the neighborhood of a point. This clearly implies that the ratio of the gravitational mass to the inertial mass of all bodies must be the same. The Dicke-Eotvos⁽⁶⁾ experiment has established that, at least for aluminum and gold, the ratio is the same to within one part in 10^{-11} . However, the principle of equivalence as used in the general theory is a stronger statement, for it implies that the neighborhood of a point in a freely falling frame at which the gravitational field has been cancelled by an acceleration is locally an inertial frame that is equivalent to all other inertial frames. Measurements that are insensitive to gravity gradients, such as measurement of the ratios of fundamental interaction constants, must give the same results in freely falling frames near massive objects as well as far away from them. In other words, the numerical content of physical laws is independent of the gravitational field. This is the statement of the strong principle of equivalence which, regarded as a potentially verifiable hypothesis, has not been experimentally verified for all the presently known physical interactions. An experimental program to measure the fundamental interaction constants as a function of gravitational potential may result in null experiments. However, such a program must be performed to establish the strong principle. In particular, the Dicke-Brans⁽⁷⁾ gravitational theory which adds a scalar gravitational interaction to the Einstein tensor field is still a viable gravitational theory which violates the strong principle. This theory makes the specific prediction that the gravitational constant, G , which is a constant in the Einstein theory, depends on the gravitational potential. For weak fields, the dependence is given by

$$\frac{\Delta G}{G} = \frac{1}{(\omega+2)} \frac{\phi}{c^2} \quad (1)$$

where G is the Newtonian gravitational constant, ϕ , the Newtonian gravitational potential, c , the velocity of light and ω a coupling constant which is equal to 0 if there is no tensor interaction and approaches ∞ if there is no scalar interaction. At present ω can be set to $\omega \geq 6$ without conflicting with the measurements of the perihelion rotation^{(7) (8)}. The experiment suggested by this is some form of Cavendish experiment that can be transported to different gravitational potentials; the measurement however, does not have to be absolute.

An earth-based experiment to measure G as a function of time throughout the year is a possibility⁽⁹⁾. The eccentricity of our orbit around the sun provides a 1% modulation of the solar gravitational potential at the position of the earth with a yearly amplitude such that $\Delta G/G \approx 3 \times 10^{-11}$. This could be measured with stable gravimeters if the geophysical phenomena with yearly periods were better understood. Moreover, since the fractional change is so small, a terrestrial experiment that does not use the earth as one of the attracting masses looks difficult. Larger variations in gravitational potential are provided in space, for example the relative change in G between near earth orbit and close orbit to Jupiter is $\Delta G/G \approx 3 \times 10^{-9}$; or better still between earth orbit and a solar orbit of 0.1 A.U. radius might give $\Delta G/G \approx 3 \times 10^{-8}$.

Instruments designed to measure gravitational forces can be distinguished by the nature of the restoring force used. These instruments fall into two major areas: those using mechanical or electrical forces, in the sense of springs, fibers or electromagnetic devices*; and those using inertia reaction forces exclusively. In the first group, we have the classical torsion balances of Cavendish and Eotvos, along with a number of modern improved versions, such as those by Heyl⁽¹⁰⁾, Dicke⁽⁶⁾ and Douglass⁽¹¹⁾: in addition, we have an array of modern gravimeters, accelerometers, and gradiometers. The second group is primarily restricted to instruments designed for use in free-fall and hence have been of interest only with the advent of space

* perhaps in conjunction with inertia reaction forces

operations. (A notable exception to the space application of the second group is the work of Beams, et al.⁽¹²⁾) Berman and Forward have proposed measuring the period of 2 equal spheres in close orbit around each other, or that of a small mass in close orbit around a large sphere⁽¹³⁾. As another experiment they have proposed measuring the period of a test mass oscillating about the mid-point of a tunnel bored through a large sphere⁽¹³⁾.

Apparatus utilizing inertia reaction methods include: tangential acceleration balance systems - wherein the test mass is restrained from relative radial motion, and the tangential force component of inertia reaction is balanced against the tangential component of gravitational attraction; centrifugal balance systems, wherein the test mass is restrained from relative tangential motion and the centrifugal force component of inertia reaction is balanced against the radial component of gravitational attraction; and orbital systems, wherein the test mass is not restrained and the test mass is in orbital motion.

The primary purpose of this Section of the Progress Report is to present four schemes that might be used to measure variations of G in space. These are in the categories of tangential acceleration balance systems (Gravitational Clock as suggested by Weiss⁽¹⁾⁽¹⁴⁾ and the Beams Balance as suggested by Blood), centrifugal balance systems (Centrifugal Balance Sphere as suggested by Wilk), and orbital systems (Synchronous Orbit Sphere as suggested by Chapman). From the nature of the equipment the first two schemes can be carried out with a single instrument, while the second two schemes use a second instrument.

A. Gravitational Clock

A self contained scheme to compare the gravitational interaction with the nuclear and electromagnetic interactions would be to make an oscillatory system for which the restoring force is primarily gravitational - a gravitational clock - and measure its periodicity using an atomic clock; both instruments mounted in the same space probe. A typical although not necessarily optimum gravitational oscillator is shown in Figure 1. There are three stator masses, in this case balls with a slot cut in them and three spherical rotor masses mounted on a rigid equilateral triangle that travel in the stator slots. The rotation axis is centered on the equilateral triangle and is normal to the plane of the triangle. The period of the oscillator is close to

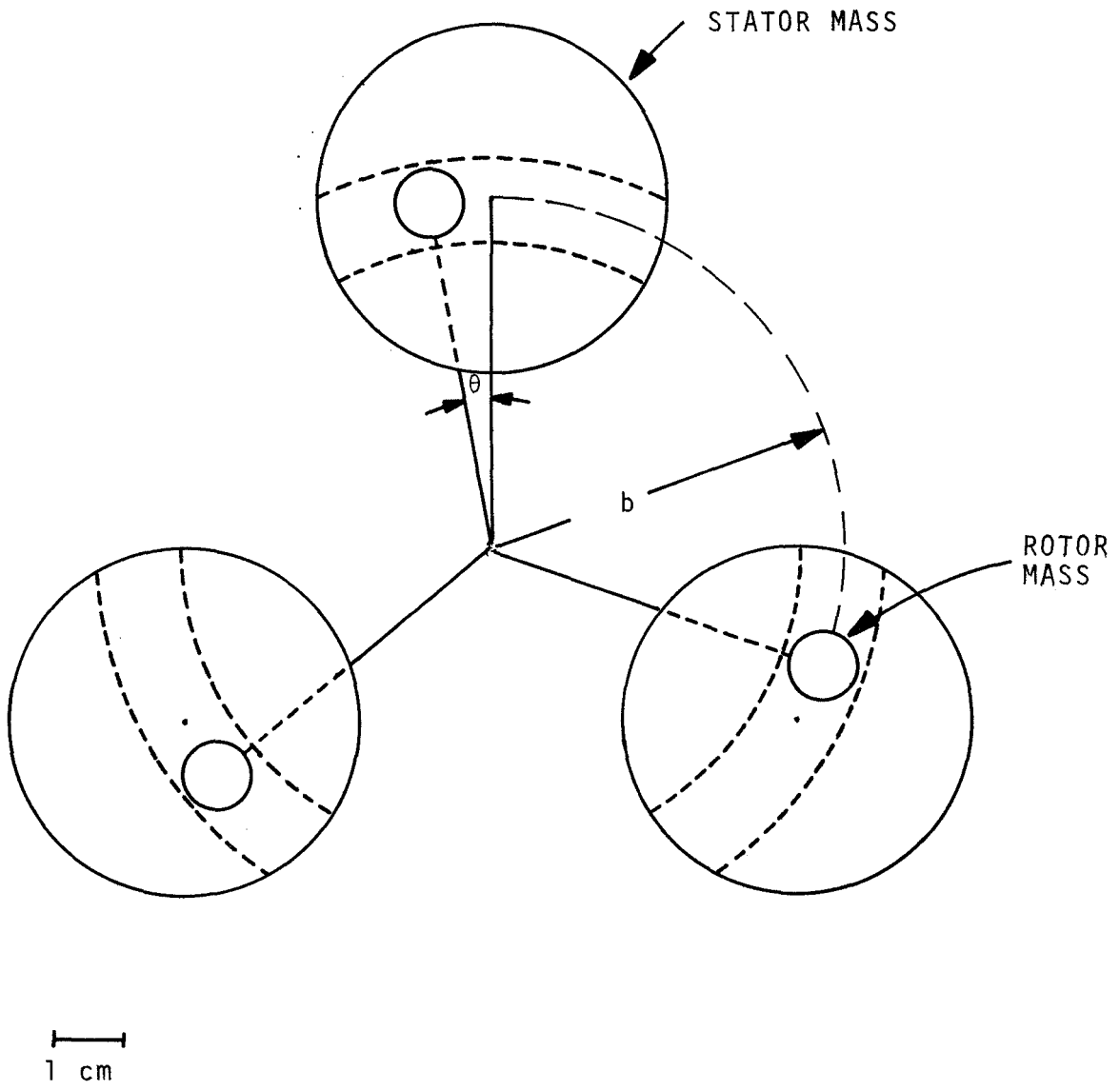


Figure 1 Gravitational Oscillator Configuration

$$\tau = \left(\frac{G\rho}{3\pi}\right)^{-1/2} \quad (2)$$

$$\frac{\Delta\tau}{\tau} = \frac{1}{2} \frac{\Delta G}{G}$$

G is the local value of the Newtonian gravitational constant and ρ the density of the stator masses. Eq. (2) neglects the influence of the slot and the moment of inertia of the structural members of the equilateral triangle, both of which increase the period. If the stator is made of gold or platinum, density 20, the minimum period is approximately 45 minutes.

The period of the oscillator is amplitude dependent because of anharmonic terms in the rotor gravitational potential energy in the field of the stator. The potential energy of the rotor expanded in a power series in θ , the rotation angle measured from the null point is given by

$$U(\theta) = a_2\theta^2 + a_4\theta^4 + a_6\theta^6 + \dots \quad (3)$$

The dominant term is $a_2\theta^2$, the harmonic term. The fourth order term has two contributions, the principle one due to the curved path of the rotor ball in the nearest stator mass and a smaller contribution from the other stator masses. The fourth order term however, can be reduced to zero by cutting a cylindrical slot in the stator. More subtle distributions of mass may be able to reduce the sixth order term, however this is not a simple analytic problem. Most likely the best method is to use a trimming stator mass that can be moved about to empirically reduce the anharmonicity. Classical perturbation theory leads to a change in period with amplitude given by

$$\frac{\Delta\tau}{\tau} = \frac{\langle E_p \rangle}{E_0} \quad (4)$$

where E_0 is the energy of the harmonic oscillator and $\langle E_p \rangle$ is the energy of the anharmonic term averaged over a cycle of the unperturbed motion. For the configuration of Figure 1,

$$\frac{\Delta\tau}{\tau} \sim \frac{15}{48} \frac{a_6}{a_2} \theta_{\max}^4 \qquad \frac{a_6}{a_2} \sim 10^{-2} \qquad (5)$$

so that if the amplitude dependence is not to affect the measurement of the period by more than 1×10^{-9} , $\theta_{\max} < 3 \times 10^{-2}$ radians. This assumes that the amplitude of the oscillator is uncontrolled or not measured.

Sensitivity of the period to gravity gradient due to external masses is small because of the triangular structure of the rotor. The potential due to a mass at distance r from the oscillator is given by

$$U(\theta) \cong \left(\frac{9GM}{r} \frac{b^3}{r^3} \sin^2 \alpha \right) \theta^2 + \dots \qquad (6)$$

if

$$b \ll r$$

where b is the radius of the circumscribed circle around the rotor equilateral triangle, M the perturbing mass, and α the angle between r and the rotation axis. The fractional change in period is

$$\frac{\Delta\tau}{\tau} = \frac{9}{2\pi} \frac{Mb}{r^4 S} \sin^2 \alpha \qquad (7)$$

For $b \approx 5$ cm, a man at 10 meters produces at worst a fractional change in period of 1×10^{-8} while the sun at 0.1 A.U. produces 3×10^{-16} .

A fundamental limit to the precision of the period measurement is established by the thermal noise which causes a fractional fluctuation in the zero crossing time on the average per cycle given by

$$\frac{\Delta\tau}{\tau} = \frac{1}{2\pi\theta_M} \left(\frac{\pi}{Q} \frac{KT}{I\omega_0^2} \right)^{1/2} \qquad (8)$$

K is Boltzmann's constant, T the absolute temperature of the damping mechanism, ω_0 the resonance frequency of the oscillator, Q/ω_0 the time for the energy in the oscillator to be damped to $1/e$ of its initial value, I the moment of inertia of the motor and θ_M the angular amplitude of the oscillation. For typical parameters,

$$I = 10^3 \text{ gm cm}^2$$

$$\omega_0 \sim 2 \times 10^{-3} \text{ radians/sec}$$

$$\theta_{\text{max}} = 3 \times 10^{-2} \text{ radians}$$

$$T = 4^\circ\text{K}$$

$$\frac{\Delta\tau}{\tau} \text{ measurement} \sim \frac{3 \times 10^{-6}}{Q^{1/2}} \quad (9)$$

If the system is evacuated we may have $Q > 10^6$; however this depends on the details of the suspension.

The rotation angle θ is to be measured by a differential, rotation sensitive, laser interferometer as shown in Figure 2. The interferogram is first order insensitive to translation and insensitive to rotations about an axis perpendicular to the free rotation axis. The principle components of the interferometer are a pair of small corner reflectors mounted on a beam that is attached to the rotor. The remaining components, all 50-50 beam splitters, are external to the oscillator chamber and mounted on a single rigid structure. Using the typical parameters mentioned previously, the fringe frequency is ≈ 6 hz near null. With a 1 mw laser limited by Poisson noise, the passage of a single fringe can be measured to 10 sec or give a fractional period measurement $\Delta\tau/\tau \sim 10^{-8}$. The time series that makes up the interferogram carries all the information needed to make a complete period, amplitude and time varying perturbation torque measurement. It also includes information concerning space craft motion.

Some difficulties with the proposed scheme:

(1) Temperature dependence of the oscillator period. The period depends on the density of the stator masses and in detail on the moment of inertia of the rotor. Both of these parameters vary with temperature in the same direction. The oscillator period varies with T as

$$\frac{\Delta\tau}{\tau} = \frac{3}{2} \left(\frac{\Delta\rho}{\rho} / \Delta T \right) \Delta T \quad (10)$$

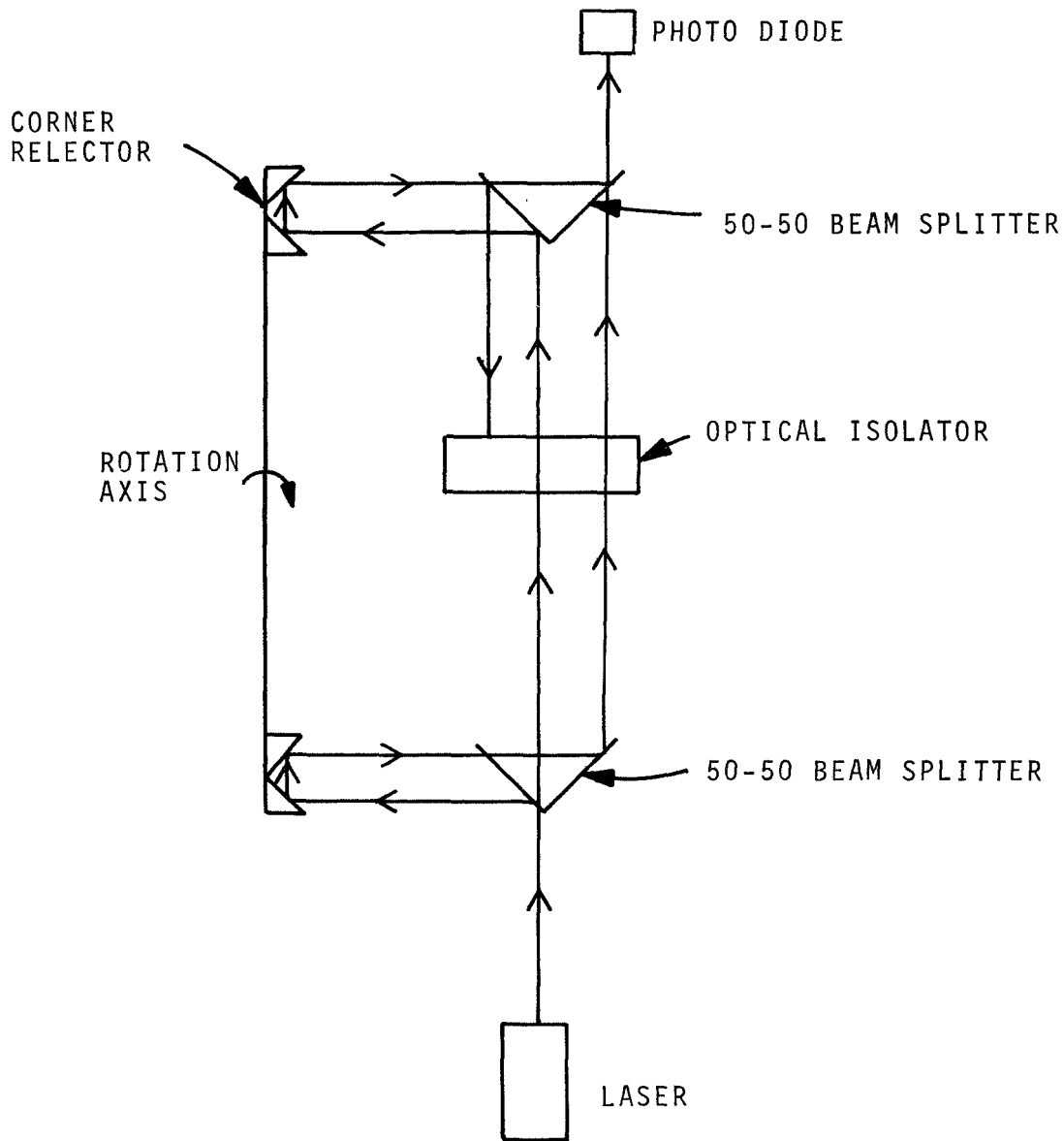


Figure 2 Rotation Sensitive Differential Interferometer.
 The output signal is insensitive to translation and rotation about any axis perpendicular to the principle rotation axis.

The linear expansion coefficients $\Delta l/l/^\circ\text{C}$ of gold or platinum are of the order 10^{-5} at room temperature, which would require temperature measurement or stabilization to 10^{-4}°C . At 4°K however, the expansion coefficient is down to 6×10^{-9} (See also Appendix G).

(2) The suspension. The nub of the experimental problem resides in the torsion suspension which has to be sufficiently isotropic to let the gravity restoring torques dominate. This means the torsion constant of the suspension must be much less than 1×10^{-3} dyne cm/radian and furthermore be constant in time and independent of temperature. Since the thermal noise depends on $Q^{-1/2}$, the suspension should permit a $Q > 10^6$. A major requirement of the suspension is that the unwanted modes of motion in the remaining degrees of freedom both rotational and translational, have high frequencies and are well damped. Excitation of these modes can effect the period of the oscillator by modulating the gravitational potential of the stator masses or by changing the effective moment of inertia of the rotor about the free rotation axis. A superconducting suspension proposed by M. Blich⁽¹⁴⁾ that satisfies some of the requirements is shown schematically in Figure 3. The suspension employs the diamagnetism of a superconductor and provides eddy current damping in copper for all motions that are not pure rotations about the free axis.

(3) Electrostatic and magnetostatic torques. It is clear that electrostatic forces between the rotor and stator as well as magnetic forces between stray fields and ferromagnetic impurities in the rotor are a serious problem. If the rotor float has no electrical connection to the stator, a charge servo that can hold the rotor to a charge unbalance less than 100 electron charges is required. If the rotor is grounded, the contact potential difference between rotor and stator has to be less than $1 \mu\text{v}$ or at least held constant to less than $1 \mu\text{v}$.

B. Beams Balance

If we modify the Gravitational Clock configuration such that the attracting (stator) masses are rotated in such a fashion that the angle (θ) between it and the rotor system does not change, then the angular accelerations of the instrument will provide a measure of the

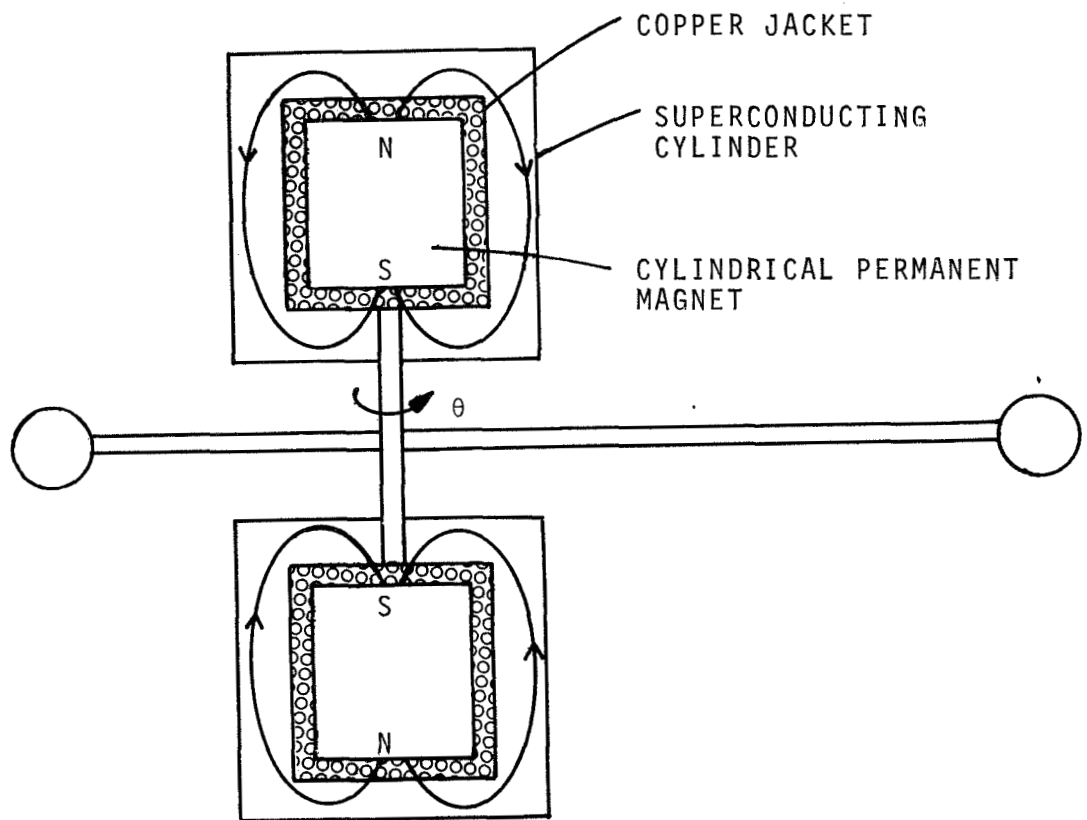


Figure 3 Schematic of a Superconducting Suspension

The suspension has a high Q and is isotropic for the principle rotation axis but is stiff and has a low Q for other motions.

gravitational attraction between the stator and motor masses⁽¹²⁾. In principle, one would monitor the angle θ and drive the stator such that θ remains constant. Of course, as with any instrument of this type, it is desirable to design it such that the operation is incrementally insensitive to the angle θ and that the spheres are sized to provide a maximum of gravitational attraction. Under these conditions, and for an instrument configuration consisting of spheres at the ends of n massless arms, the acceleration will be

$$\alpha = \left[\frac{\pi \rho}{6} \right] G \frac{(1+h^2-2h \cos \theta_p)}{h(1.1+\frac{.1}{h^2} - \frac{.2}{h} \cos \theta_p)} \sum_{i=1}^n \frac{\sin(\theta_p + \frac{i}{n} 360)}{[1+h^2-2h \cos(\theta_p + \frac{i}{n} 360)]^{3/2}} \cdot \quad (11)$$

where

G = gravitational constant

ρ = density of spheres

h = length ratio of moving arm to fixed arms

θ_p = angle between arms for zero torque variation

As shown in Appendix A, a four arm device has a significant advantage in terms of size vs. effect of disturbance masses. Figure 4 shows a plot of Eq. (11), for a four arm instrument. Note that a maximum acceleration occurs near $h = 0.5$. Figure 5 is a full scale sketch of four arm instrument with $h = 0.5$. If fabricated of platinum it would provide a gravitational torque of 0.001 dy-cm. and have an angular acceleration of 0.284×10^{-6} rad/sec. The total mass (of spheres) is 1.24 kg.

We can determine the angular acceleration by timing the passage of angular increments. If the increments are of angle ϕ and τ_1 and τ_2 are the times for the passage of successive increments, then the value

* These results are abstracted from Appendices A, B, C and D.

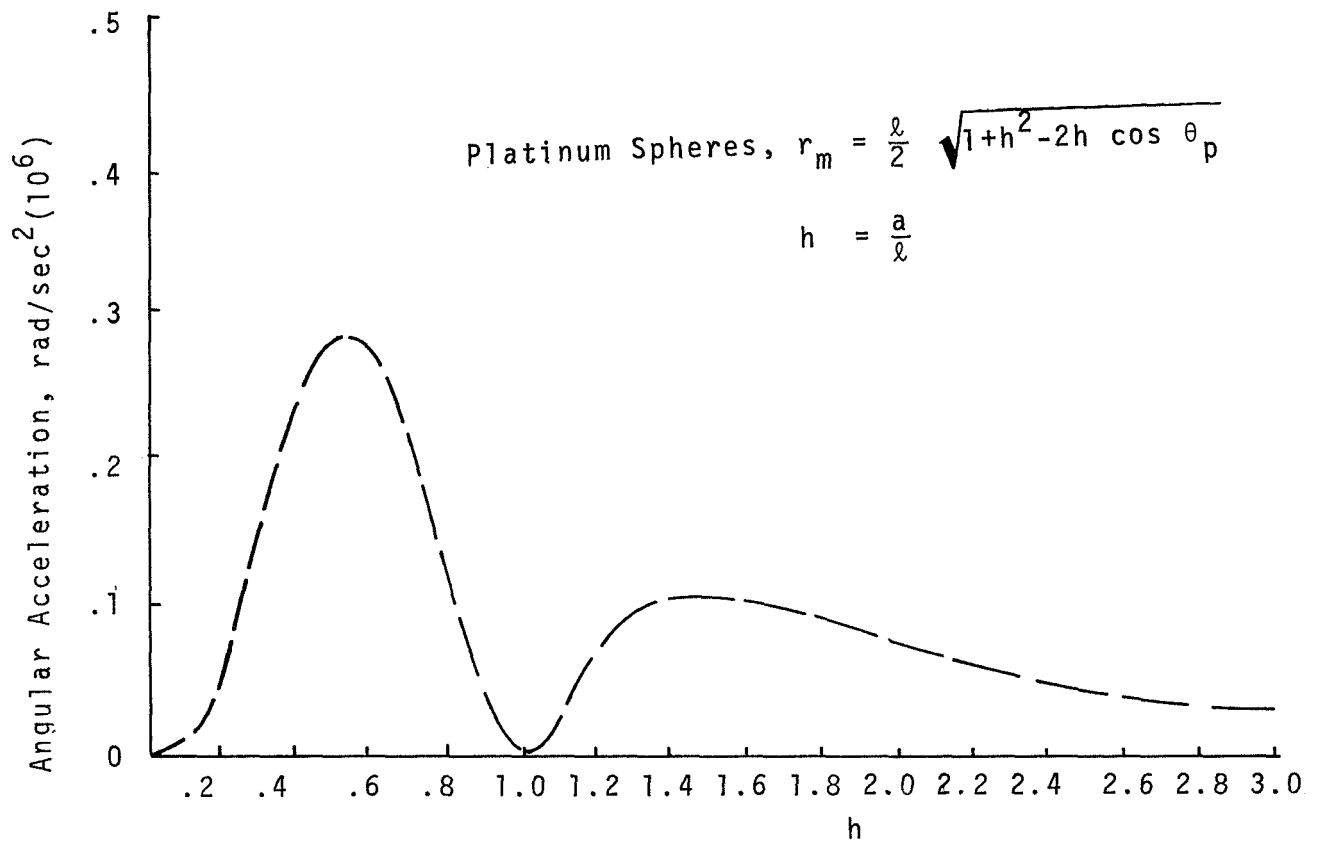


Figure 4 Angular Acceleration of a Four-Armed Device

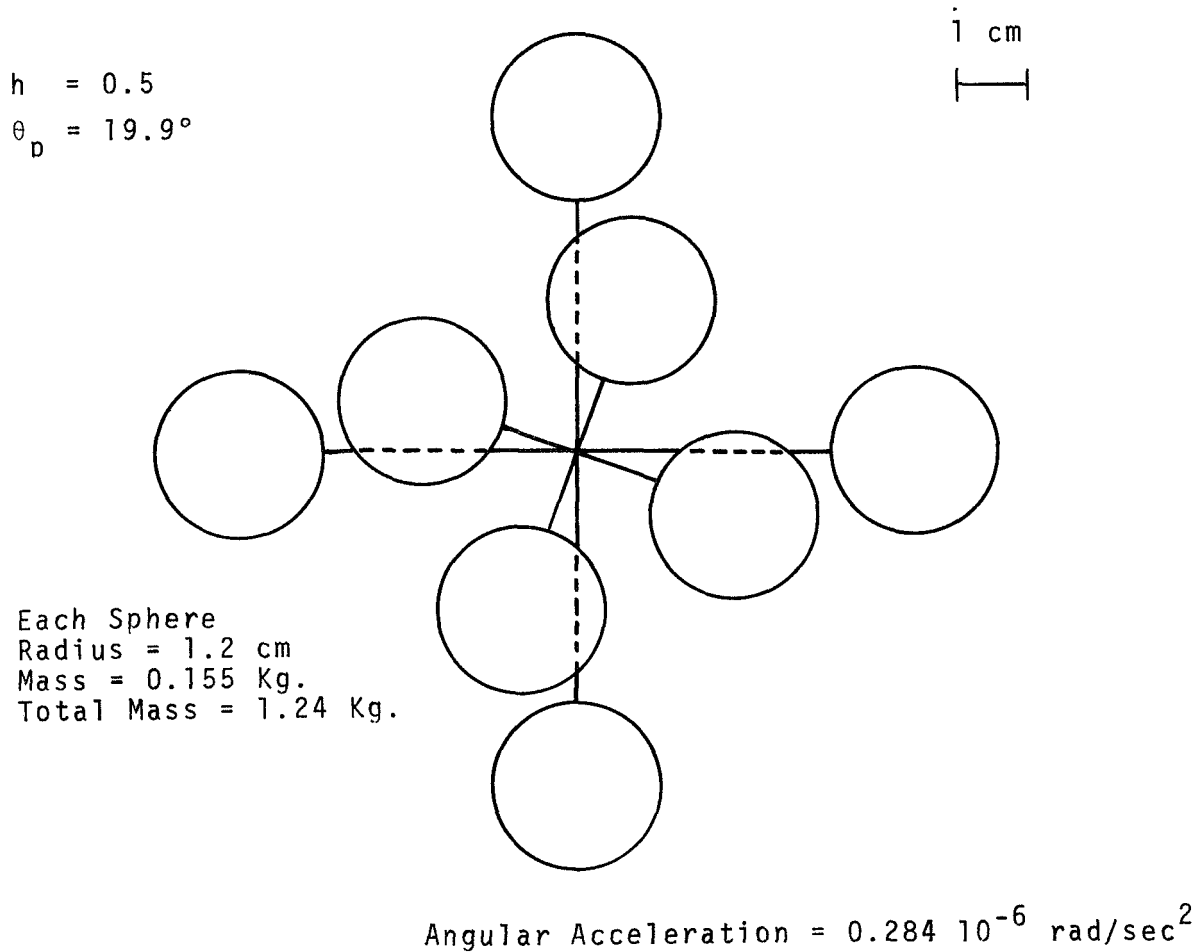


Figure 5 Full-Scale Sketch of a Four-Armed Device
 (Gravitational Torque = 0.001 dyne-cm)

of the gravitational constant will be given by

$$G = \left\{ 2\phi \frac{\tau_1 - \tau_2}{(\tau_1 \tau_2)(\tau_1 + \tau_2)} \right\} \left\{ \frac{1}{M} \frac{\frac{2}{5} r_m^2 + a^2}{a \lambda \sum_j \frac{\delta_{oj} \sin \theta - \delta_{ej} \cos \theta}{[\ell^2 + a^2 - 2a\lambda(\delta_{oj} \cos \theta + \delta_{ej} \sin \theta)]^{3/2}} \right\}$$

$$\equiv \left\{ 2\phi \frac{\tau_1 - \tau_2}{(\tau_1 \tau_2)(\tau_1 + \tau_2)} \right\} \left\{ K \right\}. \quad (12)$$

We see that G is determined by using measured time increments to calculate the first bracket which is then multiplied by a constant, K . The second bracket, K , is determined by the parameters of the experimental setup. Clearly, for a precise measurement of G , we need a correspondingly precise knowledge of K . This calibration constant is fixed by the manufacturing tolerances and metrology. Since our experiment is not to determine the absolute value of G , but rather to detect variations, then K need not be precisely known, but it must remain constant to parts in 10^{10} .

Appendix B further shows that in order to hold K constant to parts in 10^{10} in a room temperature environment, thermal expansion dictates that we need to achieve a temperature stability on the order of 10^{-6} °C. Thus requirement indicates that it may be best to perform the experiment at cryogenic temperature.

Disturbance force inputs can arise from a variety of sources: also, their importance may be related to the off-nominal conditions of the instrument. Disturbance forces due to gravity gradients, linear accelerations, electrostatic and magnetic fields and gas pressure effects are considered in Appendix B. The major negative conclusion is that the spacecraft aerodynamic drag variations (combined with a postulated mass variation of the arms of 1 part in 10^5) must be less than 2×10^{-8} cm sec² during a full revolution of the experimental apparatus. This may require that an earth orbit space experiment be conducted in a "drag free" spacecraft mode, or else that the experiment be conducted in solar orbit. The other main conclusion is that the electrostatic charge accumulation must be limited to 10^{-16} coulombs (i.e. 600 electron charges). This condition may necessitate a charge-control system, or else it precludes a suspension system that

electrically isolates the rotor.

In Eq. (12), the τ 's represent the times for rotational displacements, ϕ , of the moving test body with respect to inertial space. In a practical case, the time periods will be measured as the fiducial marks on the table supporting the attracting masses cross a fiducial mark on the frame supporting the table. If the frame is non-rotating in inertial space, the measurement times will be in error by the difference between the angular displacement of the table and the angular displacement of the test body. This difference is represented by variations in the servo signal $\Delta\theta$. However, we must also expect that the rigid frame supporting the table will have angular motion with respect to inertial space. To eliminate the effect of this angular motion, we can take two separate set-ups mounted on the same frame, such that the rotation vectors of the test bodies are parallel but in opposite directions. For one of the set-ups, the frame's angular motion will increase our time measurements and in the other set-up it will decrease the time measurement. By combining the data (obtained over the same time interval) from the two set-ups, we can eliminate the effect of the frame's angular motion.

Under these conditions, an error analysis of the first bracket in Eq. (12) was undertaken by means of a simulation, which is described in Appendix C, and the results are detailed in Appendix B. The simulation utilized an optimal estimator and used as input values an rms error of 1 second of arc in the measurement of ϕ , fiducial marks every degree (360 marks per revolution), a base (spacecraft) angular acceleration given as noise with an rms level of 10^{-6} rad/sec², and a nominal angular acceleration of the table (due to G) of 10^{-6} rad/sec².

The basic conclusions of the simulation can be summarized by four main points:

- 1) The time required to reduce the table angular acceleration measurement uncertainty to 1 part in 10^{10} is decreased as the initial table velocity is increased, but at the expense of an enormous increase in the amount of data to be handled.

- 2) The time to reach 1 part in 10^{10} is not affected appreciably by the accuracy of the initial estimate of the table angular acceleration.

- 3) The primary hardware limitation on the estimation process is the measurement error variance of ϕ .

4) The estimation process is quite insensitive to the angular acceleration variance of the spacecraft.

Although subject to many trade-offs, a reasonable experimental choice might be to give the tables and initial angular velocity of 0.02 rad/sec. Under the condition stated, an angular acceleration measurement uncertainty of 1 part in 10^{10} could be achieved in 14 hours and would require the reduction of 132,000 data points.

The operation of the Beams Balance might be improved if a mass shape other than spherical is used, since, for example the attractive force between adjoining square blocks (of optimized thickness) is 79% greater than the force between adjoining spheres of the same mass (adjoining optimum cylinders provide an increase of 86%; adjoining hemispheres provide an increase of 89%; while adjoining optimum half-spheroids provide an increase of 92%). The problem of determining a mass shape that provides a maximum of specific forces is formidable* and not necessarily pertinent since the sensitivity of the experiment is more related to either the level of angular acceleration or the level of torque achieved by the apparatus. These factors are examined in Appendix D. By means of a straightforward computer model, a simple analysis is made of a one-arm Beams Balance with hemispheres compared to a one-arm Beams Balance with Spheres. This analysis indicates that the performance (acceleration and specific torque) can indeed be improved, but this improvement is less than the factor of 2 implied by the specific force increase. There is evidence, however, that more improvement, particularly in the level of angular acceleration, may well show up in a four-arm device; and by a more thorough design and analysis effort.

C. Centrifugal Balance Sphere**

Consider a sphere of uniform density (ρ) with 3 orthogonal cylindrical tunnels passing through the center. In each tunnel is a test mass that is constrained to remain along the central axis of the tunnel and whose position along the axis can be determined. A coordinate system (rotating) aligned to these axes is chosen as shown in Figure 6. The rotation of the sphere is controlled by an external servomechanism. The (instantaneous) components of (inertial) angular velocity are shown. The following assumptions are made:

* Also, any significant increase over the optimum half-spheroids is doubtful

** See Appendices E, F, and G

- 1) The sphere is true and has uniform density.
- 2) The gravitational attraction within and due to the sphere is unmodified due to the tunnels and test masses.
- 3) The gravitational gradients due to external sources are uniform throughout the sphere.

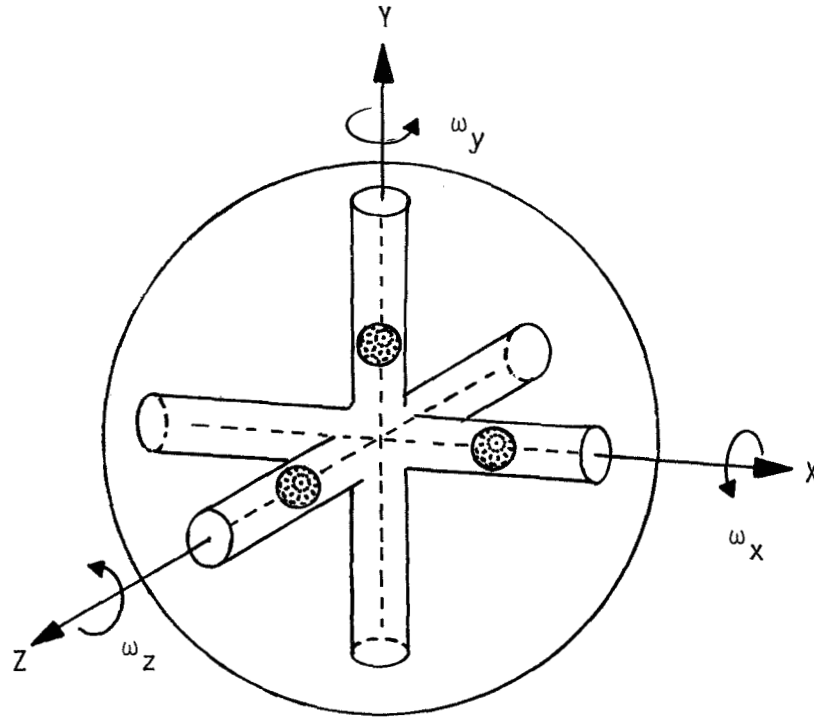


Figure 6 Centrifugal Balance Instrument and Coordinate System

Under these circumstances, the equations of motion of test masses m_x , m_y , and m_z will be (respectively)

$$\begin{aligned}
 \ddot{X} + \frac{C_x}{m_x} \dot{X} + \left(\frac{4}{3} \pi \rho G - \omega_y^2 - \omega_z^2 - \frac{\partial^2 U}{\partial x^2} \right) X &= \frac{f_x}{m_x} \\
 \ddot{Y} + \frac{C_y}{m_y} \dot{Y} + \left(\frac{4}{3} \pi \rho G - \omega_x^2 - \omega_z^2 - \frac{\partial^2 U}{\partial y^2} \right) Y &= \frac{f_y}{m_y} \\
 \ddot{Z} + \frac{C_z}{m_z} \dot{Z} + \left(\frac{4}{3} \pi \rho G - \omega_x^2 - \omega_y^2 - \frac{\partial^2 U}{\partial z^2} \right) Z &= \frac{f_z}{m_z}
 \end{aligned} \tag{13}$$

where C_x, C_y, C_z is damping in the respective tunnel, U is the gravitational potential within the sphere due to external masses, and f_x, f_y, f_z are all other forces on the test masses. If the instrument is in free-fall, and the disturbance forces are ignored, then

$$f_x = f_y = f_z = 0$$

If the servomechanism rotates the sphere so that the test mass radial motions are stabilized, then

$$\ddot{X} = \dot{X} = \ddot{Y} = \dot{Y} = \ddot{Z} = \dot{Z} = 0$$

Thus

$$\frac{4}{3} \pi \rho G - \omega_y^2 - \omega_z^2 - \frac{\partial^2 U}{\partial x^2} = 0$$

$$\frac{4}{3} \pi \rho G - \omega_x^2 - \omega_z^2 - \frac{\partial^2 U}{\partial y^2} = 0$$

$$\frac{4}{3} \pi \rho G - \omega_x^2 - \omega_y^2 - \frac{\partial^2 U}{\partial z^2} = 0 \quad (14)$$

Hence

$$4\pi\rho G - 2(\omega_x^2 + \omega_y^2 + \omega_z^2) - \left(\frac{\partial^2 U}{\partial x^2} + \frac{\partial^2 U}{\partial y^2} + \frac{\partial^2 U}{\partial z^2}\right) = 0 \quad (15)$$

Since

$$\frac{\partial^2 U}{\partial x^2} + \frac{\partial^2 U}{\partial y^2} + \frac{\partial^2 U}{\partial z^2} = \nabla^2 U = 0 \quad (16)$$

in the mass-less tunnels, and the total angular speed of rotation is

$$\omega_x^2 + \omega_y^2 + \omega_z^2 \equiv \omega^2$$

it follows that

$$G = \frac{\omega^2}{2\pi\rho} \quad (17)$$

We also note that

$$\begin{aligned}\omega_x^2 &= \frac{2}{3} \pi \rho G + \frac{\partial^2 U}{\partial x^2} \\ \omega_y^2 &= \frac{2}{3} \pi \rho G + \frac{\partial^2 U}{\partial y^2} \\ \omega_z^2 &= \frac{2}{3} \pi \rho G + \frac{\partial^2 U}{\partial z^2}\end{aligned}\tag{18}$$

Thus we see that, to a first order, the sphere will rotate at a constant (inertial) angular speed which is simply related to the density of the sphere and the universal gravitational constant. Further, the components of the (inertial) angular speed provide a measure of the (instantaneous) in-line gravity gradient components. (These components are referred to a coordinate system fixed to the sphere.) We note further that (knowing the density) a measure of ω , which is constant, provides a measure of G which is independent of all (uniform) gravity gradients arising from sources external to the sphere including those due to the astronauts, the spacecraft, and nearby planets, even if these (uniform) gradients vary with time. Further the determination is independent of the size and shape of the test masses, their radial position and their damping constraints - requiring only that the servo be stable.

One important advantage of this proposed instrument is that there are few inherent initial condition requirements on the experiment. (Perhaps it may be necessary or advantageous to add some due to the design of the servo.) Another advantage lies with the capability of checking the operation of the instrument in a laboratory before launch. This can be done by orienting the sphere so that tunnels are all at nearly equal angles to the vertical and the test masses are above the center of the sphere. The operation of the instrument in this mode will present a much different set of conditions to the servo and to the suspension restraints than in space, but the loops could be closed. (In another mode, two horizontal tunnels could be operated, with the other disabled.)

A more complete analysis of the equations of motion of the apparatus, including the effects of the spacecraft can be found in Appendix D. Appendix E derives the modifications of the gravitational field within the sphere due to the presence of the three tunnels,

and the primary error analysis of this experiment is documented in Appendix F. For the convenience of the reader, we will provide the summary of that report.

Summary of Appendix F

Purpose and Scope

The purpose of this program was to study and recommend the material and fabrication techniques for laboratory size primary masses whose physical and geometrical characteristics are very accurately known. In addition, studies were made of suspension systems for a test mass within the primary masses and techniques for cooling experiments to cryogenic temperatures.

The program included investigation of materials suitable for fabricating the primary masses by considering gravitational field uncertainties due to density, density inhomogeneity, temperature, strain, geometry, the presence of suspension systems and other sources of uncertainty. The suitability of elemental materials whose density is greater than 15 grams per cubic centimeter are discussed from the point of view of density, homogeneity, strength, fabricability, costs, availability, and the associated contribution to gravitational uncertainties. These materials are categorized according to their state of technology for fabrication, developments required to achieve a uniform mass, and the probability of success of achieving a primary mass of known uniform density. The general applicability of diamagnetic suspension systems to space gravity experiments is discussed. The applicability of a quadropole and sextipole system for suspension of a test mass in a tunnel within the primary mass of the proposed experiment are discussed. Experiment cooling requirements are estimated and both open-cycle and closed-cycle cryogenic refrigeration techniques are examined.

Conclusions and Recommendations

1. The $\Delta G/G$ experiment to test the Brans-Dicke theory is most difficult if carried out at 300°K but has a reasonable chance of success at liquid helium temperature. The measurement of the absolute value of G to an improved accuracy is feasible at either temperature. The proposed earth-orbital mission is to measure both G and to

test the suitability of the apparatus for later experiments in highly elliptical solar orbit to measure $\Delta G/G$. To accomplish the latter missions in a meaningful way, it is essential that the earth-orbital experiments be performed at cryogenic temperatures.

2. The primary sphere should be rotated in such a way that the test particle always stays in the same longitudinal position in the tunnel within a very close tolerance. This is necessary because of considerable non-linearity in the longitudinal force due to the tunnel itself and to possible defects in fabrication of the sphere.
3. The support system must be capable of holding the test particle at all times within 1 micron of the tunnel axis. This is necessary because of significant variation of the longitudinal force with distance from the tunnel axis.
4. The primary sphere should be round to 10^{-5} cm.
5. Gross density variation across the sphere should be less than 1 part in 10^{-6} .
6. Fine scale density variations of 2% on a scale of 10^{-4} cm are tolerable.
7. The test mass should be made from a diamagnetic material and should be supported in a quadropole superconducting magnetic field which has superconducting current elements to avoid dissipation within the sphere.
8. Tungsten is the primary candidate for fabrication of the principal mass. Fabrication techniques have been demonstrated for achieving spheres of 99% theoretical density. Uranium is unsuitable because of non-crystallographic phase changes below 43°K , its non-cubic structure (causing an isotropy in its properties), and poor oxidation resistance. Tantalum will be a good candidate if its lower density is acceptable in the experiment.

9. An excessively long time may be required to achieve equilibrium cryogenic temperatures if the experiment is cooled radiatively.
10. Open-cycle helium refrigeration systems in zero gravity require an as yet unproven liquid vapor separator to ensure the venting overboard of only gaseous phase helium.
11. A mechanical helium refrigeration system with long life and smaller size and weight than an open-cycle system is the best selection for both earth-orbital and solar-orbital gravitational experiments.

In addition to the above considerations, it must be noted that a test mass is subject to extraction from its tunnel under certain circumstances. If the experiment is conducted so that the sphere is in a free-fall condition, gravity gradients can operate to bring about this extraction. From Eq. (13) we see that we require

$$4/3 \pi \rho G > \frac{\partial^2 U}{\partial v^2} \quad (19)$$

(where $v = x, y, \text{ or } z$) for stable solutions. For an earth orbit, Eq. (19) is approximately

$$\rho > \frac{2\rho_{\oplus}}{(1+h/R_{\oplus})^3} \quad (20)$$

where h is the orbital altitude and ρ_{\oplus} is the average density and R_{\oplus} the average radius of the earth. For a low ($h \sim 100$ n.mi.) earth orbit, the density of the sphere must be greater than about 11 gm/cm^3 .

This extraction can occur whenever the radially outward force (at $\omega_v = 0$) is greater than the gravitational attraction of the sphere. If the sphere is not in free-fall but is translationally constrained to the spacecraft, then forces additional to gravity gradients can bring about extraction. (In fact, the gravity gradient extraction conditions must also be reevaluated). The extraction conditions will be dependent upon a number of factors, including the size, density and location of the sphere. For instance, a worst case analysis can show that extraction due to gravity gradients alone will occur when

$$\frac{R_d}{R_s} > \frac{1}{2} \left(1 + \frac{h}{R_\oplus}\right)^3 \frac{\rho}{\rho_\oplus} - 1 \quad (21)$$

where R_d is the displacement of the sphere from the C.M. of the spacecraft, and R_s is the radius of the sphere. Selecting a 10 cm radius tungsten ($\rho = 19.3 \text{ gm/cm}^3$) sphere, we see that the sphere must be located such that $R_d < 8.8 \text{ cm}$, (and also note that the sphere weight 81 kg.).

If we neglect forces due to gravity gradients then note that extraction can occur if the spacecraft acceleration (or drag) is

$$a_{sc} > \frac{4}{3} \pi \rho G R_s \quad (22)$$

in the worst case. For the sphere selected above, Eq. (22) requires the spacecraft drag to be less than about $5 \times 10^{-5} \text{ cm/sec}^2$. Depending upon the drag coefficient of the spacecraft, this could preclude a low earth orbit.

If we select a sphere location of $R_d = \frac{1}{2} R_s$ from the C.M. then, in the worst case, angular rotation of the spacecraft of 3 millirad/sec., or an angular acceleration of 0.01 millirad/sec² can cause extraction.

Each of these extraction conditions examined above was considered independently. They do support, however, the conclusion that this experimental configuration must be operated in a free-fall condition, and not constrained to the spacecraft during data-taking intervals.

D. Synchronous Orbit Sphere

A massive, homogeneous sphere of density ρ is in a circular orbit of radius R about the earth. A small test mass moves in a radial hole drilled in the sphere, which is servoed in angle to follow the test mass so that it does not touch the sides of the hole.

In a local vertical coordinate system [2-axis down, 3-axis along the orbital angular momentum, 1-axis chosen to make a right triad], with origin at the C.M. of the sphere, the equation of motion of the test mass is

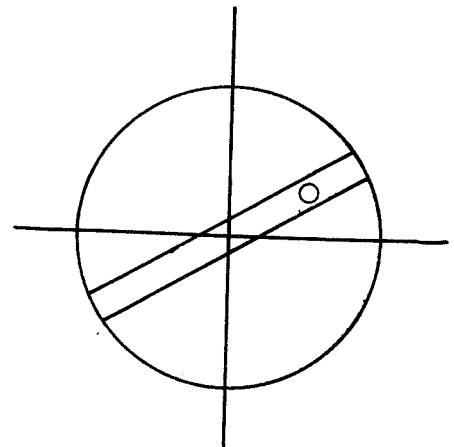


Figure 7 Synchronous Orbit Sphere

$$\ddot{\underline{r}} = -k\underline{r} + \underline{g} - \underline{g}_0 - 2 \underline{\Omega} \times \dot{\underline{r}} - \underline{\Omega} \times (\underline{\Omega} \times \underline{r}) + \underline{f} \quad (23)$$

$$k = \frac{4}{3} \pi G \rho \quad (24)$$

where $\underline{\Omega}$ is the orbital angular velocity and \underline{g} , \underline{g}_0 are the accelerations of terrestrial gravity at the test mass and the origin, respectively, \underline{f} represents any additional perturbing accelerations.

If the orbit is sufficiently high, so that $\underline{\Omega}$ and the terrestrial gravity gradient may be neglected, the equation of motion becomes

$$\ddot{\underline{r}} + k\underline{r} = 0 \quad (25)$$

The components of this equation represent three sinusoidal motions of equal period, so the orbit is clearly a plane ellipse with the C.M. of the massive sphere as center (not, as in the more familiar case of an inverse-square force, as a focus), and the period is

$$T = 2\pi/\sqrt{k} = \sqrt{\frac{3\pi}{G\rho}} \quad (26)$$

independent of any orbital parameters of the test mass. If the density is accurately known, measurement of the period would allow determination of G. In practice, however, it is necessary to take account of the terrestrial gravity gradients and orbital d'Alembert forces.

The terrestrial gravitational field at a point of radius vector \underline{R} from the center of the earth is

$$\underline{g} = - \frac{GM_{\oplus}}{R^3} \underline{R} \quad (27)$$

where M_{\oplus} is the mass of the earth, so the first-order gravity gradient tensor is

$$\begin{aligned} G_{ij} &= \left. \frac{\partial g_i}{\partial R_j} \right|_{R_j=R_j, \text{ the C.M. of the sphere.}} \\ &= -GM \left. \frac{\partial}{\partial R_j} \left(\frac{R_i}{R^3} \right) \right|_{R_j=R_j} \\ &= -\Omega^2 [\delta_{ij} - \frac{3}{R^2} R_i R_j] \end{aligned} \quad (28)$$

since, for a circular orbit, $\Omega^2 = GM_{\oplus} R^{-3}$. In this expression, δ_{ij} is the Kronecker delta, unity for $i=j$ and zero for $i \neq j$.

If we also write

$$\delta_{ij} = \Omega \begin{vmatrix} 0 & -1 & 0 \\ 1 & 0 & 0 \\ 0 & 0 & 0 \end{vmatrix} = \text{"}\Omega \times \text{"} \quad (29)$$

then Eq. (23) may be written, to first order in the gravity gradients, in the tensor form

$$\begin{aligned} \ddot{r}_i &= -kr_i + G_{ij}r_j - 2\Omega_{ij}\dot{r}_j - \Omega_{ik}\Omega_{kj}r_j + f_i \\ &= -kr_i + \Gamma_{ij}r_j - 2\Omega_{ij}\dot{r}_j + f_i \end{aligned} \quad (30)$$

where

$$\Gamma_{ij} = G_{ij} - \Omega_{ik}\Omega_{kj} = \Omega^2 \begin{vmatrix} 0 & 0 & 0 \\ 0 & +3 & 0 \\ 0 & 0 & -1 \end{vmatrix} \quad (31)$$

The components of (30) are

$$\begin{aligned} \ddot{r}_1 &= -kr_1 + 2\Omega\dot{r}_2 + f_1 \\ \ddot{r}_2 &= -(k-3\Omega^2)r_2 - 2\Omega\dot{r}_1 + f_2 \\ \ddot{r}_3 &= -(k+\Omega^2)r_3 + f_3 \end{aligned} \quad (32)$$

The last of these represents a simple harmonic motion, perpendicular to the orbit of the primary sphere, at an angular frequency $\sqrt{(k+\Omega^2)}$, but the other two equations are coupled through the Coriolis terms. Taking Laplace transforms and writing

$$k' = k - 3\Omega^2 \quad (33)$$

yields

$$\begin{vmatrix} (s^2+k) & -2\Omega s \\ +2\Omega s & (s^2+k') \end{vmatrix} \begin{vmatrix} r_1 \\ r_2 \end{vmatrix} = \begin{vmatrix} u_1+sr_1(0) \\ u_2+sr_2(0) \end{vmatrix} \quad (34)$$

where

$$\begin{aligned} u_1 &= f_1 + v_1(0) - 2\Omega r_2(0) \\ u_2 &= f_2 + v_2(0) + 2\Omega r_1(0) \end{aligned} \quad (35)$$

and $r_1(0)$, $r_2(0)$, $v_1(0)$, $v_2(0)$ are the initial values of the coordinates and velocity components. Eq. (34) may be solved, to give

$$\begin{vmatrix} r_1 \\ r_2 \end{vmatrix} = [(s^2+k)(s^2+k')+4\Omega^2 s^2]^{-1} \begin{vmatrix} (s^2+k') & +2\Omega s \\ -2\Omega s & (s^2+k) \end{vmatrix} \begin{vmatrix} u_1+sr_1(0) \\ u_2+sr_2(0) \end{vmatrix} \quad (36)$$

The denominator in this expression is, from (33),

$$s^4 + (2k+\Omega^2)s^2 + k(k-3\Omega^2) = (s^2+a^2)(s^2+b^2) \quad (37)$$

where

$$a^2, b^2 = k + \frac{1}{2} \Omega^2 \pm \frac{1}{2} \Omega \sqrt{(\Omega^2+16k)} \quad (38)$$

Of the four roots $\pm a$, $\pm b$ of (37), two are always real, but the other pair will be imaginary unless

$$k > 3\Omega^2 \quad (39)$$

which is thus the condition for stability of the system; if it is not fulfilled, gravity gradient forces will extract the test-mass from the primary sphere. From (24) and the expression for Ω^2 , this condition may also be written in the form

$$\rho > 3\rho_{\oplus} \left(\frac{R_{\oplus}}{R} \right)^3 \quad (40)$$

where ρ_{\oplus} is the average density of the earth and R_{\oplus} is its radius. For low earth orbit (~ 100 n.m. altitude), the density of the primary

sphere must be greater than about 16 gm/cc. Lighter materials could of course be used if the experiment were conducted in a higher orbit.

When the disturbing accelerations f_i are zero, the solution of (32) may be written as

$$\begin{aligned} r_1 &= A_1 \cos(at + \alpha_1) + B_1 \cos(bt + \beta_1) \\ r_2 &= A_2 \sin(at + \alpha_2) + B_2 \sin(bt + \beta_2) \end{aligned} \quad (41)$$

The phase and amplitude constants in these expressions are not all independent; their relationships to the initial conditions are complicated, but may be obtained by Laplace transforming (36), or by insertion of (41) in (32). The important point, however, is that the frequencies a and b do not depend on the parameters of the orbit, but only on k and Ω , so that sufficient information is available to allow determination of G from frequency measurements, without any requirement that accurate initial conditions be established.

In practice, it is almost certainly more convenient to carry out the measurements in an inertially non-rotating frame, which is rotating relative to the orbital frame of the calculation at an angular velocity $-\Omega$. In this frame, the coordinates of the test-mass are given by

$$\begin{vmatrix} r_1' \\ r_2' \\ r_3' \end{vmatrix} = \begin{vmatrix} \cos \Omega t & -\sin \Omega t & 0 \\ \sin \Omega t & \cos \Omega t & 0 \\ 0 & 0 & 1 \end{vmatrix} \begin{vmatrix} r_1 \\ r_2 \\ r_3 \end{vmatrix} \quad (42)$$

The effect of this transformation is to split the frequencies, so that four components at $(a \pm \Omega)$, $(b \pm \Omega)$ appear, as may readily be seen by substituting (41) in (42). If the measured frequencies are

$$\begin{aligned} \omega_1 &= a - \Omega \\ \omega_2 &= a + \Omega \\ \omega_3 &= b - \Omega \\ \omega_4 &= b + \Omega \end{aligned} \quad (43)$$

then, for example,

$$\begin{aligned} \frac{1}{4}(\omega_1 + \omega_2)^2 + \omega_3 \omega_4 &= a^2 + b^2 - \Omega^2 \\ &= 2k \end{aligned} \quad (44)$$

from (38)

Spacecraft gravity gradients:

Suppose that the primary sphere is in free fall inside an inertially non-rotating spacecraft whose mass distribution produces a gravity-gradient tensor G'_{ij} at the C.M. of the sphere. For simplicity, we first consider the case in which the spacecraft is in such a high orbit that the terrestrial gravity gradients may be neglected. The equation of motion of the test mass is then

$$\ddot{r}_i + kr_i - G'_{ij}r_j = 0 \quad (45)$$

The frequencies of oscillation in this case are given by the roots of the determinantal equation

$$|(s^2 + k)\delta_{ij} - G'_{ij}| = 0 \quad (46)$$

which are clearly

$$w_\gamma^2 = k - \lambda_\gamma \quad (\gamma = 1, 2, 3) \quad (47)$$

where the λ_γ are the eigenvalues of the tensor G'_{ij} . While it may not be possible to calculate the λ_γ precisely, because of the complexity of the mass distribution of the spacecraft, the sum of the eigenvalues of a tensor is equal to its trace, so that

$$\begin{aligned} \sum_\gamma w_\gamma^2 &= 3k - G'_{ii} \\ &= 3k - \frac{\partial^2 U}{\partial r_i \partial r_i} = 3k - \nabla^2 U = 3k \end{aligned} \quad (48)$$

where U is the gravitational potential at the C.M. of the sphere due to the spacecraft; the last equality is due to the fact that U is a solution of Laplace's equation.

In this simple case, then, the effect of the spacecraft gravity gradient is to split the frequency of oscillation into three components; but k , and hence G , may be determined from the average value of the squares of these three components.

When both terrestrial and spacecraft gravity gradients are present, the equation of motion of the test mass, Eq. (30) is modified to read*

$$\ddot{r}_i + kr_i - \Gamma_{ij}r_j + 2\Omega_{ij}\dot{r}_j - G'_{ij}r_j = f_i \quad (49)$$

In general, the spacecraft gravity gradients couple all three of these equations together; by inspection of Eqs. (32), the frequencies a' , b' , c' appearing in the components of the motion of the test mass are given by

$$\begin{vmatrix} (s^2+k)-G'_{11} & -2\Omega s-G'_{12} & -G'_{13} \\ +2\Omega s-G'_{21} & (s^2+k')-G'_{22} & -G'_{23} \\ -G'_{31} & -G'_{32} & (s^2+k'')-G'_{33} \end{vmatrix} = (s^2+a'^2)(s^2+b'^2)(s^2+c'^2) = 0$$

where $k' = k-3\Omega^2$, $k'' = k+\Omega^2$. Equating the coefficients of s^4 on the two sides of this equation yields

$$\begin{aligned} k + k' + k'' - (G'_{11}+G'_{22}+G'_{33}) + 4\Omega^2 &= 3k + 2\Omega^2 \\ &= a'^2 + b'^2 + c'^2 \end{aligned} \quad (51)$$

the trace G'_{ii} being zero.

If the motion of the test-mass is resolved in an inertially non-rotating frame, the measured frequencies are split (analogously to Eq.(43)) into six components

* It is assumed the spacecraft is in a local vertical attitude hold, so that the G'_{ij} are constants in the orbital frame of this equation

$$\begin{aligned}
a_+ &= a' + \Omega \\
a_- &= a' - \Omega \\
b_+ &= b' + \Omega \\
b_- &= b' - \Omega \\
c_+ &= c' + \Omega \\
c_- &= c' - \Omega
\end{aligned}
\tag{52}$$

Ample information is then available to determine k . For example, substituting from (52) and using (51), it is easy to show that

$$a_+^2 + a_-^2 + b_+^2 + b_-^2 + c_+^2 + c_-^2 + 10[a_+a_- + b_+b_- + c_+c_-] = 36k
\tag{53}$$

Other organizations of the data are of course possible. The important point, however, is that self-contained frequency measurements within the apparatus, using a suitable inertial reference (gyros or star-trackers) to resolve the test-mass motion into components, provide sufficient data for the determination of G even in the presence of both terrestrial and spacecraft gravity gradients. If available to sufficient accuracy, an external measurement of the spacecraft orbital angular velocity could be used in processing the data, but this is not essential. The only requirement on the spacecraft gravity gradients is that they be constant in time, in the local vertical orbital frame; a more thorough error analysis is required to determine the effects of deviations from this condition, due to motion of parts and/or astronauts within the spacecraft as well as unavoidable changes in spacecraft attitude. In general, it may be assumed that changes in spacecraft gravity gradients are important only when they contain frequency components fairly close to the oscillation frequencies of the test-mass.

Non-Linearity of the Primary Force Field

In practice, it can be expected that the gravitational field within the primary sphere will deviate slightly from the linear form of Eq. (3), and this will introduce some dependence of the period of the motion of the test mass on its orbital parameters. The principal

reasons for this are as follows:

i) Perturbation due to the tunnel drilled through the sphere. This perturbation and the resultant effects on the orbit of the test mass may presumably be calculated numerically to any desired accuracy. However, some control of the initial conditions for the test mass may be required. The effect may be minimized by minimizing the ratio of the tunnel diameter to the radius of the primary sphere. For a given mechanization with a consequent minimum tunnel diameter and given accuracy of initial conditions (caging and release mechanism for the test mass), a minimum size of the primary sphere may be required in order to achieve a desired accuracy in the measurement of G. This is important, because the overall weight of the experiment of course increases with the cube of the radius of the sphere.

ii) Non-sphericity of primary. If the primary is a slightly oblate or prolate spheroid, with the tunnel along the symmetry axis, the equation of motion of the test-mass is ⁽¹⁵⁾

$$\ddot{\underline{r}} \sim -k(1+\epsilon)\underline{r} \quad (54)$$

where ϵ is the fractional deviation of the polar radius of the spheroid from the mean radius, and the plus or minus signs refer to the prolate and oblate cases, respectively. The fractional error in the measurement of G due to this effect is thus approximately equal to the fractional tolerance in manufacture of the primary sphere. As discussed by Berman and Forward ⁽¹³⁾, a tolerance of one part in a million is not unreasonable. Furthermore, if it is possible to measure the first harmonic of the spheroid with an accuracy better than the manufacturing tolerance, the equations of motion may be corrected to the same order. This effect is therefore not expected to be a limitation on the attainable accuracy in the determination of G.

iii) Density inhomogeneity of primary sphere. While the shape and mass, and hence the mean density, of the primary can be measured with an accuracy better than one part in 10^6 , small density inhomogeneities are likely to exist, and these will certainly produce errors in the measured value of G. Some averaging will be achieved as the test-mass

moves along the tunnel (a circular orbit not being possible in the presence of gravity gradient forces). Also, Forward⁽¹⁶⁾ has suggested a possible modification of the experiment in which the test mass moves, not in a tunnel, but in a disc-shaped region obtained by removing an equatorial slice through the center of the primary sphere, which is spun at a relatively high angular velocity about an axis perpendicular to the slice, as well as being servoed in the other two axes to follow the motion of the test mass: this averages the effects of density inhomogeneities over a much larger region of the primary sphere, although of course it would considerably complicate the mechanization of the experiment. Further study of these questions must be postponed until more information has been obtained concerning the degree of density homogeneity which is feasible in the manufacture of the sphere.

Eccentricity of the Spacecraft Orbit

If the orbit of the spacecraft is elliptical, the orbital angular velocity becomes⁽¹⁷⁾

$$\Omega = \Omega_0 (1-e^2)^{-3/2} (1+e \cos \theta)^2 = \dot{\theta} \quad (55)$$

where Ω_0 is the mean angular motion (i.e., the angular velocity in a circular orbit of the same period), e is the eccentricity, and θ is the true anomaly. Furthermore, the coefficient in the gravity gradient tensor G_{ij} (cf. Eq. (28)) becomes

$$\frac{GM_{\oplus}}{R^3} = \Omega_0^2 (1-e^2)^{-3} (1+e \cos \theta)^3 \quad (56)$$

Finally it is necessary to add to the equations of motion a term $(\dot{\underline{\Omega}} \times \underline{r})$, representing tangential acceleration, where

$$\dot{\Omega} = -2\Omega_0^2 e (1-e^2)^{-3} (1+e \cos \theta)^3 \sin \theta \quad (57)$$

For small e , the equations of motion (32) become a set of Matthieu-type equations, the first two being coupled through the Coriolis and tangential accelerations. To first order e , we have

$$\Omega^2 = \Omega_0^2 (1 + 4e \cos \Omega_0 t) \quad (58)$$

$$GM_{\oplus}/R^3 = \Omega_0^2(1 + 3e \cos \Omega_0 t) \quad (59)$$

$$\dot{\Omega} = -2\Omega_0^2 e \sin \Omega_0 t$$

In low earth orbit, an eccentricity of 10^{-5} means that the apogee and perigee differ in altitude by only about 0.1 n.m. If this experiment is not to constitute a serious mission constraint, eccentricities an order of magnitude or higher than this must be expected. The implication is that corrections to the equations of motion, to the first order in e , should be considered. This is a matter for further study, perhaps by computer simulation.

Conclusion

This preliminary analysis of the rotating tunneled sphere Cavendish experiment in earth orbit has shown that the proposed apparatus offers considerable promise of substantially improving knowledge of the Newtonian gravitational constant. The principle problem areas appear to be the effects of density inhomogeneities in the primary sphere and of eccentricity of the spacecraft orbit. Further study of these areas is required in order to form a realistic estimate of the attainable accuracy in the measurement of G . So far, however, nothing has been discovered which should prevent achievement of an accuracy of a few parts in a million.

SECTION III

Measurement of the Eotvos Ratio

1. Objective

The objective of the experiment is to measure the Eotvos ratio for gold and aluminum (and possibly other materials) with an accuracy of one part in 10^{14} or better.

2. Significance

A fundamental assumption in all current gravitational theories is that all bodies fall with the same acceleration in a given gravitational field. If $m_p(A)$ is the passive gravitational mass of a body of material A, a measure of the strength of its interaction with a gravitational field, and $m_i(A)$ is its inertial mass, the Eotvos ratio for a pair of bodies of materials A and B, respectively, is defined as

$$\eta(A,B) = \frac{2[m_p(A)/m_i(A) - m_p(B)/m_i(B)]}{[m_p(A)/m_i(A) + m_p(B)/m_i(B)]} \quad (61)$$

If this ratio were found experimentally not to vanish identically for all pairs of materials, a major revision in current understanding of gravitation would be required. Since such a result would imply anomalous gravitational behavior for some of the fundamental constituents of matter, new light might also be cast on profound problems concerned with the relationship between particle physics and the structure of space-time. The accuracy of the proposed experiment is sufficient to investigate the effects of gravitation on all forms of mass-energy making up matter except that stored in the gravitational interaction itself. In particular, it should be possible to determine whether energy stored in the weak interaction (which is known to violate another well-established physical principle, that of parity conservation) violates the principle of equivalence of inert and gravitational mass.

The theoretical rationale for the proposed experiment results from extending a line of reasoning given by Schiff. He points out that the total mass-energy of any atom has several distinct components.

One part is due to the masses of the three types of elementary particles in an atom:

- 1) Protons
- 2) Neutrons
- 3) Electrons

The rest of the atom's total mass-energy is due to the four types of binding energy which hold the atom together.

- 1) Strong interactions, which bind together the neutrons and protons in a nucleus.
- 2) Electromagnetic interactions, causing protons to repel one another in a nucleus, making electrons bind with nuclei to form atoms, and causing atoms to form molecules.
- 3) Weak interactions, responsible for the β -decay process.
- 4) Gravitational interactions.

To put it another way, atoms and molecules have masses which are different from the sum of the masses of the individual free protons, neutrons, and electrons; these differences are due to the binding energies produced by the strong, weak, electromagnetic, and gravitational interactions between the particles. It might be possible for certain types of particles to have inertial-to-passive mass ratio $\underline{\gamma}$ that differed from other particles; in addition, any one of the interactions could produce binding energies for which the inertial mass equivalents and the passive-mass equivalents had an anomalous ratio $\underline{\gamma}$. Placing accurate experimental limits on the differences in $\underline{\gamma}$ for various kinds of particles and binding energies is thus essential to give the theorist an idea of the nature of the particles and their interactions.

Elementary particle theory can provide quantitative estimates of the accuracy to which $\eta(A,B)$ need be known in order to rule out anomalous Eotvos ratios for the various kinds of binding energies which hold an atom together. The following equation shows the sources of the different kinds of mass which make up an atom of atomic number Z , neutron number N , and mass number $A = N+Z$:

$$Mc^2(\text{real atom}) = Zm_p c^2 + Nm_n c^2 + Zm_e c^2 - B_E - B_S(Z,A) - B_{ER} - B_W - B_G \quad (62)$$

m_p = proton mass, m_n = neutron mass, m_e = electron mass

$B_E \approx 15.6 Z^{7/3} \text{eV}$ = electronic binding energy or total ionization potential

$B_S(Z,A)$ = strong-interaction binding-energy of the nucleus

$B_{ER} = \frac{0.6Z(Z-1)e^2}{A^{1/3} \times (1.4 \times 10^{-13} \text{cm})}$ = electromagnetic repulsion energy of the protons

B_W = weak-interaction part of binding energy

B_G = gravitational part of binding energy

Note that the nuclear binding energy measured by nuclear physicists is actually

$$B(Z,A) = B_S(Z,A) + B_{ER} + B_W + B_G \quad (63)$$

B_{ER} can be computed to a reliable accuracy, as given above. B_W , the weak-interaction contribution to nuclear binding cannot be rigorously computed using present-day theories; we can, however, make a fairly reliable estimate using Fermi's phenomenological theory of weak interactions. Fermi's universal weak coupling constant is

$$G_W = 10^{-5} m_p^{-2} \quad (64)$$

as measured in β -decay reactions. The contribution of the weak force is then assumed to be a certain fraction of the strong force given by the dimensionless number $m^2 G_W$, where m is a mass characterizing the strong interactions. In the least advantageous case, m would be the mass of the pi-meson, which is largely responsible for the strong internuclear force. We would then have

$$B_W \approx m_\pi^2 G_W B(Z,A) = 2 \times 10^{-7} B(Z,A) \quad (65)$$

This estimate agrees with the more rigorous nuclear physics calculation of the Blin-Stoyle⁽³³⁾.

The gravitational binding energy is estimated by using the nuclear radius formula

$$r_A = 1.4 A^{1/3} \times 10^{-13} \text{ cm} \quad (66)$$

and computing the gravitational potential energy of one half of the nucleus acting on the other, using Newton's gravitational constant $G = 6.67 \times 10^{-8} \text{ cm}^3 \text{ gm}^{-1} \text{ sec}^{-2}$. The result is

$$B_G = \frac{G \left(\frac{1}{2} A m_p\right) \left(\frac{1}{2} A m_n\right)}{(1.4) A^{1/3} \times 10^{-13} \text{ cm}} = 2.08 \times 10^{-31} A^{5/3} \text{ eV} \quad (67)$$

We now list in Table I the estimates of the relative contributions of each kind of energy in electron-volts for aluminum (Al) and gold (Au).

We see that if the Eotvos anomaly lies all in the electron masses, for example, the electronic Eotvos ratio η_e will be given by the expression

$$\eta_e \left| \frac{Z m_e}{M} - \frac{Z' m_e}{M'} \right| = \eta(Z, Z'), \quad (68)$$

where $\eta(Z, Z')$ is the total anomaly measured in the Eotvos experiment.

Suppose we decide to believe that η_e is satisfactorily close to zero if we show

$$\eta_e = 0 \pm 10^{-3}. \quad (69)$$

Then, for gold and aluminum, we need to show

$$\eta < \left| 10^{-3} \left(\frac{Z m_e}{M} - \frac{Z' m_e}{M'} \right) \right| = 1.78 \times 10^{-7} \quad (70)$$

Similar calculations for the other types of energy give the required upper limits of $\eta(\text{Au}, \text{Al})$ listed in Table II.

Z	N	A	M(total)C ²	Zm _p c ²	Nm _n c ²	Zm _e c ²	B _E	B(Z,A)	B _{ER}	B _W	B _G	
Al	13	14	27	25.13x10 ⁹	12.2x10 ⁹	13.15x10 ⁹	6.643x10 ⁶	6.21x10 ³	225x10 ⁶	3.12x10 ⁷	45	5x10 ⁻²⁹
Au	79	118	197	183.5x10 ⁹	74.1x10 ⁹	110.9x10 ⁹	4.037x10 ⁶	4.18x10 ⁵	1.56x10 ⁹	6.35x10 ⁸	312	1.4x10 ⁻²⁷
$\left \frac{E(\text{Au})}{M(\text{Au})} - \frac{E(\text{Al})}{M(\text{Al})} \right =$.081	.081	2.4x10 ⁻⁴	2.03x10 ⁻⁶	4.5x10 ⁻⁴	2.2x10 ⁻³	9x10 ⁻¹¹	5x10 ⁻³⁹	

Table I

A comparison of the relative energy contents of gold and aluminum. In the third row of the table, the symbol E refers to each of the particular types of energy given in the column headings. All energies are in units of electron volts.

$\eta_p(Zm_p)$	$< 10^{-3}$	if	$\eta < 10^{-4}$
$\eta_n(Nm_n)$	$< 10^{-3}$	if	$\eta < 10^{-4}$
$\eta_e(Zm_e)$	$< 10^{-3}$	if	$\eta < 10^{-7}$
$\eta_E(B_E)$	$< 10^{-3}$	if	$\eta < 10^{-9}$
$\eta_S(B_S(Z,A))$	$< 10^{-3}$	if	$\eta < 10^{-7}$
$\eta_{ER}(B_{ER})$	$< 10^{-3}$	if	$\eta < 10^{-6}$
$\eta_W(B_W)$	$< 10^{-3}$	if	$\eta < 10^{-14}$
$\eta_G(B_G)$	$< 10^{-3}$	if	$\eta < 10^{-42}$

Table II

We are now in a position to see the strongest argument as to why the Eotvos experiment should be improved beyond Dicke's limit, $\eta(\text{Au,Al}) = \leq 10^{-11}$. Table II shows us that Dicke's number confirms $\eta(\text{Au,Al})$ to be very near zero for every type of energy down to but not including the weak-interaction energy. To rule out an anomalous Eotvos ratio for weak-interaction binding energies, we must show

$$\eta(A,B) < 10^{-14} \tag{71}$$

In addition, as previously mentioned, if any interaction would be expected to give an anomalous Eotvos ratio, it would be the weak interaction. The weak force has a long history of upsetting supposedly well-established assumptions in physics; in 1956, physicists were profoundly surprised to discover that the weak interactions violated the parity conservation symmetry and the charge-conjugation symmetry obeyed by the strong interactions. Increasing the accuracy of the Eotvos experiment would conceivably demonstrate a similar weak-interaction violation of the principle of equivalence of inertial and passive mass.

3. Disciplinary Relationship

a. Brief history of related work

The field of experimental gravitation was for many years restricted to the study of the three famous tests proposed by Einstein himself⁽¹⁹⁾ to verify his theory of general relativity. The only three measurable differences between Newton's law of gravitation and Einstein's theory were the gravitational red shift of stellar spectral lines, the bending of starlight passing the limb of the sun during the solar eclipse, and the non-Newtonian part of the precession of the perihelion of Mercury's orbit about the sun.

Recent advances in technology have opened up several new areas of experimental investigation. Using the Mossbauer effect⁽²⁰⁾ Pound and Rebka⁽²¹⁾ measured the violet frequency shift of light falling in the earth's gravitation field. Using new radar technology, Shapiro⁽²²⁾ has measured the gravitational time delay in the return of a radar pulse from a planet on the other side of the sun. Weber⁽²³⁾ appears to have detected gravitational radiation. Future experiments include that of Fairbank⁽²⁴⁾, who, acting on a proposal by Schiff⁽²⁵⁾, is preparing to use a super-conducting gyroscope to measure the non-Newtonian precession which is predicted by general relativity. Kleppner, Vessot, and Ramsey⁽²⁶⁾ were until recently contemplating the use of a hydrogen maser to measure the effect of the gravitational potential on the rate of a clock.

Curious enough, it seems that the fundamental assumption of Einstein's theory of gravitation cannot be directly tested, although the agreement of the above-mentioned experiments with the theoretical predictions can certainly be regarded as an indirect test. Einstein's theory of general relativity is based on the so-called "strong principle of equivalence", which states that in an infinitesimal region of space-time, it is impossible to distinguish between a gravitational field and an acceleration of the coordinate frame. Treating gravitational fields as equivalent to accelerating coordinate systems leads fairly directly to the curvature of space-time which Einstein's theory holds responsible for all gravitational effects⁽¹⁹⁾. It is impossible to measure the space-time curvature, since the measurable numerical predictions of Einstein's curved-space theory are exactly reproduced by Thirring's flat-space formulation of gravitation⁽²⁷⁾. In the latter theory, the gravitational field is interpreted as distorting measuring instruments while leaving space-time itself unaffected. The flat-space

formulation does not depend on the strong principle of equivalence, but does require the "weak principle of equivalence", which states that a body's inertial mass, measuring its resistance to a known force, is exactly equivalent to the body's passive gravitational mass, which measures its response to a given gravitational field. The weak principle of equivalence, which obviously follows from the strong principle, says that the ratio

$$\gamma = \frac{m_{\text{passive}}}{m_{\text{inertial}}} \quad (72)$$

is a universal constant for all materials (taken by convention to be unity) regardless of composition. We are thus led to the conclusion that we can come no closer to testing the basic postulates upon which experimentally-verified theories of gravitation are based than an examination of the validity of the weak principle of equivalence.

A classic series of experiments aimed directly at testing the weak principle of equivalence was begun around 1890 by Baron Roland von Eotvos.⁽²⁸⁾ His apparatus consisted of a torsion balance with a different material attached to each end of the beam. When in equilibrium at latitude λ , the materials were acted upon by the $(3.39 \cos \lambda \sin \lambda) \text{cm/sec}^2$ acceleration due to the earth's rotation on its axis (λ is the geographic latitude) and by an equal and opposite component of the earth's gravitational attraction. If we label the two materials at opposite ends of the beam as \underline{A} and \underline{B} , then, at respective positions \underline{R}_A and \underline{R}_B relative to the center of the earth, the center of gravity \underline{R} of the balance beam is

$$\underline{R} = [m_p(A)\underline{R}_A + m_p(B)\underline{R}_B] / (m_p(A) + m_p(B)). \quad (73)$$

The component of the torque on the beam acting perpendicular to the earth's surface is given by

$$\begin{aligned} T = & [m_i(A) - m_p(A)] (\underline{R}_A - \underline{R}) \times (-\underline{\omega} \times (\underline{\omega} \times \underline{R}_A)) \cdot \underline{R} / |\underline{R}| \\ & + [m_i(B) - m_p(B)] (\underline{R}_B - \underline{R}) \times (-\underline{\omega} \times (\underline{\omega} \times \underline{R}_B)) \cdot \underline{R} / |\underline{R}| \end{aligned} \quad (74)$$

where ω is the angular velocity of the earth's rotation and m_i and m_p

refer of course to the inertial and passive gravitational masses of the materials. If the apparatus is aligned so that $\omega \cdot \underline{R}_A = \omega \cdot \underline{R}_B$, we have

$$T = \eta(A,B) \left[\frac{m_i(B)m_p(A) - m_p(B)m_i(A)}{2(m_p(A)+m_p(B))} \right] [\omega(\underline{R}_B \times \underline{R}_A) (\omega \cdot \underline{R}_A) / |\underline{R}|] \quad (75)$$

where we have defined the "Eotvos ratio", $\eta(A,B)$ as

$$\eta(A,B) = \frac{\frac{m_p(A)}{m_i(A)} - \frac{m_p(B)}{m_i(B)}}{\frac{1}{2} \left[\frac{m_p(A)}{m_i(A)} + \frac{m_p(B)}{m_i(B)} \right]} \quad (76)$$

The Eotvos experiment therefore consists of the determination of the measurable quantity

$$\eta(A,B) = \frac{\gamma_A - \gamma_B}{\frac{1}{2}[\gamma_A + \gamma_B]} \quad (77)$$

where in the second line we have arbitrarily chosen our mass units so that $m_p(B) = m_i(B)$. In the original experiment $\eta(A,B)$ was measured by comparing the equilibrium position of the torque arm in one orientation to that when the supporting frame was rotated 180° . If $\eta(A,B)$ were non-zero, the torque would change sign under the 180° rotation and give rise to a slight difference in the equilibrium orientation of the torque arm relative to the supporting framework. A representative upper limit on the value of $\eta(A,B)$ for a variety of pairs of materials as determined by this method is 10^{-9} . Thus the experiment of Eotvos provides quite a respectable experimental basis for the theory of gravitation.

As technological developments have allowed new experiments in other areas of gravitation, they have also permitted improvements in the Eotvos experiment. In a series of measurements ending in 1964, R.H. Dicke and his collaborators⁽²⁹⁾ were able to reduce the upper limit

on η (Gold, Aluminum) to one part in 10^{11} . This experiment used a balance beam similar to that of Eotvos, but suspended so that the 0.59 cm/sec^2 centrifugal acceleration of the earth's motion about the sun was counteracted by the equal and opposite gravitational attraction toward the sun. The rotation of the earth on its axis introduced a characteristic 24-hour period into the torque which would act on the balance beam if $\eta(A,B)$ were non-zero, thus facilitating the data analysis. The paper describing the experiment mentions that it was generally difficult to obtain reliable data continuously for more than three 24-hour periods because of earth-based disturbances, such as construction activity and rapid weather changes, and because of gravity-forced convection, even in the reduced atmosphere of the highly-evacuated pendulum environment.

b. State of present development in the field.

The technology appears to have advanced to the point where the experimental upper limit on $\eta(A,B)$ can be significantly reduced. In particular, the possibility of performing the experiment in the space environment originally suggested by Dicke⁽²⁹⁾, permits the elimination of the earth-based noises and convection problems which plagued Dicke, the utilization of free-fall techniques unavailable on earth, and full exploitation of the $700\text{-}800 \text{ cm/sec}^2$ centrifugal and gravitational acceleration acting on a body in earth orbit⁽³⁰⁾. Combining these advantages with those of modern control systems, measurement devices, and data reduction techniques, we hope to demonstrate that a device can be constructed in the near future which will be capable of decreasing the upper limit on $\eta(A,B)$ by several orders of magnitude.

4. Experiment Approach

a. Detailed description of the experiment concept.

We now present a possible method of improving the Eotvos experiment by adapting it to the space environment. Our method makes use of a large rotating mass of one material, an oscillating small mass of the same material and an oscillating small mass of a different material. We proposed to use servo devices to control the various aspects of the suspension and detection systems. The resulting short time scale of

the potential Eotvos oscillations will, it is hoped, reduce problems of long-term stability of the instrument. The limiting error source appears at present to be thermal noise, yielding at normal temperature, an upper limit on $\eta(\text{Au,Al})$ of about 10^{-14} . With this accuracy, we hope to demonstrate whether or not the weak-interaction binding energy of nuclei possesses an anomalous Eotvos ratio.

As shown in Figure 8, the proposed system consists basically of an aluminum wheel, spinning with an angular velocity ω , the direction of which lies along the normal to the plane of a low, circular orbit about the earth. This orientation is, of course, stable under gravity-gradient effects. A sensitive accelerometer is mounted radially in the plane of the wheel; it contains two independent proof masses, one of gold and one of aluminum, suspended coaxially.

Since our technique directly measures the differential Eotvos force instead of converting the small forces involved into torques as in the earth-bound experiments of Eotvos and Dicke, the gravity-gradient forces can for physical reasons be directly distinguished from the Eotvos forces during the measurement process. This cannot be done as readily in the former experiments.

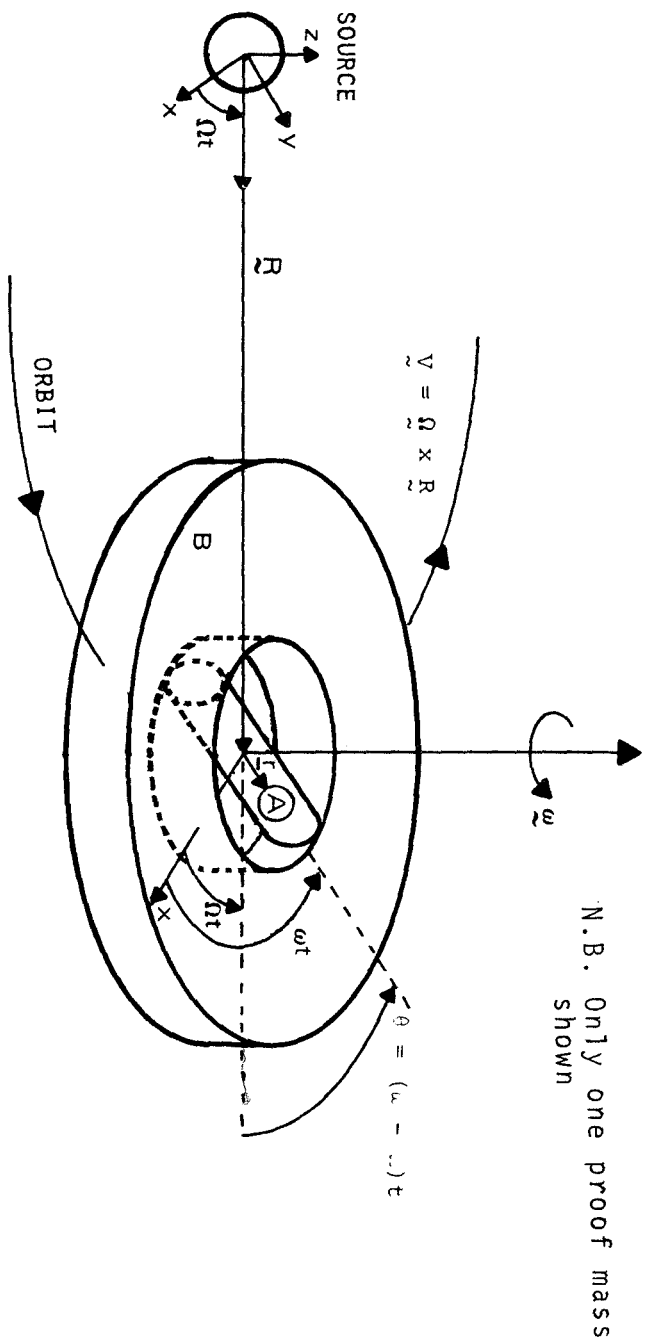
Let m_i and m_p be the inert and gravitational masses of the gold proof mass, and r its position vector relative to the center of mass of the system. It is assumed that the mass of the wheel is so large that motion of the proof mass does not appreciably shift the position of the C.M. within the system. Since the axis of the accelerometer may not, in general, pass through the C.M., we write

$$\underline{r} = \underline{x} + \underline{d} \quad (78)$$

where \underline{d} is the position vector of the null of the accelerometer. The equation of motion along the accelerometer axis is then

$$m_i \ddot{x} = -m_i \ddot{q} + m_i \omega^2 \underline{r} \cdot \underline{i} + (m_p \underline{g} + m_i \underline{g}_0) \cdot \underline{i} - m_i \underline{f} \cdot \underline{i} \quad (79)$$

where $m_i \ddot{q}$ represents a servo restraint force applied to the proof mass, \underline{i} is a unit vector along the axis, \underline{g} is the gravitational field of the Earth at the proof mass, \underline{g}_0 is the inertial acceleration of the C.M. due to gravitation, and \underline{f} is any disturbing acceleration applied to the C.M. In this equation, terms such as that due to the Coriolis acceleration, which is always perpendicular to the axis, have been dropped.



N.B. Only one proof mass shown

Figure 8 The Orbital Eotvos Apparatus

if the passive-inertial mass ratio of aluminum is taken as unity, and if it is assumed that there is too little gold or other non-aluminum material in the system to affect the overall Eotvos ratio significantly, then

$$\underline{g}_0 = \underline{\Omega} \times (\underline{\Omega} \times \underline{R}) = +\underline{R}\Omega^2 \quad (80)$$

where $\underline{\Omega}$ is the instantaneous orbital angular velocity of the system (and is a function of \underline{R}) and \underline{R} is the geocentric position vector of the C.M. If we consider the earth as a perfect sphere of mass M, the gravitational acceleration at a distance \underline{X} from the center is

$$\underline{g} = -GM \underline{X}/|\underline{X}|^3 = -\underline{X}\Omega^2 \quad (81)$$

where $G = 6.6732 \times 10^{-8} \text{ cm}^3 \text{ gm}^{-1} \text{ sec}^{-2}$ is Newton's gravitational constant.

We now expand the gravitational term in Eq. (79) about the C.M. position \underline{R} by letting $\underline{X} = \underline{R} + \underline{r}$. The result is

$$\begin{aligned} m_p \underline{g} + m_i \underline{g}_0 &= \left[m_i^{-\gamma} \frac{GM(\underline{R} + \underline{r})}{|\underline{R} + \underline{r}|^3} + \underline{R}\Omega^2(\underline{R}) \right] \\ &= -m_i \Omega^2(\underline{R}) [\eta \underline{R}' + \gamma(\underline{r} - 3\underline{R}(\underline{r} \cdot \underline{R})/\underline{R}^2) + \dots] \end{aligned} \quad (82)$$

where $\gamma = m_p/m_i$ is the passive inertial mass ratio of gold and $\eta \equiv \eta(\text{Au}, \text{Al})$ is the Eotvos ratio for gold and aluminum. Substituting Eq. (81) in (99), we have

$$\begin{aligned} \ddot{\underline{x}} &= -\underline{g} + \omega^2 \underline{x} - \eta \underline{g}_0 \cdot \underline{i} - \gamma \Omega^2 [1 - 3\underline{R}^{-2}(\underline{R} \cdot \underline{i})^2] \underline{x} - \underline{f} \cdot \underline{i} \\ &\quad + (\omega^2 - \gamma \Omega^2) \underline{d} \cdot \underline{i} + 3\underline{R}^{-2}(\underline{R} \cdot \underline{d})(\underline{R} \cdot \underline{i}) \gamma \Omega^2 \end{aligned} \quad (83)$$

The term in $\underline{d} \cdot \underline{i}$ is a constant, which may be minimized by choosing \underline{d} as nearly as possible along the spin axis of the wheel. Since this is nominally along the orbital angular momentum, this choice also minimizes $\underline{R} \cdot \underline{d}$. Then, since \underline{R} and \underline{g}_0 are rotating at the orbital angular velocity $\underline{\Omega}$, and \underline{i} is rotating at $\underline{\omega}$ about the same axis, the equation becomes

$$\ddot{x} + q - [\omega^2 + \frac{1}{2}\gamma\Omega^2 + \frac{3}{2}\gamma\Omega^2 \cos 2(\omega - \Omega)t]x = \eta g \cos(\omega - \Omega)t - f' \quad (84)$$

If we neglect constant terms, and assume f lies in the orbital plane, f' is given by $\gamma\Omega^2$

$$f' = f \cos(\omega - \Omega)t + \frac{3}{2}\Omega^2 (d_1^2 + d_2^2)^{1/2} \cos [2(\omega - \Omega)t + \alpha] \quad (85)$$

where d_1, d_2 are the components, if any, of d in the plane of the wheel, and $\tan \alpha = d_2/d_1$.

If q is a simple spring restraint (say, $q = kx$, $k > \omega^2 + \frac{1}{2}\gamma\Omega^2$), then Eq. (84) is recognized as a standard Mathieu equation.

For the aluminum proof mass (which has $\gamma \equiv 1$), an identical calculation yields the equation of motion

$$\ddot{x}' + q' - [\omega^2 + \frac{1}{2}\Omega^2 + \frac{3}{2}\Omega^2 \cos 2(\omega - \Omega)t]x' = 0 - f' \quad (86)$$

On the right-hand side of this equation, it is assumed that the null positions of the gold and aluminum proof masses are identical, a condition which should be realizable to within a fraction of the wavelength of light, because of the coaxial design.*

The quantities which can be measured directly in this system are x , x' and $y = x - x'$. By subtraction, the equation of relative motion of the two proof masses is, to an entirely sufficient accuracy,

$$\ddot{y} - [\omega^2 + \frac{1}{2}\Omega^2 + \frac{3}{2}\Omega^2 \cos 2(\omega - \Omega)t]y + q - q' = \eta g \cos(\omega - \Omega)t \quad (87)$$

The orbital angular velocity is of order 0.01 rpm, whereas the wheel angular velocity may be 10-100 rpm. The time-varying coefficient in Eqs. (86) and (87) is then 6 to 8 orders of magnitude smaller than ω^2 , and may be neglected in the initial stages of the servo design (although it must be taken into account in the final analysis, since it may cause instability). The Laplace transform of (86) is then

* Since, from Eq. (85), a deviation of the null positions of the two proof masses results in a double-frequency input signal, it may be necessary to design a separate, slow servo loop to maintain coincidence.

$$[s^2 + A(s) - \omega^2 - \frac{1}{2} \Omega^2] x' = f' \quad (88)$$

where the transform of q' has been chosen as $A(s)x'$. The transform of q is chosen to be

$$q(s) = B(s)y + (1+\delta)A(s)x' \quad (89)$$

which, from Eqs. (87) and (88), gives

$$y = \frac{1}{[s^2 + B(s) - \omega^2 - \Omega^2/2]} [\epsilon - H(s)f'] \quad (90)$$

Here

$$\epsilon = \frac{\eta g s}{s^2 + (\omega - \Omega)^2} \quad (91)$$

is the Laplace transform of the very small Eotvos acceleration which it is desired to detect, and

$$H(s) = \frac{\delta A(s)}{[s^2 + A(s) - \omega^2 - \Omega^2/2]} \quad (92)$$

The function of the aluminum proof-mass system is to filter disturbing accelerations, thus giving only the differential displacement y as the output. Common electronics can be used for $A(s)$ in both the x' - and y -loops, so that the value of δ depends only on the difference in the sensitivity of the force transducers used to command the two proof masses: a value as low as 0.001 should be attainable. The optimum choice for $A(s)$, consistent with stability in the x' -loop, must await specification of the statistics of the disturbing accelerations and is thus dependent on the overall vehicle design. Reducing the disturbing accelerations essentially to zero still leaves the gravity-gradient-induced, double-frequency component of f' in Eq. (85). Reducing this component to $10^{-11}g$, the present lower limit on the Eotvos acceleration, would require that the accelerometer null lie on the spin axis of the wheel with an accuracy of about 50 microns. The design should be such

that the disturbance-filtering capability of the proposed system will allow the apparatus to be mounted in a low-pass suspension to the spacecraft structure. In this case, the spectrum of f' should be contained in narrow bands around $(\omega-\Omega)$ and $2(\omega-\Omega)$, a situation allowing $H(s)$ to be designed for strong rejection of the disturbances.

It is a simple matter to assure stability of the x' -loop of this system, but stability of the y -loop may be affected by the time-varying term in the equation, which can also cause spurious responses which might be mistaken for the Eotvos effect. To investigate this, we assume that the disturbing accelerations have been effectively reduced to an acceptable value, rewrite Eq. (87) as

$$\ddot{y} + [w^2 - \Lambda \cos 2(\omega-\Omega)t]y = \eta g \cos (\omega-\Omega)t \quad (93)$$

where w^2 has the Laplace transform

$$w^2(s) = B(s) - \omega^2 - \frac{1}{2} \Omega^2 \quad (94)$$

and Λ is used in the time-varying coefficient to allow for the possibility of computing a correction term in the servo from external measurements, if this should prove necessary.

For maximum resonance, the first choice of $w^2(s)$ is apparently a real quantity

$$w^2 = (\omega-\Omega)^2 \quad (95)$$

but such an ideal, infinite- Q case results in one of the unstable regions for solutions of the Mathieu equation⁽³¹⁾. Examination of the stability boundaries shows, however, that stability can be achieved by operating off the resonant frequency by a fractional amount

$$\frac{w - (\omega-\Omega)}{(\omega-\Omega)} > \frac{1}{4} \frac{\Lambda}{(\omega-\Omega)^2} \quad (96)$$

In order to maintain the desired response to the Eotvos driving force, the overall Q of the system must then be limited:

$$Q < 4(\omega-\Omega)^2/\Lambda \quad (97)$$

If stability is assured, and the time-varying term is sufficiently small, its effects may be calculated by a perturbation technique; choosing

$$w^2(s) = s^2 + 2\mu s \quad (98)$$

with $\mu = w/2Q$. Neglecting starting transients, Eq. (93) may be written to first order as

$$\begin{aligned} \ddot{y} + 2\mu\dot{y} + w^2y &= (\eta)g[\cos(\omega-\Omega)t + \Lambda b \cos 2(\omega-\Omega)t \cos((\omega-\Omega)t + \theta)] \\ &= (\eta)g[\cos(\omega-\Omega)t + \frac{\Lambda b}{2} \cos((\omega-\Omega)t - \theta) + \frac{\Lambda b}{2} \cos(3(\omega-\Omega)t + \theta)] \end{aligned}$$

where

$$b = [(w^2 - (\omega - \Omega)^2)^2 + (w(\omega - \Omega)/Q)^2]^{-1/2} \quad (100)$$

and

$$\tan \theta = -2\mu(\omega - \Omega) / (w^2 - (\omega - \Omega)^2). \quad (101)$$

In order that the Mathieu term may be regarded as a perturbation, it is necessary that

$$\frac{\Lambda b}{2} \ll 1 \quad (102)$$

or, for operation near resonance,

$$Q \ll 2(\omega - \Omega)^2 / \Lambda \quad (103)$$

a more stringent limitation than (97). If Λ has its natural value $\frac{3}{2}\Omega^2$, and ω is taken as 100 rpm (10.47 rad/sec), (103) implies that the Q must be small compared to 10^9 . On the other hand, a reasonable value of Q , within the limits of mechanical feasibility, is 10^5 ; this would allow starting transients to die away in a period of order 5 hours. The conclusion is thus that it is unnecessary to compute a compensation in the servo for the Mathieu term.

b. Method and procedures for carrying out the experiment

While these are roughly outlined above, they remain to be worked out in detail. However, the following considerations are applicable.

In the steady state, the amplitude will be given by

$$Y = \frac{\eta g Q}{(\omega - \Omega)^2} \quad (104)$$

Thus we see that with $\eta = 10^{-11}$, a Q of 10^5 and a spin of 100 rpm, the amplitude of the displacement of gold proof mass is of the order of 10^3 \AA or 10^{-5} cm . However, displacements of 10^{-11} cm have been detected in the laboratory by laser interferometry⁽³²⁾. This implies a limit for the accuracy of the comparison of gravitational to inert mass of one part in 10^{17} . While it is undoubtedly impossible to approach this displacement accuracy in an operational system, it appears that the displacement detector will not impose a design limitation.

The principal transverse force on the accelerometer (a force which must be opposed by the suspension system) is that due to Coriolis acceleration. If κ is the cross-coupling between the support and sensitive axes of the accelerometer, the disturbance due to the support will be less than the force the device is intended to measure if $Q < \frac{1}{\kappa}$. Current practice with electrostatic accelerometers gives a value for the cross-coupling of about 10^{-5} . This value could certainly be improved in an accelerometer designed specifically for the space environment, but cross-coupling could impose a limit on the maximum useable Q .

There are many other error sources which have not been considered here, such as nutation of the wheel, deviation of the spin axis from the direction of the orbital angular momentum, eccentricity of the orbit and deviation of the null point of the accelerometer from the spin axis of the wheel. The analysis which has been carried out to date, however, indicates that this device may nevertheless offer a technique for increasing the sensitivity of the Eotvos by three to five orders of magnitude.

c. Measurements to be made and ranges of numerical values expected

An orbital Eotvos force just at the outer limit of detectability of the most refined experiment to date (Dicke's) will yield a displacement of the gold mass relative to the aluminum proof mass of about 10^3 \AA amplitude with an angular velocity of the aluminum wheel of 10 rad/sec. This displacement may be measured by laser interferometry.

The result is expected to be a continuous real-time record of mass-displacements, with steady-state, after a short disturbance, attained after an orbital period ($\sim 5 \times 10^3$ sec), with a Q of 10^5 . Data-taking could be automatic and require only occasional monitoring.

d. Method for analysis and interpretation of data

This has yet to be worked out in detail. The aforementioned mass-displacement record would be analyzed for the presence of otherwise unaccounted-for sinusoidal displacement components having that period corresponding to the difference of the disc angular velocity relative to the orbit and relative to the earth.

e. Prime obstacles and uncertainties which can be anticipated

The system may of course turn out to be infeasible in the course of development. In any case, it seems unlikely that it will be possible to carry out adequate performance checks of the accelerometer in a terrestrial environment, so a test of this subsystem may be regarded as a preliminary experiment to be conducted in a manned space laboratory. In view of the expense and difficulty of providing a "pure gravity orbit" windshield for the system, if that should prove necessary, it may also be desirable to carry out a manned orbital test of the complete wheel assembly, before proceeding to the design of such ancillary apparatus, even if it is necessary to launch the actual, complete experiment on an unmanned vehicle. By that time, however, it may well be possible to have the experiment assembled and calibrated in a manned orbital facility, and then launched gently into the required orbit. A development program making optimum use of both the manned and unmanned capabilities of the national space program offers the only feasible approach to the design of mechanical systems of the sensitivity contemplated here.

In the steady state, the amplitude of the displacement due to the Eotvos force is calculable as follows. At room temperature, with a proof mass of 5 gm, equipartition of thermal energy produces an oscillation of amplitude 10^{-8} cm; the threshold of suitable displacement detectors (e.g., using laser homo-dyne techniques⁽³²⁾) is several orders of magnitude lower than this. This thermal limit corresponds to an anomalous gold/aluminum Eotvos ratio of 10^{-14} , a value which could

be improved by an order of magnitude or so by reducing the temperature of the apparatus and/or increasing the size of the proof masses. Further improvement is possible by decreasing the wheel angular velocity and increasing the Q.

These considerations lead to an expected threshold of about 10^{-15} in measurement of the anomalous Eotvos ratio with this apparatus, if the effective disturbing forces can be reduced to a sufficiently small value. Whether this is possible in a conventional spacecraft (i.e., without employing the pure gravity orbit technique) depends on (i) the spectrum of disturbances in the spacecraft and the rejection characteristics of the dual accelerometer servo; and (ii) design of the accelerometer proof mass suspension to minimize coupling of support forces into the sensitive axis.

f. The significance of the astronaut in performing the experiment

A technically-trained astronaut in a space station will be able to conduct development tests in free fall of parts of the apparatus at relatively low cost; the resultant confidence in the design may substantially simplify the engineering. The astronaut can also be used to set up, calibrate, and deploy the experiment in its operating environment, so that it is not necessary to design complex caging devices to enable it to withstand the stresses of launch. Finally, it will be possible to monitor the experiment at intervals to effect routine maintenance, to repair or replace defective parts, to gather data records, and perhaps to modify the equipment in the light of experience with the experiment. The reliability specifications may then be relaxed to a level comparable to that of high-quality terrestrial systems, a factor which can by itself reduce hardware costs by an estimated factor of 10.

5. Baseline or Control Data

The following list identifies by title support studies and concurrent investigations that must be conducted to augment the flight investigation. The requirements for these studies are discussed in the foregoing sections.

- (1) Study of the deliberate modulation of the "elastic constant" of the test masses to assure accurate location of the equilibrium position.
- (2) Study and computer simulation of a system to keep the disk's spin angular velocity vector in a fixed orientation with respect to the orbital angular velocity vector
- (3) Engineering study and computer simulation of data-handling systems.
- (4) Computer servo-design study, to determine optimum Q for test-mass motion.
- (5) Study, by computer, of the stability of the system, especially its response to expected disturbing accelerations with various mounting methods.
- (6) Computer simulation of the overall experiment, creating artificial data.
- (7) Computer simulation of data-processing methods.
- (8) Experimental and theoretical study of a suspension system for the test-masses (including superconductive suspensions).
- (9) Experimental study of a laser-interferometer for measuring test-mass position, including new methods of application.
- (10) Engineering design of a calibration scheme for positioning test-masses concentrically with the large disk.
- (11) Engineering design of power-transfer system from spacecraft to the spinning disk.
- (12) Analysis of resolution of disturbances and signals with frequencies near those of Eotvos force.

SECTION IV

Summary and Conclusions

In the period to 1 April 1971 we have continued to study several proposed space experiments involving the measurement of gravitational inertial forces. Specifically, these are null-experiments with respect to Einstein's General Theory of Relativity and, as such, require an unprecedented degree of precision. This precision may be attainable by the proper exploitation of the outer space environment, which is now available.

A. Measurement of Variations of the Gravitational Constant

We have examined, with varying comprehensiveness, four devices conceivably capable of measuring the possible variations (with gravitational potential) of the Newtonian gravitational constant. Some of these devices are capable of operation only in a "zero-g" laboratory as approximated by a spacecraft in orbit about the earth or the sun; and all of them require the benign aspects of space environment if they are to achieve the required resolution. The space environment is also required to provide a substantial variation in the gravitational potential, for the comparative measurements.

The four devices are: 1) the Gravitational Clock, where a set of non-rotating attracting masses provides a gravitational potential well for the oscillation of a test body rotor and the relevant measurement is the frequency of oscillation of the rotor; 2) the Beams Balance, where the attracting masses are rotated so that the test body rotor is subjected to a constant torque, and the relevant measurement is the angular acceleration of the rotor; 3) the Centrifugal Balance Sphere, where a homogeneous sphere provides gravitational attraction for three test objects which are constrained to the axis of internal tunnels, and the relevant measurement is the angular rate required of the sphere to keep the test bodies axially motionless and; 4) the Synchronous Orbit sphere, where a homogeneous sphere provides gravitational attraction for one test body which is unconstrained in an internal tunnel, and the relevant measurement is the angular rate required of the sphere to keep the test body from colliding with the sides of the tunnel.

The Gravitational Clock is a possible approach which can be operationally checked in earth orbit, but would require a solar orbit for a viable experiment. The primary difficulties are: 1) the harmonicity of the restoring force; 2) the requirement for cryogenic temperatures; 3) the development of a superconducting isotropic suspension with a $Q > 10^6$; and 4) the development of an adequate charge control technique.

The Beams Balance also is a possible approach which can be operationally checked in earth orbit, but would require a solar orbit for a viable experiment. Its suspension requirements are considerably relaxed from the Gravitational Clock, but would also require operations at cryogenic temperature, and a charge control technique. A preferred configuration would utilize two Balances back-to-back to eliminate the need for an inertial reference, and would utilize hemisphere masses rather than spheres. An experiment to achieve a resolution of 1 part in 10^{10} in detecting $\Delta G/G$ would take about 14 hours and require the reduction of 132,000 data points. Of the four devices studied, the Beams Balance has the best potential for detecting variations in the gravitational constant with a resolution of 1 part in 10^{10} , but still has many instrument design requirements that are unprecedented.

The Centrifugal Balance Sphere and the Synchronous Orbit Sphere appear to have identical serious flaws. In order to avoid extraction of the test masses, because of gravity gradients, the sphere must be made of a very dense material (viz. tungsten). In order to avoid extraction, because of spacecraft acceleration (drag, angular motion), and in order to avoid excessive miniaturization of ancillary equipment, the sphere must have a radius on the order of 10 to 20 cm. This provides for a minimum device weight in the range of 200 to 800 lbs. Additionally the equipment must be operated at liquid helium temperature; and the tolerances on the radial and axial position of each test mass in its tunnel is critical.

B. Measurement of the Eotvos Ratio

Although the major effort in this reporting period was devoted to the G-Constancy Experiment, the analytic derivation of the major factors of the Eotvos Experiment, as presented in Section III, provides a high degree of optimism for this proposed space experiment. This approach consists of measuring the differential force between two materials with differing proportions of weak interaction binding energy (viz. aluminum and gold), which have identical orbital conditions. This force is measured by observing the individual amplitudes of oscillation of the test bodies (near resonance) in a rotating structure.

The anticipated resolution of the measurement of the Eotvos ratio (1 part in 10^{14}) will provide a highly accurate check (1 part in 10^3) of any anomaly in the equivalence of inertial and passive gravitational mass. Further, it will significantly decrease the possible anomalous contribution which could be attributable to the other, larger, sources of atomic mass. This result will place a significant restriction on the viability of any gravitational theory. The proposed experiment is a unique exploitation of space operations in that the effect being observed is enhanced in earth orbit, and the external disturbances are reduced, compared to an earth based experiment.

References

1. J. Hovorka, M.I.T. Letter, MSL-127-69 to NASA, MSC, (15 September 1969).
2. R.V. Pound and J.L. Snider, Phys. Rev., 140, B788 (1965).
3. H. Von Klüber, Vistas in Astronomy, New York, Pergamon Press, 3, 47 (1960).
4. I.I. Shapiro, G.H. Pettengill, M.E. Ash, M.L. Stone, W.B. Smith, R.P. Ingalls, and R.A. Brockelman, Phys. Rev. Letters, 20, 1265 (1968).
5. R.H. Dicke, AP 3., 159, 1 (1970).
6. P.G. Roll, R. Krotkov, and R.H. Dicke, Ann. of Phys., 26, 442 (1964).
7. C. Brans and R.H. Dicke, Phys. Rev., 124, 925 (1961).
8. R.H. Dicke, The Theoretical Significance of Experimental Relativity, Gridon & Breach, N.Y., (1964).
9. R. Weiss, "Quarterly Progress Report", Research Laboratory of Electronics, M.I.T., 77, 59 (1965).
10. P.R. Heyl, Bur. Stds. J. Res., 5, 1243 (1930).
11. D.H. Douglas, Jr., "Two Gravity Experiments", a paper presented at the Third Cambridge Conference on Relativity, Goddard Institute for Space Studies, 8 June 1970.
12. J.W. Beams, R.D. Rose, H.M. Porter, R.A. Lowry and A.R. Kuhethan, Phys. Rev. Letters, 23, 655 (1969).
13. D. Berman, R.L. Forward, "Free-Fall Experiments to Determine the Newtonian Gravitational Constant", Vol. 24, Science and Technology Series, American Astronautical Soc., (1968)
14. M.G. Blicht, "The Feasibility of a Gravitational Clock to Test the General Theory of Relativity", S.M. Physics Thesis, M.I.T. (1969).
15. J.M.A. Danby, Fundamentals of Celestial Mechanics, MacMillan, N.Y. p. 103, (1964).
16. R.L. Forward, private communication
17. R.H. Battin, Astronautical Guidance, McGraw-Hill, N.Y., p. 16, (1964).
18. L.I. Schiff, Proc. Nat. Acad. Sci., 45, 69 (1959).
19. See for example: A. Einstein, in H.A. Lorentz, A. Einstein, H. Minkowski, and H. Weyl, The Theory of Relativity, p. 109, Dover Publications Inc., reprinted from the original edition (1923).

20. R.L. Mossbauer, Z. Physik, 151, 124 (1958).
21. R.V. Pound and G.A. Reblea, Jour. Phys. Rev., Letters, 4, 337 (1960).
22. I.I. Shapiro, Phys. Rev. Letters, 26, 789 (1964).
23. J. Weber, Phys. Rev. Letters, 22, 1320 (1964).
24. C.W.F. Everitt and W.M. Fairbank, Proc. Tenth International Conf. of Low Temperature Physics, Moscow, Aug. 1966.
25. L.I. Schiff, Proc. Nat. Acad. Sci., 46, 871 (1960).
26. D. Kleppner, R.F.C. Vessot, and N.F. Ramsey, Astrophysics and Space Science, 6, 13 (1970).
27. W. Thirring, Annals of Physics, 16, 96 (1961). See also R.P. Feynman, "Lectures on Gravitation", Cal. Inst. of Tech. (1962-63) and P.K. Chapman, M.I.T. Experimental Astronomy Laboratory Report TE-16, (1966).
28. R.V. Eotvos, Math. u. Naturw. Ber. ans Ungarn, 8, 65 (1890);
R.V. Eotvos, D. Pekar, And E. Feteke, Ann. Physic, 68, 11 (1922).
29. P.G. Roll, R. Krotkov, and R.H. Dicke, Annals of Physics, 26, 442 (1964).
30. A.J. Hanson, M.I.T. Measurement Systems Laboratory Research Note RN-58, preliminary (1970).
31. P.M. Morris and H. Feshback, Methods of Theoretical Physics, McGraw-Hill, N.Y., p. 556 (1953).
32. G. Gerziger and H. Lindner, Phys. Letters, 12, 658 (1967).
33. R.J. Blin-Stoyle, Phys. Rev., 118, 1605 (1960).

APPENDIX A

AN ELEMENTARY ANALYSIS OF THE ADAPTATION
OF THE BEAMS' EXPERIMENTAL CONCEPT TO
 $\Delta G/G$ DETECTOR TO BE USED IN SPACE

RN-60

AN ELEMENTARY ANALYSIS OF THE ADAPTATION
OF THE BEAMS' EXPERIMENTAL CONCEPT TO
A $\Delta G/G$ DETECTOR TO BE USED IN SPACE

B. E. Blood

June 1970

Massachusetts Institute of Technology
Measurement Systems Laboratory
Cambridge, Massachusetts 02139

ABSTRACT

This research note presents an elementary analysis for an experimental apparatus. In order to detect changes in the gravitational attraction between two or more test bodies, the experiment uses inertial angular acceleration as a balance torque (in a D'Alembertian sense). The Dicke-Brans theory General Relativity predicts a different value for the Newtonian Gravitational Constant, G , in regions of different gravitational potential. This difference is very small for gravity fields of objects in the solar system. For an initially remote observor approaching the earth, the maximum difference is

$$\frac{\Delta G}{G} \sim - 7 \times 10^{-11}$$

This note contains a discussion of the problems associated with adapting an experimental concept of J.W. Beams to an apparatus that can be used in a spacecraft. The experiment will detect $\Delta G/G$ as the craft orbits to regions of different gravitational potential. The chief results of the analysis are

1. Establishment of an idea of the size (and mass) of the experiment
2. Isolation of problems to be considered in subsequent analyses.

ACKNOWLEDGEMENT

This work was performed under National Aeronautics and Space Administration contract NAS 9-8328 (MIT DSR 71390).

NOTE

This research note is one of a series of reports published by the MIT Measurement Systems Laboratory. The "RN" designation indicates a semi-formal presentation of research results. These presentations represent work in progress so the results are not necessarily complete or fully refined.

TABLE OF CONTENTS

I.	Detection of $\Delta G/G$	5
II.	Beams' Experimental Concept.....	8
III.	Adaptation of the Beams' Concept to a Space Experiment.....	10
IV.	Preliminary Design Considerations.....	11
V.	Geometric Design Considerations.....	15
VI.	Size of the Experiment.....	22
VII.	Further Analyses.....	34
VIII.	References.....	38

I. Detection of $\Delta G/G$

The Dicke-Brans scalar-interaction theory in General Relativity predicts a different value for the Newtonian Gravitational Constant, G , in regions of different gravitational potential. This effect is very small for gravity fields of objects in the solar system. For an initially remote observer approaching the earth, the maximum difference is

$$\frac{\Delta G}{G} \sim -7 \times 10^{-11}.$$

To make a measurement of $\Delta G/G$, we require instrumentation of unprecedented sensitivity. The Measurement Systems Laboratory (MSL) has been working on the design of an apparatus that can be used in a spacecraft to detect $\Delta G/G$ as the craft orbits to regions of different gravitational potential.

In general the experimental apparatus, as presently conceived (at MSL and elsewhere), will involve a set of precisely known test-masses disposed in a precisely known geometry. In one version, gravitational forces between the test masses are exactly balanced by some other calibrated forces† (presumably not subject to change with gravitational potential). These calibrated forces can be adjusted to account for Dicke-Brans changes in the gravitational forces. The balance is detected by observing the relative displacements of the masses. In a second version, the masses are arranged to permit relative periodic motion, either libration or rotation.^{(1), (2)*} With

*Superscript numbers refer to the list of references

†We include here and throughout this note the notion of inertial reaction as a force in the D'Alembertian sense.

gravitational attraction as the restoring force (alone or in combination with some other calibrated force⁽³⁾), the period of the motion is related to G.

This note is concerned with a few aspects of the force-balance version. It seems reasonable to assume that the most precise force balance is that in which we counteract gravitational attraction with an inertial force.* Since inertial forces can be determined by the direct measurements of mass, length, and time, we then have the possibility of making an absolute determination (in terms of present mass, length, and time standards) of G (at a given point) in the process of detecting $\Delta G/G$.

Each of the three inertial forces that arise in rotational motion has been suggested for a balance force. Centrifugal force as a balance is the design basis for a device consisting (in part) of a massive sphere of uniform density, ρ , and a small test mass, m , free to move without friction in a radial tunnel.⁽⁴⁾ The sphere is given an inertial angular velocity, ϕ , such that

$$m \phi^2 r = \frac{4}{3} \pi \rho G r m$$

and then we can get

$$G \propto \phi^2 \frac{1}{\rho} .$$

Coriolis force (in the form of a gyroscopic torque) also has been considered, as in the use of a Pendulous Integrating Gyro Accelerometer (PIGA)[†] mounted on a massive sphere⁽⁵⁾.

* The use of inertial forces is in contradistinction to establishing the force balance with electromagnetic, elastic, or other physical forces.

† An accelerometer used in inertial guidance and navigation systems.

Here the balance equation is

$$H \dot{\psi} = K G$$

in which

H = a constant gyro angular momentum

$\dot{\psi}$ = an inertial angular velocity, applied transverse to H , to provide the torque balance

K = a constant determined by the mass of the sphere, the pendulosity and geometric factors.

The third inertial force (torque) reaction to angular acceleration, has been used by J.W. Beams and others (all at the University of Virginia) in an experiment to measure the absolute value of G .⁽⁶⁾ The force balance equation is

$$I \ddot{\phi} = - \frac{\partial (P.E.)}{\partial \theta}$$

in which

I = moment of inertia of a pivoted test body

θ = relative angle between the test body and a set of known attracting masses

P.E. = potential energy (proportional to G) of the test body in the field of the attracting masses

$\ddot{\phi}$ = an inertial angular acceleration imparted to the whole apparatus to effect a torque balance.

In this note we are specifically concerned with some preliminary thoughts on adapting the Beams' method to a space experiment for the detection of $\Delta G/G$.

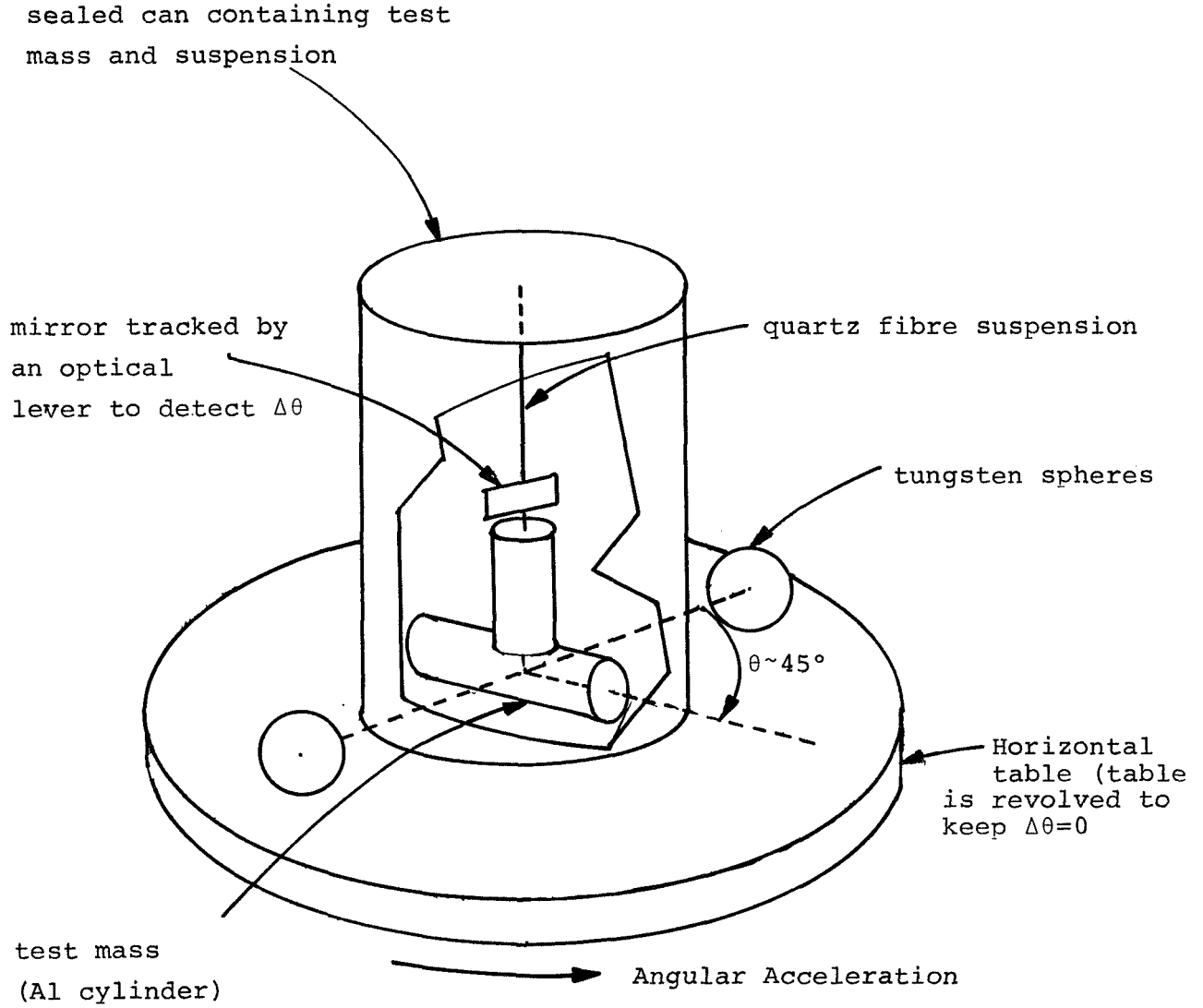
II. Beams' Experimental Concept

Newton's Gravitational Constant, G , is measured in the Beams' experiment by balancing a gravitational torque acting on a pivoted test body with an inertial angular acceleration. As shown in Fig. I, the test body is torqued by the gravitational attraction of two spheres, while an equal and opposite torque is provided by accelerating the table that holds the apparatus so that the relative displacement, θ , remains constant.*

The theoretical gravitational torque can be calculated to great precision (except for the constant factor G) since spheres of uniform density are used and the dimensions of the experiment are determined accurately. The dimensions are held to their measured values by running the experiment in a temperature controlled environment. The angular acceleration of the table is proportional to G , so the data taken are the time increments for successive rotations. These time increments are then used to calculate the acceleration.

The test body is, of course, subject to gravitational torques due to other objects than the spheres. However, by the conservative nature of gravitational fields, external (to the table) stationary masses have effects that are averaged to zero for complete (relative to the laboratory) revolutions of the table. The data taken are then the time increments for complete revolutions. Torques arising from masses (other than the spheres) on the table, as well as the effects of the fibre suspension are

* The situation is analogous to the case of linear motion when we have a test mass, m "freely falling" in the field of another body, M . The relative separation between m and M is maintained constant by accelerating M so that, in effect, m is "chasing" M .



Note: Not to scale. Spheres would be 3".

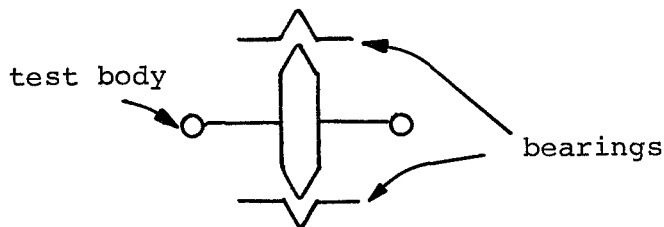
FIG. I. BEAMS' EXPERIMENT

calibrated out by running the experiment with and without the spheres on the table.

The Beams' experiment has been built and operated at the University of Virginia. Experimental results have confirmed the presently accepted value of G (known to one part in 500).⁽⁶⁾ Further results show that the apparatus gives consistent measurements to one part in 34,000 or about 3 parts in 10^{-5} .*

III. Adaptation of the Beams' Concept to a Space Experiment

For operation in a spacecraft, the most obvious change in the Beams' device is the suspension of the test body. In view of the single-degree-of-freedom nature of the experiment, we require a suspension that permits the test body to rotate in a set of bearings something like a watch balance wheel.



Since θ is to be held constant during the experiment, the bearing need only be "frictionless" over a small range around the operating value, θ_p .†

*Verbal communication with J.W. Beams.

†Suspensions that can be considered are

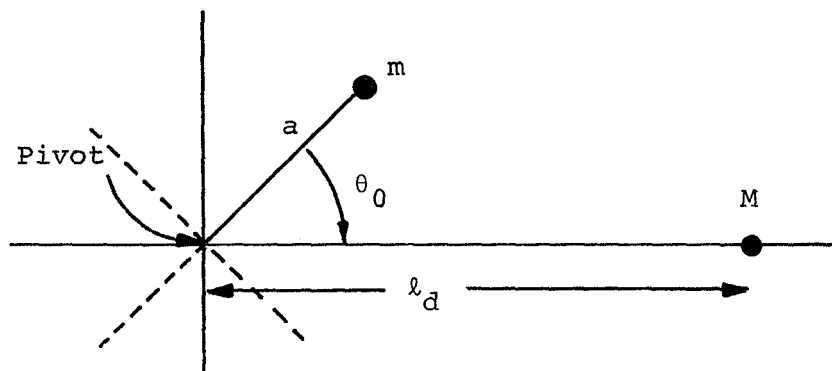
1. Double torsion fibre
2. Magnetic - Servo controlled electromagnets⁽⁷⁾
3. Magnetic - Diamagnetic substance at room temperature⁽⁸⁾
4. Magnetic - Meissner effect at cryogenic temperatures⁽⁹⁾ (1)
5. Electrostatic.

Of these, 3 and 4 seem the most promising, at least for an initial analysis.

Before the selection and design of a suspension system, we need to answer some questions about the size, mass, and geometry of the experiment. Most of the remainder of this note is concerned with these preliminary design questions.

IV. Preliminary Design Considerations

One of the compelling features of the Beams' concept is that external stationary masses have effects, which average to zero for complete revolutions of the experiment. In a spacecraft, however, we will have the motion of astronauts and the changing mass of the craft as fuel is expended, as well as a changing position in the gravity gradient field of the orbited body. To minimize the effects of these moving objects, we can consider making the test body of a number of symmetrically arranged arms. To show this, we make some calculations based on the idealized representation of the arms by massless rods of length, a , with point masses, m , at the ends. In the sketch we show a disturbing mass, M , (taken



as a point or spherical mass for simplicity) at a distance l_d from the pivot. The potential energy of m in the field of M is

$$P.E. = \frac{m M G}{\sqrt{a^2 + \ell_d^2 - 2a\ell_d \cos \theta_0}} \quad (1)$$

For the case of n symmetrical arms, we have

$$P.E. = \sum_{i=1}^n mMG \frac{1}{\ell_d} (1+h^2-2h \cos \theta_i)^{-1/2} \quad (2)$$

in which

$$h \equiv \frac{a}{\ell_d}$$

and

$$\theta_i \equiv \theta_0 + \frac{i}{n} (360) \text{ degrees.}$$

We can expand the radical in (2) in terms of Legendre polynomials

$$(1+h^2-2h \cos \theta_i)^{-1/2} = \sum_{k=0}^{\infty} (h)^k P_k(\cos \theta_i).$$

Equation (2) becomes

$$P.E. = \frac{mMG}{\ell_d} \sum_{i=1}^n \sum_{k=0}^{\infty} (h)^k P_k(\cos \theta_i). \quad (3)$$

The first few polynomials are

$$P_0(\cos \theta_i) = 1$$

$$P_1(\cos \theta_i) = \cos \theta_i$$

$$P_2(\cos \theta_i) = \frac{1}{2} (\cos^2 \theta_i - 1)$$

$$P_3(\cos \theta_i) = \frac{1}{2} (5 \cos^3 \theta_i - 3 \cos \theta_i)$$

$$P_4(\cos\theta_i) = \frac{1}{8} (35 \cos^4\theta_i - 30 \cos^2\theta_i + 3) .$$

Presuming that the disturbing mass is at some greater distance than the arm length or $h < 1$, we write (3) out to the precision of h^4 .

$$\begin{aligned} \text{P.E.} = \frac{mMG}{\ell_d} & \left[\sum_{i=1}^n P_0(\cos\theta_i) + h \sum_{i=1}^n P_1(\cos\theta_i) + h^2 \sum_{i=1}^n P_2(\cos\theta_i) \right. \\ & \left. + h^3 \sum_{i=1}^n P_3(\cos\theta_i) + h^4 \sum_{i=1}^n P_4(\cos\theta_i) \right] . \end{aligned}$$

Substituting the expressions for the P_k 's and rearranging the terms gives us

$$\begin{aligned} \text{P.E.} = \frac{mMG}{\ell_d} & \left[n \left(1 - \frac{h^2}{2} + \frac{3h^4}{8} \right) + \sum_{i=1}^n \cos\theta_i \left(h - \frac{3}{2} h^3 \right) \right. \\ & \left. + \sum_{i=1}^n \cos^2\theta_i \left(\frac{3}{2} h^2 - \frac{30}{8} h^4 \right) \right. \\ & \left. + \sum_{i=1}^n \cos^3\theta_i \left(\frac{5}{2} h^3 \right) + \sum_{i=1}^n \cos^4\theta_i \left(\frac{35}{8} h^4 \right) \right] . \end{aligned}$$

For $n=3$, the summations give us*

*We ignore $n=1$ and $n=2$, since in the first case M gives a direct torque and in the second case the gradient of M 's field will torque the arms.

$$\begin{aligned} \text{P.E.} = \frac{mMG}{\ell_d} & \left[3 \left(1 - \frac{h^2}{2} + \frac{3h^4}{8} \right) + \frac{3}{2} \left(\frac{3}{2} h^2 - \frac{30}{8} h^4 \right) \right. \\ & \left. + \frac{3}{4} \cos 3\theta_0 \left(\frac{5}{2} h^3 \right) + \frac{9}{8} \left(\frac{35}{8} h^4 \right) \right] \end{aligned}$$

and for $n = 4$,

$$\begin{aligned} \text{P.E.} = \frac{mMG}{\ell_d} & \left[4 \left(1 - \frac{h^2}{2} + 3 \frac{h^4}{8} \right) + 2 \left(\frac{3}{2} h^2 - \frac{30}{8} h^4 \right) \right. \\ & \left. + \left(\frac{12}{8} + \frac{1}{2} \cos 4\theta_0 \right) \left(\frac{35}{8} h^4 \right) \right]. \end{aligned}$$

To determine the torque exerted by M's field, we have

$$T \equiv \text{Torque} \equiv \frac{\partial \text{P.E.}}{\partial \theta_0} .$$

For $n=3$,

$$T_{n=3} = \frac{-mMG}{\ell_d} \frac{45}{8} h^3 \sin 3\theta_0 \quad (4)$$

and for $n=4$,

$$T_{n=4} = \frac{-mMG}{\ell_d} \frac{35}{4} h^4 \sin 4\theta_0 . \quad (5)$$

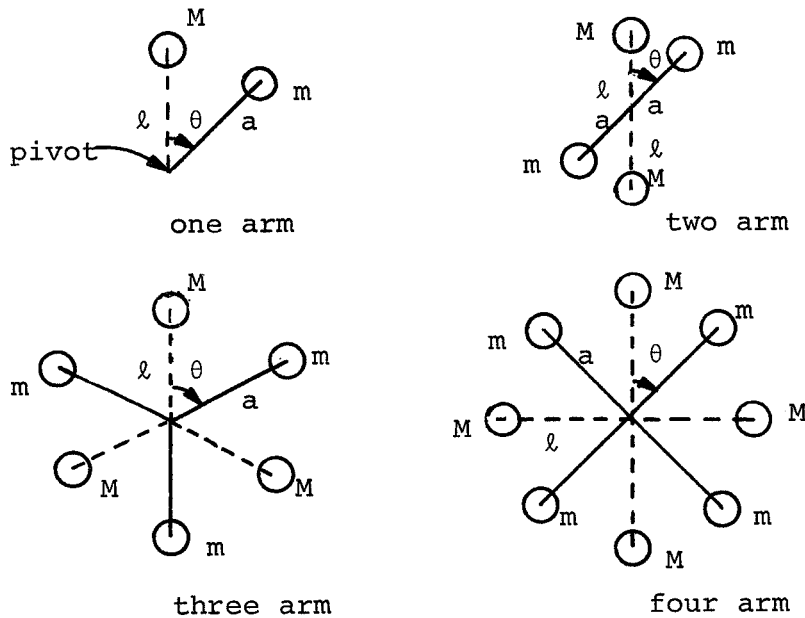
With the disturbing mass, M , at a distance, ℓ_d , we see that the peak torque on the 4-arm device is about $3/2 h$ of that on the 3-arm device. We conclude that the 4-arm device has a distinct advantage (if $h < 2/3$) especially in the changing mass environment

of a manned spacecraft.

V. Geometric Design Considerations

Increasing the number of arms reduces the sensitivity to external fields -- yet we can not increase the number of arms indefinitely because we must still apply a torque by placing our calibrated masses in some sort of known juxtaposition to the moving arms.*

For our simple analysis, a pivoted device consisting of n symmetrically disposed massless rods tipped with point (spherical) masses, m , are attracted by n symmetrically disposed fixed spheres, M . The sketch shows the configurations to be analyzed. We can determine the torque expression for these configurations by differentiating (2) with respect to θ and multiplying by n



*In the absurd extreme we could increase the number of arms until we had a wheel. Then no torques could be applied, disturbance or otherwise. We obviously have a design "trade-off" between sensitivity to external masses and the efficient use of the calibrated masses.

(for the n M's). Equation (2) (with $\ell_d \rightarrow \ell$) gives

$$T = n \frac{mMG}{\ell} \sum_{i=1}^n \frac{h \sin \left(\theta + \frac{i}{n} 360 \right)}{\left[1+h^2 - 2h \cos \left(\theta + \frac{i}{n} 360 \right) \right]^{3/2}} \quad (6)$$

in which

$$h = \frac{a}{\ell}, \text{ a design parameter}$$

a = length of the pivoted arm

ℓ = distance from the pivot to the calibrated attracting mass.

For given values of our design parameter, h , we can calculate an operating angle, θ_p , for maximum torque. Setting

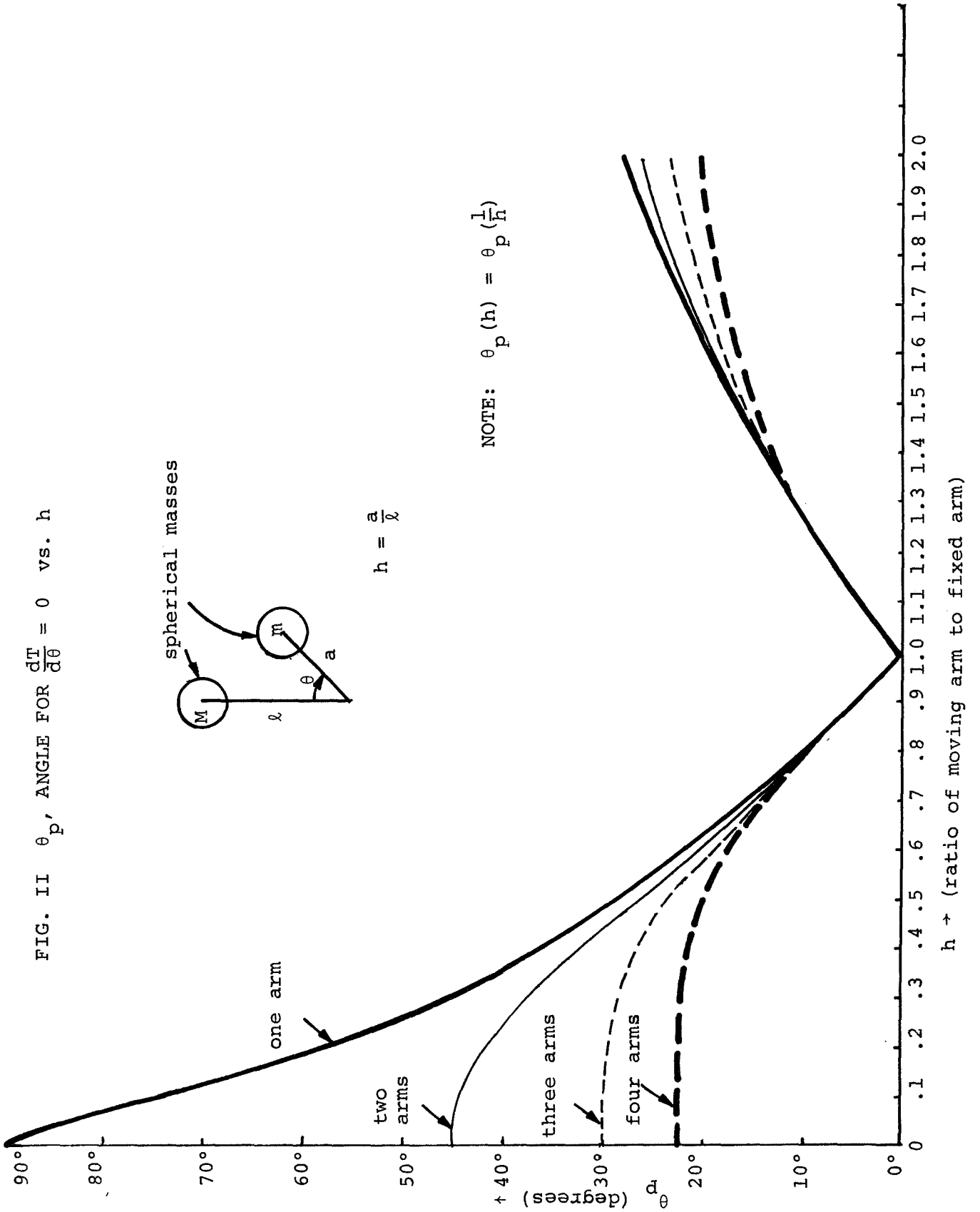
$$\frac{dT}{d\theta} = 0$$

we obtain for $n=1$

$$\cos \theta_p = \frac{1}{2} \left[-\frac{1+h^2}{h} + \sqrt{\left(\frac{1+h^2}{h} \right)^2 + 12} \right]. \quad (7)$$

For other values of n , we must calculate $\cos \theta_p$ by numerical methods. Fig. II shows the results of these calculations. Fig. III gives the same information in a more instructive manner. If M , the attracting mass, lies as shown, then the moving mass, m , must lie on the curve as shown if $dt/d\theta = 0$.

FIG. II θ_p , ANGLE FOR $\frac{dT}{d\theta} = 0$ vs. h



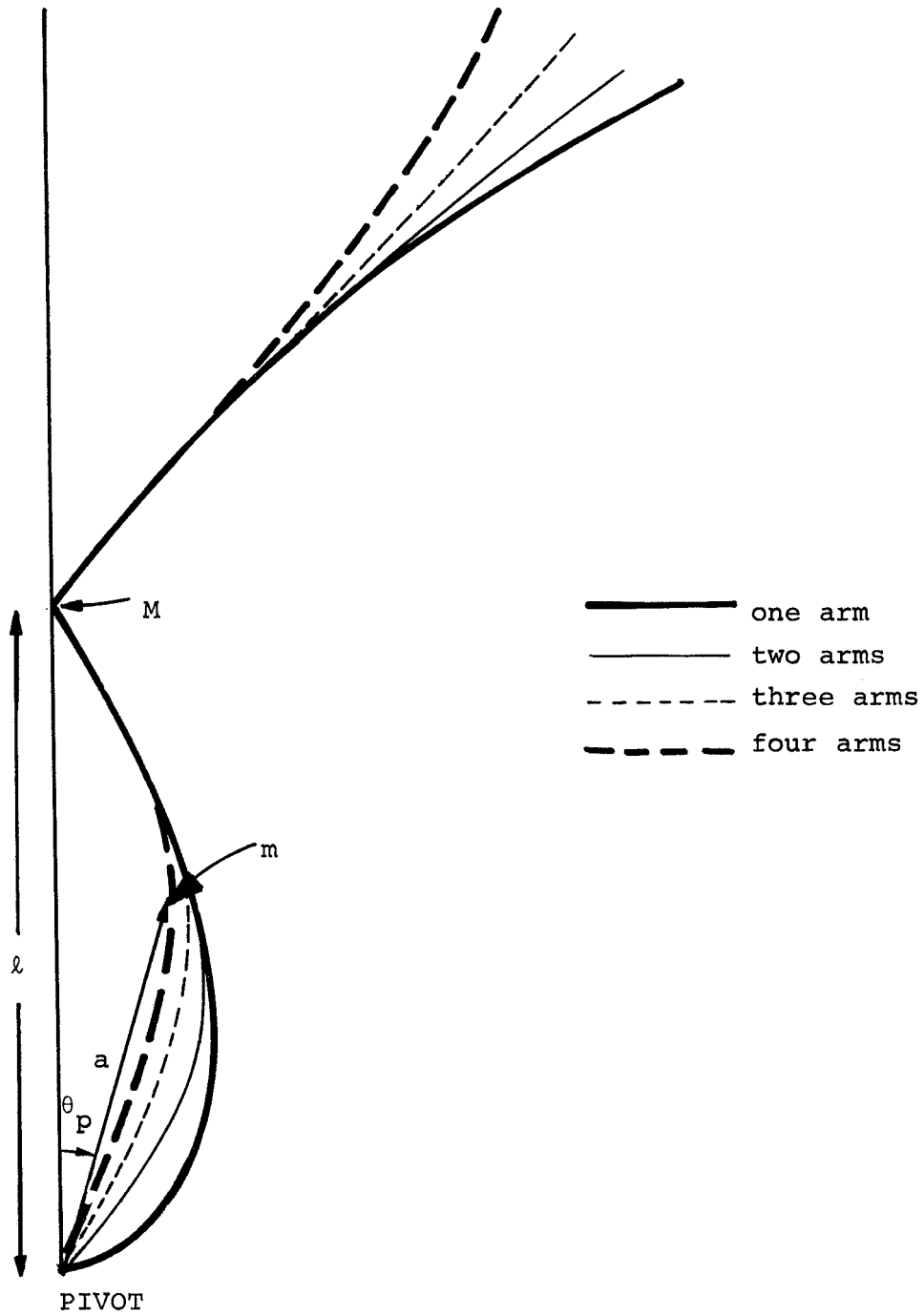


FIG. III. CURVES ON WHICH m MUST LIE FOR $\frac{dT}{d\theta} = 0$

In addition to the desirability of placing m so that the torque is a maximum (for a given h), it is also important to operate at an angle θ_p , the angle at which the magnitude of the torque is relatively insensitive to changes in θ . In general, $\Delta\theta$ will be the error signal to the servo that accelerates the experiment.* Operating at θ_p , we can make an estimate of the change in torque, ΔT , with $\Delta\theta$, by expanding the torque expression in a Taylor series around $\theta = \theta_p$ to get

$$T(\theta_p + \Delta\theta) = T(\theta_p) + T''(\theta_p) \frac{\Delta\theta^2}{2} + \dots$$

in which we have used

$$T'(\theta_p) \equiv 0.$$

Now we have

$$\frac{\Delta T}{T} = \frac{T(\theta_p + \Delta\theta) - T(\theta_p)}{T(\theta_p)} = \frac{T''(\theta_p) \frac{\Delta\theta^2}{2}}{T(\theta_p)}.$$

Differentiating (6) twice and using $T'(\theta_p) \equiv 0$, we get

*It can be argued that $\Delta\theta$ could be monitored and then applied with a correction factor in the data reduction. This is true for operation at any θ ; however, the sensitivity of our result to errors in $\Delta\theta$ and the correction factor will be reduced if θ_p is used.

$$\frac{\Delta T}{T} = \frac{T''(\theta_p) \frac{\Delta\theta^2}{2}}{T(\theta_p)} = \frac{\sum_{i=1}^n \frac{-\sin(\theta_p + \frac{i}{n} 360) [2h \cos(\theta_p + \frac{i}{n} 360) + (1+h^2)]}{[1+h^2 - 2h \cos(\theta_p + \frac{i}{n} 360)]^{5/2}}}{\sum_{i=1}^n \frac{\sin(\theta_p + \frac{i}{n} 360)}{[1+h^2 - 2h \cos(\theta_p + \frac{i}{n} 360)]^{3/2}}} \frac{\Delta\theta^2}{2}$$

Using the values of θ_p shown in Fig. II, we can evaluate this equation for the different values of n . The results are shown in Fig. IV. A value for $\Delta\theta$ of one arc second was used. This value was selected as a reasonable tracking error for instrument servomechanisms. From the curves in Fig. IV, we see that for high precision ($\Delta T/T < 1.5 \cdot 10^{-10}$)

$$h > 1.7 \text{ or } h < 0.5$$

at least for the simple model used in these calculations.

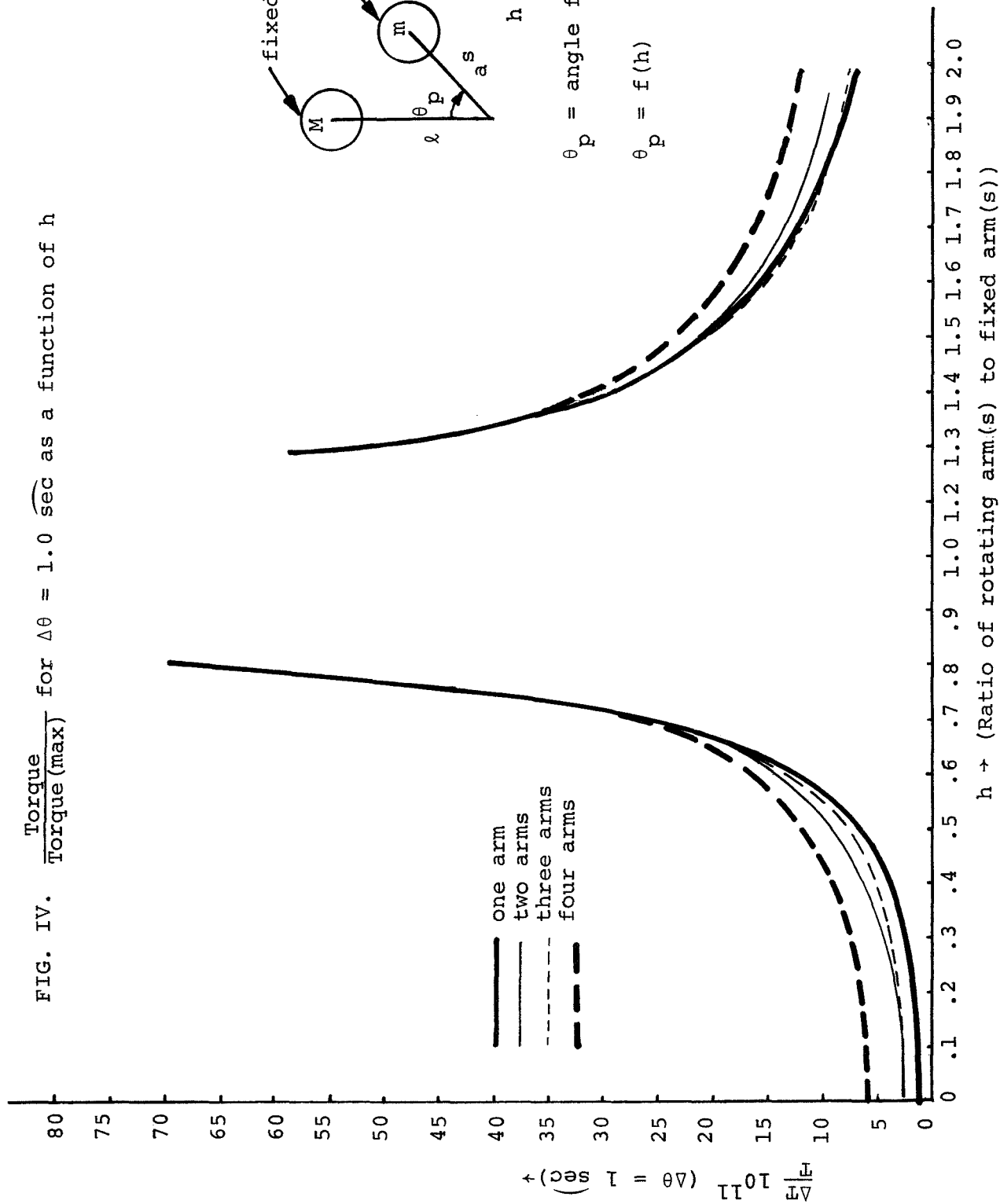
The significance of operating at θ_p can be illustrated by an example. Using the simple model, we will assume a two-arm device with $h = 0.15$ and an operating angle, $\theta = 45^\circ$.* (From Fig. II, we note that for $h = 0.15$, $\theta_p = 43.2^\circ$.) Using (6), we get for $n=2$

$$[(h \cos^2\theta + (1+h^2)\cos\theta - 3h)]$$

$$\frac{dT/d\theta}{T} = \frac{(1+h^2+2h \cos\theta)^{-5/2} (h \cos^2\theta - (1+h^2)\cos\theta - 3h) + [(1+h^2-2h \cos\theta)^{-5/2}]}{\sin\theta [(1+h^2-2h \cos\theta)^{-3/2} - (1+h^2+2h \cos\theta)^{-3/2}]}$$

* These are very nearly the conditions for the Beams' experiment, if we approximate the moving cylinder (see Fig. I) by a dumbbell of equal mass and moment of inertia.

FIG. IV. $\frac{\text{Torque}}{\text{Torque (max)}}$ for $\Delta\theta = 1.0 \text{ sec}$ as a function of h



Evaluating this expression for $h = 0.15$ and $\theta = 45^\circ$, we get

$$\frac{dT/d\theta}{T} = 0.13.$$

For a servo error angle, $\Delta\theta = 20$ seconds of arc we have

$$\frac{\Delta T}{T} = \frac{dT/d\theta}{T} \Delta\theta \approx (0.13)10^{-4} = 1.3 \cdot 10^{-5}.$$

In this simple example, servo error angles of 20 seconds of arc cause variations in our assumed value of T to a part in 10^{-5} . * For contrast we see from Fig. IV that operation at $\theta = \theta_p = 43.2^\circ$ would give

$$\begin{aligned} \frac{\Delta T}{T} (\Delta\theta = 20 \text{ sec. of arc}) &\rightarrow 3 \cdot 10^{-11} (400) \\ &\rightarrow 1.2 \cdot 10^{-8}, \end{aligned}$$

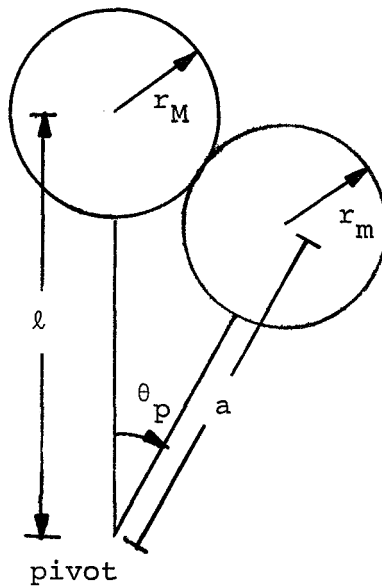
an improvement approaching 3 orders of magnitude.

VI. Size of the Experiment

To get an idea of the magnitudes of the torques and accelerations as a function of the size of the experiment, we proceed by assuming

*Reference 6 on the Beams' experiment reports tracking errors as large as 20 seconds of arc for short periods of time; however, in general they assumed the tracking error to be less than 0.2 seconds of arc. For the latter error angle, operation at $\theta = 45^\circ$ would not contribute an appreciable error to their present results. However, for a refined version of the Beams' experiment, it would seem prudent to operate at $\theta = \theta_p$ as calculated for the particular mass configuration used.

spherical masses of maximum size for a given θ_p .* Further, to maximize the torque, we will apportion the total mass of the experiment equally between the fixed and moving arms. From the sketch we see the maximum diameter spheres that we can fit in for a given θ_p .



$$r_M = r_m$$

$$h = \frac{a}{2}$$

$$\theta_p \equiv F(h)$$

$$m = M = \frac{4}{3} \pi \rho r_m^3$$

ρ = density of the spheres

The maximum radii are

$$r_m = r_M = \frac{\ell}{2} \sqrt{1+h^2-2h \cos\theta_p} \quad . \quad (8)$$

Equation (6) now becomes

$$T = n \left[\frac{\pi \rho}{6} \right]^2 G (1+h^2-2h \cos\theta_p)^3 \ell^6 \frac{h}{\ell} \sum_{i=1}^n \frac{\sin(\theta + \frac{i}{n} 360)}{[1+h^2-2h \cos(\theta + \frac{i}{n} 360)]^{3/2}} \quad . \quad (9)$$

* We will assume that the experiment will operate at $\theta = \theta_p$ in this analysis.

Taking

$$\rho = 21.45 \text{ grams/cm}^3 \quad (\text{platinum})$$

and

$$G = 6.675 \cdot 10^{-8}$$

we get

$$T = n \cdot 8.07 \cdot 10^{-6} \ell^5 h (1+h^2 - 2h \cos \theta_p)^3 \sum_{i=1}^n \frac{\sin(\theta + \frac{i}{n} 360)}{[1+h^2 - 2h \cos(\theta + \frac{i}{n} 360)]^{3/2}} \quad (10)$$

We see from the above sketch that the attractive force between the spheres creates a torque about the pivot that is the same in magnitude whether M is the fixed mass and m moves or m is fixed and M moves. For convenience, we introduce

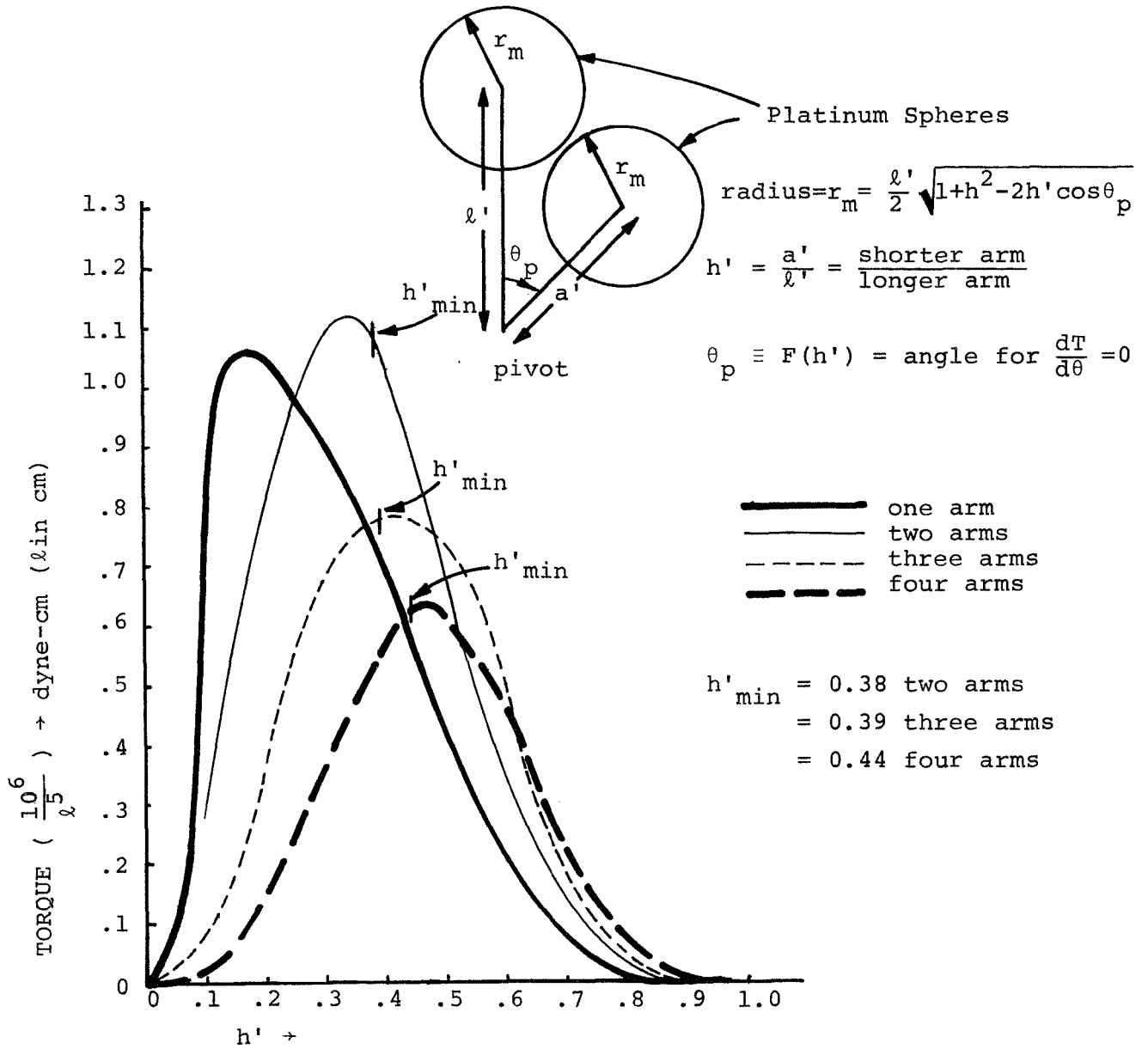
$$h' = \frac{\text{length of shorter arm}}{\text{length of longer arm}}$$

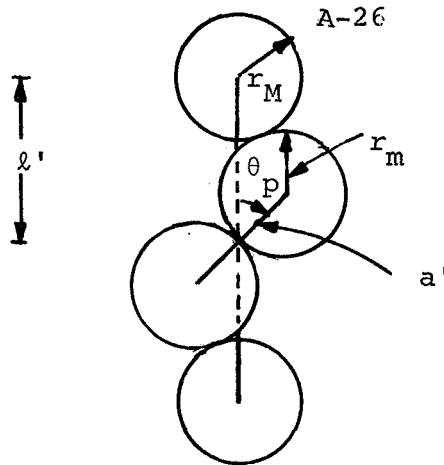
$$\ell' = \text{length of longer arm.}$$

Equation (9) remains the same with $h \rightarrow h'$ and $\ell \rightarrow \ell'$. Torque normalized to $(\ell')^5$ is given as a function of h' in Fig. V. Before discussing the curves, we note that there are minimum values for h' established by mechanical interference, as illustrated in the following sketch.*

* This interference arises because our model calls for spheres that have diameters which are functions of h' and $\theta_p = F(h')$.

FIG. V. MAXIMUM GRAVITATIONAL TORQUE NORMALIZED TO $(\ell')^5$





Mechanical interference occurs when the two inner spheres become tangent. At this point

$$r_m = a'$$

and using (8)

$$r_m = \frac{l'}{2} \sqrt{1+h'^2 - 2h' \cos \theta_p} = a'.$$

Then

$$\frac{a'}{l'} = h' = \frac{1}{2} \sqrt{1+h'^2 - 2h' \cos \theta_p}.$$

Using (7) for $\cos \theta_p$ and solving for h' , we get

$$h'_{\min} = 0.38 \text{ for two arms}$$

Similar arguments give

$$h'_{\min} = 0.39 \text{ for three arms}$$

and

$$h'_{\min} = 0.44 \text{ for four arms.}$$

From Fig. V, we note that for any ℓ' , maximum torque occurs at a particular h' . For the 4-arm device, optimum torque occurs at $h' \sim 0.46$ and with $\ell' = 16$ cm, for example, the torque is 0.64 dyne-cm.

This optimization is important for keeping the experiment size small and yet getting the maximum torque for mass (spheres in this model) used. Continuing on this line of thought, we can divide (9) by $n a^2 m$ to get

$$\frac{T}{n a^2 m} = \left[\pi \frac{\rho}{6} \right] G \frac{1}{h} (1+h^2-2h \cos \theta_p)^{3/2} \sum_{i=1}^n \frac{\sin(\theta_p + \frac{i}{n} 360)}{[1+h^2-2h \cos(\theta_p + \frac{i}{n} 360)]^{3/2}} \quad (11)$$

This expression is plotted in Fig. VI. Using (3) we can calculate the maximum disturbance torque caused by a 150 lb. astronaut (taken as a spherical object) at 2 meters from a 4-arm device. This disturbance torque is

$$T_d = m a^4 (.124 \cdot 10^{-12}) \text{ dyne-cm}$$

or

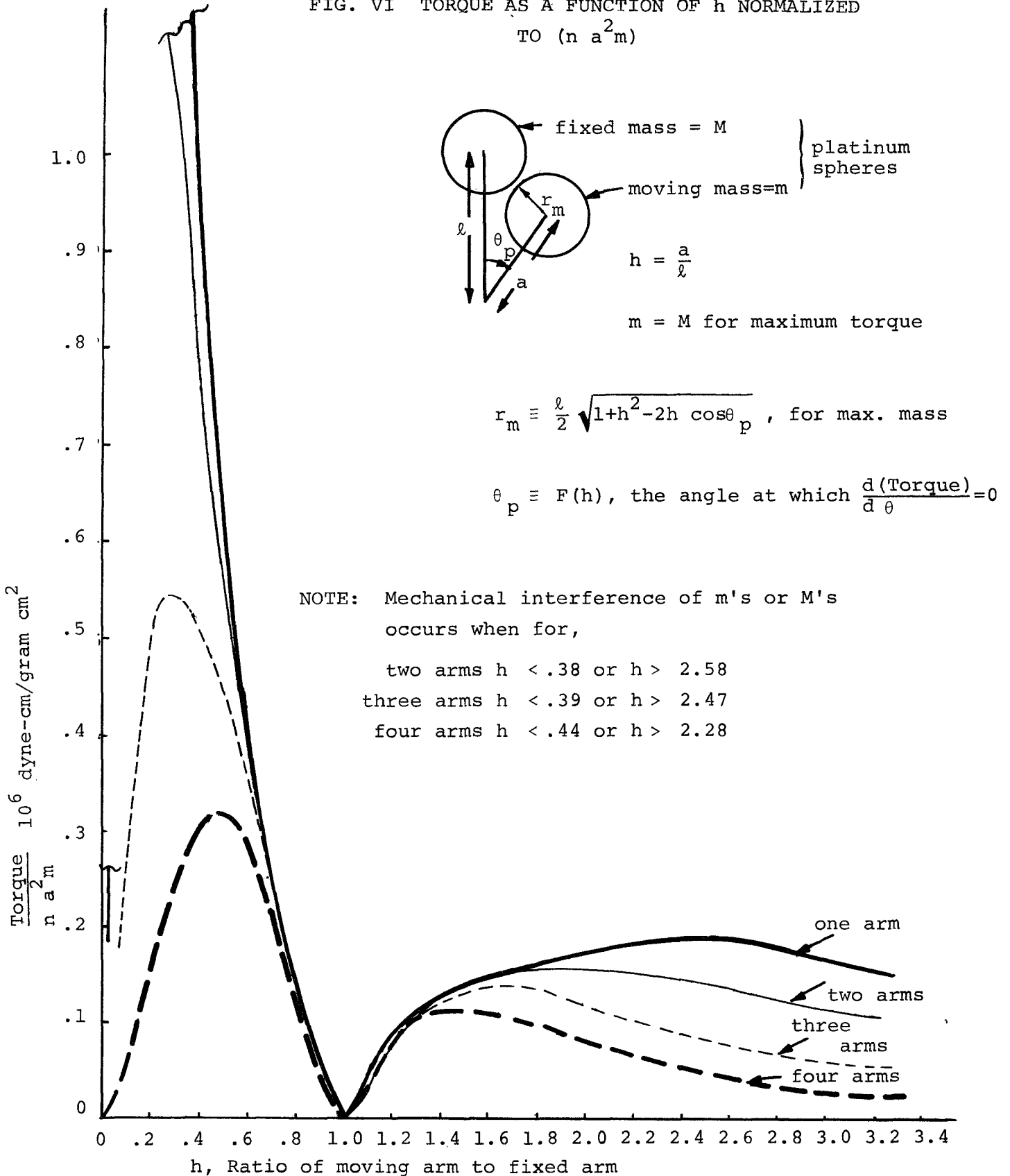
$$\frac{T_d}{m a^4} = .124 \cdot 10^{-12}. \quad (12)$$

We can divide (12) by (11) to get an expression for a^2 in terms of T_d/T . For example, say we wish to limit

$$\frac{T_d}{T} < 10^{-6}$$

then from Fig. VI (4-arm) we have the maximum $T/4a^2 m = 0.32 \cdot 10^{-6}$ at $h \sim 0.5$. Dividing (12) by this gives

FIG. VI TORQUE AS A FUNCTION OF h NORMALIZED TO $(n a^2 m)$



$$a^2 = 10.3$$

or

$$a = 3.2 \text{ cm (4-arm device).}$$

This is the maximum size for "a" if we want to limit the effect of the astronaut to 1 part in 10^6 . If we want to put the same limit on this disturbance torque's effect on a 3-arm device, we get

$$a_{\text{max}} = 0.13 \text{ cm (3 arms)}$$

For this simple model, the 4-arm device has a significant advantage in terms of size vs. effect of disturbance masses.

Using Fig. 6, we can select the value of h that gives the maximum torque for given values of a and m^* . For the four arm device, maximum torque occurs at $h \sim 0.5$.

Up to this point, we have only considered the gravitational torque acting on the arms; now we can calculate the angular acceleration needed to balance this torque by dividing (9) by the moment of inertia of the moving arms. For the model of spheres on massless rods, the moment of inertia about the pivot is

$$I = n \left[\frac{2}{5} m r_m^2 + m a^2 \right] .$$

Using (8) gives

$$r_m^2 = \frac{a^2}{4} \left[\frac{1}{h^2} + 1 - \frac{2}{h} \cos \theta_p \right]$$

*We recall that the total mass of the 4-arm experiment is 8 m.

and then

$$I = n m a^2 \left[1.1 + \frac{.1}{h^2} - \frac{.2}{h} \cos \theta_p \right]. \quad (13)$$

Dividing (9) by (13) gives the acceleration

$$\frac{T}{I} = \left[\frac{\pi \rho}{6} \right] G \frac{(1+h^2-2h \cos \theta_p)}{h(1.1+\frac{.1}{h^2} - \frac{.2}{h} \cos \theta_p)} \sum_{i=1}^n \frac{\sin(\theta_p + \frac{i}{n} 360)}{[1+h^2-2h \cos(\theta_p + \frac{i}{n} 360)]^{3/2}}. \quad (14)$$

This expression for $n=4$ is plotted in Fig. VII. The peak acceleration occurs near $h \sim 0.5$. From the results shown in Figs. V, VI, and VII it appears that $h = 0.5$ would be a near optimum choice for the design of the 4-arm device.*

Fig. VIII is a full-scale sketch of a 4-arm device that has $h = 0.5$ and a peak gravitational torque of 0.01 dyne-cm. For comparison purposes, Fig. IX shows a full-scale sketch of a 4-arm device that has $h = 0.5$ and a peak gravitational torque of 0.001 dyne-cm. If we use platinum spheres to make a 4-arm device ($h = 0.5$), the total mass of the experiment $\sim 8 \cdot 10^4 T^{3/5}$ grams.† Fig. X shows the torque vs. the total mass and size

*Some caution must be used in interpreting Figs. V, VI and VII, since the results shown represent variations with design parameters. The curves do not represent the operation of a particular device. For example, the variation of torque with h (Figs. V and VI) can not be used (at least directly) in a temperature-sensitivity analysis because we are also changing the mass with h in these figures.

†Here we mean, of course, only the mass that is active in the gravitational torque equations

FIG. VII Angular Acceleration of a Four-Armed Device

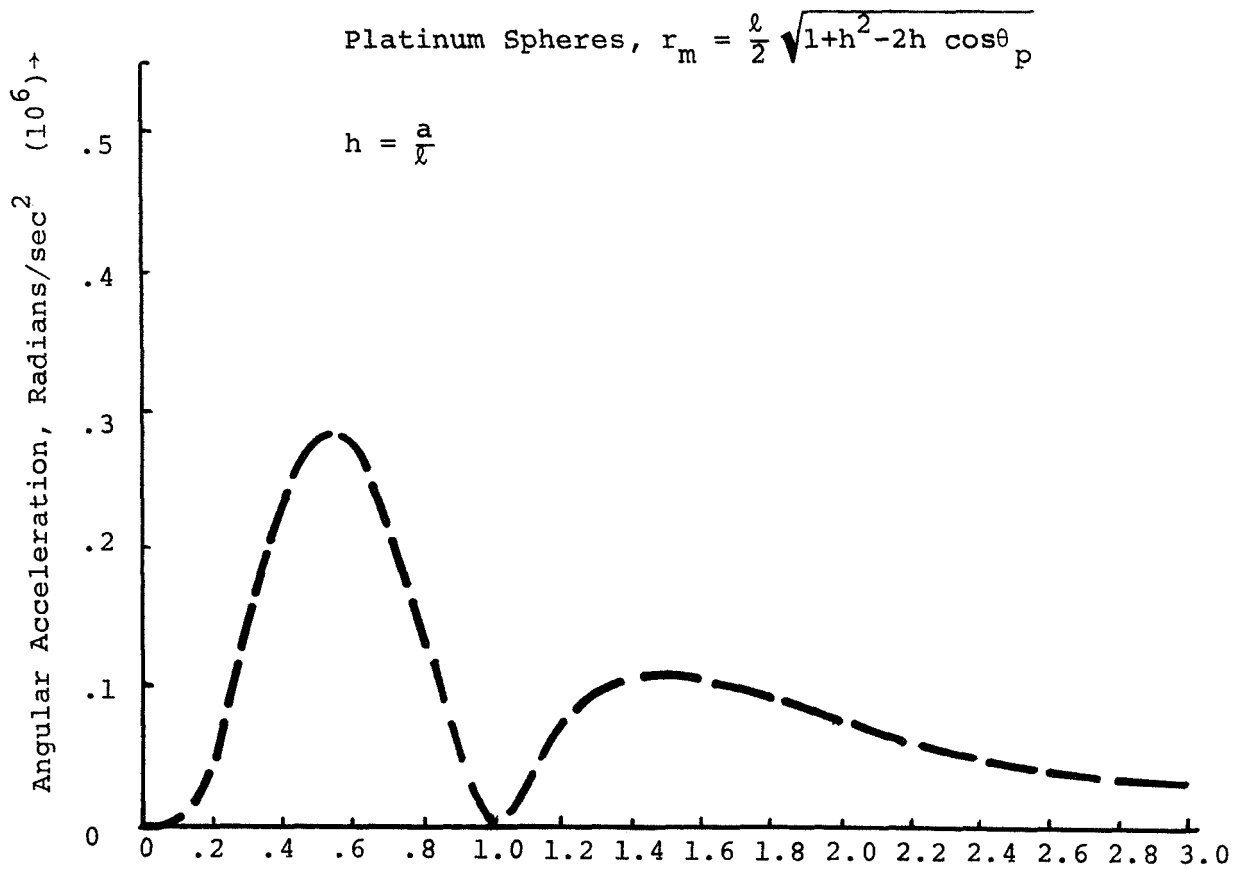
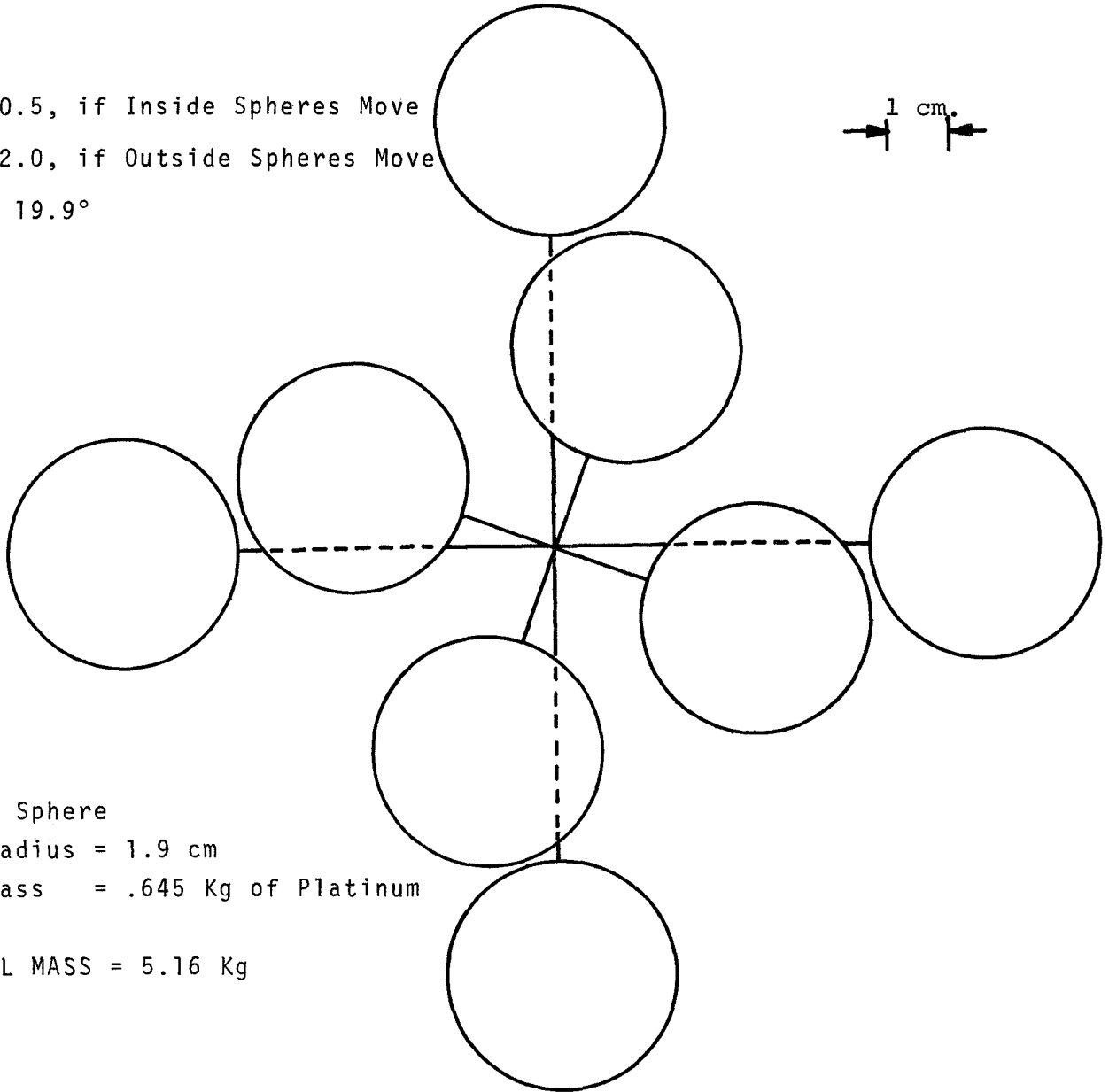
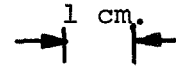


FIG. VIII - FULL-SCALE SKETCH OF A FOUR-ARMED DEVICE
 (Gravitational Torque = 0.01 DYNE-CM)

h = 0.5, if Inside Spheres Move
 h = 2.0, if Outside Spheres Move
 $\theta_p = 19.9^\circ$



Each Sphere
 Radius = 1.9 cm
 Mass = .645 Kg of Platinum

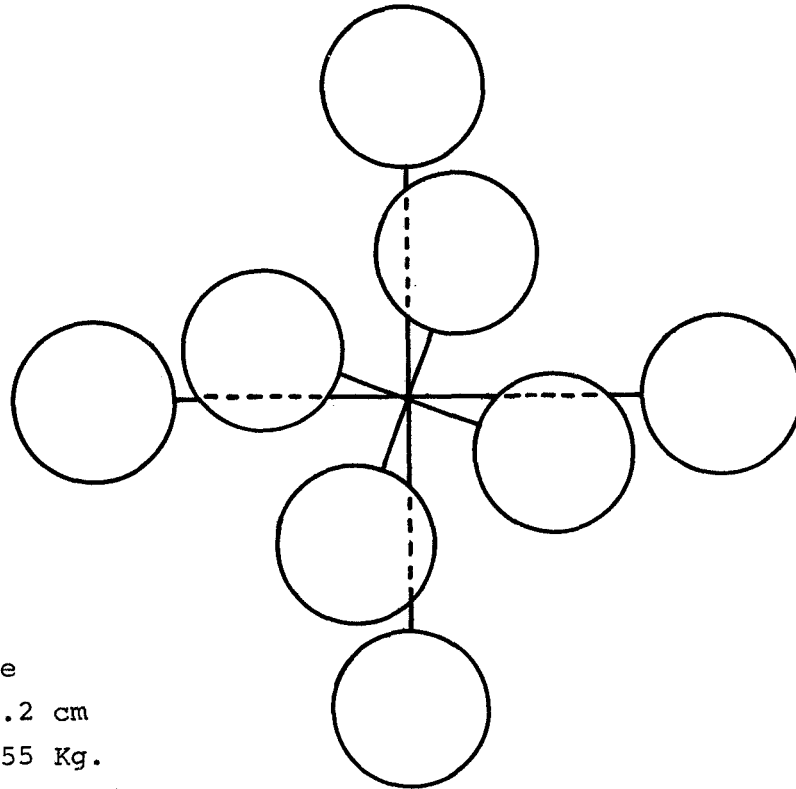
TOTAL MASS = 5.16 Kg

For h = 0.5, Angular Acceleration = $.284 \cdot 10^{-6} \text{ rd/sec}^2$
 h = 2.0, Angular Acceleration = $.076 \cdot 10^{-6} \text{ rd/sec}^2$

FIG. IX FULL-SCALE SKETCH OF A FOUR ARMED DEVICE
(GRAVITATIONAL TORQUE = 0.001 dyne-cm)

$h = 0.5$ if inside spheres move
 $h = 2.0$ if outside spheres move
 $\theta_p = 19.9^\circ$

1 cm



Each Sphere
 Radius = 1.2 cm
 Mass = 0.155 Kg.
 Total Mass = 1.24 Kg.

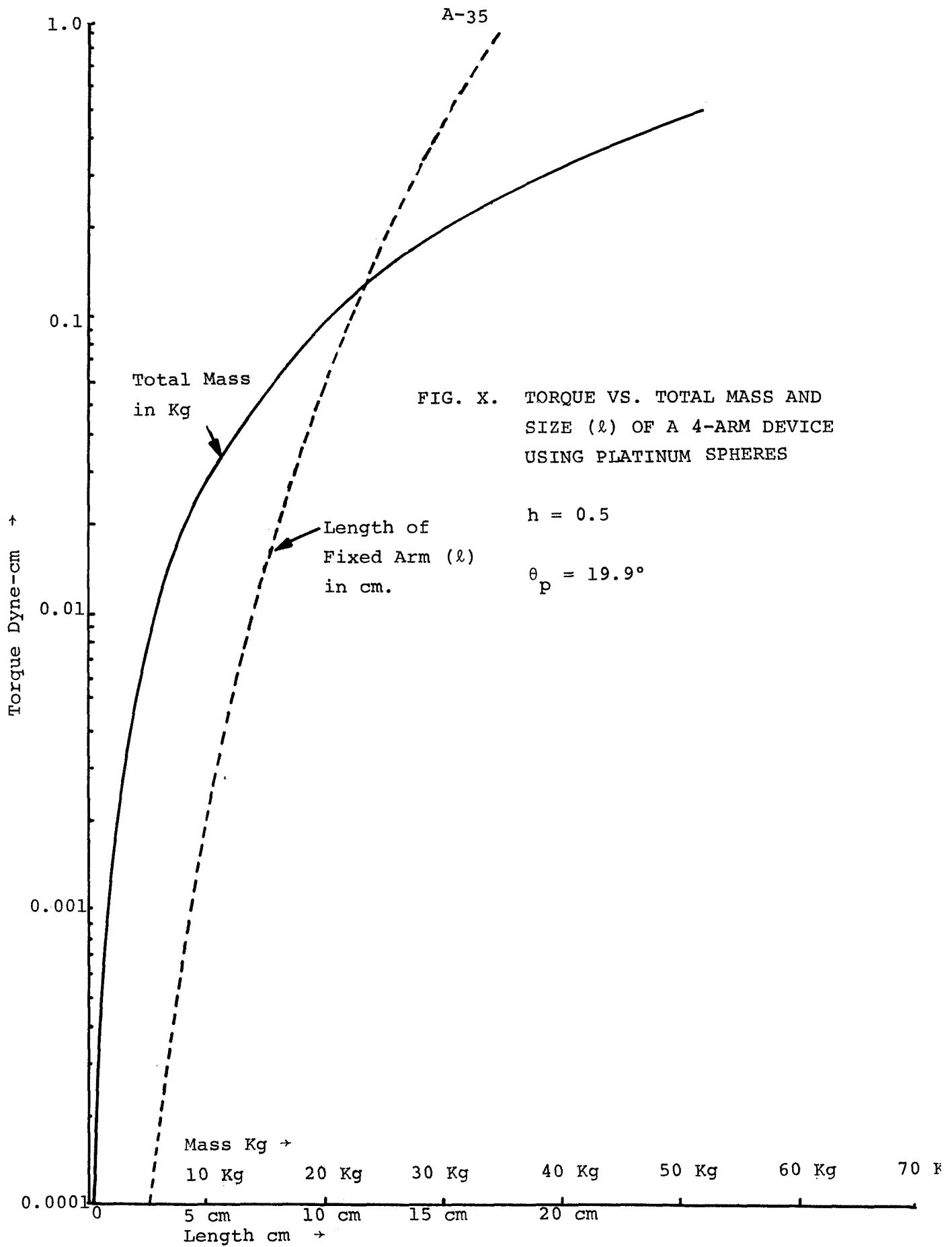
For $h = 0.5$ Angular Acceleration = $0.284 \cdot 10^{-6}$ rd/sec²
 $h = 2.0$ Angular Acceleration = $0.076 \cdot 10^{-6}$ rd/sec²

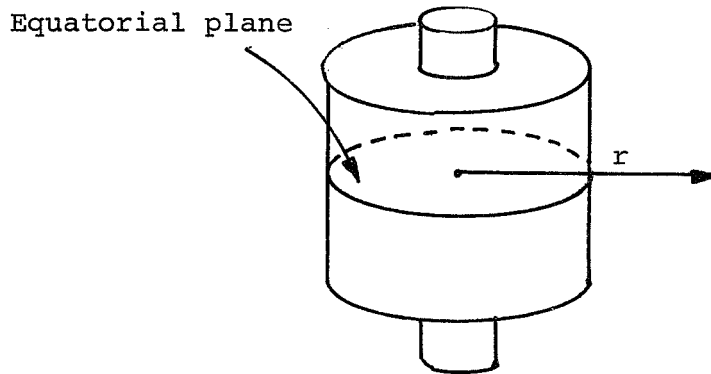
(ℓ) of a 4-arm ($h = 0.5$) experiment with platinum spheres. In a rough way, we can use Fig. X to estimate the size and mass needed to get a certain accuracy in the face of suspension and other uncertainty torques. We note in this connection that the torque level in the Beams' experiment was about $0.2 \cdot 10^{-4}$ dyne-cm.

VII. Further Analysis

In the foregoing analysis, we used an idealized test body made of spheres and massless rods. This made the analysis tractable for slide-rule calculations and also made the results easy to visualize. These results do have practical validity for the classical configurations of the Cavendish experiment. Traditionally, spheres and cylinders have been employed as test masses in experiments on gravitational attraction. Beyond the obvious analytical advantages, spheres (of small size) and cylinders are practical objects to fabricate with precise dimensions and uniform density. A.H. Cook, in a contemporary Cavendish experiment, has found it expedient to use cylindrical test masses to avoid fabrication difficulties.^{(10)*} For the fixed attracting masses, Cook uses cylinders of radius "a" and length $2\sqrt{3} a$. With these dimensions and the addition of some small cylindrical end caps, the composite object (see sketch)

*In a description of a new Cavendish Experiment A.H. Cook says, "The masses attached to the pendulum will be in the form of spheres, since it is not difficult to make spheres of about 10 Kg with high accuracy and with reasonable assurance that the density is uniform..... The stationary attracting masses are to be made much larger, 500 Kg and cannot be spheres, both because of the difficulty of handling them and because of the difficulty of ensuring that the density is indeed uniform."⁽¹⁰⁾





has a field in its equatorial plane equivalent to that of a sphere (at least up to correcting terms proportional to r^{-9} or less).

However, we can use any object as a test mass if it can be fabricated (or measured) to the required dimensional and density tolerances. With a digital computer, we can easily overcome the analytical difficulties of gravitational-field calculations. Considering the stringent size and mass limits on space experiments, it would be useful to examine test-mass shapes that give optimum torque levels for the amount of mass used.* Also, in this analysis of optimum configurations, it would be useful to consider the criteria of the foregoing analysis (e.g., operating at a θ_p , $dT/d\theta = 0$) as well as other criteria which would reduce the sensitivity of the apparatus to dimensional changes (e.g., temperature effects).

In addition to the study of optimum configurations, we must do an analysis of the dynamics of the Beams' experimental concept for operation in a spacecraft. Since a spacecraft is generally in accelerated motion with respect to inertial space, we need to make certain corrections in the experimental measurements. Spacecraft angular acceleration is an interfering quantity that adds (or subtracts) directly in the force-balance equation of

*In these examinations, we would also consider the effects of test-body density variations, surface roughness, and other effects such as Van der Waal force.

the experiment. We can remove this interference by measuring the angular acceleration of the experiment with respect to an inertial reference device. This reference device could be a gyroscopic stable-element or a set of star trackers.

There is a way, however, to avoid the use of an inertial reference device. Consider two separate experimental setups mounted (close together) such that the angular accelerations (needed for force balance) are colinear but in opposite directions. For one of the setups, the spacecraft angular acceleration will add in the force balance and in the second, it will subtract. By combining the data (obtained over the same time intervals) from both setups, we can (in concept, at least) remove the effect of spacecraft angular acceleration. One of the difficulties with this technique is that the two setups will experience different (integrated) effects from external fields, since their rotational periods will necessarily be different. This difficulty needs to be analyzed in terms of experiment size and the expected spectrum of spacecraft motions.

Finally it would be useful to extend our analysis to the design of a laboratory prototype of a space experiment using Beams' concept. This design would be based on a detailed consideration of the suspension system. For this prototype it seems prudent (from cost and ease of construction considerations) to base the initial design on a simple mass configuration and a simple suspension scheme.

VIII. List of References

1. Blitch, M.G., "The Feasibility of a Gravitational Clock to Test the General Theory of Relativity," S.M. Thesis in Physics, M.I.T., August 1969.
2. Chapman, P.K., "A Cavendish Experiment in Earth Orbit," unpublished note, December 1969.
3. Douglas, D.H. Jr., "Two Gravity Experiments: Time Variation of G and Gravitational Wave Detectors at Low Frequencies," A paper presented at the Third Cambridge Conference on Relativity, New York, June 1970.
4. Lee, W.N., "A Space Experiment to Determine the Constancy of the Gravitational Constant G," Measurement Systems Laboratory Report PR-7, "Review of NASA-Sponsored Research at the Measurement Systems Laboratory," May 1970.
5. Hovorka, J., "A Force-Measurement in Orbit to Check Scalar Gravitational Theory," Measurement Systems Laboratory Report RN-57, August, 1969.
6. Rose, D.R., "A New Method for Determination of Newton's Gravitational Constant," D.Sc. Dissertation, University of Virginia, August, 1969.
7. Beams, J.W., "Magnetic Bearings", A paper presented to the Automotive Engineering Congress, Detroit, Mich., January 1964.
8. Fischback, D.B., "Diamagnetic Susceptibility of Pyrolytic Graphite," Physical Review, Vol. 123, No. 5, September 1961.
9. Ezekiel, S., Chapman, P.K., and Egan, J.T., "Analytical and Experimental Investigations of Low-Level Acceleration Measurement Techniques," M.I.T. Experimental Astronomy Laboratory Report, RE-23, April, 1966.

10. Cook, A.H., "A New Determination of the Constant of Gravitation," *Contemp. Phys.*, 1968, Vol. 9, No. 3, 227-238.

APPENDIX B

ERROR STUDY OF THE BEAMS' EXPERIMENTAL
CONCEPT USED IN A $\Delta G/G$ DETECTOR

RN-63

Error Study of the Beams' Experimental Concept
Used in a $\Delta G/G$ Detector

by

Bernard E. Blood

January 1971

Approved:

W. Markey
Director
Measurement Systems Laboratory

Massachusetts Institute of Technology
Measurement Systems Laboratory
Cambridge, Massachusetts 02139

ABSTRACT

This research note presents an elementary evaluation of error sources in a proposed apparatus for the detection of variations in the gravitational constant, G . The experiment is based on a concept used by J.W. Beams to measure the absolute value of G in his laboratory. The Dicke-Brans theory of General Relativity predicts that the magnitude of G will vary with the local magnitude of gravitational potential. Our proposed experiment would detect changes in the gravitational attraction between calibrated test-bodies in an orbiting spacecraft as it moves to points of different gravitational potential. The theory predicts a $\Delta G/G \sim 10^{-9}$ for the extreme positions in an eccentric solar orbit. Instrumentation for this case should be designed, then, to keep individual error effects to less than a part in 10^{10} .

The error sources considered are

1. Thermally caused dimensional variations
2. Interfering inputs
3. Resolution in the measurement of angular acceleration.

Beams' concept involves the use of a controllable angular acceleration to achieve a torque balance (in a D'Alembertian sense) with a gravitational torque on a pivoted test-body.

The simple analyses of this note do not uncover any insuperable problems in achieving a resolution of 10^{-10} in detecting $\Delta G/G$. However, many of the instrument design requirements are unprecedented and may prove to very difficult to meet.

ACKNOWLEDGEMENTS

This work was performed under National Aeronautics and Space Administration Contract NAS 9-8328 (MIT DSR 71390).

Mr. Harold Jones did the analysis in Chapter 3.

TABLE OF CONTENTS

1. Experiment Design Concept	1
1.1 Beams' Experimental Concept	2
1.2 Sensitivity of the Calibration Constant	5
2. Sources of Error	11
2.1 Dimensional Variations	11
2.2 Interfering Inputs	12
2.3 Errors in Measuring Angular Acceleration	15
3. Data Reduction (by Harold Jones)	17
3.1 Simplified Estimator	17
3.2 Minimum Variance Estimator	19
3.2.1 Mathematical Model of Systems	19
3.2.2 Estimator Statistics	30
3.2.3 Simulation Results	34
4. References	47
Appendix A - Design for $\partial K/\partial a = 0$	49
Appendix B - Suspension Stiffness	53

Chapter 1

Experiment Design Concept

According to the Dicke-Brans theory of General Relativity, the magnitude of G (the Newtonian Gravitational Constant) varies with gravitational potential. For example,

$$\frac{\Delta G}{G(\text{initial})} = -2 \times 10^{-8}$$

as an observer moves from a very remote initial position up to a distance of ten solar radii from the Sun.^{(1)*} For a measurement of $\frac{\Delta G}{G}$ in a spacecraft in an eccentric solar orbit, we might expect the variation to be

$$\frac{\Delta G}{G} \sim 10^{-9}.$$

An apparatus (in a solar orbiter) for $\frac{\Delta G}{G}$ detection should, then, have a resolution to parts in 10^{-10} , obtainable in reasonable averaging times compared to the orbital period.

In this note we examine some of the error contributors in a measurement apparatus that uses a concept of J.W. Beams.⁽²⁾ In a 1964 paper Dicke evaluates some of the sources of error in his Eötvös experimental apparatus. Because of the similarity in experimental setups and desired precision, his results are apropos this note.⁽³⁾ Other relevant results are contained in an S.M. thesis by Blicht who considers error sources in a gravitational clock apparatus.⁽¹⁾ The gravitational clock is also a $\frac{\Delta G}{G}$ detector; however, Blicht concludes that the errors due to thermal noise make it impossible to get resolution to parts in 10^{10} in reasonable averaging times. The Beams' method has the advantage of giving a much higher data rate and hence the possibility of having reasonable averaging times to get the desired resolution.

*Superscript numbers refer to items in the list of References.

1.1 Beams' Experimental Concept

To measure the magnitude of G, the Beams' method uses a pivoted test-body which is accelerated by the gravitational torque provided by a set of calibrated attracting masses. The relative separation of the test-body and the attracting masses is maintained constant by a servo that accelerates the attracting masses. The servo acceleration, α , is then proportional to G. Ideally,

$$\alpha = \frac{T}{I} = \frac{\text{Gravitational Torque}}{\text{Moment of Inertia of the Test-Body}} \quad (1a)$$

If, as in Ref. 4, the test body is a rigid, symmetrical arrangement of four spheres on massless arms and the four attracting masses are also symmetrically disposed,

$$T = mMG \sum_{i=1}^4 \sum_{j=1}^4 \frac{al[\delta_{oj}(\delta_{oi}\sin\theta - \delta_{ei}\cos\theta) + \delta_{ej}(-\delta_{oi}\cos\theta + \delta_{ei}\sin\theta)]}{\{l^2 + a^2 - 2al[\delta_{oj}(\delta_{oi}\cos\theta + \delta_{ei}\sin\theta) + \delta_{ej}(\delta_{oi}\sin\theta + \delta_{ej}\cos\theta)]\}^{3/2}} \quad (1)$$

in which we have used the following convenient notation

n	1	2	3	4
δ_{on}	1	0	-1	0
δ_{en}	0	1	0	-1

The remaining notation is defined in Fig. I.

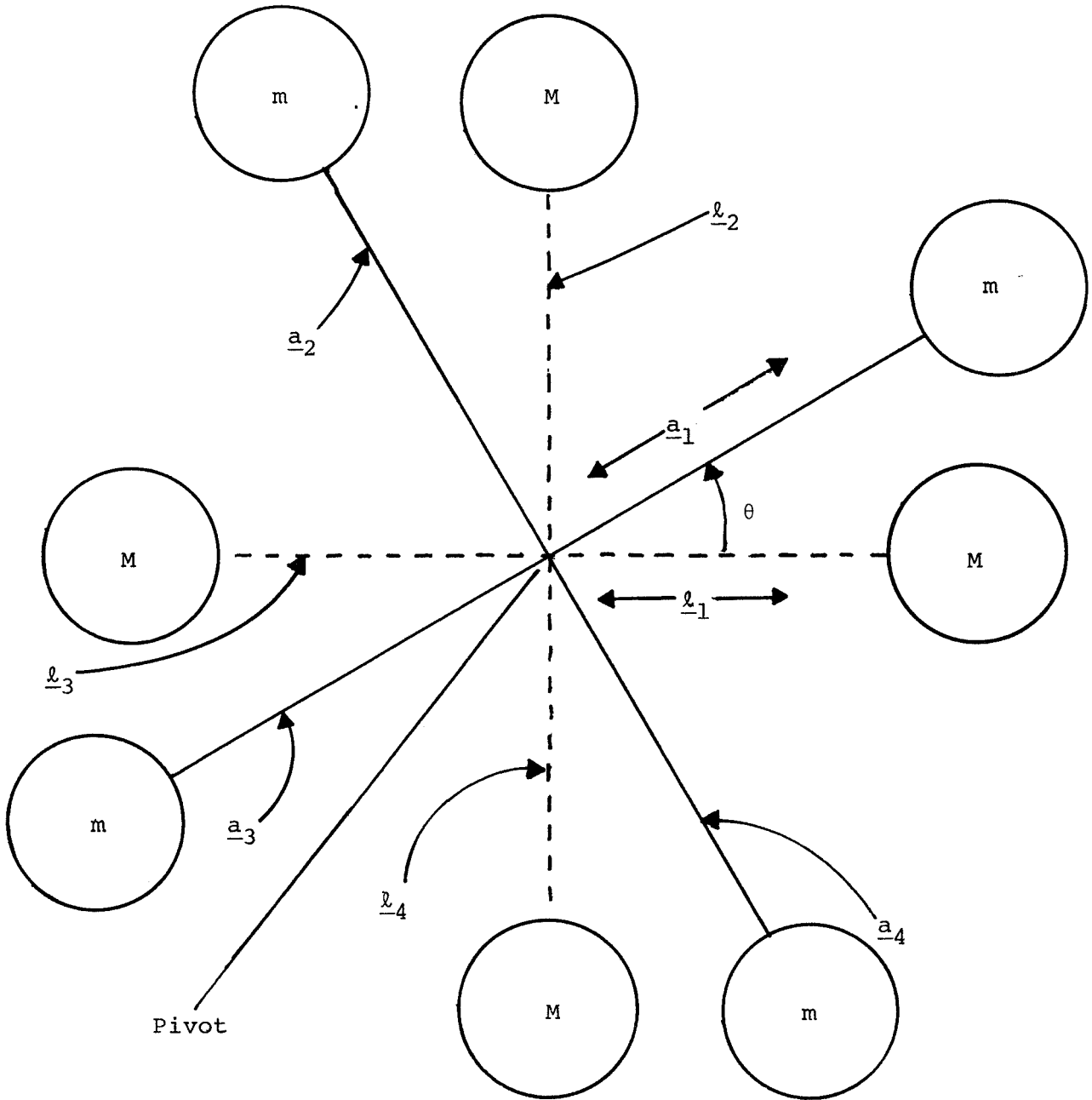


FIG. I Four-Arm Apparatus

M - attracting masses

m - test body masses

\underline{a}_i - vector position of i^{th} arm of the test body

\underline{l}_j - vector positions of the j^{th} attracting mass

The moment of inertia of the test-body is

$$I = 4m\left(\frac{2}{5} r_m^2 + a^2\right) \quad (2)$$

in which

$$r_m = \text{radius of the masses, } m.$$

The experiment is conducted by accelerating a table (on which the M's are mounted) such that θ remains constant. The table angular acceleration is determined by timing angular increments. If we time two successive, equal increments, ϕ , we can get

$$\alpha = 2\phi \frac{\tau_1 - \tau_2}{(\tau_1 \tau_2)(\tau_1 + \tau_2)}. \quad (3)$$

From symmetry considerations we can set $i = 1$ in Eq. 1 and get

$$\frac{T}{4} = mMG \sum_j \frac{a\lambda[\delta_{oj}\sin\theta - \delta_{ej}\cos\theta]}{[\lambda^2 + a^2 - 2a\lambda(\delta_{oj}\cos\theta + \delta_{ej}\sin\theta)]^{3/2}}. \quad (4)$$

Now combining Eqs. 2, 3, and 4

$$G = \left\{ 2\phi \frac{\tau_1 - \tau_2}{(\tau_1 \tau_2)(\tau_1 + \tau_2)} \right\} \left\{ \frac{1}{M} \frac{\frac{2}{5} r_m^2 + a^2}{a\lambda \sum_j \frac{\delta_{oj}\sin\theta - \delta_{ej}\cos\theta}{[\lambda^2 + a^2 - 2a\lambda(\delta_{oj}\cos\theta + \delta_{ej}\sin\theta)]^{3/2}}} \right\}$$

$$\equiv \left\{ 2\phi \frac{\tau_1 - \tau_2}{(\tau_1 \tau_2)(\tau_1 + \tau_2)} \right\} \left\{ K \right\}. \quad (5)$$

We see that G is determined by using measured time increments to calculate the first bracket which is then multiplied by a constant, K.* The second bracket, K, is determined by the parameters of the experimental setup. Clearly, for a precise measurement of G, we need a correspondingly precise knowledge of K. This calibration constant is fixed by the manufacturing tolerances and metrology. Since our experiment is not to determine the absolute value of G, but rather to detect variations, then K need not be precisely known, but it must remain constant to parts in 10^{10} .

1.2 Sensitivity of the Calibration Constant

For an uncomplicated analysis of the dependence of K on the parameters of the experimental setup, we take

$$K = \frac{a}{M \sin \theta} \left[\frac{\frac{2}{5} r_m^2 / a^2 + 1}{\ell} (\ell^2 + a^2 - 2a\ell \cos \theta)^{3/2} \right]. \quad (6)$$

This expression was obtained by setting $j = 1$ in the second bracket of Eq. 5. Effectively, this K is appropriate for a device consisting of a single arm and single attracting mass.

For the simple case of Eq. 6, we see that K is sensitive to variations in M , r_m , a , ℓ , and θ . From a practical point of view we assume that M is unlikely to change, but that a , ℓ , and r_m are subject to thermal effects and θ has variations due to servo errors. To reduce the sensitivity of K to variations in these dimensional parameters, we would ideally like to choose values for a , ℓ , r_m , and θ such that K (as a function of these independent design variables) is at a stationary point, i.e.

$$\frac{\partial K}{\partial a} = \frac{\partial K}{\partial \ell} = \frac{\partial K}{\partial r_m} = \frac{\partial K}{\partial \theta} = 0$$

*In Chapter 3 we show that many sets of time increments are used in an optimal estimation procedure to get the desired resolution in our result.

or

$$\frac{dK}{K} = \frac{\partial K/\partial \theta}{K} d\theta + \frac{\partial K/\partial a}{K} da + \frac{\partial K/\partial r_m}{K} dr_m + \frac{\partial K/\partial \ell}{K} d\ell = 0$$

Using Eq. 6, we can get

$$\frac{\partial K/\partial \theta}{K} = \frac{h}{\sin \theta [1 + h^2 - 2h \cos \theta]} [\cos^2 \theta + \frac{1 + h^2}{h} \cos \theta - 3], \quad (7)$$

$$\frac{\partial K/\partial a}{K} = \left\{ \frac{1}{a} \frac{1}{\left(\frac{2}{5} \frac{r_m^2}{a^2} + 1\right) (1 + h^2 - 2h \cos \theta)} \left[\frac{2}{5} \frac{r_m^2}{a^2} (2h^2 - 1 - h \cos \theta) + (4h^2 + 1 - 5h \cos \theta) \right] \right\}, \quad (8)$$

$$\frac{\partial K/\partial \ell}{K} = \frac{1}{\ell} \left[\frac{2 - h^2 - h \cos \theta}{1 + h^2 - 2h \cos \theta} \right], \quad (9)$$

and

$$\frac{\partial K/\partial r_m}{K} = \frac{1}{r_m} \left[\frac{.8}{.4 + a^2/r_m^2} \right] \quad (10)$$

in which

$$h = \frac{a}{\ell}.$$

The greatest variation in parameters is likely to be in θ , since it represents a degree of freedom in the experiment and is held to a nominal value by servo action. In Ref. 4, we examined in detail the conditions required for $\frac{\partial K}{\partial \theta} = 0$. That report concluded that it was indeed physically possible to adjust the design parameters so that $\frac{\partial K}{\partial \theta} = 0$. The report further showed, for a four-arm device, with

$$\frac{\partial K}{\partial \theta} = 0,$$

$$h \sim 0.45$$

that

$$\frac{dK}{K} < 10^{-10}$$

for $\Delta\theta \sim 1$ second of arc.

On the other hand, examination of Eq. 10 shows that $\frac{\partial K}{\partial r_m} = 0$ only for $r_m = 0$, a physically impossible condition.

For getting the conditions for $\frac{\partial K}{\partial a} = 0$, we set the right-hand-side of Eq. 8 = 0*. If we then use $\frac{\partial K}{\partial \theta} = 0$, we have an expression⁽⁴⁾

$$\cos\theta = f(h)$$

Using this $f(h)$, we can then get an expression

$$\frac{r_m}{a} = g(h)$$

to establish the condition $\frac{\partial K}{\partial a} = 0$. We examine this proposition in Appendix A, where it is shown that, with a four-arm device, we can not get a physically realizable arrangement for $\frac{\partial K}{\partial a} = 0$ (with $\partial K / \partial \theta = 0$) unless a second set of attracting masses is introduced.

For getting the conditions for $\frac{\partial K}{\partial \ell} = 0$, we have from (9)

$$2 - h^2 - h \cos\theta = 0. \tag{11}$$

Now if $\frac{\partial K}{\partial \theta} = 0$, we have from (7)

$$\cos\theta = \frac{1}{2} \left[\frac{1+h^2}{h} + \sqrt{\left(\frac{1+h^2}{h}\right)^2 + 12} \right] \quad (12)$$

Substitution of (12) into (11) and solving for h gives

$$h = 1^*$$

which is a physically unrealizable solution (i.e. the masses m and M would need to be points). We could proceed here in a manner similar to that of Appendix A and calculate the conditions for $\frac{\partial K}{\partial \ell} = 0$, using two masses on the pivoted arms. Fig. II illustrates the idea. From the figure we see that the parameters can be set so that if M moves a distance $\Delta \ell$ the increase in torque on m_2 is exactly offset by the decrease in torque on m_1 .

*We note here that since both the torque T, and inertia, I of Eq. 1 are functions of "a," that making $\partial K / \partial a = 0$ is equivalent to adjusting the parameters so that

$$\frac{T}{I} = \frac{T + \frac{dT}{da} \Delta a}{I + \frac{\partial I}{\partial a} \Delta a}$$

*This solution also holds for a four-arm device.

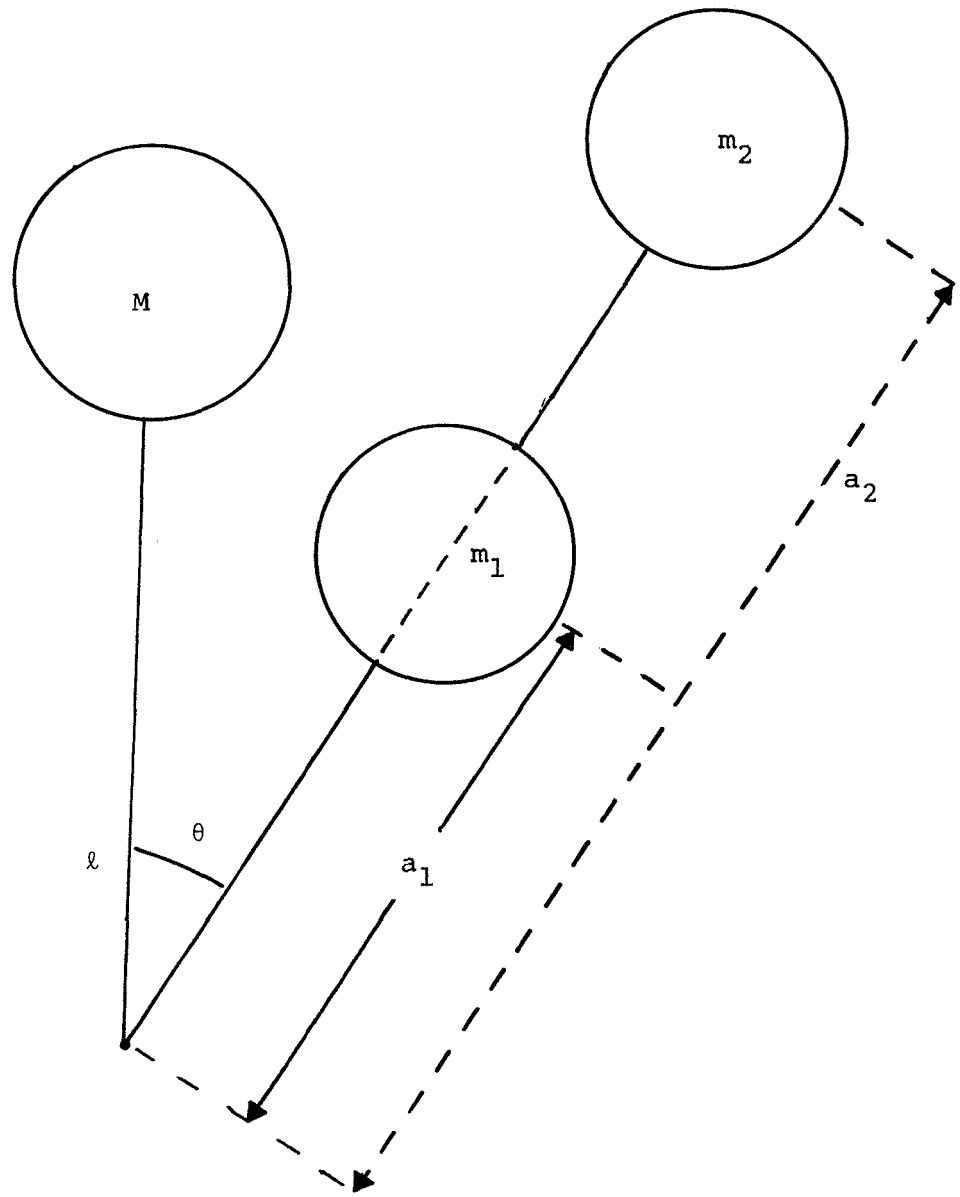


FIG. II. Double Set of Masses on the Moving Arms

Note: h_1 and h_2 set for $\frac{dK}{d\theta} = 0$. $h_1 = \frac{1}{h_2}$. See Ref. 1.

We conclude from the above discussion that if we adjust the parameters for $\frac{\partial K}{\partial a} = 0$, then $\frac{\partial K}{\partial a}$ can be made zero by using an additional set of attracting masses or $\frac{\partial K}{\partial \ell}$ can be made zero by using two masses on the pivoted arms. With our simple models* it does not seem physically possible to make both $\frac{\partial K}{\partial a} = 0$ and $\frac{\partial K}{\partial \ell} = 0$ for the same device.

For the hypothetical device of Fig. VIII, Ref. 4, we made no attempt to make $\frac{\partial K}{\partial a} = 0$ or $\frac{\partial K}{\partial \ell} = 0$.** For this device we have from Eqs. 3,9, and 10

$$\frac{\partial K}{\partial \theta} = 0$$

$$\frac{\Delta K}{K} \sim 1.74 \frac{\Delta a}{a}$$

$$\frac{\Delta K}{K} \sim 4.25 \frac{\Delta \ell}{\ell}$$

$$\frac{\Delta K}{K} \sim 0.12 \frac{\Delta r_m}{r_m} .$$

(13)

We note the K is less sensitive to variations in r_m by over an order of magnitude. Examination of Eq. 10 will show that this will generally be the case since for most physically realizable arrangements $a > r_m$.

In general we conclude that we must maintain $\Delta a/a$, $\Delta \ell/\ell$ and $\Delta r_m/r_m$ to be less than about $1/2 \times 10^{-10}$ to achieve the desired precision in K if no attempt is made to set $\frac{\partial K}{\partial a}$, $\frac{\partial K}{\partial \ell}$, and $\frac{\partial K}{\partial r_m}$ to zero.

*Spherical masses on massless rods

**Actually in this device we adjusted the parameters to make α a maximum under the conditions $\partial K/\partial \theta = 0$.

CHAPTER 2
Sources of Error

To discuss sources of error in our $\Delta G/G$ detection, we classify the effects in three general categories.

1. Dimensional Variations
 - Servo Errors
 - Thermal Effects
2. Interfering Inputs (Extraneous Torques)
 - External Gravity Fields
 - Linear Acceleration
 - Electrostatic Forces
 - Gas Pressure Effects
 - Magnetic Forces
 - Cosmic Ray Protons
3. Errors in Measuring Angular Acceleration
 - Brownian Motion/Thermodynamic Fluctuations
 - Spacecraft Angular Accelerations

Each of these items is discussed in more less detail in terms of magnitude and design requirements to keep the effect in general to less a part in 10^{10} .

2.1 Dimensional Variations

Dimensional variations introduce errors in the calibration constant, K , as discussed in the previous Chapter. Here we are concerned with the factors $\Delta\theta$, $\Delta a/a$, $\Delta l/l$, and $\Delta r_m/r_m$ of Eq. 13.

Servo Errors

As detailed in Reference 4 the nominal operating angle, θ_p , can have variations due to non-ideal operation of the servo. With $\Delta\theta \sim 1$ second of arc, $\Delta K/K$ can be $< 10^{-10}$, if the experiment's parameters are properly adjusted. There is another $\Delta\theta$ effect, however, which is discussed below in 2.3.

Thermal Effects

At room temperatures the coefficient of thermal expansion for most metals (including platinum) is about 10^{-5} per °C. We might expect to achieve temperature control to 10^{-3} °C. (5) This will give use $\Delta l/l$, $\Delta a/a$, and $\Delta r_m/r_m$ 10^{-8} . Yet, from Eq. 13, we require

$$\frac{\Delta l}{l} \sim .2 \cdot 10^{-10}$$

$$\frac{\Delta a}{a} \sim .5 \cdot 10^{-10}$$

$$\frac{\Delta r_m}{r_m} \sim 10^{-9}$$

to keep $\frac{\Delta K}{K} < 10^{-10}$. With a very refined temperature control and using a quartz base for the attracting spheres, setting $\frac{\partial K}{\partial a} = 0$ by the method of Appendix A, and making $r_m \ll a$ we might barely achieve $\Delta K/K < 10^{-10}$ at room temperature. However it seems more feasible to achieve the required insensitivity by operating at cryogenic temperature where the coefficient of thermal expansion is on the order of 10^{-8} per °C.

Other sources of dimensional variations include the effects of centrifugal force on "a". For example, if the angular velocity of the test body is 0.2 rd/sec., and m is a 645 gram weight at the end of a slender rod, then the area of the rod, A, must be 1.29 cm^2 to maintain $\Delta a/a < 10^{-10}$. In the calculation of A we have taken Young's Modulus to be 10^{13} dynes/cm². This particular Δa is more or less deterministic and the effect could be compensated in the data reduction.

2.2 Interfering Inputs (Extraneous Torques)

In discussing interfering inputs, we must consider the effects on an non-ideal device (one with deviations from perfect symmetry) as well as the ideal.

Gravity Fields

As discussed in Reference 4, one of the advantages of the Beams' device is that the gravity fields of fixed external objects do not

affect the experiment if the timing data is taken for full revolutions of the experiment. In an environment of moving external masses (during a revolution period of the experiment) there are three general ways to minimize the effect on the ideal instrument.

1. The moving test body is constructed of 4 symmetric arms (see Reference 4) to minimize the effects of gravity gradients.
2. The moving test body is made so that arm length, a is much shorter than the distance to the disturbing object.
3. The experiment is run at relatively high angular velocities so that the rotation period is short compared to the period of motion of the external disturbing masses.

An extreme example in Reference 4 showed that a 150 lb. astronaut at 2 meters from a 4-arm rotor (arm length = 3.2 cm) introduced an extraneous torque of 1 part in 10^6 . We can calculate what deviation from symmetry in our 4-arm device will give an equal extraneous torque for this object. Suppose we model the dissymmetry by an excess of mass, Δm , at the end of one of the 4-arms, then $\Delta m/m$ must be less than $0.4 \cdot 10^{-4}$ to limit the extraneous torque (because of the astronaut) to 1 part in 10^6 . Establishment of a manufacturing tolerance on the mass, m , to 10^{-5} is not unreasonable. (6)

Although each specific case would need be analyzed, it does not seem unreasonable to conclude that effect of extraneous gravitational torques can be reduced to parts in 10^{10} by experiment design, manufacturing tolerances, and control of the environment.

Linear Acceleration

Just as gravity fields of fixed external objects do not affect the ideal experiment, constant linear acceleration does not as well. Variations in linear acceleration will, however, affect the non-symmetrical device. Using the example of Figure VIII, Reference 4, i.e., $a=3.2\text{cm}$ and $m=645$ grams we can calculate the maximum change in linear acceleration permissible if the extraneous torque is to be less than 1 part in 10^{10} . We again take the effective dissymmetry to be $\Delta m/m = 10^{-5}$. Under these conditions, $\Delta(\text{linear acceleration})$ must

be less than $2 \cdot 10^{-8}$ cm/sec² (during the period of the experiment's full revolution).*

Another effect of linear acceleration and external gravity fields is to pull the center of mass of the test body off the center of symmetry. In Appendix B we show that reasonable suspension stiffness will easily limit this effect on the constant K. For a constant acceleration of 10^{-5} cm/sec² and a test body mass of 2.58 kg.

$$\frac{\Delta K}{K} < 10^{-10}$$

if the suspension stiffness is 890 dynes/cm. In a practical case we can expect a suspension stiffness on the order of 10^6 dynes/cm. (1)

Electrostatic Forces

The rotating test body has small clearances with the attracting masses to maximize the gravitational torque. With these small clearances, a small difference in electric potential between the test body and the attracting masses will give a relatively large electrostatic force. If the device shown in Figure VIII, Reference 4 has suspension that electrically isolates the test body, we get an extraneous torque of

$$\Delta T \sim 2V^2 10^{-2} \text{ dyne cm}^{**}$$

in which V = potential difference. Since, for this device T = .01 dyne cm and we want $\Delta T/T < 10^{-10}$, then we must have

$$V < 10^{-5} \text{ volts.}$$

With V = 10^{-5} volts and the assumed capacities = 10^{-11} farads we have a charge, Q = 10^{-16} coulombs or about 600 electron charges. In view of the difficulties (see Reference 3) of controlling such low potential differences or small charge concentrations it may be wise to consider suspension systems that do not electrically isolate the test body.

* Such small variations in spacecraft acceleration would be difficult to assume for low earth orbit where the drag acceleration is on the order of 10^{-5} cm/sec².

** This relationship represents a very rough calculation in which we have used an estimated capacitance on the order of 10^{-11} farads.

Gas Pressure Effects are treated by Roll, Krotkov, and Dicke in Reference 3. They conclude that to keep gas pressure forces to less than 10^{-10} dynes per cm^2 in a vacuum of 10^{-6} mm, the temperature difference of gas streaming in two opposite directions in the chamber must be less than $3 \times 10^{-6} \text{ }^\circ\text{C}$. Since the Beams' experiment requires as low or lower effects, the same good vacuum and control of temperature uniformity is needed as in Dicke's Eötvös experiment.

Magnetic Forces on the test body are only eliminated by making the apparatus as free of magnetic contaminants as possible and using good shielding. Roll, Krotkov, and Dicke report (Reference 3) that the measured sensitivity of their Eötvös apparatus was about 7×10^{-12} dyne $\text{cm}/10^{-5}$ gauss (external field).

In addition to the above error sources, Blich (Reference 1) considers the effects of Cosmic ray protons. He concludes that with proper shielding the effect can be limited.

2.3 Errors in Measuring Angular Acceleration

From Equation 5 we have

$$G = \left\{ 2\phi \frac{\tau_1 - \tau_2}{\tau_1 \tau_2 (\tau_1 + \tau_2)} \right\} \left\{ K \right\} \quad (5)$$

The τ 's represent the times for rotational displacements, ϕ , of the moving test body with respect to inertial space. In a practical case the time periods will be measured as fiducial marks on the table (holding the attracting masses) cross a fiducial mark on the frame holding the experiment. If the frame is non-rotating in the inertial space, the measured times will be in error by the difference between the angular displacement of the table and the angular displacement of the test body. This difference is represented by variations in the servo error signal $\Delta\theta$. In general with careful servo design, we can expect noise in θ to be on the order of a few tenths of a second arc rms.*

* In Beams' experimental set up it was assumed that noise in θ was generally about 0.2 seconds of arc rms.²

Other sources of error in the time measurements come from thermodynamic fluctuations in the position of the fiducial marks (in practice the coincidence detection of fiducial marks will be optical). In the next chapter on data reduction we lump all noise effects together and assume that there is an rms error of 1 second of arc in each displacement measurement.

In general the rigid frame holding the experiment will have angular motions with respect to inertial space. To eliminate the effect of angular motion we can take two separate set ups mounted on the same frame such that the rotation vectors of the test bodies are parallel but in opposite directions. For one of the set ups, the frame's angular motion will increase our time measurements and in the other set up it will decrease the time measurement. By combining the data (obtained over the same time interval) from the two set ups we can eliminate the effect of the frame's angular motion. This arrangement is assumed in the next chapter in which we take the frame's angular motion to be an angular acceleration given by a constant term plus noise with an rms level of 10^{-6} rad/sec².

Chapter 3
Data Reduction

3.1 Simplified Estimator

The least amount of information required to compute an estimate of G is the passage time for the table through a set of three fiducial marks. If the times are $\tau_{n,n+1}$ and $\tau_{n+1,n+2}$ respectively, the estimate for G is given by (5):

$$\hat{G}_n = 2\phi \left\{ \frac{\tau_{n,n+1} - \tau_{n+1,n+2}}{\tau_{n,n+1}\tau_{n+1,n+2}(\tau_{n,n+1} + \tau_{n+1,n+2})} \right\} K \quad (5)$$

If the passage times for N such fiducial marks are measured, the best estimate for G is:

$$\hat{G}_N = \frac{1}{N-2} \sum_{i=2}^{N-1} h(i) \hat{G}_i \quad (14)$$

The weighting factor, $h(i)$, is a function of the variance of the estimate \hat{G}_i . If all of the \hat{G}_i have the same variance, then $h(i)$ is unity; but this will not in general be the case. The variance of \hat{G}_i is determined by the variance of the passage time measurements which in turn is determined by the table angular velocity. For long experiment runs, the velocity will vary significantly and $h(i)$ will not be unity. In general, the individual estimates, \hat{G}_i , at a high angular velocity will be less accurate, but more numerous.* This fact should not be construed to suggest that the most accurate estimate of \hat{G}_N is obtained for low table angular velocities. In Section 3.2.3,

*See Appendix E of Forward for details.

the opposite is shown to be true.

The variance of \hat{G}_N is not trivial to compute since the errors in \hat{G}_N are not independent. This is obvious since a large measurement error in the passage time for the $(n+1)^{\text{th}}$ fiducial mark affects the measurement of $\tau_{n,n+1}$ and $\tau_{n+1,n+2}$ and this directly affects G_{n-1} , \hat{G}_n , and \hat{G}_{n+1} . The statistics for the passage time measurement must be known to determine $h(i)$. The variance of \hat{G}_N can in principle be computed from the same information. For the volume of data required to attain the necessary accuracy, the computation would be tedious.

The mathematical model upon which the above estimator is based assumes that the angular acceleration of the table is constant between fiducial marks and that the base acceleration is zero. The only error sources which are accounted for are the direct measurement errors in the passage time measurement and in the value of K . If the fiducial marks correspond to full revolutions of the table, the conservative torques from fixed masses within the spacecraft will not affect the true passage times and can be ignored. Two disturbances which will affect the true passage times are:

- 1) torques from moving masses within the spacecraft, and

- 2) base angular accelerations of the spacecraft.

The simplified estimator proposed above cannot account for the effect of either of these disturbances on either the estimate, \hat{G}_N , or the variance of the estimate. Although the estimator may be used in the real experiment to reduce the data, an estimator based on a more detailed mathematical model is necessary to study the importance of the disturbances.

It is possible to devise a more complicated estimator which will

allow for the effect of random base angular accelerations. The moving mass torques cannot be so readily accommodated except by order-of-magnitude comparisons with the base accelerations. Such an estimator and its statistics are investigated in the remainder of this chapter.

3.2 Minimum Variance Estimator

3.2.1 Mathematical Model of System

The gravitational constant can be estimated directly from:

$$\hat{G} = \hat{\alpha}\hat{K} \quad (15)$$

if the estimates

\hat{K} are independent, then the variance in \hat{G} is the product of the variances:

$$\sigma_G^2 = (\sigma_\alpha^2 + \alpha^2)(\sigma_K^2 + K^2) \quad (16)$$

The minimum variance estimator developed in this section determines $\hat{\alpha}$ in such a manner as to minimize σ_α^2 . The estimator is optimal to the extent that the assumptions to be made are valid. If the minimum variance estimator were used to effect the actual data reduction, it would provide at least as accurate an estimate as any other estimator based upon the same mathematical model.*

The minimum variance estimator is presented here in a general form which includes optimal position and angular velocity estimates for

*For linear systems with Gaussian noise sources, the estimator to be used is alternatively called a Kalman estimator or a conditional mean estimator. See Bryson and Ho for details.

the test tables. If the estimator were to be used for the actual data reduction, the amount of computation could be reduced to a level more competitive with that of the simple estimator of Section 3.1 by solving the derived equation in component form rather than matrix form. Many of the matrix elements are identically zero and need not be continually updated.

For a minimum variance estimator for a linear system, the estimate variance σ_{α}^2 may be precomputed for the experiment if the times at which the state measurements are made are known. Unfortunately, for the Beams-type configuration the measurements are not of the state but of the passage times of a particular set of states (fiducial marks). In order to determine σ_{α}^2 it is necessary to know the passage time measurements and then to relate the time measurement error to an equivalent position measurement error. Any analysis of the variance must be based upon a simulation in order to obtain a set of realistic passage times. A mathematical model used for such an analysis is described in this section. The estimator itself is discussed in 3.2.2 along with the necessary mathematics for the variance computation. In 3.2.3 the simulation results are used to estimate the dependence of σ_{α}^2 on the length of the experiment runs and the initial angular velocities of the tables and also to determine the sensitivity of σ_{α}^2 to model parameter variations. The simulation is not used to compute $\hat{\alpha}$ since the estimate would have no particular significance, but only to study the variance of the estimator.

The angular acceleration of the table with respect to the frame can be modeled as:

$$\ddot{\theta}(t) = \alpha + A \sin(2\theta + \phi_1) + B(t) \sin(2\theta + \phi_2) + a_{O_x} + a_b + v(t) \quad (17)$$

where α is from the primary gravitational interaction,

$A \sin(2\theta + \phi_1)$ is due to the fixed mass distribution of the spacecraft,

$B(t) \sin(2\theta + \phi_2)$ is due to the moving mass distribution of the spacecraft,

a_{o_x} is the acceleration bias due to configuration uncertainties,

a_b is the average base angular acceleration, and

$v(t)$ is the zero mean spacecraft angular acceleration profile.

Any servo uncertainties are lumped into a_b and $v(t)$. If the spacecraft is in a local vertical or sun-oriented attitude, the bias term a_b will vary as a function of the position of the spacecraft along its orbit. The experiment running times will be short relative to the orbital period and the orbital angular acceleration can be assumed constant over that time. The bias a_{o_x} may or may not be invariant between experimental runs.

It is difficult to develop a model involving the mass distribution terms that is mathematically tenable. The fixed mass contribution is conservative and can be ignored if the fiducial marks coincide with full revolutions; however, practical considerations will dictate a much more closely spaced set of measurements. The approach to be taken is to assume that a linear model is valid by supposing that the mass distribution accelerations are small when compared to the base accelerations.

A reasonable value of A and $B(t)$ would be 10^{-8} rad/sec² or less. The variance of $v(t)$ to be assumed is on the order of 10^{-6} rad/sec². Thus it would seem reasonable that the mass distribution terms are

of secondary importance. The acceleration model used to determine the minimum variance estimator for $\hat{\alpha}$ is:

$$\ddot{\theta}(t) = \alpha + a_{o_x} + a_b + v(t) \quad (18)$$

It is shown in Section 3.3 that the qualitative results derived from the ensuing analysis appear to be valid independent of the error in (18). Before the minimum variance estimator is utilized for data reduction, however, the effect of the mass distribution terms should be more carefully investigated.

The experimental apparatus is expected to incorporate two tables with opposite directions of rotation. The equation of motion for the X-table is given by (18). The equation of motion for the Y-table is given by:

$$\ddot{\phi}(t) = \alpha + a_{o_y} - a_b - v(t) \quad (19)$$

The configuration uncertainty bias is particular to a given table. The remaining accelerations are common to both tables.

If the constant accelerations are defined:

$$\alpha_x = \alpha + a_{o_x} + a_b \quad (20)$$

$$\alpha_y = \alpha + a_{o_y} - a_b$$

then in terms of the optimal estimates $\hat{\alpha}_x$ and $\hat{\alpha}_y$, the optimal estimator for α is defined to be:

$$\hat{\alpha} = \frac{1}{2} (\hat{\alpha}_x + \hat{\alpha}_y) \quad (21)$$

The estimates $\hat{\alpha}_x$ and $\hat{\alpha}_y$ will be shown to be unbiased in 3.2.2. The estimate $\hat{\alpha}$ is biased by the configuration bias accelerations:

$$E[(\hat{\alpha} - \alpha)] = \frac{1}{2} (a_{o_x} + a_{o_y}) \quad (22)$$

The variance in the estimate is:

$$\sigma_{\alpha}^2 = \frac{1}{4} (\sigma_{\alpha_x}^2 + \sigma_{\alpha_y}^2 + \sigma_{\alpha_x \alpha_y}^2) \quad (23)$$

where $\sigma_{\alpha_x}^2$ and $\sigma_{\alpha_y}^2$ are the variances in $\hat{\alpha}_x$ and $\hat{\alpha}_y$ respectively and $\sigma_{\alpha_x \alpha_y}^2$ is the covariance between the two estimates. Since the Y-table will experience the same noise profile as the X-table but of opposite polarity, the covariance between the two estimators is significant and cannot be ignored.

Since the experiment is to estimate $\Delta\alpha/\alpha$, the bias in $\hat{\alpha}$ is unimportant if a_{o_x} and a_{o_y} are invariant for the series of test runs. If the biases change between test runs, the effect will be to increase σ_{α}^2 but not to change the form of the estimator. If direct estimates of a_{o_x} and a_{o_y} are made, they may be incorporated into (21) with an attendant decrease in σ_{α}^2 . For the remainder of the present analysis the biases are assumed to be invariant but unknown.

The random nature of the experiment is modeled by the base acceleration profile, $v(t)$, and the passage time measurement errors. The base acceleration profile is modeled as Gaussian white noise with

a variance, Q_v , which is constant:

$$E[v(t)] = 0$$
$$E[v(t)v(\tau)] = Q_v \delta(t-\tau)$$
(24)

where $\delta(t-\tau)$ is the unit impulse function. The base acceleration model is assumed to account for all continuous, random accelerations in the system. The nominal value of Q_v used is $10^{-12} \text{ (rad/sec}^2\text{)}^2$.

The passage time measurement is corrupted by two noise sources; the timing uncertainty in the sensor and the resolution of the fiducial marks. The timing uncertainty is of the order of one microsecond or less and can be ignored. A reasonable estimate for the attainable resolution is a standard deviation of a few tenths of a second of arc. The nominal value used is a standard deviation of one second of arc. The larger value was chosen in an attempt to account for other error sources.

The resolution measurement errors comprise an independent random sequence. If the X-table and Y-table have p fiducial marks distributed uniformly about their circumferences, the n^{th} and m^{th} position measurements respectively at the true passage times will be:

$$\theta(t_n) = \frac{2\pi n}{p} + w_n$$
$$\phi(t'_m) = \frac{2\pi m}{p} + u_m$$
(25)

where w_n and u_m can be modeled as zero-mean, normally distributed,

*The simplified estimator of Section 3.1 illustrates that the state estimate is determined from time interval measurements. Thus timing biases are subtracted out and need not be modeled.

independent random variables:

$$E[w_n w_j] = Q_w \delta_{nj}$$

$$E[u_m u_i] = Q_w \delta_{mi}$$

$$E[w_n u_m] = 0$$

in which δ_{ij} has the properties that:

$$\begin{aligned} \delta_{ij} &= 1 \text{ if } i = j \\ &= 0 \text{ otherwise.} \end{aligned}$$

From (25) the passage time measurements can be approximated by:

$$\tau_n = t_n - \frac{w_n}{\dot{\theta}(t_n)}$$

(26)

$$\tau'_m = t'_m - \frac{u_m}{\dot{\phi}(t'_m)}$$

The passage time measurements have the desired statistical properties of the measurement system. If the simulation were to be used to calculate $\hat{\alpha}$, the passage time errors would correspond to first order to the position measurement errors of (25).

The variance for both the base acceleration model and the measurement error model may differ significantly in the actual experiment from the chosen values. The sensitivity of σ_α^2 to changes in Q_v and Q_w is investigated in 3.2.3.

The remaining element of the model to be developed is the dynamics of the two tables. For the remainder of the chapter it is convenient to use state-space notation. The notation is assumed to be self-explanatory. Athens and Falb is a general reference for the mathematical approach.^[7]

The tables can be modeled as second order integrators which integrate angular acceleration about their input axes twice to determine angular displacement. Defining the elements of the three dimensional state vectors X and Y respectively as:

$$\begin{aligned}
 x_1 &= \theta \\
 x_2 &= \dot{\theta} = \dot{x}_1 \\
 x_3 &= \alpha_x \\
 \dot{x}_2 &= x_3 + v(t)
 \end{aligned}
 \tag{27}$$

and

$$\begin{aligned}
 y_1 &= \phi \\
 y_2 &= \dot{\phi} = \dot{y}_1 \\
 y_3 &= \alpha_y \\
 \dot{y}_2 &= y_3 - v(t)
 \end{aligned}
 \tag{28}$$

The purpose in including α_x and α_y in the state vector relates to the properties of a minimum variance estimator. Even though only part of the state vector is measured (in this case the angular positions x_1 and y_1), the minimum variance estimator provides the

best possible estimate of the entire state vector. Consequently, if $\hat{\alpha}_x$ and $\hat{\alpha}_y$ are to be computed for substitution into (21), they must be included in the state.

If the state matrices are defined:

$$A = \begin{bmatrix} 0 & 1 & 0 \\ 0 & 0 & 1 \\ 0 & 0 & 0 \end{bmatrix} \quad (29)$$

$$B_x = \begin{bmatrix} 0 \\ 1 \\ 0 \end{bmatrix} \quad (30)$$

$$B_y = \begin{bmatrix} 0 \\ -1 \\ 0 \end{bmatrix} \quad (31)$$

and:

$$H = [1 \quad 0 \quad 0] \quad (32)$$

then the equations of motion for the two tables can be expressed as first-order vector differential equations:

$$\dot{X}(t) = AX(t) + B_x v(t) \quad (33)$$

$$Z_x(\tau'_n) = HX(\tau_n) + w_n \quad (34)$$

and:

$$\dot{Y}(t) = AY(t) + B_y v(t) \quad (35)$$

$$Z_Y(\tau'_m) = HY(\tau'_m) + u_n \quad (36)$$

where $Z_X(\tau_n)$ and $Z_Y(\tau'_m)$ are the measured states corresponding to the fiducial mark measurements:

$$Z_X(\tau_n) = \frac{2\pi}{p} n \quad (37)$$

$$Z_Y(\tau'_m) = \frac{2\pi}{p} m \quad (38)$$

The presence of the noise signals in (34) and (36) should serve as a reminder that the measured fiducial mark crossings at τ_n and τ'_m are not the true positions of the tables. The true fiducial mark crossings occur at t_n and t'_m respectively.

The state equations (33)-(36) are sufficient to define minimum variance estimators for α_x and α_y if the motions of the two tables are assumed to be statistically independent. This is not the case. Since the tables are driven by the same base acceleration noise, as well as the same α , a measurement $Z_Y(\tau'_m)$ on the Y-table provides information on the true position of the X-table and thus improves the estimate of $\hat{\alpha}_x$ along with $\hat{\alpha}_y$. In addition, to compute σ_α^2 from (23) it is necessary to know $\sigma_{\alpha_x \alpha_y}^2$. To make the best possible estimates of α_x and α_y , it is necessary to consider the two tables as part of a single experimental apparatus where different functions of the apparatus state are measured at different times.

Define the six-dimensional state vector:

$$\begin{bmatrix} \xi_1 \\ \xi_2 \\ \xi_3 \\ \xi_4 \\ \xi_5 \\ \xi_6 \end{bmatrix} = \Xi(t) = \begin{bmatrix} X(t) \\ Y(t) \end{bmatrix} = \begin{bmatrix} x_1 \\ x_2 \\ x_3 \\ y_1 \\ y_2 \\ y_3 \end{bmatrix} \quad (39)$$

The state-vector differential equation is then:

$$\dot{\Xi}(t) = A_{\xi} \Xi(t) + B y(t) \quad (40)$$

where:

$$A_{\xi} = \begin{bmatrix} A & 0 \\ 0 & A \end{bmatrix}$$

and:

$$B = \begin{bmatrix} B_x \\ B_y \end{bmatrix}$$

To include measurements on both the X-table and the Y-table in the measurements history, define the list $\{\tau_{\beta n}\}$ as an ordered, increasing list of times at which a state measurement is made. A value $\beta = 1$ indicates a measurement on the X-table is taken and $\beta = 2$ indicates a measurement on the Y-table is taken. The state description is completed by defining the measurement system:

$$z_{\beta}(\tau_{\beta n}) = H_{\beta} \Xi(\tau_{\beta n}) + w_n \quad (41)$$

where:

$$H_{\beta} = [1 \ 0 \ 0 \ 0 \ 0 \ 0] \text{ if } \beta = 1$$

and:

$$H_{\beta} = [0 \ 0 \ 0 \ 1 \ 0 \ 0] \text{ if } \beta = 2.$$

3.2.2 Estimator Statistics*

The mathematical model developed in (40) and (41) is for a continuous dynamic system with measurements occurring at discrete intervals. To employ the minimum variance estimator it is necessary to write the true state at the n^{th} measurement time recursively in terms of the true state at the $(n-1)^{\text{th}}$ measurement time. This requires a discrete formulation of (40). The minimum variance estimator is also defined recursively. The minimum variance estimate of the entire six-dimensional state vector based on the first n data points, $\hat{\Xi}(\tau_{\beta n})$, is defined recursively in terms of the n^{th} measurement and $\hat{\Xi}(\tau_{\beta(n-1)})$. The initial state estimate is propagated recursively through the set of measurements to arrive at the final state estimate based upon all the measurements available. The final state estimate yields $\hat{\alpha}_x$ and $\hat{\alpha}_y$ as its third and sixth elements respectively.

*The material in this section on minimum variance estimators is taken from Bryson and Ho, Chapters 12 and 13. The properties of state transition matrices and the state vector approach to dynamic systems are presented in Chapters 3 and 4 of Athens and Falb.

At the time $\tau_{\beta n}$, the state can be written in terms of the state at the previous measurement time, $E(\tau_{\beta(n-1)})$, the state transition matrix, $\Phi(\tau_{\beta n}, \tau_{\beta(n-1)})$, and a random variable $g(\tau_{\beta n})$:

$$E(\tau_{\beta n}) = \Phi(\tau_{\beta n}, \tau_{\beta(n-1)}) E(\tau_{\beta(n-1)}) + g(\tau_{\beta n}) \quad (42)$$

The vector $g(\tau_{\beta n})$ is a six-dimensional vector random variable and is defined as the time integral of $v(t)$ from (40). The elements of the vector are zero-mean and normally distributed with covariance:

$$E[g(\tau_{\beta n})^2] = Q_g = \int_{\tau_{\beta(n-1)}}^{\tau_{\beta n}} \Phi(\tau_{\beta n}, t) B Q_v B^T \Phi^T(\tau_{\beta n}, t) dt \quad (43)$$

$$E[g(\tau_{\beta n})g(\tau_{\beta m})] = 0 \quad n \neq m$$

The off-diagonal elements of Q_g are non-zero, indicating that the six random variables which comprise $g(\tau_{\beta n})$ are correlated. A general procedure for generating correlated random numbers was developed for the simulation to facilitate the computation of $g(\tau_{\beta n})$.

The state transition matrix is best defined in terms of its Laplace transform:

$$\Phi(s) = (Is - A_{\xi})^{-1} \quad (44)$$

where I is the identity matrix.

If $\Delta\tau_n$ is defined as:

$$\Delta\tau_n = \tau_{\beta n} - \tau_{\beta(n-1)} \quad (45)$$

then the expressions for these matrices become:

$$Q_g = \begin{bmatrix} \frac{1}{3}\Delta\tau_n^3 & \frac{1}{2}\Delta\tau_n^2 & 0 & -\frac{1}{3}\Delta\tau_n^3 & -\frac{1}{2}\Delta\tau_n^2 & 0 \\ \frac{1}{2}\Delta\tau_n^2 & \Delta\tau_n & 0 & -\frac{1}{2}\Delta\tau_n^2 & -\Delta\tau_n & 0 \\ 0 & 0 & 0 & 0 & 0 & 0 \\ -\frac{1}{3}\Delta\tau_n^3 & -\frac{1}{2}\Delta\tau_n^2 & 0 & \frac{1}{3}\Delta\tau_n^3 & \frac{1}{2}\Delta\tau_n^2 & 0 \\ -\frac{1}{2}\Delta\tau_n^2 & -\Delta\tau_n & 0 & \frac{1}{2}\Delta\tau_n^2 & \Delta\tau_n & 0 \\ 0 & 0 & 0 & 0 & 0 & 0 \end{bmatrix} \quad (46)$$

and:

$$\Phi(\tau_{\beta n}, \tau_{\beta(n-1)}) = \begin{bmatrix} 1 & \Delta\tau_n & \frac{1}{2}\Delta\tau_n^2 & 0 & 0 & 0 \\ 0 & 1 & \Delta\tau_n & 0 & 0 & 0 \\ 0 & 0 & 1 & 0 & 0 & 0 \\ 0 & 0 & 0 & 1 & \Delta\tau_n & \frac{1}{2}\Delta\tau_n^2 \\ 0 & 0 & 0 & 0 & 1 & \Delta\tau_n \\ 0 & 0 & 0 & 0 & 0 & 1 \end{bmatrix} \quad (47)$$

The recursive expression for the state estimate can be written in terms of the quantities defined in (40)-(47):

$$\hat{\Xi}(\tau_{\beta n}) = \bar{\Xi}(\tau_{\beta n}) + K(\tau_{\beta n}) [Z_{\beta}(\tau_{\beta n}) - H_{\beta} \bar{\Xi}(\tau_{\beta n})] \quad (48)$$

where:

$$K(\tau_{\beta n}) = P(\tau_{\beta n}) H_{\beta}^T Q_w^{-1} \quad (49)$$

and:

$$\bar{\Xi}(\tau_{\beta n}) = \Phi(\tau_{\beta n}, \tau_{\beta(n-1)}) \bar{\Xi}(\tau_{\beta(n-1)}) \quad (50)$$

$P(\tau_{\beta n})$ is the covariance matrix for the state estimate, $\hat{\Xi}(\tau_{\beta n})$, and is defined recursively below. The solution of (48) requires an initial state estimate, $\hat{\Xi}(0)$, and a corresponding initial covariance matrix, $P(0)$. If the experiment generates a large quantity of data, the effect of the initial state estimate is quickly dissipated. (48) and (50) are the equations that would be used in reducing the actual experimental data.

The covariance matrix is defined recursively:

$$P(\tau_{\beta n}) = P'(\tau_{\beta n}) - P'(\tau_{\beta n}) H_{\beta}^T [H_{\beta} P'(\tau_{\beta n}) H_{\beta}^T + Q_w]^{-1} H_{\beta} P'(\tau_{\beta n}) \quad (51)$$

where:

$$P'(\tau_{\beta n}) = \Phi(\tau_{\beta n}, \tau_{\beta(n-1)}) P(\tau_{\beta(n-1)}) \Phi^T(\tau_{\beta n}, \tau_{\beta(n-1)}) + Q_g \quad (52)$$

Again, $P(0)$ must be specified. The recursive relationship for $P(\tau_{\beta N})$ can be solved in principle without knowledge of the state measurements, $Z_{\beta}(\tau_{\beta N})$. Since the measurement times, $\tau_{\beta N}$, are themselves determined by the measurements, the solution of (51) does require either real or simulated data for this particular application.

If $\tau_{\beta N}$ is the last measurement, then:

$$\begin{aligned}\hat{\alpha}_x &= \hat{x}_3(\tau_{\beta N}) = \hat{\xi}_3(\tau_{\beta N}) \\ \hat{\alpha}_y &= \hat{y}_3(\tau_{\beta N}) = \hat{\xi}_6(\tau_{\beta N})\end{aligned}\tag{53}$$

The covariance for $\hat{\alpha}$ is:

$$\sigma_{\alpha}^2 = \frac{1}{4}[P_{33}(\tau_{\beta N}) + P_{66}(\tau_{\beta N}) + 2P_{36}(\tau_{\beta N})]\tag{54}$$

3.2.3 Simulation Results

The simulation consisted of determining the true state of the two tables at discrete time intervals, $\Delta\tau_1$, using the discrete formulation of (40):

$$E(n\Delta\tau_1) = \Phi(n\Delta\tau_1, (n-1)\Delta\tau_1) E((n-1)\Delta\tau_1) + g(n\Delta\tau_1)\tag{55}$$

where $g(n\Delta\tau_1)$ is defined similar to (43). The fiducial marks were distributed uniformly every .0175 radians (360 measurements per revolution). The true passage times were interpolated from the true state profiles and the measured passage times were computed using (26):

$$\tau_n = t_n - \frac{w_n}{\xi_2(t_n)}$$

$$\tau'_m = t'_m - \frac{w_m}{\xi_4(t'_m)}$$
(56)

The measured passage times for the two tables were then formed into the list $\{\tau_{\beta n}\}$ and (51) was solved for $P(\tau_{\beta n})$. σ_α^2 was then computed from (54).

The nominal parameter values for the simulation are listed in Table 1. The primary variables in the simulation were the table velocity at the beginning of the experimental run and the time required to reduce the standard deviation in $\hat{\alpha}$ to 10^{-16} rad/sec². The sensitivity of the results to variations of the parameters in Table 1 was also investigated.

The limiting factor with the simulation was the amount of computation required to complete one experimental run. The results indicate that to reduce σ_α to 10^{-16} rad/sec² would require an experimental run of 50,000 seconds duration (approximately 14 hours) and the analysis of 140,000 data points. The computation involved in solving (51) and (55) iteratively 140,000 and 300,000 times respectively was prohibitive from an economical point of view.

$$\begin{aligned}
\alpha &= 10^{-6} \text{ rad/sec}^2 \\
Q_w &= (1 \text{ arc second})^2 \\
Q_v &= 10^{-12} (\text{rad/sec}^2)^2 \\
P_{11} &= P_{44} = 2.5 \times 10^{-11} \text{ rad}^2 \\
P_{22} &= P_{55} = 10^{-8} (\text{rad/sec})^2 \\
P_{33} &= P_{66} = 10^{-16} (\text{rad/sec}^2)^2 \\
P_{ij} &= 0 \quad i \neq j \\
&360 \text{ measurements per revolution}
\end{aligned}$$

TABLE 1 Nominal parameter values for simulation.

The alternative was to run the simulation for a shorter time and extrapolate the value of σ_α to $10^{-16} \text{ rad/sec}^2$. Very clear trends were observed for the 500 second to 5,000 second segments which were run and it is felt that the extrapolations are not without justification and provide at least nominal estimates of the experiment requirements.

The basic results of the simulation are qualitative and not related to the extrapolation process. These can be summarized by four main points:

- i) the requirement to reduce σ_α to $10^{-16} \text{ rad/sec}^2$ is reached in less time as the initial table velocity is increased, but at the expense of an enormous increase in the amount of data to be reduced.

ii) the time to reach 10^{-16} rad/sec² is not effected appreciably by the accuracy of the initial estimate of α .

iii) the primary hardware limitation on the estimation process is the measurement error variance, Q_w .

iv) the estimation process is quite insensitive to the base acceleration variance, Q_v .

The first result is a contradiction of the results presented by Parker.^[9] It is discussed on a quantitative basis later in this section.

The last three points can be analyzed quite satisfactorily on a qualitative basis. If the measurement error variance, Q_w , is reduced by a factor of two, then, regardless of initial table velocity, the standard deviation, σ_α , of the estimate, $\hat{\alpha}$, after a specified time interval is .707 what it would have been for the same initial conditions but the greater measurement error variance. The effect of this sensitivity on the time required to reduce σ_α to 10^{-16} rad/sec² is discussed later.

Alternatively, if the variance of the base acceleration, Q_v , is decreased by a factor of 100, the effect on σ_α is negligible. If Q_v is increased by a factor of 10,000 from the nominal value, for an initial table velocity of .002 rad/sec the increase in σ_α is a factor of two over the nominal value after 1000 seconds and a factor of three over the nominal value after 2000 seconds. If the base acceleration variance used in the simulation is nominally accurate, base acceleration contributions to the experiment are not important. This would indicate that the simplified estimator of Section 3.1 may

have some merit.

The value of σ_{α} as a function of time for initial table velocities of .2 rad/sec, .02 rad/sec, and .002 rad/sec is presented in Figure 1. The simulations run for 1000 seconds for the two slower velocities and 500 seconds for the .2 rad/sec velocity. In Figure 2 the simulation for .002 rad/sec is extended to 5500 seconds.

The basis for iii) above can be obtained from Figure 1. The initial standard deviation for $\hat{\alpha}$ for the simulation was 10^{-8} rad/sec². If this was to be decreased by a factor of ten, the result would be roughly to save the 140 seconds that it took the experiment starting at .002 rad/sec to obtain that accuracy in its estimate, or the 95 seconds for the table at .02 rad/sec, etc. For an operating time in excess of 10,000 seconds, these savings would be negligible.

Observation i) above can be substantiated quantitatively by extrapolation of the available data. Two trends of σ_{α} are very clear from Figures 1 and 2. The first is that the ratio of the standard deviations corresponding to two different initial velocities is very nearly a constant independent of the time at which the ratio is calculated. The second is that after the first 50 seconds, the decay in σ_{α} is geometric, decaying by a factor of 5.65 every time the experiment running time is doubled. The data upon which these results are based is presented in Tables 2 and 3.

The deviation from the factor at 5.65 for the slower run and times greater than 1000 seconds is due to the fact that the time integration of α becomes the dominant factor in determining the table angular velocity. The initial angular velocity becomes relatively important.

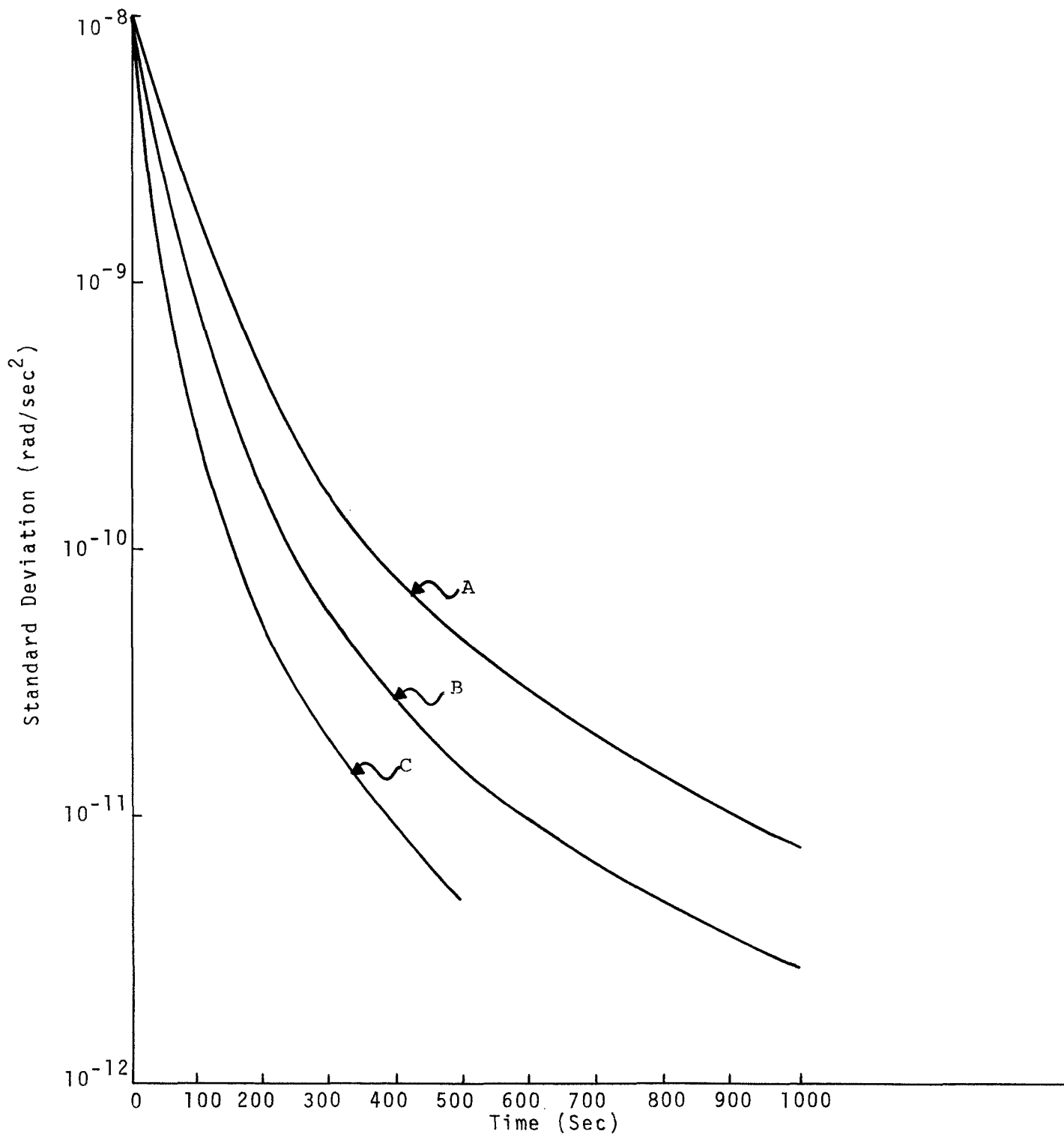


Figure 1 Standard deviation of $\hat{\alpha}$ as a function of time for three B-39 initial table velocities. The initial velocities for A, B, and C are respectively .002 rad/sec, .02 rad/sec, and .2 rad/sec. The model parameter values are those of Table 1.

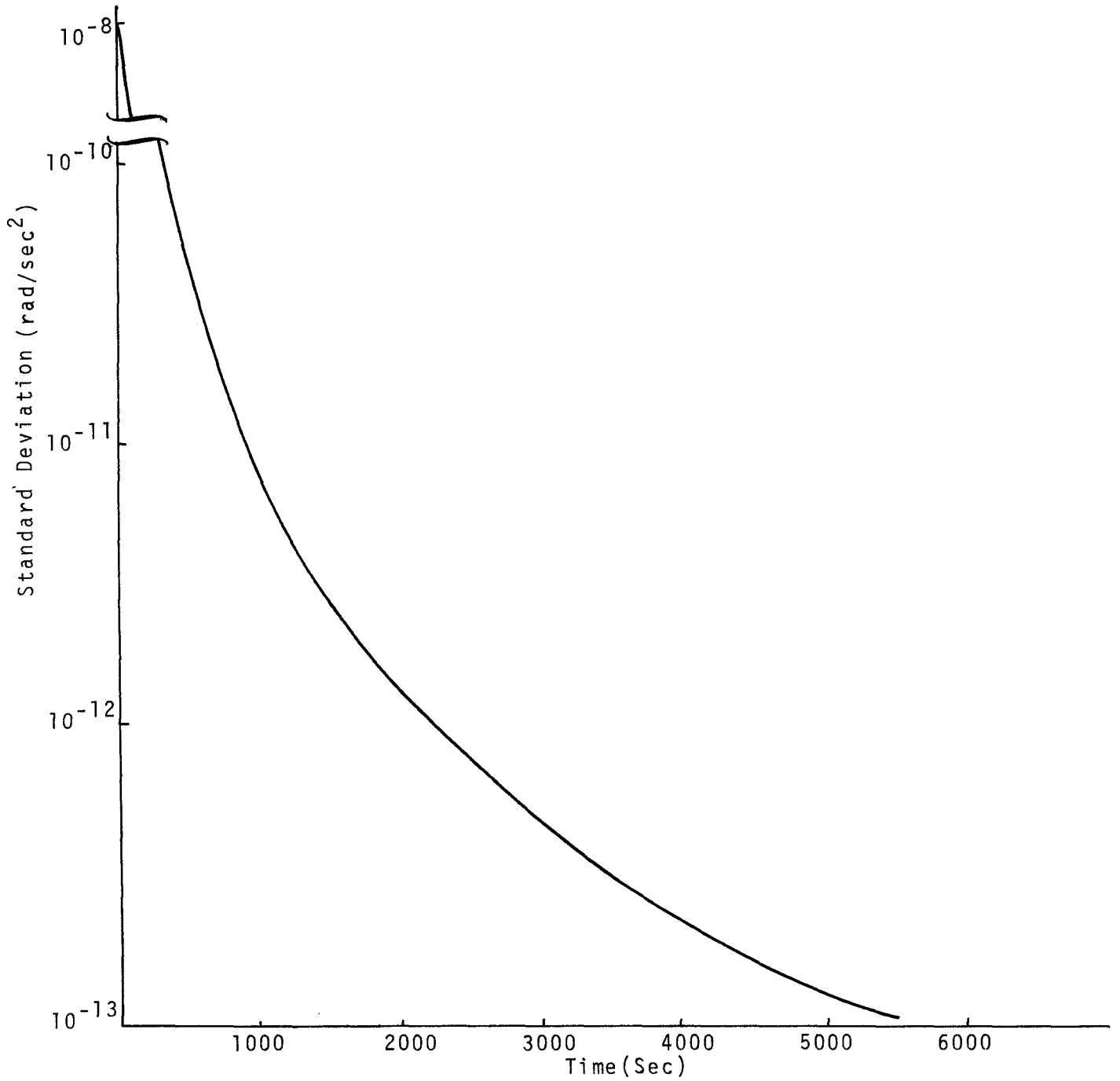


Figure 2 Standard deviation of $\hat{\alpha}$ as a function of time for an initial table angular velocity of .002 rad/sec. The model parameter values are those of Table 1.

For an initial velocity of .002 rad/sec, the velocity is .003 rad/sec at 1000 seconds and increases .001 rad/sec per 1000 seconds thereafter. The effect of the increased velocity is to cause the standard deviation for the slower table to asymptotically approach the standard deviation for the table starting at .02 rad/sec.

The results of Table 3 suggest that the value of σ_α as a function of time can be satisfactorily modeled when the velocity is constant as:

$$\sigma_\alpha(t) = \frac{K_0(\dot{\theta}(0), \dot{\phi}(0))}{t^{2.5}} \quad (56)$$

for:

$$t < \frac{\alpha}{\dot{\theta}(0)} = \frac{\alpha}{\dot{\phi}(0)}$$

and when the integrated velocity from α is dominant as:

$$\sigma_\alpha(t) = \frac{K_1(\theta(0), \phi(0))}{t^{2.7}} \quad (57)$$

for:

$$t > \frac{\alpha}{\dot{\theta}(0)} = \frac{\alpha}{\dot{\phi}(0)}$$

The values for the constants are summarized in Table 4. The accuracy for (56) is easily checked by comparison with Figure 1. Between 50 seconds and 1000 seconds, the error is less than 5% for all three initial velocities. The exponent of 2.5 corresponds to the ratio of 5.65 which appeared to be the norm in Table 2. The extrapolation of (56) to greater times for initial velocities of .02 rad/sec and .2 rad/sec should yield results with a high confidence level.

The model for the time region when the table velocity is essentially independent of the initial velocity is not quite so satisfactory. The exponent of 2.7 was determined from analyzing the decay of σ_α between 5000 seconds and 5500 seconds in Figure 2 with consideration for the fact that the initial velocity of the platform is not quite

Initial Velocity rad/sec	Time Interval (Seconds)							
	32 to 64	64 to 128	128 to 256	256 to 512	500 to 1000	1000 to 2000	2000 to 4000	2750 to 5500
.002	--	--	5.50	5.67	5.75	6.07	6.27	6.45
.02	2.62	5.35	5.52	5.68	5.68	--	--	--
.2	4.55	5.55	5.65	5.65	--	--	--	--

Table 2 Factor by which σ_α is reduced when the running time is doubled as a function of initial table velocity.

Ratio of σ_α for A over σ_α for B	Time (Seconds)						
	50	100	200	400	600	800	1000
	1.48	2.69	2.91	2.86	2.94	2.84	2.83

Ratio of σ_α for B over σ_α for C	Time (Seconds)						
	50	100	200	300	400	500	--
	2.76	3.10	3.12	3.13	3.12	3.11	--

Table 3 Ratios of σ_α for different initial table velocities. A corresponds to .002 rad/sec, B to .02 rad/sec, and C to .2 rad/sec.

Initial Angular Velocity	K_0 (rad/sec ²)	K_1 (rad/sec ²)
.002	2.5×10^{-4}	1.05×10^{-3}
.02	8.9×10^{-5}	5.1×10^{-4}
.2	2.8×10^{-5}	--

Table 4 Constant parameter values for geometric models of σ_α .

negligible for the data analyzed. The value for K_1 was determined from the value of σ_α at 5500 seconds. The model is in error at 5000 seconds by 2% and at 4000 seconds by 8%.

It is felt that (57) is useful in estimating the time required to reduce σ_α to 10^{-16} rad/sec. Certainly the use of (56) alone would overestimate by a considerable amount the time required to reach that accuracy for the low initial angular velocities. Different methods for estimating the parameter values for (57) suggest that the time estimate for an initial velocity of .02 rad/sec may be accurate to within 2000 seconds and for an initial velocity of .002 rad/sec to within 5000 seconds. These error estimates assume that the initial model (56) is relatively precise.

The estimates for total time required and total data required to achieve a value of 10^{-16} rad/sec² for σ_α are summarized in Figure 3 and Figure 4. The time required clearly must approach a maximum value somewhere in the vicinity of 70,000 seconds. The number of data points required must approach a corresponding lower limit of around 125,000 data points. No such limit for higher velocities exists. As a rule of thumb, increasing the velocity by a factor of ten in the high velocity region of Figures 3 and 4 reduces the time requirement by 25% to 30%, but increases the total amount of data acquired by a factor of between 8 and 9.

The total time and total data requirements are quite sensitive to the measurement error variance of the mathematical model. The measurement errors for the simulation had a standard deviation of one second of arc. If this is reduced by a factor of two, the corresponding total time and total data requirements for the same

initial conditions are decreased by 26%. If the standard deviation is reduced by a factor of four, the savings is 42%. The latter accuracy has been suggested as feasible. If it can be attained with a 360 measurement per revolution measurement system, the required accuracy in $\hat{\alpha}$ can be reached in 30,000 seconds with 76,000 data points for an initial velocity of .02 rad/sec.

All of the data for Figures 3 and 4 is based upon a sample rate of 360 measurements per revolution. For the faster velocities, a change in the fiducial mark spacing is equivalent to a change in the table angular velocity. For the slower velocities the quantitative analysis of fiducial mark density changes would require an additional simulation.

The conclusion to be drawn from Figures 3 and 4 is that a definite engineering tradeoff exists in the choice of initial table angular velocities. If an experimental run of 50,000 seconds is acceptable, only 132,000 data points need be stored and analyzed. If mission constraints require a shorter experimental run, the penalty is a vast increase in the data storage and transmission requirements.

The simulation has dealt only with the case for accelerating tables. A corresponding case for decelerating tables exists. It is expected that the qualitative results would be similar to those which have been presented.

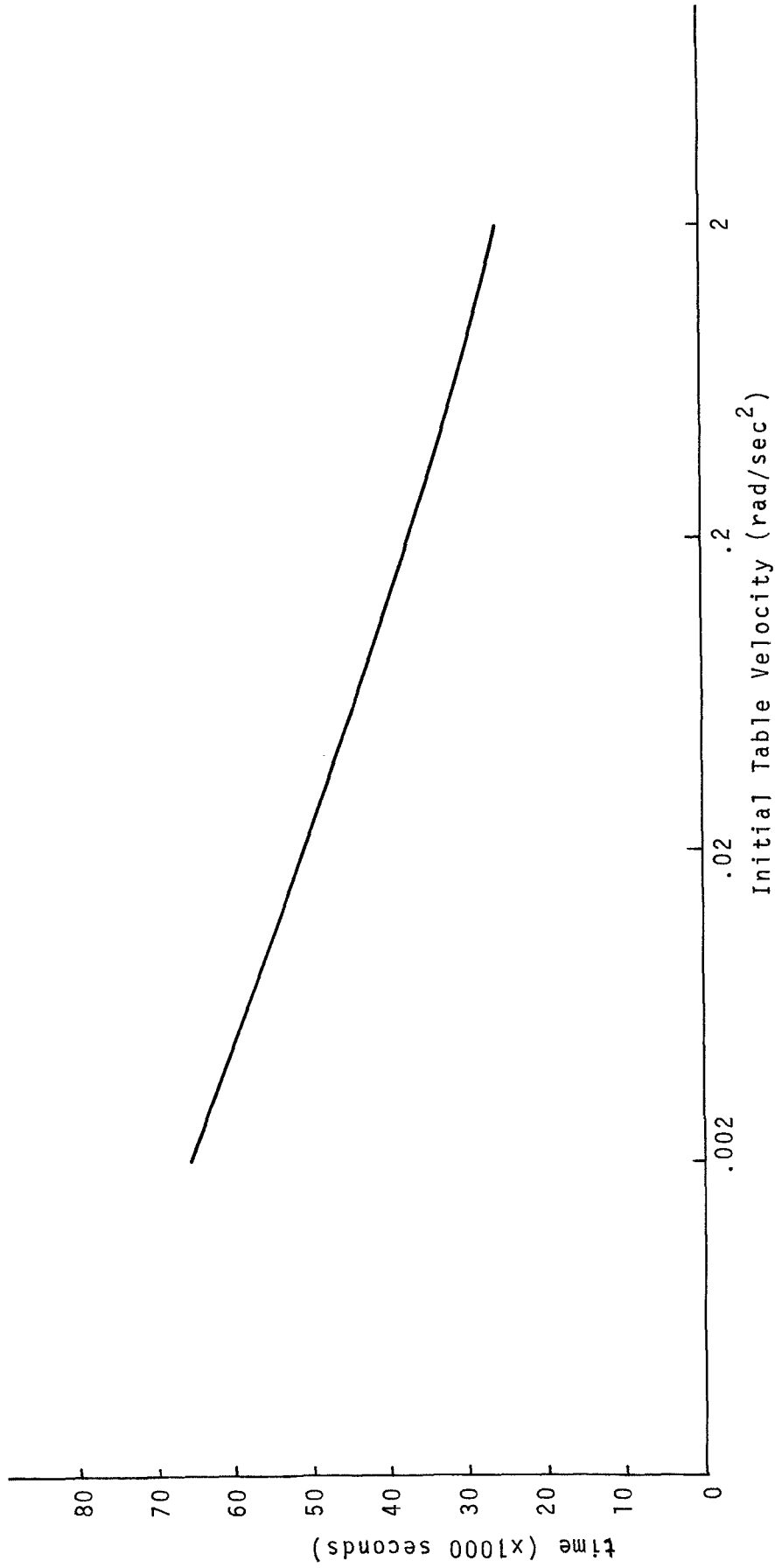


Figure 3 Time required to reduce σ_α to 10^{-16} rad/sec² as a function of initial table angular velocity. The system has 360 measurements per revolution with a measurement error standard deviation of one arc second.

DATA POINTS REQUIRED ($\times 10^5$)

100

50

20

10

5

2

1

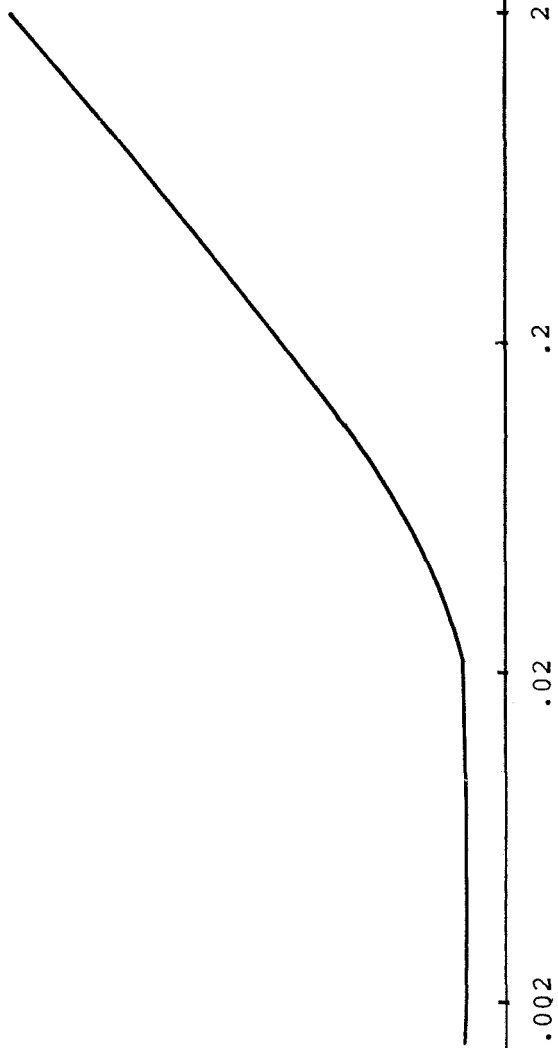


Figure 4 Total number of data points required to reduce σ_a to 10^{-16} rad/sec² as a function of initial table angular velocity. The system has 360 measurements per revolution with a measurement error standard deviation of one arc second.

4. References

1. Blicht, M.G., "The Feasibility of a Gravitational Clock to Test the General Theory of Relativity," S.M. Thesis in Physics, M.I.T., August 1969.
2. Rose, D.R., "A New Method for Determination of Newton's Gravitational Constant," D.Sc. Dissertation, University of Virginia, August 1969.
3. Roll, P.G., Krotkov, R., and Dicke, R.H., "The Equivalence of Inertial and Passive Gravitational Mass," *Annals of Physics*: 26, 442-517 (1964).
4. Blood, B.E., "An Elementary Analysis of the Adaptation of the Beams' Experimental Concept to a $\Delta G/G$ Detector to Be Used in Space," Measurement Systems Laboratory Report RN-60, June 1970.
5. Arabian, J.H., "Advanced Inertial Gyro Test Equipment Designs," Instrumentation Laboratory, E-1613, October 1964.
6. Green, E., and Grimm, M.J., "Density by Hydrostatic Weighing," *Metrologia*, Vol. 6, No. 4, October 1970.
7. Athans, M., and Falb, P.L., Optimal Control. New York: McGraw-Hill, 1966.
8. Bryson, A.E., and Ho, Y., Applied Optimal Control, Waltham, Massachusetts: Baisdell, 1969.
9. Forward, R.L., "Research toward Feasibility of an Instrument for Measuring Vertical Gradients of Gravity," Air Force Cambridge Research Laboratory Report 67-0631, October 1967.

Appendix A

Design for $\frac{\partial K}{\partial a} = 0$

The condition $\frac{\partial K}{\partial a} = 0$ is equivalent to $\frac{\partial \alpha}{\partial a} = 0$. If we set $i = 1$ in Eq.(1), we have an expression for the torque on one arm of the test body in the fields of four attracting masses. The angular acceleration,

$$\alpha = \frac{T}{I} = \frac{mMG}{m(\frac{2}{5}r_m^2 + a^2)} \sum_{j=1}^4 \frac{al[\delta_{oj}\sin\theta - \delta_{ej}\cos\theta]}{\left[\ell^2 + a^2 - 2al(\delta_{oj}\cos\theta + \delta_{ej}\sin\theta)\right]^{3/2}} \quad (A1)$$

Differentiating with respect to "a" gives us

$$\begin{aligned} \frac{1}{MG} \frac{\partial \alpha}{\partial a} &= \frac{\frac{2}{5}r_m^2 - a^2}{(\frac{2}{5}r_m^2 + a^2)^2} \sum_j \frac{1}{R_j^3} [-\delta_{oj}\sin\theta + \delta_{ej}\cos\theta] \\ &+ \frac{a}{(\frac{2}{5}r_m^2 + a^2)} \sum_j \frac{-3}{R_j^5} \left[al - \ell^2(\delta_{oj}\cos\theta + \delta_{ej}\sin\theta) \right] \left[-\delta_{oj}\sin\theta + \delta_{ej}\cos\theta \right] \end{aligned} \quad (A2)$$

in which

$$R_j^2 = a^2 + \ell^2 - 2al(\delta_{oj}\cos\theta + \delta_{ej}\sin\theta).$$

Setting $\frac{\partial \alpha}{\partial a} = 0$ and doing the summations gives us

$$\frac{r_m^2}{a^2} = \frac{5}{2} \frac{\frac{1+4h^2}{h} \left[\frac{1}{\cos\theta} \left(\frac{R_1^5}{R_3} - 1 \right) + \frac{1}{\sin\theta} \left(\frac{R_1^5}{R_2} - \frac{R_1^5}{R_4} \right) \right] + 5 \left[\left(1 + \frac{R_1^5}{R_3} \right) - \left(\frac{R_1^5}{R_2} + \frac{R_1^5}{R_4} \right) \right]}{\frac{1-2h^2}{h} \left[\frac{-1}{\cos\theta} \left(\frac{R_1^5}{R_3} - 1 \right) + \frac{1}{\sin\theta} \left(\frac{R_1^5}{R_2} - \frac{R_1^5}{R_4} \right) \right] - \left[\left(1 + \frac{R_1^5}{R_3} \right) - \left(\frac{R_1^5}{R_2} + \frac{R_1^5}{R_4} \right) \right]} \quad (A3)$$

in which $h = \frac{a}{\ell}$.

If we establish the condition $\frac{\partial \alpha}{\partial \theta} = 0$, then from Ref. 1 we have θ equal to some function of h or

$$\theta = f(h)$$

We can write Eq.(A3) as

$$\frac{r_m^2}{a^2} = \frac{5}{2} \frac{N(h)}{D(h)}, \quad (\text{A4})$$

since

$$\frac{R_1^5}{R_3^5} = \left[\frac{1 + h^2 - 2h \cos \theta}{1 + h^2 + 2h \cos \theta} \right]^{5/2} = \left[\frac{1 + h^2 - 2h \cos f(h)}{1 + h^2 + 2h \cos f(h)} \right]^{5/2}$$

Using the $\theta = f(h)$ shown in Fig. II of Ref. 4, we can calculate $\frac{r_m}{a}$ for $\frac{\partial \alpha}{\partial a} = 0$. These calculations reveal that we cannot get a real value for $\frac{r_m}{a}$ for any value of h .

If, however, we introduce another set of attracting masses, each with mass, M' at a distance ℓ' from the pivot, we can rewrite Eq.(A4) as

$$\frac{r_m^2}{a^2} = \frac{5}{2} \frac{N(h) + \frac{M'}{M} N(q)}{D(h) + \frac{M'}{M} D(q)} \quad (\text{A5})$$

in which

$$q = \frac{a}{\ell},$$

For the second set of masses we also have $\frac{\partial \alpha}{\partial \theta'} = 0$. Then we have

$$\theta' = f(q).$$

As a not necessarily optimum example, we choose

$$h = 0.5, \quad \theta = 19.95^\circ$$

$$q = 2.5, \quad \theta' = 21.45^\circ,$$

and $\frac{M'}{M} = .312.$

For these values we get

$$\frac{r_m}{a} = .256.$$

This example is illustrated in Fig. AI.

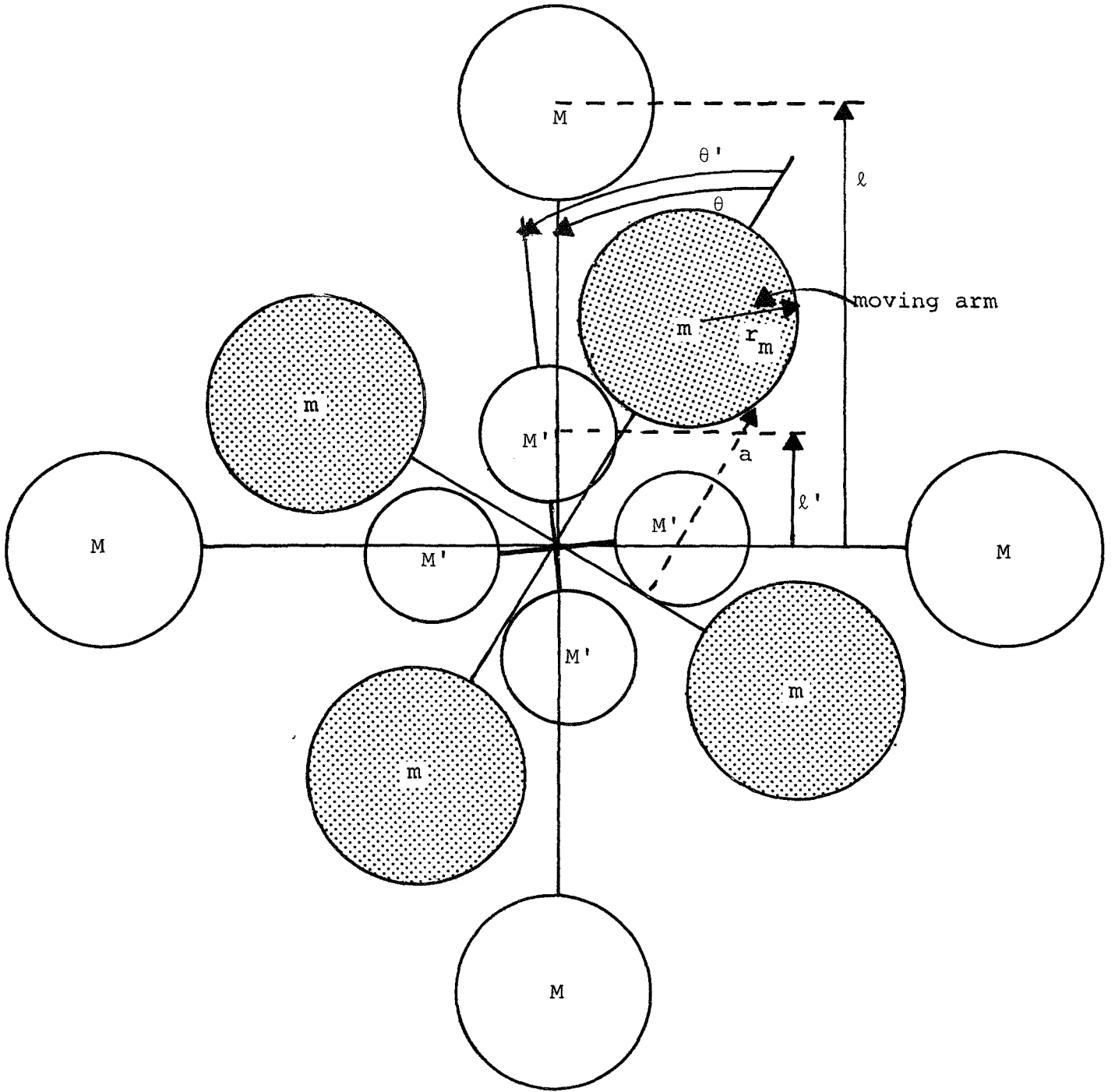


FIGURE A1 Example for $\frac{\partial \alpha}{\partial a} = 0$.

Appendix B
Suspension Stiffness

To calculate the required suspension stiffness to maintain $\frac{\Delta K}{K} < 10^{-10}$ (or equivalently $\frac{\Delta T}{T} < 10^{-10}$), we first calculate the effect of a small vector deflection, \underline{x} , of the center of the test body. Using the notation of Paragraph 1.1, we can write for the potential energy of the test body (in the field of the attaching masses)

$$P.E. = mMG \sum_{i=1}^4 \sum_{j=1}^4 \frac{1}{\{x^2 + a_i^2 + l_j^2 + 2a_i^T l_j + 2a_i^T x - 2l_j^T x\}^{1/2}} \quad (B1)$$

in which we have defined

$$R_{ij} = \sqrt{a_i^2 + l_j^2 - 2a_i^T l_j} \quad (B2)$$

to be the distance between the mass on the i^{th} arm and the j^{th} attaching mass.

Then

$$P.E. = mMG \sum_i \sum_j \frac{1}{R_{ij}} \left\{ \frac{1}{x^2 + 2(a_i^T - l_j^T)x} \right\}^{1/2} \quad (B3)$$

Now keeping terms to order of x^2

$$P.E. = mMG \sum_i \sum_j \frac{1}{R_{ij}} \left[1 - \frac{1}{2} \frac{x^2 + 2(a_i^T - l_j^T)x}{R_{ij}^2} \right] \quad (B4)$$

so we have

$$\Delta P.E. = \frac{mMG}{2} \sum_i \sum_j \frac{x^2}{R_{ij}^3} + mMG \sum_i \sum_j \frac{x^T (a_i - l_j)}{R_{ij}^3} \quad (B5)$$

By symmetry

$$\sum_i \sum_j \frac{a_i - l_j}{R_{ij}^3} \equiv 0$$

Then

$$\Delta P.E. = \frac{mMG}{2} \sum_i \sum_j \frac{x^2}{R_{ij}^3} \quad (B6)$$

To calculate ΔT we differentiate

$$\Delta T = \frac{d}{d\theta} \Delta P.E. = \frac{-mMG}{2} \sum_i \sum_j \frac{3x^2}{2R_{ij}^5} \frac{dR_{ij}^2}{d\theta} \quad (B7)$$

Using Eqs. B(1) and B(2) ($\underline{x} = 0$),

$$T = -mMG \sum_i \sum_j \frac{1}{2R_{ij}^3} \frac{dR_{ij}^2}{d\theta} \quad (B8)$$

Now

$$\frac{\Delta T}{T} = \frac{3}{2} x^2 \frac{\sum_i \sum_j R_{ij}^{-5} \frac{dR_{ij}^2}{d\theta}}{\sum_i \sum_j R_{ij}^{-3} \frac{dR_{ij}^2}{d\theta}} \quad (B9)$$

Doing the summations in B(9) for the example shown in Figure VIII, Reference 4 gives us

$$\frac{\Delta T}{T} \sim .1x^2$$

or for

$$\frac{\Delta T}{T} < 10^{-10}$$

$$x < 3 \cdot 10^{-3} \text{ cm.}$$

The total mass of the test body in Figure VIII, Reference 4 is 2.58Kg, so, for example, the suspension stiffness, k, needed to limit x in the face of an acceleration of 10^{-5} cm/sec² is

$$k = \frac{(2.58 \cdot 10^3) 10^{-5}}{310^{-5}}$$

$$= 890 \text{ dynes/cm.}$$

APPENDIX C

DIGITAL SIMULATION OF A SPACE EXPERIMENT
TO MEASURE THE NEWTONIAN GRAVITATIONAL
CONSTANT

RN-61

Digital Simulation of a Space Experiment
to Measure the Newtonian Gravitational Constant

by

Harold L. Jones

October 1970

Approved:

W. Markley

Director

Measurement Systems
Laboratory

Massachusetts Institute of Technology
Measurement Systems Laboratory
Cambridge, Massachusetts 02139

ABSTRACT

A digital simulation package has been developed in support of current Measurement System Laboratory research on an experiment to measure the Newtonian gravitational constant in earth orbit. The apparatus for the experiment is similar to that developed by J.W. Beams in an earth-fixed experiment.

The mathematical model upon which the simulation is based accounts for earth orbital dynamics, vehicle dynamics, and a generalized experimental configuration. The simulation package is structured to allow the user to make necessary modifications in the mathematical model relatively easily. The procedure for adding disturbance force models or modifying existing models is outlined.

ACKNOWLEDGEMENT

This work was performed under National Aeronautics and Space Administration contract NAS 9-8328 (MIT DSR 71390).

NOTE

This research note is one of a series of reports published by the MIT Measurement Systems Laboratory. The "RN" designation indicates a semi-formal presentation of research results. These presentations represent work in progress so the results are not necessarily complete or fully refined.

DIGITAL SIMULATION OF A SPACE EXPERIMENT
TO MEASURE THE NEWTONIAN GRAVITATIONAL CONSTANT

1.	Introduction	1
2.	Mathematical models	4
2.1	Coordinate systems	5
2.2	Dynamics for rotating coordinate systems	8
2.3	Control law	13
2.4	Force models	14
2.5	Vehicle motion	18
2.6	Orbit determination	18
3.	Program Implementation	21
3.1	Program structure and function.	23
3.2	Input/output specifications	28
3.3	Integration error analysis	31
4.	Possible Program Modifications	33
Appendix A	Source deck listing	37
B	Program variable definitions	39
C	Auxiliary subroutine functions	45
D	2 nd order Runge-Kutta	47

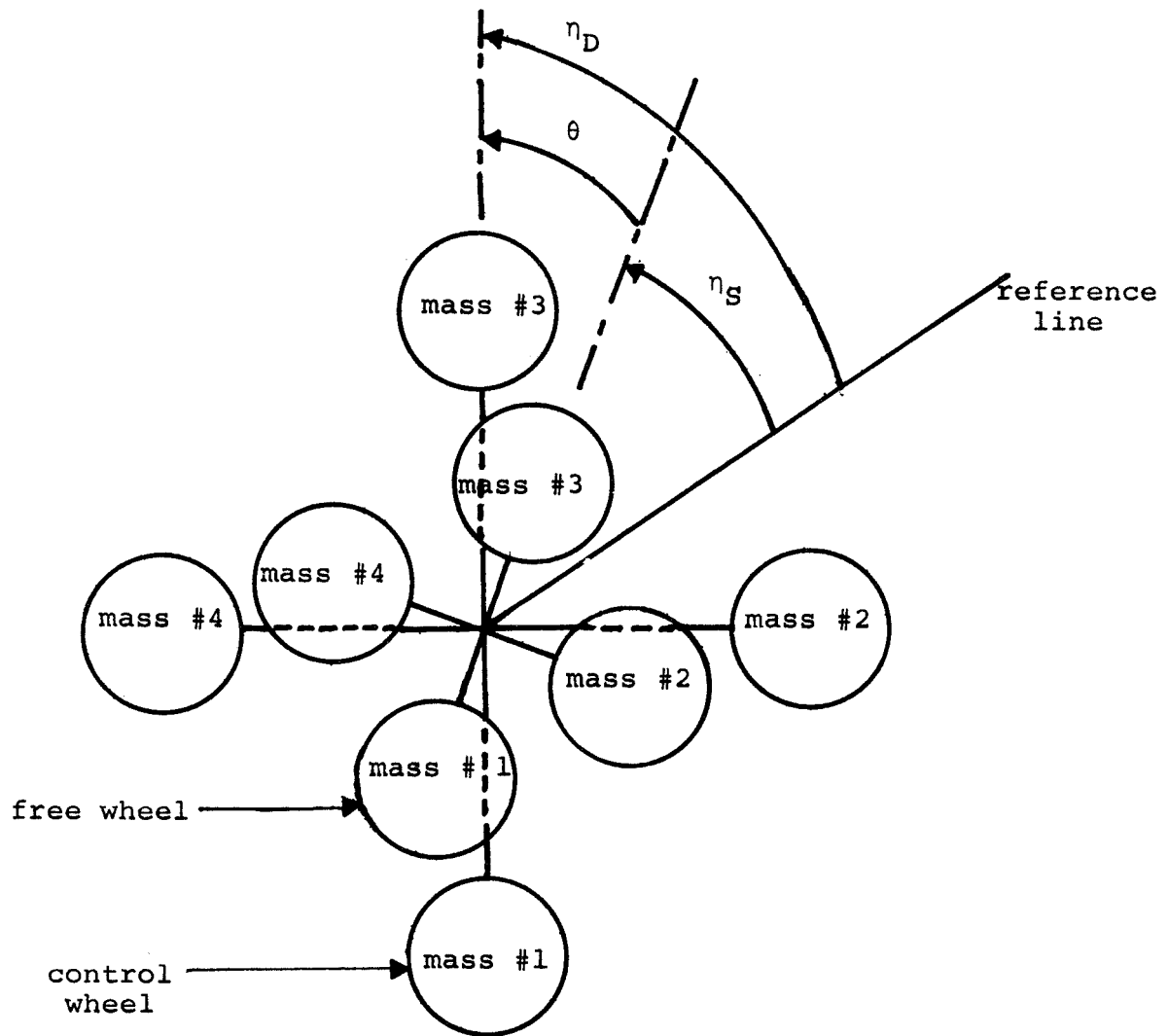


Figure 1 Sketch of a four-armed Beams-type experimental apparatus. The direction of rotation is counter-clockwise.

The feasibility of an experiment to measure the Newtonian Gravitational Constant, G , in earth orbit has been the subject of investigations at the Measurement Systems Laboratory by Blood [2], Chapman [3], and Lee [5]. The general experimental approach is to balance the gravitational force between two sets of calibrated masses by some precisely measurable inertial force. The literature should be consulted for a detailed analysis of the experimental concept.

One proposed experimental configuration is the apparatus used by J.W. Beams in an earth-fixed Cavendish experiment [7]. The apparatus consists of a set of masses mounted on the spokes of a suspended wheel with one degree of freedom about its axis of symmetry. The wheel is free to accelerate about that axis in response to externally applied torques. The control torque is provided by a second wheel which is rotated through an angle θ relative to the free wheel (See Figure 1.). The control wheel is servoed to maintain the angle θ near a nominal value, η_0 . The equations of motion for the free wheel are specified by:

$$I_M \ddot{\eta}_S = \frac{\partial (P.E.)}{\partial \theta} \quad (1)$$

where I_M is the moment of inertia of the free wheel,
P.E. is the potential energy of the free wheel in the field
of the control wheel, and
 $\ddot{\eta}_S$ is the angular acceleration of the free wheel.

In the absence of disturbing torques, the free wheel will experience a constant acceleration and the servo will provide an identical acceleration to the control wheel. The quantity $\ddot{\eta}_S$ is directly measurable within experimental uncertainties.

The intent of the digital simulation of the Beams experiment was to provide a general framework for the study of :

- 1) experiment sensitivity to disturbance effects, and
- 2) data reduction procedures required to minimize the effect of stochastic disturbances.

The simulation package developed has stressed a modular design concept to allow modification of the experiment model and the environment model with a minimum of knowledge of the program mechanics. Each of the environmental factors (atmospheric drag, earth gravity gradient, etc.) is defined independently as a subroutine

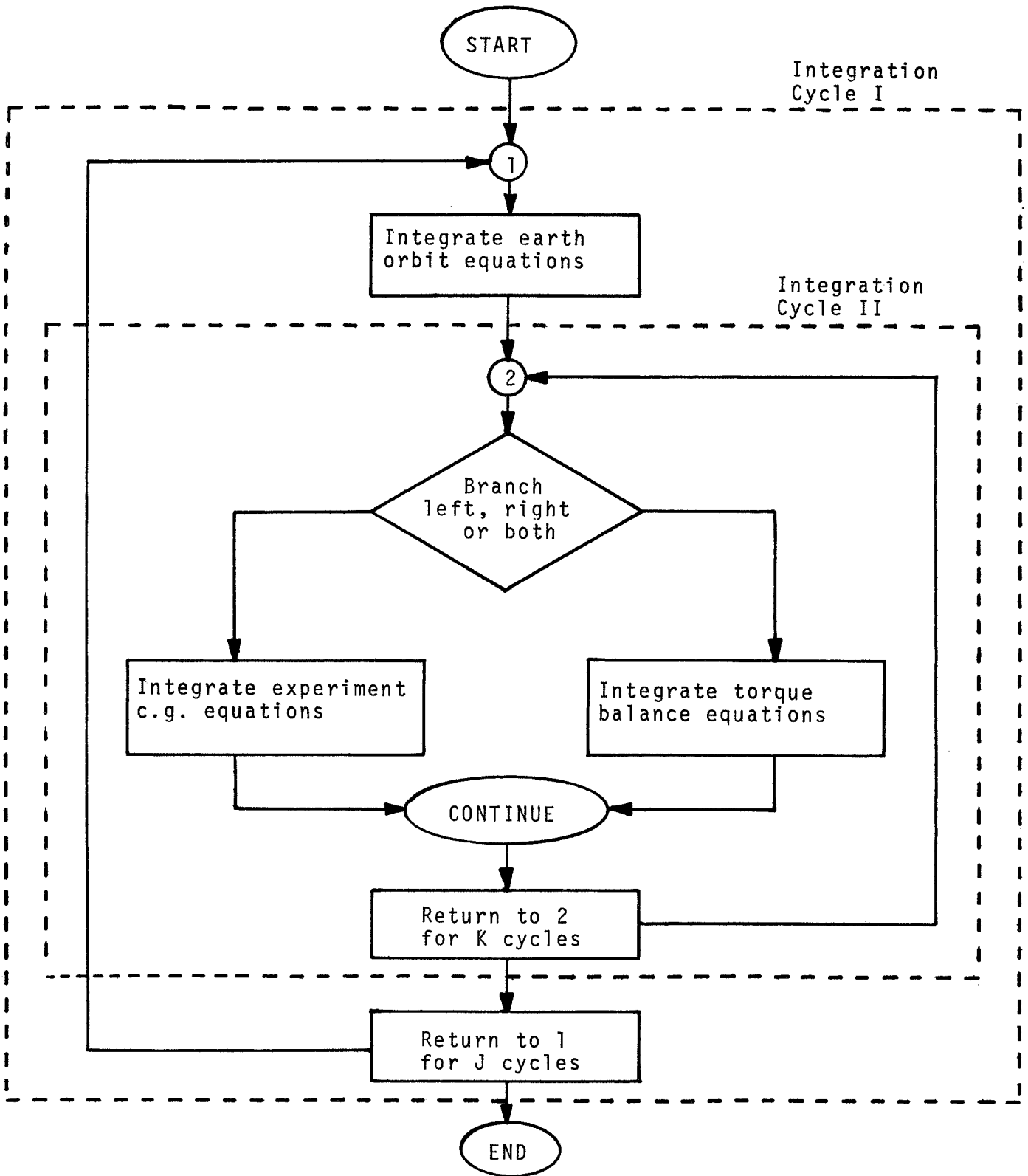


Figure 2. Macrostructure of the simulation package

The cycle II integrations (experiment c.g. equations and torque balance equation) are nested inside the cycle I integration (earth orbit equations) to allow different integration time intervals

with explicitly defined calling parameters. The shape of the two test wheels can be chosen arbitrarily without program modification if all test masses are spheres. Non-spherical test masses can be accommodated if a subroutine specifying the gravitational interaction between the two sets of masses is substituted for the model employed in the simulation. The experiment can be simulated in either free fall or bolted to the spacecraft without program modification.

The subroutines modeling the measurement system for $\ddot{\eta}_S$ and the data reduction procedures are under development and are not included in the present package. They will be added to a revised simulation package at a later date.

The macrostructure of the program is governed by the three sets of integrations performed involving respectively:

- 1) the orbital equations of motion of the spacecraft,
- 2) the equations of motion of the experiment c.g. with respect to the spacecraft c.g. if the experiment is in free fall, and
- 3) the equations of motion of the fixed and the free wheels relative to the experiment c.g. (torque balance equations).

As indicated in Figure 2, the integrations involving the experiment c.g. motion and the torque balance are nested within the earth orbit integration cycle to allow an integration interval which is a submultiple of the earth orbit integration interval. The earth orbit parameters are interpolated to provide the increased data density required for the nested integrations. The experiment c.g. integrations and torque balance integrations are performed in parallel if both are required. The integration algorithm employs a 2nd order Runge-Kutta procedure. The integration interval for both the inner and outer loops is directly accessible as a program input parameter. Throughout this report, the outer and inner integration loops will be referred to as cycle I and cycle II respectively.

The mathematical models upon which the simulation is based are developed in Section 2. A modular flow chart for the program is provided in Section 3 along with an input/output specification and comments upon the range of problems the simulation is directly applicable to. Section 4 is of interest only if modifications to these models are being considered.

2. Mathematical Models

The mathematical models upon which the simulation is based are detailed in this section. The coordinate frames are defined in Section 2.1.

The simplest model is the equation of motion for the earth orbit integration:

$$\underline{a}_E = \underline{g} + \underline{a}_D \quad (2)$$

where \underline{a}_E is the acceleration of the spacecraft c.g., \underline{g} is the earth gravitation, and \underline{a}_D is atmospheric drag. The integration is performed in the I-frame. The algorithm for the integration is detailed in Appendix D. The models for \underline{g} and \underline{a}_D are specified in Section 2.4.

The equation of motion for the free wheel is given by:

$$\ddot{\eta}_S = \frac{1}{I_M} \sum_J m_{JS} (\underline{a}_{J/N} \times \underline{R}_{J/N}) \quad (3)$$

where I_M is the total inertia of the wheel,
 m_{JS} is the mass of the J^{th} sphere of the free wheel,
 $\underline{R}_{J/N}$ is the vector to the J^{th} sphere from the origin of the N-frame, and
 $\underline{a}_{J/N}$ is the acceleration of the J^{th} sphere as seen in the N-frame.

The N-frame is the reference coordinate system for the integration. The relationships defining $\underline{a}_{P/N}$ and $\underline{R}_{P/N}$ for an arbitrary point P in the N-frame are given in Section 2.2.

The equation of motion for the experiment c.g. is derived in Section 2.2.

The mathematical models described in this section deal with some physical aspects of the experiment and its environment analytically, some in an approximate manner, and some not at all. In the latter two cases it is conceivable that the model would have to be expanded in order to accurately describe certain phenomena. It is hoped that if the user can adequately describe the necessary expansions mathematically, Sections 3 and 4 will make the manner in which the program can be modified apparent.

2.1 Coordinate Systems

For purposes of generality the program maintains six coordinate systems with sufficient transformation matrices to facilitate a coordinate transformation between any two frames. In addition, the O-frame is directly calculable using the E-frame and the true anomaly, f_0 , if it is required. The frames available are described in Table 1.

Frame	Type	z-axes	REFERENCE	
			x-axes	y-axes
I	inertial, earth centered	north	complete triad	complete triad
E	inertial, earth centered	orbital angular momentum vector	orbit perigee	complete triad
O	rotating with respect to E, earth centered	angular momentum vector	vector to spacecraft c.g.	complete triad
B	spacecraft centered, fixed to spacecraft	complete triad	complete triad	longitudinal axis of spacecraft
N	nonrotating with respect to B, experiment c.g. centered	axis of rotation of experiment	complete triad	complete triad
D	experiment c.g. centered, fixed to control wheel	axis of rotation of experiment	complete triad	complete triad
S	experiment c.g. centered, fixed to free wheel	axis of rotation of experiment	complete triad	complete triad

TABLE 1 Coordinate frames maintained in simulation. The essential axis orientations are specified. The remaining axis orientations are chosen to complete a right-handed coordinate system.

The coordinate transformation matrices maintained by the simulation are listed in Table 2. The algorithm for calculating C_I^E is provided in 2.6 where the general problem of orbital parameter determination is dealt with. C_B^N is time invariant. C_D^S and C_N^S are calculated explicitly from (4) and (5) respectively if the torque

TRANSFORMATION MATRIX	FUNCTION	COMPUTATION METHOD	COMPUTATION INTERVAL
C_I^E	from I to E	explicit	start only
C_B^N	from B to N	-----	-----
C_D^S	from D to S	explicit	half cycle II
C_N^S	from N to S	explicit	half cycle II
C_E^S	from E to S	update	half cycle II
C_B^S	from B to S	explicit	half cycle II
C_E^B	from E to B	update	half cycle II
$C_E^{B'}$	from E to B	update	half cycle II

TABLE 2 Coordinate transformation matrices maintained in simulation.

balance equations are being integrated and not otherwise:

$$C_D^S = \begin{bmatrix} \cos\theta & -\sin\theta & 0 \\ \sin\theta & \cos\theta & 0 \\ 0 & 0 & 1 \end{bmatrix} \quad (4)$$

$$C_N^S = \begin{bmatrix} \cos\eta_S & \sin\eta_S & 0 \\ -\sin\eta_S & \cos\eta_S & 0 \\ 0 & 0 & 1 \end{bmatrix} \quad (5)$$

C_B^S and C_E^S are computed as products:

$$C_B^S = C_N^S C_B^N \quad (6)$$

$$C_E^S = C_B^S C_E^B \quad (7)$$

when the torque balance equations are integrated. C_E^B is calculated from the update algorithm:

$$C_E^B(t + \Delta t) = (I + \Delta t \underline{\psi}_{EB}^B)^T C_E^B(t) \quad (8)$$

with:

$$\underline{\psi}_{EB}^B = \begin{bmatrix} 0 & -\psi_Z^B & \psi_Y^B \\ \psi_Z^B & 0 & -\psi_X^B \\ -\psi_Y^B & \psi_X^B & 0 \end{bmatrix} \quad (9)$$

where $\underline{\psi}^B$ is the angular rate of the B-frame with respect to the E-frame coordinatized in the B-frame, Δt is the update interval, and I is the identity matrix.

The integrations in cycle II are only approximately simultaneous and it is necessary to maintain C_E^B for the torque balance integrations and $C_E^{B'}$ for the c.g. integrations.

2.2 Dynamics for Rotating Coordinate Systems

If the spacecraft is maintained in a true inertial mode the dynamics of the experiment c.g. motion and of the torque balance can be described by a linear relationship if time histories for the inertial forces are known. If the spacecraft is to be maintained in a non-inertial mode, however, or if vehicle motion disturbances in an essentially inertial mode are to be analyzed, then it is necessary to consider the form of the dynamical relationships as viewed in the rotating coordinate system attached to the spacecraft. The development of this relationship requires consideration of the dynamics of several intermediate coordinate systems.

O-frame--The O-frame is earth-centered and rotating with an angular velocity $\underline{\Omega}$ relative to the earth-centered I-frame. The state vector relationships are given by (10):

$$\begin{aligned}\underline{R}_I &= \underline{R}_O \\ \underline{V}_I &= \underline{V}_O + \underline{\Omega} \times \underline{R}_O \\ \underline{a}_I &= \underline{a}_O + \frac{d\underline{\Omega}}{dt} \times \underline{R}_O + 2\underline{\Omega} \times \underline{V}_O + \underline{\Omega} \times (\underline{\Omega} \times \underline{R}_O)\end{aligned}\tag{10}$$

where the subscripts denote the frame in which the quantity is observed.

V-frame--The V-frame is a spacecraft-centered, local vertical navigation system. It is linearly accelerating, but non-rotating with respect to the O-frame. The state vectors in terms of the V-frame are specified by:

$$\begin{aligned}
\underline{R}_O &= \underline{R}_V + \underline{R}_{P/V} \\
\underline{V}_O &= \underline{V}_V + \underline{V}_{P/V} \\
\underline{a}_O &= \underline{a}_V + \underline{a}_{P/V}
\end{aligned}
\tag{11}$$

where \underline{R}_V , \underline{V}_V , and \underline{a}_V specify the state of the V-frame origin (spacecraft c.g.) and $\underline{R}_{P/V}$, $\underline{V}_{P/V}$, and $\underline{a}_{P/V}$ specify the state of the experiment at P with respect to that origin (Figure 3a). For the torque balance equation, P is the coordinates of one of the free wheel test masses (Equation 3).

The acceleration \underline{a}_V can be determined from (10) by considering spacecraft c.g. motions, i.e. $\underline{R}_{P/V}$, $\underline{V}_{P/V}$, and $\underline{a}_{P/V}$ are zero:

$$\underline{a}_V = \underline{a}_{g_V} + \underline{a}_D - \frac{d\Omega}{dt} \times \underline{R}_V - 2\Omega \times \underline{V}_V - \Omega \times (\Omega \times \underline{R}_V)
\tag{12}$$

where \underline{a}_{g_V} is the primary earth gravitational force at the spacecraft c.g., and \underline{a}_D is the atmospheric drag at the c.g.

B-frame--The B-frame is a vehicle-centered, vehicle-fixed coordinate system rotating with an angular velocity $\underline{\Psi}$ relative to the V-frame. The state is specified relative to the state observed in the V-frame by:

$$\begin{aligned}
\underline{R}_{P/V} &= \underline{R}_B \\
\underline{V}_{P/V} &= \underline{V}_B + \underline{\Psi} \times \underline{R}_B \\
\underline{a}_{P/V} &= \underline{a}_B + \frac{d\Psi}{dt} \times \underline{R}_B + 2\underline{\Psi} \times \underline{V}_B + \underline{\Psi} \times (\underline{\Psi} \times \underline{R}_B)
\end{aligned}
\tag{13}$$

N-frame--The N-frame is centered at the experiment and non-rotating with respect to the B-frame (Figure 3b). If the experiment is floating free in the spacecraft the N-frame will translate linearly with respect to the B-frame.

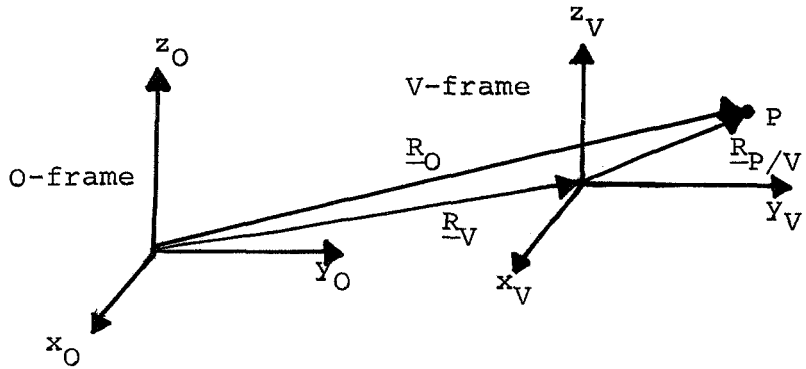


Figure 3a Translation of V-frame with respect to O-frame.

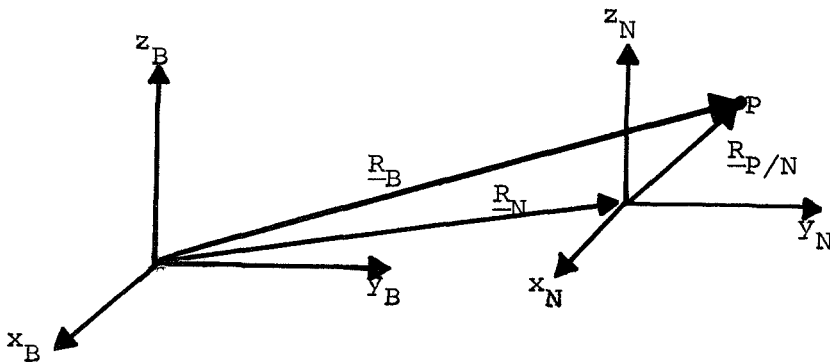


Figure 3b Translation of N-frame with respect to B-frame.

The state for this general case is given by:

$$\begin{aligned}
 \underline{R}_B &= \underline{R}_{P/N} + \underline{R}_N \\
 \underline{V}_B &= \underline{V}_{P/N} + \underline{V}_N \\
 \underline{a}_B &= \underline{a}_{P/N} + \underline{a}_N
 \end{aligned}
 \tag{14}$$

where \underline{R}_N , \underline{V}_N , and \underline{a}_N specify the state of the N-frame origin and $\underline{R}_{P/N}$, $\underline{V}_{P/N}$, and $\underline{a}_{P/N}$ specify the state of the experiment at P with respect to that origin. In the case where the experiment is free, the acceleration, \underline{a}_N , of the c.g. is \underline{a}_B if $\underline{R}_{P/N}$, $\underline{V}_{P/N}$, and $\underline{a}_{P/N}$ are set equal to zero. Substitution of (10) and (12) into (13) and (14) and rearranging yields:

$$\begin{aligned}
 \underline{a}_N &= \underline{a}_{I_B} - \underline{a}_{g_V} - \underline{a}_D - \frac{d\Omega}{dt} \times \underline{R}_N - \underline{\Omega} \times (\underline{\Omega} \times \underline{R}_N) - 2\underline{\Omega} \times (\underline{V}_N + \underline{\Psi} \times \underline{R}_N) \\
 &\quad - \frac{d\Psi}{dt} \times \underline{R}_N - 2\underline{\Psi} \times \underline{V}_N - \underline{\Psi} \times (\underline{\Psi} \times \underline{R}_N)
 \end{aligned}
 \tag{15}$$

where \underline{a}_{I_B} represents the inertially referenced forces acting on the experiment c.g.

The only forces acting on the experiment c.g. are the primary gravitation of the earth and the primary gravitation of the spacecraft. For small displacements of the experiment from the spacecraft c.g. the earth gravitational effect can be modeled as a gravity gradient. The first two terms of (15) then become:

$$\underline{a}_{I_B} - \underline{a}_{g_V} = G_{E-N} \underline{R}_N + \underline{a}_{SC_N}
 \tag{16}$$

where \underline{a}_{SC_N} is the spacecraft gravitational acceleration at \underline{R}_N , and

G_E is the earth gravity gradient matrix evaluated at the spacecraft c.g. (Section 2.4).

The equations of motion for the experiment c.g. when the experiment is free are then given by:

$$\begin{aligned} \underline{a}_N = & \underline{a}_{SC_N} + G_E \underline{R}_N - \underline{a}_D - \frac{d\underline{\Omega}}{dt} \times \underline{R}_N - \underline{\Omega} \times (\underline{\Omega} \times \underline{R}_N) - 2\underline{\Omega} \times (\underline{V}_N + \underline{\Psi} \times \underline{R}_N) \\ & - \frac{d\underline{\Psi}}{dt} \times \underline{R}_N - 2\underline{\Psi} \times \underline{V}_N - \underline{\Psi} \times (\underline{\Psi} \times \underline{R}_N) \end{aligned} \quad (17)$$

In order to write the torque balance equations it is necessary to express the acceleration $\underline{a}_{P/N}$ as seen in the N-frame. The expression for $\underline{a}_{P/N}$ is:

$$\underline{a}_{P/N} = \underline{a}_{P/V} - \frac{d\underline{\Psi}}{dt} \times (\underline{R}_{P/N} + \underline{R}_N) - 2\underline{\Psi} \times (\underline{V}_{P/N} + \underline{V}_N) - \underline{\Psi} \times (\underline{\Psi} \times (\underline{R}_{P/N} + \underline{R}_N)) - \underline{a}_N \quad (18)$$

For the case where the c.g. is free \underline{a}_N is given by (17). Substitution of \underline{R}_N and \underline{V}_N using (11), (13), and (14) and inclusion of the sphere gravitational interaction in the inertial force model yields ultimately:

$$\begin{aligned} \underline{a}_{P/N} = & G_E \underline{R}_{P/N} + \underline{a}_{SG} + G_{SC} \underline{R}_{P/N} - \frac{d\underline{\Omega}}{dt} \times \underline{R}_{P/N} - 2\underline{\Omega} \times (\underline{V}_{P/N} + \underline{\Psi} \times \underline{R}_{P/N}) \\ & - \underline{\Omega} \times (\underline{\Omega} \times \underline{R}_{P/N}) - \frac{d\underline{\Psi}}{dt} \times \underline{R}_{P/N} - 2\underline{\Psi} \times \underline{V}_{P/N} - \underline{\Psi} \times (\underline{\Psi} \times \underline{R}_{P/N}) \end{aligned} \quad (19)$$

where \underline{a}_{SG} is the sphere gravitational interaction, and G_{SC} is the spacecraft gravity gradient matrix evaluated at the experiment c.g.

For the case when the experiment is mounted rigidly in the spacecraft, $\underline{a}_N = 0$ and the torque balance equations become:

$$\begin{aligned}
\underline{a}_{P/N} = & G_E(\underline{R}_N + \underline{R}_{P/N}) + \underline{a}_{SG} + \underline{a}_{SC_P} - \underline{a}_D - \frac{d\underline{\Omega}}{dt} \times (\underline{R}_{P/N} + \underline{R}_N) \\
& - 2\underline{\Omega} \times (\underline{\Psi} \times (\underline{R}_N + \underline{R}_{P/N})) - \underline{\Omega} \times (\underline{\Omega} \times (\underline{R}_N + \underline{R}_{P/N})) \\
& - \frac{d\underline{\Psi}}{dt} \times (\underline{R}_{P/N} + \underline{R}_N) - \underline{\Psi} \times (\underline{\Psi} \times (\underline{R}_{P/N} + \underline{R}_N))
\end{aligned} \tag{20}$$

where \underline{a}_{SC_P} is the spacecraft gravitation at the point P.

(17), (19), and (20) are the state equations instrumented in the simulation. When the experiment is free, (17) and (19) are integrated in an approximately simultaneous fashion.

2.3 Control Law

To maintain a constant torque interaction between the two wheels, it is necessary to maintain the angular separation at some nominal value η_0 . The incremental control law employed in the simulation attempts to drive the error signal, $\eta_0 - \theta$, at the beginning of the integration interval to null at the end of the interval. The law assumes that the disturbances are zero mean and that all torques are constant in the interval. The angular acceleration of the control wheel is then:

$$\ddot{\eta}_D = \frac{(\eta_0 - (\eta_D - \eta_S)) - \Delta t(\dot{\eta}_D - \dot{\eta}_S) + .5 \Delta t^2 \ddot{\eta}_S}{.5 \Delta t^2} - \dot{\psi}_{N_Z} - \dot{\Omega}_{N_Z} \tag{21}$$

where Δt is the integration interval,
 $\dot{\Omega}_{N_Z}$ is the angular acceleration of the O-frame with respect to the E-frame resolved along the Z-axis of the N-frame, and
 $\dot{\psi}_{N_Z}$ is the angular acceleration of the B-frame with respect to the V-frame resolved along the z-axis of

the N-frame.

The control $\ddot{\eta}_D$ is computed at the beginning of each cycle II integration. The error signal, $\eta_0 - \theta$, used for the control law is precise. For some applications it may be desirable to replace this exact value with a noise corrupted measurement (See Section 4

2.4 Force Models

The mathematical models discussed to this point have been discrete time expressions of analytical relationships and will presumably converge as the integration time increment becomes small. The force models described below are approximate relationships. The accuracy of the simulation is a function both of the integration time increment and of the precision of the force model. It is presumed that the user is capable of supplying a more precise model where necessary.

The primary earth gravity field model at the spacecraft c.g. is:

$$\underline{g} = - \frac{GM_E}{|\underline{R}_V|^3} \underline{R}_V \quad (22)$$

where M_E is the mass of the earth. The computation is performed in the I-frame. If a more precise model is desired, the additional elements must be specified in the I-frame.

The gradient matrix is specified by:

$$G_E = \left. \frac{\partial \underline{g}}{\partial \underline{R}} \right|_{\underline{R} = \underline{R}_V} \quad (23)$$

In component form the gradient model is:

$$G_{Eij} = - \frac{GM_E}{|\underline{R}_V|^3} \left[\delta_{ij} - \frac{3}{|\underline{R}_V|^2} R_{Vi} R_{Vj} \right] \quad (24)$$

where $\delta_{ij} = 1$ if $i = j$ and zero otherwise, and R_{Vi} and R_{Vj} are the i^{th} and j^{th} components of \underline{R}_V respectively.

The force model for the gravitational interaction between the two wheels assumes that all of the test masses can be modeled as point masses. The acceleration of the J^{th} test mass of the free wheel due to the test masses of the control wheel is:

$$\underline{a}_{SG_J} = - \sum_K \frac{GM_{KD}}{|\underline{R}_{J/K}|^3} \underline{R}_{J/K} \quad (25)$$

where M_{KD} is the mass of the K^{th} sphere of the control wheel, and $\underline{R}_{J/K}$ is the vector distance from the J^{th} sphere of the free wheel to the K^{th} sphere of the control wheel, coordinatized in the S-frame.

The angular acceleration of the free wheel is computed from the torque balance equation (3) using (25). If the test masses cannot be modeled as point masses, (25) must be modified.

The simulation as presently implemented does not include a spacecraft gravity model. Development of a model is currently in progress.

The drag model in the simulation is specified by:

$$\underline{a}_D = \frac{\frac{1}{2} \rho C_d A \underline{V}_R^2}{M_S} \quad (26)$$

where M_S is the mass of the spacecraft,
 ρ is the atmospheric density,
 C_d is the drag coefficient,
 A is the cross-sectional area of the spacecraft
perpendicular to \underline{V}_R , and
 \underline{V}_R is the relative wind at the spacecraft c.g.

The relative wind is given as the vector difference:

$$\underline{V}_R = \underline{V}_V - \underline{V}_A \quad (27)$$

where \underline{V}_A is the atmospheric velocity and is a function both of latitude and altitude. In the simulation \underline{V}_A is zero.

For a circularly symmetrical spacecraft, the cross-sectional area is a function of the angle between the velocity vector, \underline{V}_R and the y-axis of the spacecraft. Defining:

$$C_{22} = \frac{\underline{V}_{RB}_y}{|\underline{V}_R|} \quad (28)$$

where \underline{V}_{RB_Y} is the y-component of \underline{V}_R coordinatized in the B-frame, then:

$$A = A_1 C_{22} + A_2 (1 - C_{22}^2)^{\frac{1}{2}} \quad (29)$$

where A_1 is the cross-sectional area perpendicular to the y-axis of the B-frame and A_2 is the cross-sectional area for any plane containing the y-axis. The cosine function C_{22} is maintained in the simulation but is not used in the drag model.

The drag model presently incorporated in the simulation does not account for either atmospheric density variations or cross-sectional area variations or relative wind considerations. The model is:

$$\underline{a}_D = 1.5 \times 10^{-17} |\underline{V}_V| \underline{V}_V \quad (30)$$

This model is within the drag range estimated by Lee [6] and summarized in Table 3.

- Conditions:
- (1) Circular orbit at 500 km.
 - (2) Drag coefficient = 2.3
 - (3) Mass of spacecraft = 4.54×10^7 gm.
 - (4) Velocity = 7.64×10^5 cm/sec²

Parameters	Probable (90 %) Lower Limit	Mean	Probable (90 %) Upper Limit
Exospheric Temp.	580 °K	812 °K	1125 °K
Density	2.0×10^{-17} gm./cm ³	1.7×10^{-16} gm./cm ³	1.1×10^{-15} gm./cm ³
Area (projected)	2.92×10^5 cm ²	5×10^5 cm ²	7.35×10^5 cm ²
Drag Acceleration	8.6×10^{-8} cm./sec ²	1.3×10^{-6} cm./sec ²	1.2×10^{-5} cm./sec ²
	8.8×10^{-11} g's	1.3×10^{-9} g's	1.2×10^{-8} g's

TABLE 3 Expected drag accelerations for Skylab B [6].

2.5 Vehicle Motion

The choice of vehicle motion model is somewhat arbitrary. The model that has been implemented is an inertial hold mode with no disturbance forces. The initial orientation of the spacecraft is user specified. In applying the simulation, the user may prefer to substitute a vehicle motion time history for the present model.

2.6 Orbit Determination

The orbit determination routines perform two functions:

- 1) computation of orbital parameters from \underline{R}_V and \underline{V}_V , and
- 2) updating the true anomaly to determine the relative position of the spacecraft in the orbit.

The second function is performed at the start of each pass through cycle I. The computation of orbital parameters is carried out only when a flag is set by the main program during execution. As currently implemented, the flag is set only to initialize the orbit. If

the flight profile to be simulated involves large drag forces or orbit changes, the main program must be altered to set the flag at the appropriate times (See Section 4).

The orbital parameters of interest are the eccentricity, e ; the true anomaly, f_0 ; the angular rate, Ω ; the angular acceleration, $\dot{\Omega}$; and the coordinate transformation matrix, C_I^E . All computations are carried out in the I-frame. The eccentricity is defined as the positive root of:

$$e^2 = \left[\frac{|\underline{h}|^2}{GM_E |\underline{R}_V|} - 1 \right]^2 + \left[\frac{|\underline{h}|}{GM_E |\underline{R}_V|} \underline{R}_V \cdot \underline{V}_V \right]^2 \quad (31)$$

where the massless orbital angular momentum is defined by:

$$\underline{h} = \underline{R}_V \times \underline{V}_V \quad (32)$$

The true anomaly can be defined uniquely from the two equations:

$$\begin{aligned} \sin f_0 &= \frac{|\underline{h}|}{GM_E e |\underline{R}_V|} \underline{R}_V \cdot \underline{V}_V \\ \cos f_0 &= \frac{|\underline{h}|^2}{GM_E e |\underline{R}_V|} - \frac{1}{e} \end{aligned} \quad (33)$$

The orbital angular rate and acceleration are given respectively by:

$$\Omega = \Omega_0 (1 - e^2)^{-3/2} (1 - e \cos f_0)^2 \quad (34)$$

and:

$$\dot{\Omega} = -2\Omega_0^2 e(1 - e^2)^{-3/2} (1 - e \cos f_0) \sin f_0 \quad (35)$$

where Ω_0 is the average angular rate:

$$\Omega_0 = \frac{(GM_E)^2 (1 - e^2)^{3/2}}{|\underline{h}|^3} \quad (36)$$

The coordinate transformation matrix, C_I^E , is determined by computing in the I-frame the unit vectors parallel to the three axes of the E-frame. The unit vector in the direction of the angular momentum is obviously:

$$\underline{i}_\xi = \frac{\underline{h}}{|\underline{h}|} \quad (37)$$

The unit vector directed at the orbital perigee from the origin is given by:

$$\underline{i}_\zeta = \frac{1}{GM_E e} \left[\left(|\underline{V}_V|^2 - \frac{GM_E}{|\underline{R}_V|} \right) \underline{R}_V - (\underline{R}_V \cdot \underline{V}_V) \underline{V}_V \right] \quad (38)$$

and the third vector is formed by the cross-product:

$$\underline{i}_\eta = \underline{i}_\zeta \times \underline{i}_\xi \quad (39)$$

The coordinate transformation matrix is then specified by:

$$C_I^E = \begin{bmatrix} i_{\xi_1} & i_{\xi_2} & i_{\xi_3} \\ i_{\eta_1} & i_{\eta_2} & i_{\eta_3} \\ i_{\zeta_1} & i_{\zeta_2} & i_{\zeta_3} \end{bmatrix} \quad (40)$$

3. Program Implementation

The specific structure of the source program is presented in this section and in Section 4. No detailed algorithm is presented; however, the program is discussed in sufficient detail to permit relatively easily the interchange of mathematical models.

The source language for the simulation is FORTRAN IV. The program was written and tested under the G-level compiler on the IBM 360/65 at MIT IPC. The standard IBM double precision library function package is required for execution.

The simulation is organized using a modular concept to facilitate program modification. The source code consists of a main program and 21 subroutines. The main program performs Input/Output operations, program initialization, and sequencing of the integration cycles. Each of the 21 subroutines is used to perform a specific function, e.g. ACCEL computes the accelerations at the test masses of the free wheel. Under certain program options, output is generated from the subroutines. All state variables and most data for the computations and output are passed through COMMON to facilitate access to the data by all subroutines. Control parameters are passed to the subroutines as dummy arguments in the calling sequence. These are discussed in Appendix A. If program modifications are made requiring state variables not available in

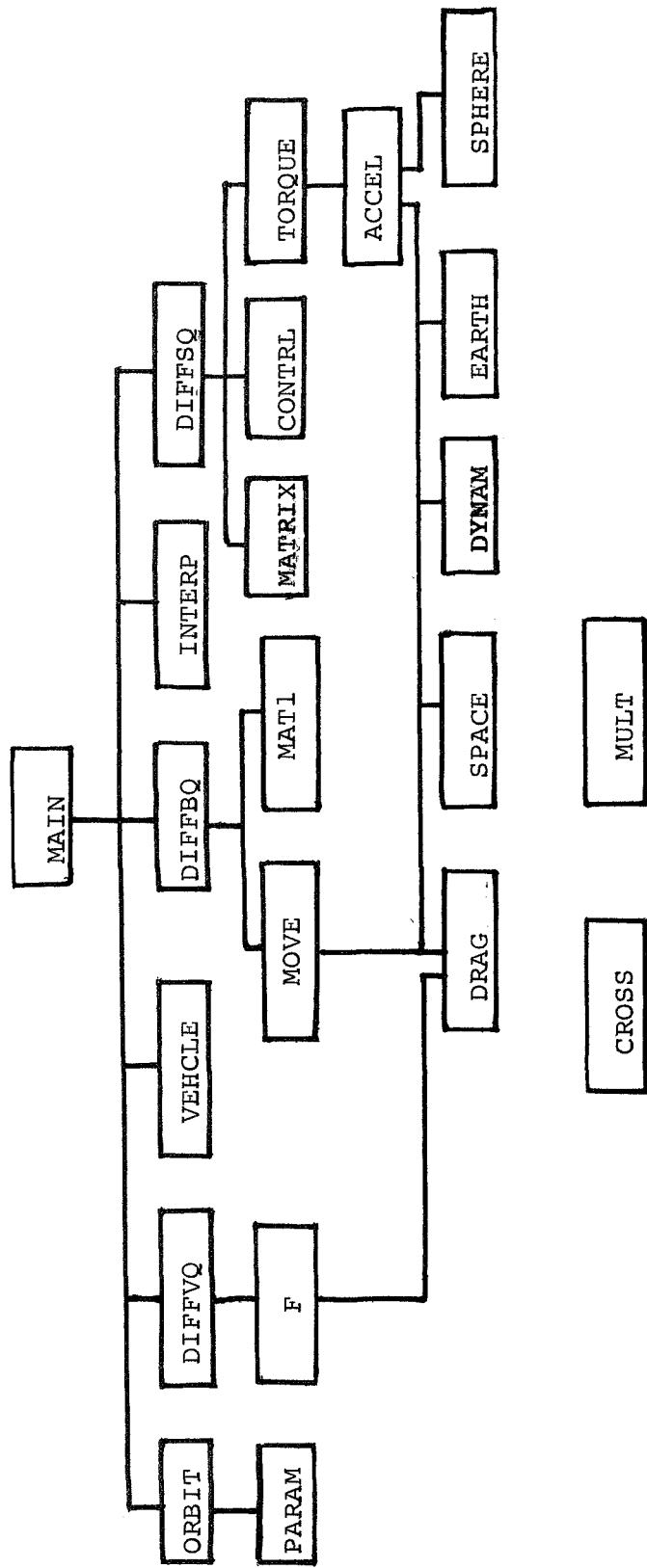


Figure 4 Control structure for the simulation package. A subroutine can be called only by a subroutine to which it is connected from above. CROSS and MULT are matrix manipulation subroutines called by several other subroutines.

COMMON, then those variables are not computed in the present package and must be supplied by an addition subroutine. The list of COMMON variables along with definitions and the subroutines in which they are computed is supplied in Appendix B.

3.1 Program Structure and Function

The control sequence for the simulation is depicted schematically in Figure 4. A subroutine can be called by any subroutine which is directly above it on the control tree. For instance, DRAG can be called only by F, MOVE, or ACCEL. Upon exit the subroutine always returns control to the subroutine from which it was called. The subroutines CROSS and MULT are matrix manipulation subroutines and are called by several other subroutines. The functions performed by MULT, CROSS, and INTERP are discussed in Appendix C.

The specific function performed by each subroutine is listed in Table 4. Complete time histories are computed and stored for:

- 1) position and velocity of spacecraft c.g.,
- 2) true anomaly,
- 3) orbital angular velocity,
- 4) position and velocity of experiment c.g.,
- 5) angular position, rate, and acceleration for control wheel,
- 6) angular position, rate, and acceleration for free wheel, and
- 7) angular separation error.

All other computed variables supersede the previous value and no history is maintained. The time histories specified by the user are printed after completion of the simulation. The storage allocation in COMMON restricts the time histories to 400 entries in each dimension.

PROGRAMFUNCTION

MAIN	Input/Output and program initialization, sequencing of integrations
DIFFSQ	Torque balance equation integration
INTERP	Interpolate orbital position, velocity, angular rate, and angular acceleration values from DIFFVQ to match integration interval of DIFFSQ and DIFFBQ(See Appendix C)
DIFFBQ	Experiment c.g. equation of motion integration
VEHICLE	Vehicle motion history
DIFFVQ	Orbital equation of motion integration
ORBIT	True anomaly, orbital rate, and orbital acceleration
PARAM	Orbital eccentricity, true anomaly, and C_I^E
F	Primary earth gravitation
MAT1	$C_E^{B'}$ coordinate transformation matrix
MOVE	Acceleration of experiment c.g.
MATRIX	C_D^S , C_N^S , C_E^S , C_B^S , and C_E^B coordinate transformation matrices; and C_{22}
CONTROL	Position, angular rate, and angular acceleration of control wheel
TORQUE	Torque and angular acceleration of free wheel
ACCEL	Accelerations at test masses on free wheel
DRAG	Atmospheric drag
SPACE	Spacecraft primary gravitation (current program is dummy)
DYNAM	Dynamics of rotational coordinate systems
EARTH	Earth gravity gradients
SPHERE	Gravitational acceleration on test spheres due to control wheel test spheres
MULT	Product of vector and matrix (See Appendix C)
CROSS	Cross product of vectors (See Appendix C)

TABLE 4 Simulation subroutine functions.

<u>CONTROL VARIABLE</u>	<u>VALUE</u>	<u>EFFECT</u>
DTIS	real	The integration interval for the cycle II integrations is DTIS seconds.
KSKIPS	integer	The state variables for the cycle II integrations are printed at KSKIPS•DTIS second intervals.
NDT	integer	The state variables for the cycle I integration are printed at NDT•KSKIPS•DTIS second intervals.
KSKIPG	integer	The integration interval for the cycle I integration is $\frac{NDT \cdot KSKIPS \cdot DTIS}{KSKIPG}$ seconds.
IFIX	0	Experiment is fixed in spacecraft. Only the torque balance equation is integrated in cycle II.
	1(default)	Experiment is free in spacecraft. The torque balance equation and the experiment c.g. equations of motion are integrated in cycle II.
	2	Experiment is free in spacecraft. Only the experiment c.g. equations of motion are integrated in cycle II.
NRR	0(default)	No force profile at experiment c.g. is printed.
	1	A force profile at experiment c.g. is printed if the c.g. equations of motion are integrated.
NSS	0(default)	No force profile at test masses is printed.
	1	A force profile is printed if the torque balance equation is integrated.
NARMS	integer	The number of arms on the free wheel.
NARMD	integer	The number of arms on the control wheel.

TABLE 5 Control variable specifications. Cycle I is the orbital equations of motion integration. Cycle II encompasses the torque balance equation and the experiment c.g. equations of motion.

VARIABLE NAME	SYMBOL	COORDINATE FRAME	PHYSICAL QUANTITY
XIS	η_S	N	Angle of S-frame relative to N-frame (about z-axis)
VIS	V_S	N	Angular rate of S-frame and D-frame relative to N-frame (about z-axis)
RNB	R_N	B	Coordinates of experiment c.g.
VNB	V_N	B	Velocity of experiment c.g.
CEB	C_E^B	-	Coordinate transformation matrix from E-frame to B-frame
CBN	C_B^N	-	Coordinate transformation matrix from B-frame to N-frame
ET0	η_0	N	Initial and optimal angular separation of free and control wheels
ARMS (K, J)	$R_{J/S}$	S	State vector to the J th free sphere from the origin of the S-frame
ARMD (K, J)	$R_{J/D}$	D	State vector to the J th control sphere from the origin of the D-frame
RMAS (J)	M_{JS}	-	Mass of the J th sphere on the free wheel
RMASD (J)	M_{JD}	-	Mass of the J th sphere on the control wheel

TABLE 6 Definition of physical parameters requiring initialization.

<u>CARD NUMBER</u>	<u>VARIABLES</u>	<u>FORMAT</u>
1	NDT, KSKIPS, KSKIPG, TIS, DTIS, TIME, XIS, VIS	3I4, 8F10.4
2	XI	3F10.4
3	VI	3F10.4
4	RNB	3F10.4
5	VNB	3F10.4
6	CEB	9F8.3
7	CBN	9F8.3
8	IFIX, NARMS, NARMD, ETO	3I4, 8F10.4
9	NRR, NSS	2I4
10 to K	ARMS	3F10.4
K+1 to J	ARMD	3F10.4
J+1	RMASS	8F10.4
J+2	RINERT	F10.4
J+3	RMASD	8F10.4

TABLE 7 Card format for input variables. The coordinates for the wheel spokes are read in one spoke per card. $K = 10 + \text{NARMS}$ and $J = 10 + \text{NARMS} + \text{NARMD}$. All vectors are read in as x-component, y-component, z-component.

3.2 Input/Output Specifications

The input variables to the simulation can be classed in two distinct categories:

- 1) control variables for the execution of the simulation, and
- 2) initial values for the physical parameters of the simulation.

The control variable specifications are detailed in Table 5. "Integer" or "real" implies that the user is free to specify the appropriate value in the indicated mode. In the remainder of the cases the user is required to choose one of the indicated integer mode values. The default option for cases in which the user specifies a value other than the permitted value is indicated in parentheses.

The physical parameters to be defined are indicated in Table 6 along with the coordinate system in which the input is to be specified. The symbols refer to the mathematical symbology used in Section 2. A complete list of program variables is given in Appendix B along with the subroutine in which the variable is computed. Program modification is required to obtain direct access to any variable not listed in Table 6.

The card format for the input variables is detailed in Table 7. Each vector is read in on a single card as: x-component, y-component, z-component. The coordinates for the wheel spokes (ARMS and ARMD) are read in one spoke at a time. The coordinate transformation matrices are read on a single card according to the element sequence: C_{11} , C_{21} , C_{31} , C_{12} , C_{22} ... The format for the remaining variables is straightforward.

Examples of simulation output for the three state integrations are presented in Figure 5. The user specifies which of the three outputs are to be computed and printed through the control variable IFIX. The definitions of the output parameters can be obtained in either Section 2 or Appendix B.

Additional output variables for the spacecraft c.g. integrations are the initial conditions on the state variables; the orbital eccentricity, e ; and the integration interval. For the experiment c.g. integrations, the initial value for the transformation matrix C_E^B is printed along with the integration interval. For the torque

balance integration; the test wheel configurations, the initial conditions, and the integration interval are printed.

If either of the control variables NSS or NRR is assigned the integer value 1, force profiles are printed as they are computed in the subroutines. The vehicle angular rates and accelerations are also printed along with the coordinate transformation matrices. The format for the output is to print the time at the top of a new page. Each line on the page then consists of the variable name used in the program (Appendix B) followed by the variable value. The output format for arrays and matrices is the same as the input format described above.

TIME	R_{O_x}	R_{O_y}	R_{O_z}	V_{O_x}	V_{O_y}	V_{O_z}	f_0	Ω
==	==	==	==	==	==	==	==	==

Figure 5a Output format for spacecraft c.g. integration.

Output variables are time, position vector, velocity vector, true anomaly, and orbital angular rate. Variables are coordinatized in I-frame.

TIME	R_{N_x}	R_{N_y}	R_{N_z}	V_{N_x}	V_{N_y}	V_{N_z}
==	==	==	==	==	==	==

Figure 5b Output format for experiment c.g. integration.

Output variables are time, position vector, and velocity vector. Variables are relative to spacecraft c.g. and coordinatized in B-frame.

TIME	η_S	η_D	$\eta_0 - (\eta_D - \eta_S)$	$\dot{\eta}_S$	$\dot{\eta}_D$	$\ddot{\eta}_S$	$\ddot{\eta}_D$
==	==	==	==	==	==	==	==

Figure 5c Output format for torque balance equation

integration. Variables are relative to N-frame and are coordinatized in N-frame.

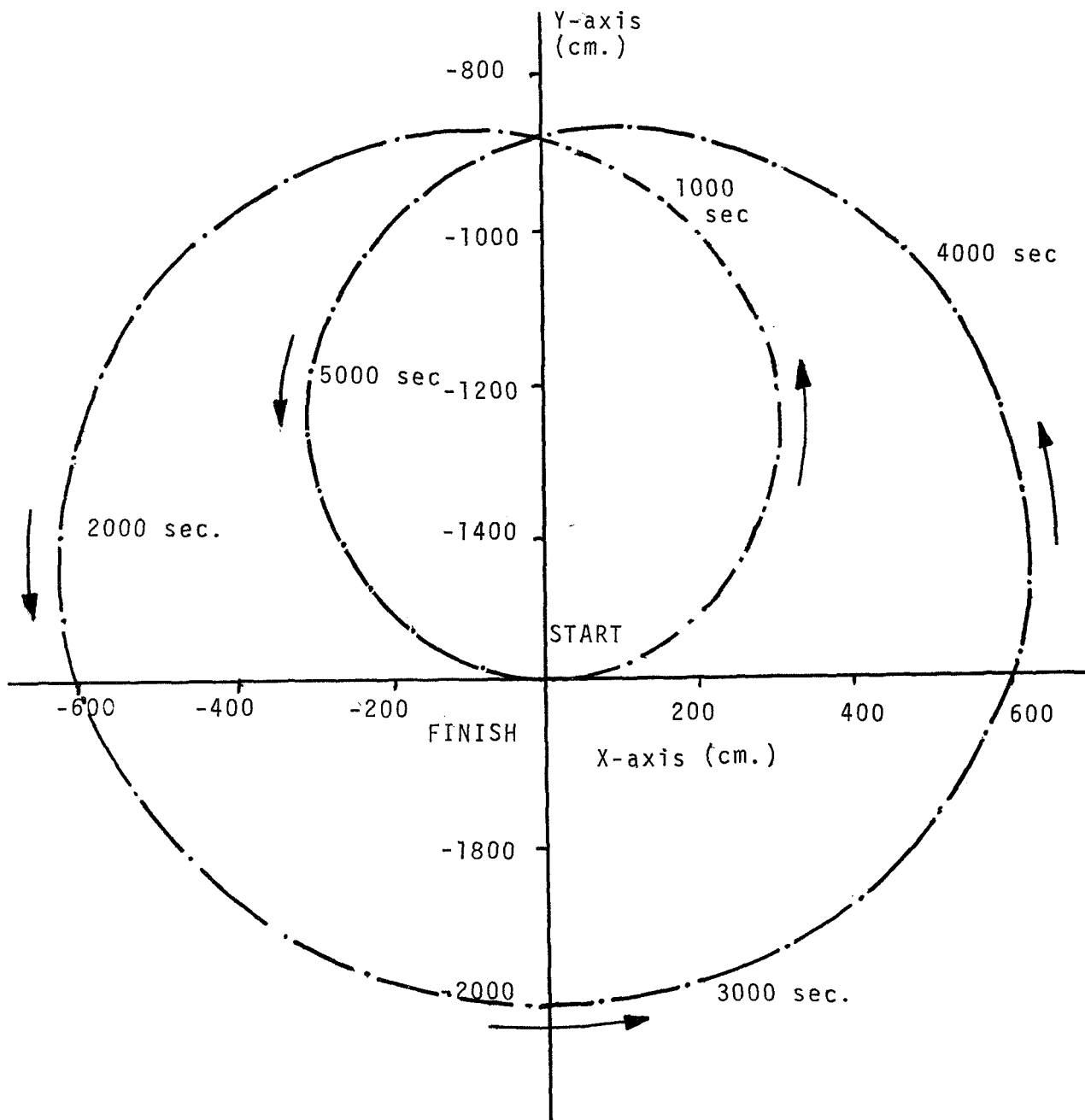


Figure 6. Simulation of motion of free floating experiment as seen in spacecraft (B-frame).

Initial conditions are $R_N = (0, -1574.8, 0)$ and $V_N = (.745, 0., 0.)$
 Experiment c.g. returns to initial state after one earth orbit of 5700 seconds. Position is shown at 100 second intervals.

3.3 Integration Error Analysis

In addition to modeling errors, the simulation is sensitive to truncation errors and finite integration interval errors. All program variables are double precision with a maximum of 15 significant digits. Although truncation errors can become significant for small integration intervals, the primary integration error is the linearization error introduced by the finite integration interval. For the earth orbit integration (cycle I), the linearization error is controlled by the integration interval, DTIG. For the cycle II integrations, the linearization error is governed by both DTIS and DTIG.

The data of Table 8 is intended as an aid in estimating the output errors associated with a particular pair of values for DTIS and DTIG. Table 8a outlines as a function of DTIG the convergence of the orbital state estimate after approximately one revolution in a drag free orbit. Accepting the one second integration interval as a base reference, the cumulative error after 5700 seconds with a 20 second integration interval is .4 cm. in the x-coordinate, 15.88 cm. in the y-coordinate, and 20.16 cm. in the z-coordinate.

Table 8b illustrates a case when the experiment is floating free in the spacecraft. Given an initial displacement from the c.g. of the spacecraft and a small initial velocity relative to the spacecraft c.g., the experiment c.g. ideally describes a closed arc as seen in the B-frame (Figure 6) and after one full orbit returns to a state close to its initial state. In a drag free orbit with the spacecraft in an inertial hold, the motion of the experiment c.g. is determined solely by the resolution of the earth gravity gradient matrix into the B-frame. Since the gravity gradient matrix is calculated by the subroutine EARTH from the orbital state estimates, DTIG indirectly affects the integration error in cycle II along with the direct effect from DTIS. The data of Figure 8b indicates that this error is quite significant. The test run with DTIS and DTIG equal to one second is assumed as a reference. When both integration intervals are 20 seconds, the cumulative error is 23.45 cm. in the x-coordinate and 73.20 cm. in the y-coordinate.

No test runs for the torque balance equations are included. The results were similar to the experiment c.g. equation error analysis.

Integration Interval (DTIG)	x-coordinate	y-coordinate	z-coordinate
20 seconds	690093936.62 cm.	-2622799.90 cm.	-3125701.86 cm.
10 seconds	690093936.96 cm.	-2622815.82 cm.	-3125720.83 cm.
5 seconds	690093937.01 cm.	-2622816.76 cm.	-3125721.95 cm.
2 seconds	690093937.02 cm.	-2622816.80 cm.	-3125722.00 cm.
1 second	690093937.02 cm.	-2622816.82 cm.	-3125722.02 cm.

Table 8a Convergence of orbital equations of motion integration as a function of integration interval, DTIG. The table entries are the coordinate estimates of a 500 km. orbit after 5700 seconds (approximately one orbit). The case with DTIG = 1 is assumed as the best estimate of the true state. The initial state is (690106000., 0., 0.) and the orbital period is 5706 seconds.

Cycle II Integration Interval (DTIS)	Cycle I Integration Interval (DTIG)	x-coordinate	y-coordinate
20 seconds	20 seconds	-27.46 cm.	-1501.26 cm.
1 second	20 seconds	-27.46 cm.	-1501.26 cm.
10 seconds	10 seconds	-9.74 cm.	-1555.80 cm.
1 second	10 seconds	-9.68 cm.	-1556.13 cm.
5 seconds	5 seconds	-5.45 cm.	-1569.91 cm.
2 seconds	2 seconds	-4.38 cm.	-1573.61 cm.
1 second	1 second	-4.01 cm.	-1574.46 cm.

Table 8b Convergence of experiment c.g. equations of motion integration as a function of the integration intervals DTIS (cycle II) and DTIG (cycle I). The table entries correspond to the trajectory of Figure 6 after 5700 seconds (approximately one orbit). The case with DTIG = DTIS = 1. is assumed as the best estimate of the true state. The initial state is (0., -1576.8) and the orbital period is 5706 seconds.

4. Possible Program Modifications

The simulation package described in this report was developed with the hope that it would be sufficiently general to accommodate a large number of applications and test configurations without requiring program modifications. Nonetheless, there will undoubtedly be application requirements for which program modifications will be necessary. Some such modifications are obvious and are presently under consideration. There are a great number of modeling requirements for which no sufficiently general simulation package can be developed, however, and a major concern in the development of the package has been to allow relatively major alterations of the mathematical model without requiring the programmer to understand the mechanics of the entire package.

Desired modifications can generally be classified into three major categories:

- 1) alteration of the sequencing logic in the main program to allow for variable integration intervals,
- 2) extended Input/Output capabilities, and
- 3) alteration of the mathematical model of the experiment and its physical environment.

The first modification is of interest because of the nature of the experiment. When the free wheel is revolving slowly, the forces at the test masses change slowly with time and a relatively long integration interval is sufficient to accurately describe the motion. After several thousand seconds of constant mean acceleration, however, the rate of change of the forces is high enough to warrant a shorter integration interval. Modifications to allow a time history for DTIS to be input are under development.

The most likely requirement for extended Input/Output is to output the data in a different format, such as Calcomp plots. With the exception of the force profiles and spacecraft angular motion profiles, all output emanates from the main program in the form of time history arrays. All that is required to modify the output format is to replace the current output package with a new package.

If time histories for any of the force profiles are desired, the simplest approach would be to set the appropriate control flag (NSS or NRR) to unity, replace the print statement in the appropriate

subroutine by a time history array assignment, and pass the array back through COMMON to the main program: If the variable of interest is computed for the torque balance integration, the array index for the assignment should be IT. If the variable originates in the experiment c.g. equation integration, the array index is IB. For the orbit integration , the array is KRG.

The number of model changes which can be made is seemingly endless. Substitution of models generally requires only modification of the subroutine implementing that model. The modifications can utilize any COMMON variable or the control variables passed through the CALL statement to the subroutine. In the event that the modification requires the current value of a variable stored in a time history array, the array index indicated in Table 9 should be used. The indexes KRG-1, IT-1, and IB-1 specify the value at the beginning of the current integration

<u>ARRAY</u>	<u>INDEX FOR CURRENT VALUE</u>
TMG,OMEGA,DOMEGA,ANSG,VELOG,TA	KRG-1
OM,DOM,PST,DPSI,XG,VG,	ND for torque balance NDB for experiment c.g. motion
AETAS,ETAS,DETAS,AETAD,ETAD DETAD,ERS	IT-1
ANSB,VELOB	IB-1
TMS	IT-1 for torque balance IB-1 for experiment c.g. motion

TABLE 9 Index required to obtain data value in time history array corresponding to value at beginning of current integration interval.

interval. The resolution of ND, and NDB is such that the value at the midpoint of the integration interval may also be accessed. The procedure for effecting model modifications is to use Appendix B

to locate the subroutine in which the variable is computed and Appendix A to determine what modifications are necessary. The documentation in Appendix A is intended to be sufficient to define the nature of the modifications.

The mathematical model for the simulation may be altered either by replacing old models or adding new ones. The most likely instances in which additional models might be added are:

- 1) a noise-corrupted measurement model, and
- 2) additional disturbance force models.

The noise-corrupted measurement model can be implemented by substituting the model for the two assignment statements for ERR in DIFFSQ. The disturbance force models can be referenced as subroutines from F, ACCEL, or MOVE depending on whether the disturbance affects the spacecraft orbital motion, the torque balance, or the experiment c.g. motion respectively. The model output must then be added in vector form to either ACD, ACC, or ACB.

As discussed in Section 2.4, any of the force models may require modification or replacement. The immediately apparent modifications were discussed in that section. It is also conceivable that the vehicle motion model may require a time history different from the inertial hold implemented. This modification can be effected by either inputting the time history directly or modifying VEHICLE to compute the vehicle motion.

A further generalization of the simulation package can be effected by allowing the possibility of impulsive orbit changes for the spacecraft. The procedure for implementing this modification is discussed in the documentation for MAIN in Appendix A.

Although additional program modifications may seem desirable, they very likely cannot be effected without a more extensive understanding of the logic structure of the program. It is expected that as the simulation is applied and its limitations more clearly delineated, modification to the general structure of the package will be forthcoming.

Appendix A

Source Deck Listing

The complete FORTRAN IV listing for the simulation package is contained in this appendix. The documentation is intended as a supplement to the textual descriptions in the body of the report. No attempt is made to detail the mechanics of the individual subroutines. The documentation in each subroutine defines the input and output variables pertinent to that subroutine and outlines the function of the control parameters. The intent is to specify the interface constraints that a user-supplied subroutine must meet if the mathematical model in the simulation package is to be replaced. Appendix B should be used in conjunction with Appendix A to relate the program source code to the text of the report.

Because of the size of the source code program, Appendix A is not included in this copy of the report. A complete listing is available on request, as TN-2.

Appendix B

Program Variable Definitions

This appendix summarizes in a table format all of the variables maintained in COMMON during execution of the simulation and a number of the more important variables which are passed through the CALL statements. Dummy calling parameters are defined in the documentation for the appropriate subroutine in Appendix A and are not included here. In addition, variables which are intermediate products within a single subroutine are omitted. In modifying a model, the user may replace these variables with variable names of his own choice. All variables necessary for communicating data between subroutines are listed in this table except for the control parameters of Table 5.

The majority of the variable values are updated and only the current value is available during execution. For those variables which constitute time histories, the data value at the beginning of each integration interval is pointed to by the appropriate index from Table 9. Those variables listed in the table and not stored in COMMON are generally accessible only to the subroutine in which they are computed and the subroutine from which that subroutine was called.

The table contains seven entries for each variable. The key letters at the top of each page denote respectively:

NAME -- the variable name used in the program.
S -- the symbol used in the mathematical model of Section 2.
-- the equation number from Section 2 which defines the variable.
SUB -- the subroutine in which the variable is computed.
C -- whether or not the variable is stored in COMMON.
F -- the coordinate frame in which the variable is coordinatized.

NAME	S	#	SUB	C	F	Physical Interpretation
ACB	\underline{a}_N	17	MOVE	N	B	acceleration of experiment c.g. as seen in B-frame
ACC	$\underline{a}_{P/N}$	19 or 20	ACCEL	N	N	accelerations at test masses on free wheel as seen in N-frame
ACD	\underline{a}_E	2	F	N	I	acceleration at spacecraft c.g. as seen in I-frame
ACT	$\ddot{\eta}_S$	3	TORQUE	N	N	net angular acceleration on free wheel (used in integration routine only)
AEG	G_{E-R-N}	16	EARTH	N	E	earth gravity gradient force
AETAC	η_D	--	CONTRL	Y	N	angle of control wheel (D-frame) relative to N-frame at midpoint of integration interval
AETAD	η_D	--	CONTRL	Y	N	angle of control wheel (D-frame) relative to N-frame at beginning of integration interval (time history)
AETAS	η_S	--	DIFFSQ	Y	N	angle of free wheel (S-frame) relative to N-frame at beginning of integration interval (time history)
AFD	\underline{a}_D	30	DRAG	N	E	atmospheric drag force
ASC	\underline{a}_{SC}	16	SPACE	N	B	primary spacecraft gravity force
ASG	\underline{a}_{SG_J}	25	SPHERE	N	N	acceleration of the J th test mass of the free wheel due to the control wheel
ANSB	\underline{R}_N	13	DIFFBQ	Y	B	position of experiment c.g. relative to spacecraft c.g. (time history)
ANSG	\underline{R}_E	--	DIFFVQ	Y	I	position of spacecraft c.g. relative to earth (time history)

Table 9 Program variable definitions. The column headings are explained in the text.

NAME	S	#	SUB	C	F	Physical Interpretation
AOB	--	17, 19, or 20	DYNAM	Y	B	rotating coordinate system force terms in equations of motion for cycle II
ARMD	--	--	MAIN	Y	D	coordinates of control wheel test masses (input variable)
ARMS	--	--	MAIN	Y	S	coordinates of free wheel test masses (input variable)
C22	C_{22}	28	MATRIX	Y	E	angle of spacecraft velocity vector with longitudinal axis of spacecraft
CBN	C_B^N	--	MAIN	Y	-	coord. trans. matrix from B-frame to N-frame (input variable)
CBS	C_B^S	6	MATRIX	Y	-	coord. trans. matrix from B-frame to S-frame
CDS	C_D^S	4	MATRIX	Y	-	coord. trans. matrix from D-frame to S-frame
CEB	C_E^B	8	MATRIX	Y	-	coord. trans. matrix from E-frame to B-frame (used for torque balance only)
CEB1	$C_E^{B'}$	8	MAT1	Y	-	coord. trans. matrix from E-frame to B-frame (used for experiment c.g. only)
CES	C_E^S	7	MATRIX	Y	-	coord. trans. matrix from E-frame to S-frame
CIE	C_I^E	40	PARAM	Y	-	coord. trans. matrix from I-frame to E-frame
CNS	C_N^S	5	MATRIX	Y	-	coord. trans. matrix from N-frame to S-frame
CSTRA	$\cos f_0$	33	ORBIT PARAM	Y	-	cosine of true anomaly
DENT	I	8	MAIN	Y	-	identity matrix
DETAD	$\ddot{\eta}_D$	21	CONTRL	Y	N	angular acceleration of control wheel (time history)

Table 9 (cont'd) Program variable definitions.

NAME	S	#	SUB	C	F	Physical Interpretation
DETAS	$\ddot{\eta}_S$	3	DIFFSQ	Y	N	angular acceleration of free wheel (time history)
DIST	$\underline{R}_{J/K}$	25	MATRIX	Y	S	vector distance from J th sphere of free wheel to K th sphere of control wheel
DOM	$\dot{\underline{\Omega}}$	--	INTERP	Y	E	orbital angular acceleration interpolated to cycle II data density
DOMEGA	$\underline{\dot{\Omega}}$	35	ORBIT	Y	E	orbital angular acceleration (time history)
DPSI	$\dot{\underline{\psi}}$	13	VEHICLE	Y	B	B-frame angular acceleration relative to V-frame
DTIG	--	--	MAIN	Y	-	cycle I integration interval
DTIS	--	--	MAIN	Y	-	cycle II integration interval
ECC	e	31	PARAM	Y	-	orbital eccentricity
EETA	\underline{i}_η	39	PARAM	N	I	y-axis of E-frame
ERR	--	--	DIFFSQ	N	N	angle position error between free wheel and control wheel
ERS	--	--	DIFFSQ	N	N	angle position error between free wheel and control wheel (time history)
ETO	η_0	--	MAIN	Y	N	nominal angle between free wheel and control wheel
ETAD	$\dot{\eta}_D$	--	CONTRL	Y	N	angular velocity of control wheel (time history)
ETAS	$\dot{\eta}_S$	--	DIFFSQ	Y	N	angular velocity of free wheel (time history)
G	G_E	24	EARTH	N	E	earth gravity gradient matrix

Table 9 (cont'd) Program variable definitions.

NAME	S	#	SUB	C	F	Physical Interpretation
H	\underline{h}	32	PARAM	N	I	orbital massless angular momentum
HOLD	--	--	CONTRL	Y	N	last computed angle and angular velocity for control wheel
OM	$\underline{\Omega}$	--	INTERP	Y	E	orbital angular velocity interpolated to cycle II data density
OMO	$\underline{\Omega}_0$	36	PARAM	Y	E	average orbital angular velocity
OMEGA	$\underline{\Omega}$	34	ORBIT	Y	E	orbital angular velocity (time history)
POS	$\underline{R}_{J/N}$	3	TORQUE	N	S	coordinates of J^{th} test mass of free wheel for force computation
PSI	$\underline{\Psi}$	13	VEHICLE	Y	B	angular velocity of B-frame relative to V-frame
RINERT	I_M	1	MAIN	Y	-	inertia of free wheel
RMASD	M_{JD}	25	MAIN	Y	-	mass of the J^{th} sphere of the control wheel
RMASD	M_{JS}	3	MAIN	Y	-	mass of the J^{th} sphere of the free wheel
RNB	\underline{R}_N	13	DIFFBQ	Y	B	position of experiment c.g. relative to spacecraft c.g. (used in force routines only)
SNTRA	$\sin f_0$	33	ORBIT PARAM	Y	-	sin of true anomaly
TA	f_0	33	ORBIT PARAM	Y	-	true anomaly
TARM	$\times \underline{R}_{J/N}$	3	MAIN	Y	S	cross product matrix used to compute torques
TIG	--	--	DIFFVQ	Y	-	clock time in cycle I
TIS	--	--	DIFFSQ	Y	-	clock time in cycle II

Table 9 (cont'd) Program variable definitions.

NAME	S	#	SUB	C	F	Physical Interpretation
TMG	--	--	DIFFVQ	Y	-	clock time in cycle I (time history)
TMS	--	--	DIFFSQ	Y	-	clock time in cycle II (time history)
XG	\underline{R}_E	--	INTERP	Y	E	position of spacecraft c.g. relative to earth interpolated to cycle II data density
XI	η_D	--	MAIN	N	N	initial angle of control wheel (D-frame) relative to N-frame
XIS	η_S	--	MAIN	N	N	initial angle of free wheel (S-frame) relative to N-frame
XXI	\underline{i}_ξ	34	PARAM	N	I	x-axis of E-frame
VELOB	\underline{V}_N	13	DIFFBQ	Y	B	velocity of experiment c.g. relative to space- craft c.g. (time history)
VELOG	\underline{V}_E	2	DIFFVQ	Y	I	velocity of spacecraft c.g. relative to earth (time history)
VG	\underline{V}_E	2	INTERP	Y	E	velocity of spacecraft c.g. relative to earth interpolated to cycle II data density
VI	$\dot{\eta}_D$	--	MAIN	N	N	initial angular velocity of control wheel (D- frame) relative to N- frame
VIS	$\dot{\eta}_S$	--	MAIN	N	N	initial angular velocity of free wheel (S-frame) relative to N-frame
VNB	\underline{V}_N	13	DIFFSQ	Y	B	velocity of experiment c.g. relative to space- craft c.g. (used in force models only)
ZETA	\underline{i}_ξ	37	PARAM	N	I	z-axis of E-frame

Table 9 (cont'd) Program variable definitions.

Appendix C

Auxiliary Subroutine Functions

The subroutine MULT, CROSS, and INTERP are data manipulation routines. Given the vector A, CROSS computes the matrix:

$$\underline{B} = \underline{A} \times \quad (C-1)$$

$$\underline{B} = \begin{bmatrix} 0 & -A_3 & A_2 \\ A_3 & 0 & -A_1 \\ -A_2 & +A_1 & 0 \end{bmatrix} \quad (C-2)$$

for use in cross-product computations. Given the vector B, the matrix A, and the control variable K; MULT computes:

$$\underline{C} = \underline{A} \underline{B} \quad (C-3)$$

if K equals zero and:

$$\underline{C} = \underline{A}^T \underline{B} \quad (C-4)$$

if K equals one. MULT is used for effecting coordinate transformations and computing cross-products in conjunction with CROSS.

INTERP performs a straight linear interpolation of the specified variables. The input data density has a spacing of DTIG seconds and the output data density has a spacing of DTIS/2 seconds.

Appendix D

2nd Order Runge-Kutta

To integrate a pair of state vectors, $\underline{x}(t_n)$ and $\underline{v}(t_n)$, for a time increment δt , the 2nd order Runge-Kutta method assumes that the derivatives can be computed as arbitrary functions of $\underline{x}(t)$, $\underline{v}(t)$, and t . From the initial state, the acceleration $f(\underline{x}, \underline{v}, t_n)$ is used to project a state estimate at $t_n + \delta t/2$:

$$f_{x_0} = \underline{v}(t_n) \quad (D-1)$$

and:

$$f_{v_0} = f(\underline{x}, \underline{v}, t_n) \quad (D-2)$$

yield:

$$\underline{x}'(t_n + \delta t/2) = \underline{x}(t_n) + \frac{\delta t}{2} \cdot f_{x_0} \quad (D-3)$$

and:

$$\underline{v}'(t_n + \delta t/2) = \underline{v}(t_n) + \frac{\delta t}{2} \cdot f_{v_0} \quad (D-4)$$

The acceleration corresponding to this projected state is then used to compute a second projected state:

$$f_{x_1} = \underline{v}'(t_n + \delta t/2) \quad (D-5)$$

and:

$$f_{v_1} = f(x', v', t_n + \delta t/2) \quad (D-6)$$

yield:

$$x''(t_n + \delta t/2) = x(t_n) + \frac{\delta t}{2} \cdot f_{x_1} \quad (D-7)$$

and:

$$v''(t_n + \delta t/2) = v(t_n) + \frac{\delta t}{2} \cdot f_{v_1} \quad (D-8)$$

This state estimate is then used to project a state estimate to the end of the interval:

$$f_{x_2} = v''(t_n + \delta t/2) \quad (D-9)$$

and:

$$f_{v_2} = f(x'', v'', t_n + \delta t/2) \quad (D-10)$$

yield:

$$x'''(t_n) = x(t_n) + \delta t \cdot f_{x_2} \quad (D-11)$$

and:

$$v'''(t_n) = v(t_n) + \delta t \cdot f_{v_2} \quad (D-12)$$

Finally, this state estimate is used to estimate the derivatives at the end of the time interval:

$$f_{x_3} = v'''(t_n) \quad (D-13)$$

and

$$f_{v_3} = f(x''', v''', t_n + \delta t) \quad (D-14)$$

The state estimates at the end of the time interval are then:

$$x(t_n + \delta t) = x(t_n) + \delta t \cdot (f_{x_0} + 2f_{x_1} + 2f_{x_2} + f_{x_3})/6 \quad (D-15)$$

and

$$v(t_n + \delta t) = v(t_n) + \delta t \cdot (f_{v_0} + 2f_{v_1} + 2f_{v_2} + f_{v_3})/6 \quad (D-16)$$

Bibliography

1. Battin, Richard H., Astronautical Guidance, McGraw-Hill, 1964.
2. Blood, B.E., "An Elementary Analysis of the Adaptation of the Beams' Experimental Concept to a $\Delta G/G$ Detector to be Used in Space," Measurement Systems Laboratory Report RN-60, June, 1970.
3. Chapman, P.K., "A Cavendish Experiment in Earth Orbit," unpublished note, December 1969.
4. Halfman, Robert L., Dynamics, Volume I, Addison-Wesley, 1962.
5. Lee, W.N., "A Space Experiment to Determine the Constancy of the Gravitational Constant G," Measurement Systems Laboratory Report PR-7, "Review of NASA-Sponsored Research at the Measurement Systems Laboratory," May 1970.
6. Lee, W.N., "Expected Drag Accelerations for Skylab B," unpublished memo, August 1970.
7. Rose, D.R., "A New Method for Determination of Newton's Gravitational Constant," D.Sc. Dissertation, University of Virginia, August 1969.
8. Wilk, Leonard S., "A Gravitational Experiment in Space," unpublished memo, December 1969.

APPENDIX D

A PRELIMINARY ANALYSIS OF THE EFFECTS
OF USING NON-SPHERICAL MASSES IN A
BEAMS-TYPE MEASUREMENT OF G OR $\Delta G/G$

RE-74

A PRELIMINARY ANALYSIS OF THE
EFFECTS OF USING NON-SPHERICAL MASSES
IN A BEAMS-TYPE MEASUREMENT OF G OR


$\Delta G/G$

by

William N. Lee

October 1970

APPROVED



Director
Measurement Systems Laboratory

MASSACHUSETTS INSTITUTE OF TECHNOLOGY

Measurement Systems Laboratory

Cambridge, Massachusetts 02139

A PRELIMINARY ANALYSIS OF THE
EFFECTS OF USING NON-SPHERICAL MASSES
IN A BEAMS-TYPE MEASUREMENT OF G OR
 $\Delta G/G$.

by

William N. Lee

ABSTRACT

A proven method of performing a Cavendish measurement of the gravitational constant G has been developed by J. W. Beams. One possible way to improve the accuracy of the measurement of G , or the measurement of $\Delta G/G$ to test the general theory of relativity, is to use masses other than spheres in the experimental set up.

This analysis considers the gravitational interaction between masses of various shapes, and examines the use of a pair of hemispheres in a Beams-type experiment.

ACKNOWLEDGEMENTS

The author wishes to express his appreciation to Mr. Leonard Wilk and Dr. Stephen Madden, Jr., for their interest and support. This research was sponsored by the National Aeronautics and Space Administration under contract NAS9-8328.

The publication of this report does not constitute approval by the National Aeronautics and Space Administration of the findings or conclusions contained therein. It is published only for the exchange and stimulation of ideas.

TABLE OF CONTENTS

	Page
I. INTRODUCTION	1
II. MAXIMIZATION OF THE FORCE BETWEEN TWO BODIES OF UNIFORM DENSITY	3
II.1 Two Spheres	3
II.2 Optimally Shaped Body Interacting with a Sphere	4
II.3 Two Hemispheres - Analytic Treatment	9
II.4 Two Hemispheres - Computer Model	12
II.5 Two Blocks	17
II.6 Two Right Cylinders	17
II.7 Two Spheroids	21
II.8 Summary of Chapter II.	23
III. THE EFFECTS OF USING HEMISPHERES INSTEAD OF SPHERES IN A BEAMS-TYPE EXPERIMENT	23
III.1 Criteria for Comparing Performances	25
III.2 Constraints on the Geometrical Configurations	27
III.3 Comparison of Results for a One Arm Device	29
IV. SUMMARY AND CONCLUSIONS	33
APPENDIX A Computer Results for the Calculations of the Force between Two Hemispheres	35
APPENDIX B Computer Results for the Calculation of the Force between Two Blocks	37
APPENDIX C Computer Results for the Calculation of the Force between Two Right Cylinders	39
APPENDIX D Computer Results for the Calculation of the Force between two Half-Spheroids	41
APPENDIX E Computer Results for the Calculation of the Torque Generated by Two Hemispheres when $\partial T / \partial \theta = 0$	43
REFERENCES	45

I. INTRODUCTION

The type of experimental set up used by J. W. Beams and his colleagues for a measurement of G consists of two sets of masses which are suspended on two sets of torque arms, anchored at a common point (Figure I).

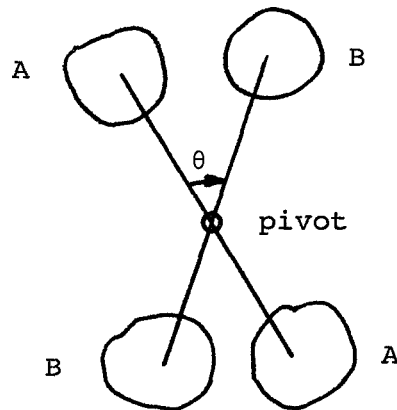


Figure I. ROTATING MASSES

One of the sets, "A" for example, is free to rotate and hence gravitate towards the fixed set "B". The magnitude of the gravitational interaction can be measured by either allowing "A" to oscillate about "B", or as Beams has done, servo "B" with an angular acceleration such that the angular separation θ is constant (Reference 1).

A preliminary design study for optimizing the geometry of Beams' method, assuming spherical masses at the ends of massless torque arms, has been carried out by B. E. Blood (Reference 2). Design considerations included minimizing the effects of disturbance torques, maximizing the magnitude of the torque, and minimizing the sensitivity to changes in θ . Based on these analyses, Blood was able to optimize the size of the experiment.

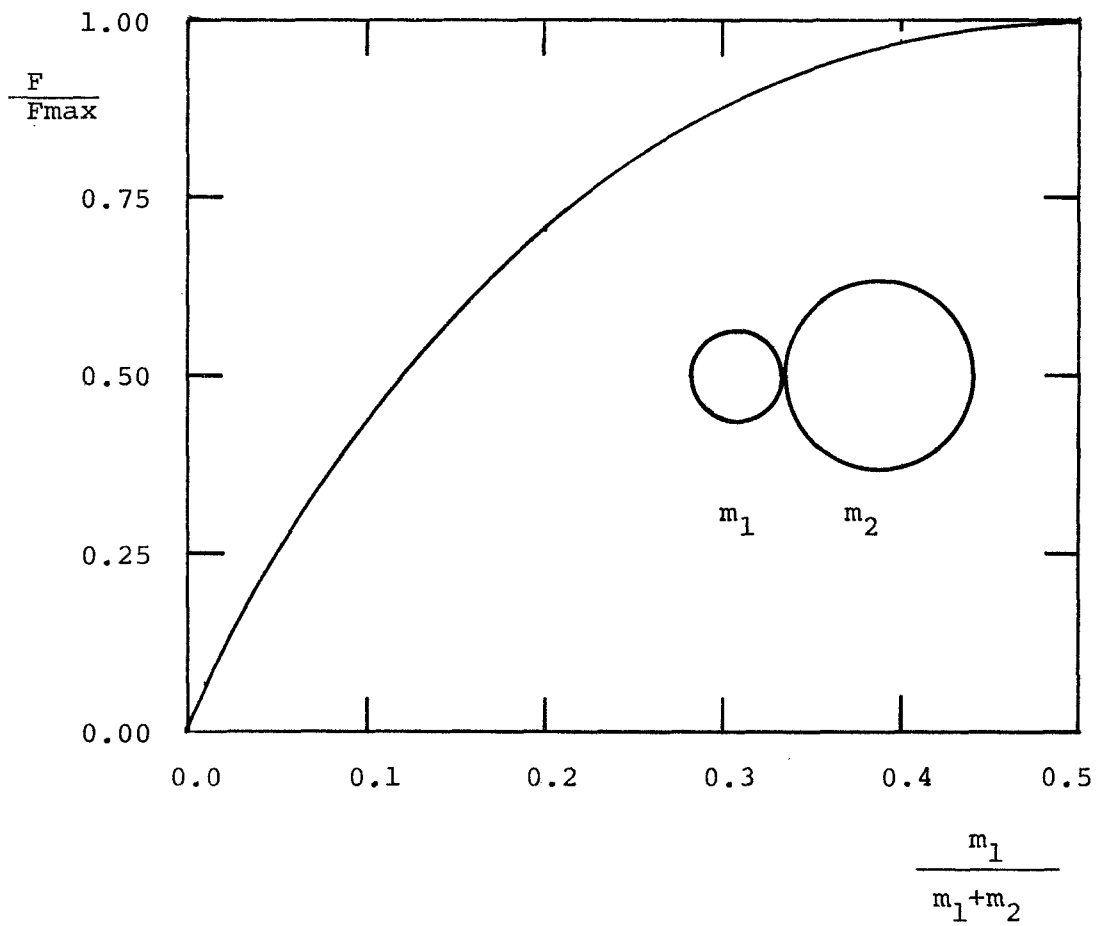


Figure II. MUTUAL FORCE FOR VARIOUS DISTRIBUTIONS OF MASS BETWEEN TWO SPHERES OF UNIFORM DENSITY

This report parallels a portion of Blood's analysis with the study of the effects of replacing the spheres with solid bodies of various shapes. The optimum shape is probably quite irregular, kidney-shaped, for example. Unfortunately, precision machining of such a shape is very difficult. The hypothesis is, however, that the performance of the experiment might very well be improved with the use of masses possessing fairly simple, but non-spherical shapes.

The problem of maximizing torque is related to that of maximizing the gravitational force between two bodies. This simpler problem is investigated first to obtain a feeling for both the shape desired, and more importantly, the magnitude of the improvement which can be expected using masses other than spheres.

II. MAXIMIZATION OF THE FORCE BETWEEN TWO BODIES OF UNIFORM DENSITY

In order to maximize the force between two bodies of uniform density, Figure II indicates the advantage of using two bodies of equal mass. Furthermore, intuitive reasoning dictates that the bodies represent mirror images of one another about the plane separating them and perpendicular to the axis passing between their centers of mass, about which they should be so-called bodies of revolution.

II.1 Two Spheres

For two identical spheres of radius r and mass m , the maximum (attractive) mutual gravitational force is

$$F = - \frac{Gm^2}{4r^2} ,$$

or normalized to $G\rho^2V^{4/3}$

$$\frac{F}{G\rho^2V^{4/3}} = - \frac{1}{4} \left(\frac{4\pi}{3}\right)^{2/3} \cong - 0.650 , \quad (1)$$

a dimensionless expression which is independent of the mass involved. The density and volume of one sphere are denoted by ρ and V , respectively. It might be noted that in general, for two bodies of different mass, the non-dimensional force expression is

$$\frac{F}{G\rho_1\rho_2V_1^{2/3}V_2^{2/3}}$$

and enables one to compare various interactions, given a specific amount of mass.

The first derivative of the force with respect to separation x , evaluated when the spheres are touching, can also be expressed in a dimensionless form which is independent of the mass involved,

$$\left. \frac{\frac{\partial F}{\partial x}}{G\rho^2V} \right|_{\text{spheres are touching}} = \frac{\pi}{3} \approx 1.047.$$

II.2 Optimally Shaped Body Interacting with a Sphere

For improvement in the magnitude of the force between two bodies, the first step was to maximize the force using a sphere and selecting the shape of a second body with equivalent mass. Due to the complete symmetry of a sphere about its center of mass, this reduces to the problem of maximizing the field of the second body at the center of the sphere.

With the coordinate system defined by Figure III in two dimensions (and assuming "B" is a body of revolution about the x axis) the

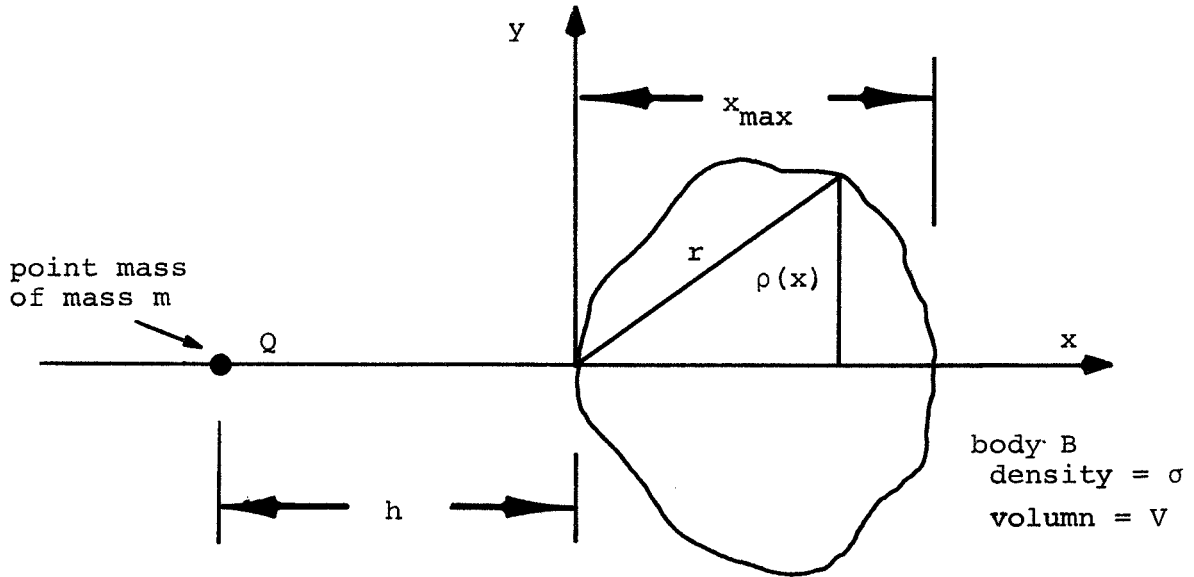


Figure III.

equation for the x-component of the field at a point "Q" on the x-axis is

$$\frac{F_x}{m} = -2\pi G\sigma \int_0^{x_{\max}} \int_0^{\rho(x)} \frac{(x+h)\rho \, dx \, d\rho}{[(x+h)^2 + \rho^2]^{3/2}}$$

where the volume is specified as

$$V = 2\pi \int_0^{x_{\max}} \int_0^{\rho(x)} \rho \, dx \, d\rho .$$

Body "B" is restricted to lie on the positive x side of the plane containing the y and z coordinate axes. The two preceding integral equations reduce to

$$\frac{F}{m} = 2\pi G\sigma \int_0^{x_{\max}} \left\{ \frac{x+h}{[(x+h)^2 + \rho^2(x)]^{1/2}} - 1 \right\} dx \quad (2)$$

and to the constraint that

$$V = \pi \int_0^{x_{\max}} \rho^2(x) dx \quad . \quad (3)$$

Using calculus of variations, the Euler equation for maximizing F_x (Reference 3) is

$$\frac{d}{dx} \left[\frac{\partial H}{\partial \left(\frac{d\rho}{dx} \right)} \right] - \frac{\partial H}{\partial \rho} = 0 \quad (4)$$

where

$$H \equiv \frac{x+h}{[(x+h)^2 + \rho^2]^{1/2}} - 1 + \frac{\lambda \rho^2}{2} \quad (5)$$

and λ is the Lagrange multiplier. The application of (4) to (5) yields the equation for $\rho(x)$ which describes the perimeter of B in the x-y plane:

$$\rho^2(x) = q^{4/3} (x+h)^{2/3} - (x+h)^2 \quad (6)$$

where $q \equiv x_{\max} + h$ and q satisfies

$$q^{4/3} \left[\frac{4}{9} q^{5/3} - h^{5/3} \right] - \frac{5}{9} \left[\frac{3V}{\pi} - h^3 \right] = 0. \quad (7)$$

A special case, and the one of interest here, is to place a homogeneous sphere of radius $R = h$, such that its center of mass coincides with the point Q. Equation (6) then takes the form

$$\left(\frac{\rho}{R}\right)^2 = p^{4/3} \left(\frac{x}{R} + 1\right)^{2/3} - \left(\frac{x}{R} + 1\right)^2 \quad (8)$$

and (7) becomes

$$f \equiv p^3 - \frac{9}{4} p^{4/3} - \frac{15}{4} = 0 \quad (9)$$

where

$$p \equiv \frac{q}{h} = \frac{x_{\max} + h}{h} \quad (10)$$

The relevant root of (9) is $p \cong 2.1555$ and the corresponding shape is indicated in Figure IV.

The expression for the mutual force between the bodies is found from (2), using (6) and (10):

$$F_{x_{\max}} = -\frac{8}{3} \pi^2 \sigma^2 R^3 G \left[\frac{2}{5} p + \frac{3}{5} p^{-2/3} - 1 \right] h .$$

For the special case of $h = R$, this reduces to

$$F_{x_{\max}} \cong -0.591 \pi^2 \sigma^2 G R^4$$

or in the dimensionless form

$$\frac{F_{x_{\max}}}{G \sigma^2 V^{4/3}} \cong -0.864 . \quad (11)$$

Finally, one can calculate the derivative of the force with respect to separation along the x axis:

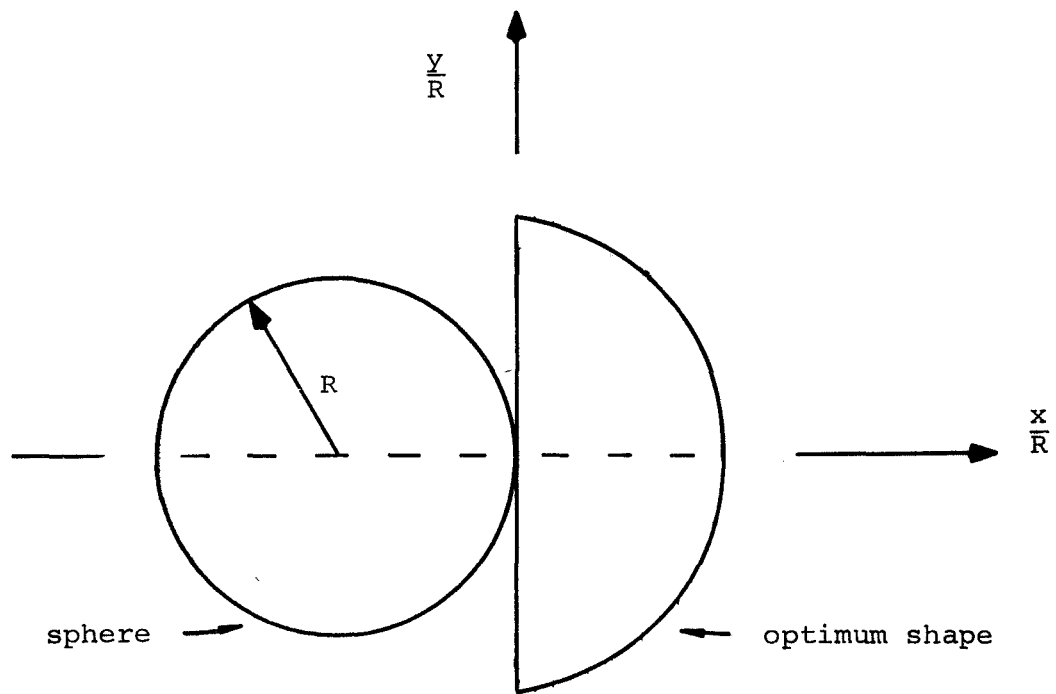


Figure IV. SHAPE OF BODY WHICH MAXIMIZES INTERACTION WITH SPHERE

$$\frac{dF_x}{dh} = \left. \frac{\partial F_x}{\partial h} \right|_{p=\text{const.}} + \left. \frac{\partial F_x}{\partial p} \right|_{h=\text{const.}} \cdot \begin{bmatrix} -\frac{\partial f}{\partial h} \\ \frac{\partial f}{\partial p} \end{bmatrix}$$

or

$$\frac{dF_x}{dh} = -\frac{8}{3} \pi \sigma^2 R^3 G \left\{ \frac{2}{5} p + \frac{3}{5} p^{-2/3} - 1 \right. \\ \left. + \frac{2}{5} (1 - p^{-5/3}) h \left[\frac{-15V}{4\pi h^4 p^{1/3} (p^{5/3} - 1)} \right] \right\}$$

which reduces in the special case of $h = R$, using

$$\frac{d}{dx} = \frac{d}{dh} ,$$

to

$$\frac{dF_x}{dx} \cong 0.557 \pi \sigma^2 R^3 G \quad \text{at } x = 0,$$

or

$$\frac{\frac{dF_x}{dx}}{G \rho^2 V} \Bigg|_{\substack{\text{bodies are} \\ \text{touching}}} \cong 1.312 .$$

II.3 Two Hemispheres - Analytic Treatment

The mutual force between two identical homogeneous hemispheres which are face-to-face can be found analytically (Reference 4). The force is calculated using the gradient theorem, once an expression for the potential of hemisphere "A" (see Figure V) is found.

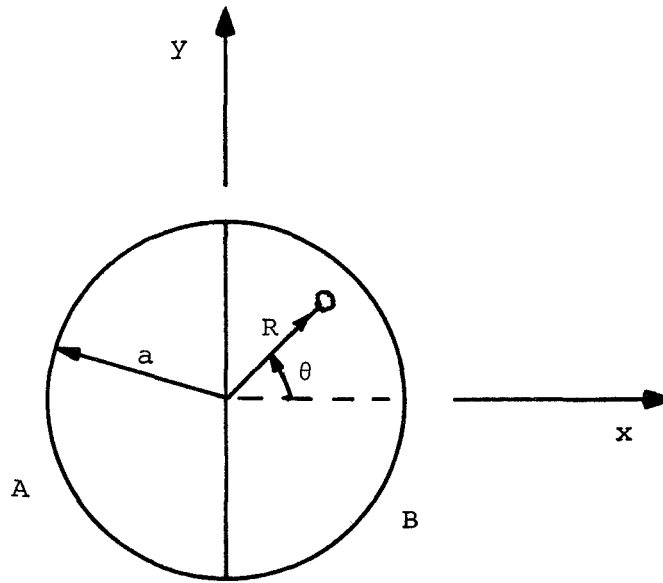


Figure V. HEMISPHERES A AND B

$$\underline{F} = \rho \int_{\text{volume of B}} \underline{\nabla}\phi d\tau = \rho \int_{\text{surface of B}} \phi \underline{n} dS \quad (12)$$

where

ϕ is the potential of hemisphere A

ρ is the mass density of B (and assumed to be the same for A in this case)

\underline{n} is the outward normal to the surface of B

$d\tau$ is volume element of B

dS is a surface element of B

One way to calculate the potential of "A" is to find the potential along the x axis, and then, since the body is one of revolution about that axis, expand the solution in Legendre polynomials for points off the axis (Reference 5). The potential along the x axis is given by

$$\phi(x) = \frac{2}{3} \pi \rho G \frac{a^3}{x} \left\{ 1 + \frac{3}{2} \left(\frac{x}{a}\right) - [1 - \left(\frac{x}{a}\right)^2]^{3/2} + \left(\frac{x}{a}\right)^3 \right\}. \quad (13)$$

A binomial expansion of (13) yields two different expressions depending on whether $\frac{x}{a}$ is less than or greater than one. In these expansions, powers of x^n are replaced by $R^n P_n(\cos \theta)$ in the first case, and $x^{-(n+1)}$ by $R^{-(n+1)} P_n(\cos \theta)$ in the second case. This results in

$$\begin{aligned} \phi_1(R, \theta) = \frac{2}{3} \pi \rho G a^2 \left\{ \frac{3}{2} - \frac{3}{2} \frac{R}{a} P_1(\cos \theta) + \left(\frac{R}{a}\right)^2 P_2(\cos \theta) \right. \\ \left. - \frac{3 \cdot 1}{2 \cdot 4} \left(\frac{R}{a}\right)^3 P_3(\cos \theta) + \frac{3 \cdot 1 \cdot 1}{2 \cdot 4 \cdot 6} \left(\frac{R}{a}\right)^5 P_5(\cos \theta) \right. \\ \left. - \frac{3 \cdot 1 \cdot 1 \cdot 3}{2 \cdot 4 \cdot 6 \cdot 8} \left(\frac{R}{a}\right)^7 P_7(\cos \theta) + \dots \dots \dots \right\} \\ 0 < R < a, \quad 0 < \theta < \frac{\pi}{2} \quad (14) \end{aligned}$$

and

$$\begin{aligned} \phi_2(R, \theta) = \frac{2}{3} \pi \rho G a^2 \left\{ \left(\frac{a}{R}\right) - \frac{3 \cdot 1}{2 \cdot 4} \left(\frac{a}{R}\right)^2 P_1(\cos \theta) + \frac{3 \cdot 1 \cdot 1}{2 \cdot 4 \cdot 6} \left(\frac{a}{R}\right)^4 P_3(\cos \theta) \right. \\ \left. - \frac{3 \cdot 1 \cdot 1 \cdot 3}{2 \cdot 4 \cdot 6 \cdot 8} \left(\frac{a}{R}\right)^6 P_5(\cos \theta) + \dots \dots \dots \right\} \\ R > a, \quad 0 < \theta < \frac{\pi}{2} \quad (15) \end{aligned}$$

When the hemispheres are face-to-face only equation (14) is necessary to evaluate (12) and hence the force between the two bodies. It should be noted that the author is currently treating an extension of this problem which will facilitate the calculation of the force regardless of the orientation of the hemispheres.

The mutual force (along the x axis) is found to be

$$F_x = -\frac{1}{3} \pi^2 \rho^2 G a^4$$

or

$$\frac{F_x}{G \rho^2 V^{4/3}} = -\left(\frac{3\pi^2}{16}\right)^{1/3} \cong -1.228 \quad . \quad (16)$$

Comparison of this result with equation (1) reveals an increase in force of about 90% for a given amount of mass, with an improvement of about 40% over (11). With improvements of this magnitude the question arises whether one could do still better with other shapes.

To attack this problem numerical techniques must be employed, as the analytic methods become quite difficult, especially when one looks for the dependence of the force upon separation of the masses.

II.4 Two Hemispheres - Computer Model

A particularly simple computational method was used to examine the interactions between various bodies. The program was not intended for highly accurate results, nor was it expected to be particularly efficient, but it represented a very straightforward approach to the problem, and was easily adaptable to bodies of various shapes.

The body in question (in this first case, a hemisphere) is divided into a number of identical cubes aligned with the coordinate axes. Each cube is treated as a point mass located at the center of the cube. The interactions among all the cubes are totaled for the force calculations. In the limit, as the number of cubes per unit volume becomes very large, the method approaches that of ordinary calculus.

For two bodies of revolution with their axes of symmetry aligned, the model can be reduced to the interaction among the cubes of one

quarter of one body and one half of the other, reducing the number of necessary calculations.

In Figure VI two arbitrary bodies are assumed to be made up of n_A and n_B cubes, each of mass m_a and m_b , respectively. The component

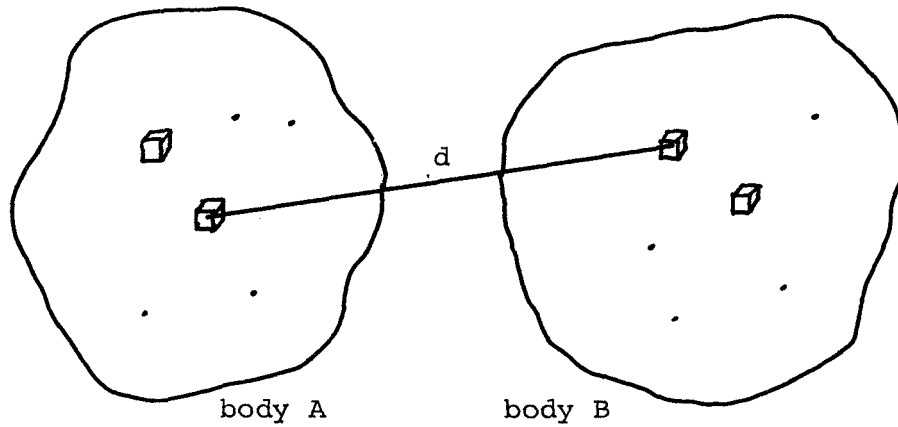


Figure VI.

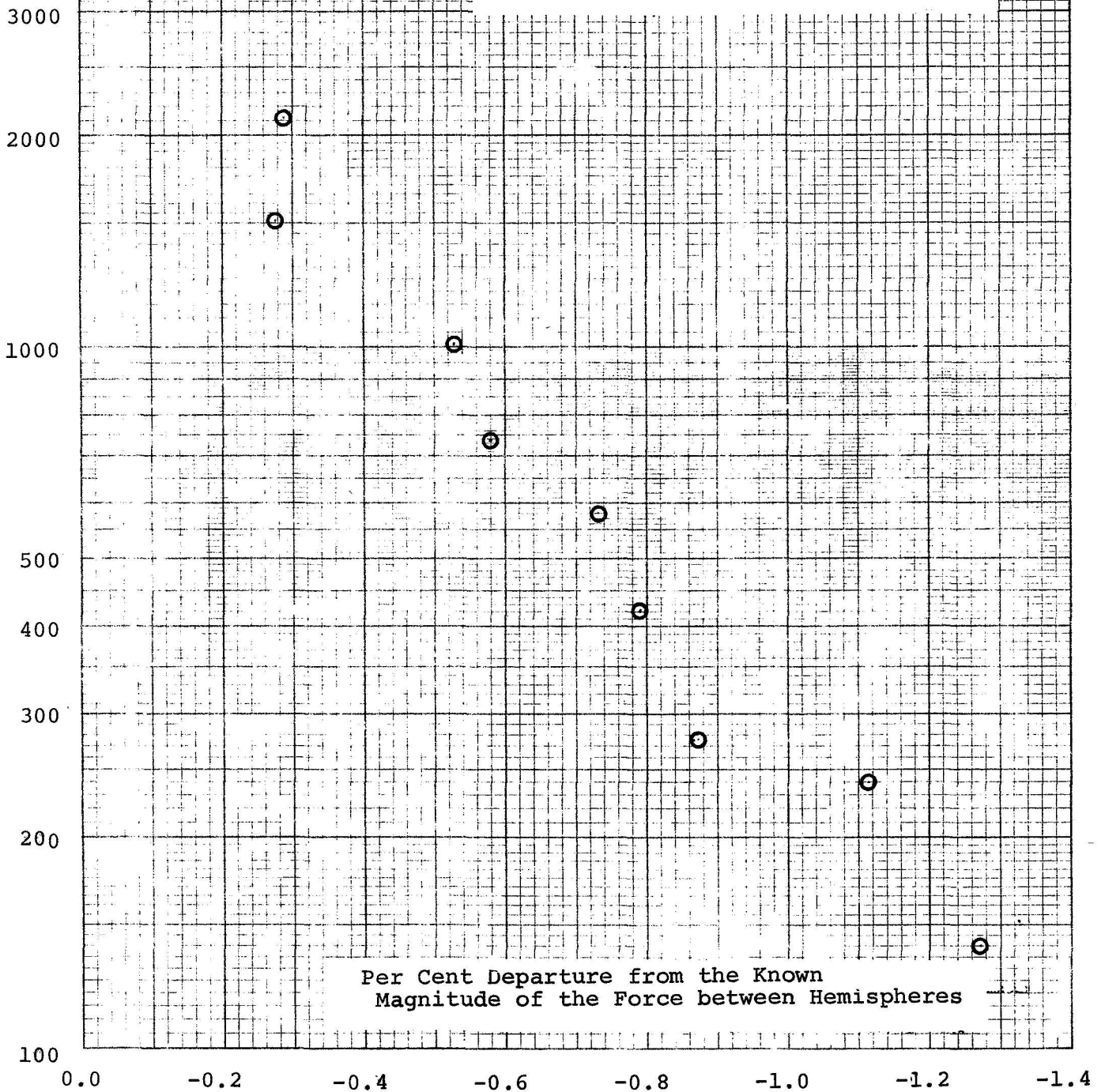
of force in the x direction is

$$\begin{aligned}
 F_x &= G \sum_{\text{body A}} m_a \sum_{\text{body B}} m_b \frac{d_{ab} \cdot \hat{x}}{d_{ab}^3} \\
 &= G m_a m_b \sum_A \sum_B \frac{d_{ab} \cdot \hat{x}}{d_{ab}^3} \tag{17}
 \end{aligned}$$

If each cube of "A" is of length ℓ_A on a side and each cube of "B" is ℓ_B on a side, and ρ_A and ρ_B are the respective mass densities, (17) becomes

Number of Cubes
per hemisphere
in Model

Figure VII. Computer Results
for the Force between Two
Hemispheres which are Face-to-Face



$$F_x = G \rho_A \rho_B l_A^3 l_B^3 \sum_A \sum_B \frac{d_{ab} \cdot \hat{x}}{d_{ab}^3}$$

or in dimensionless form

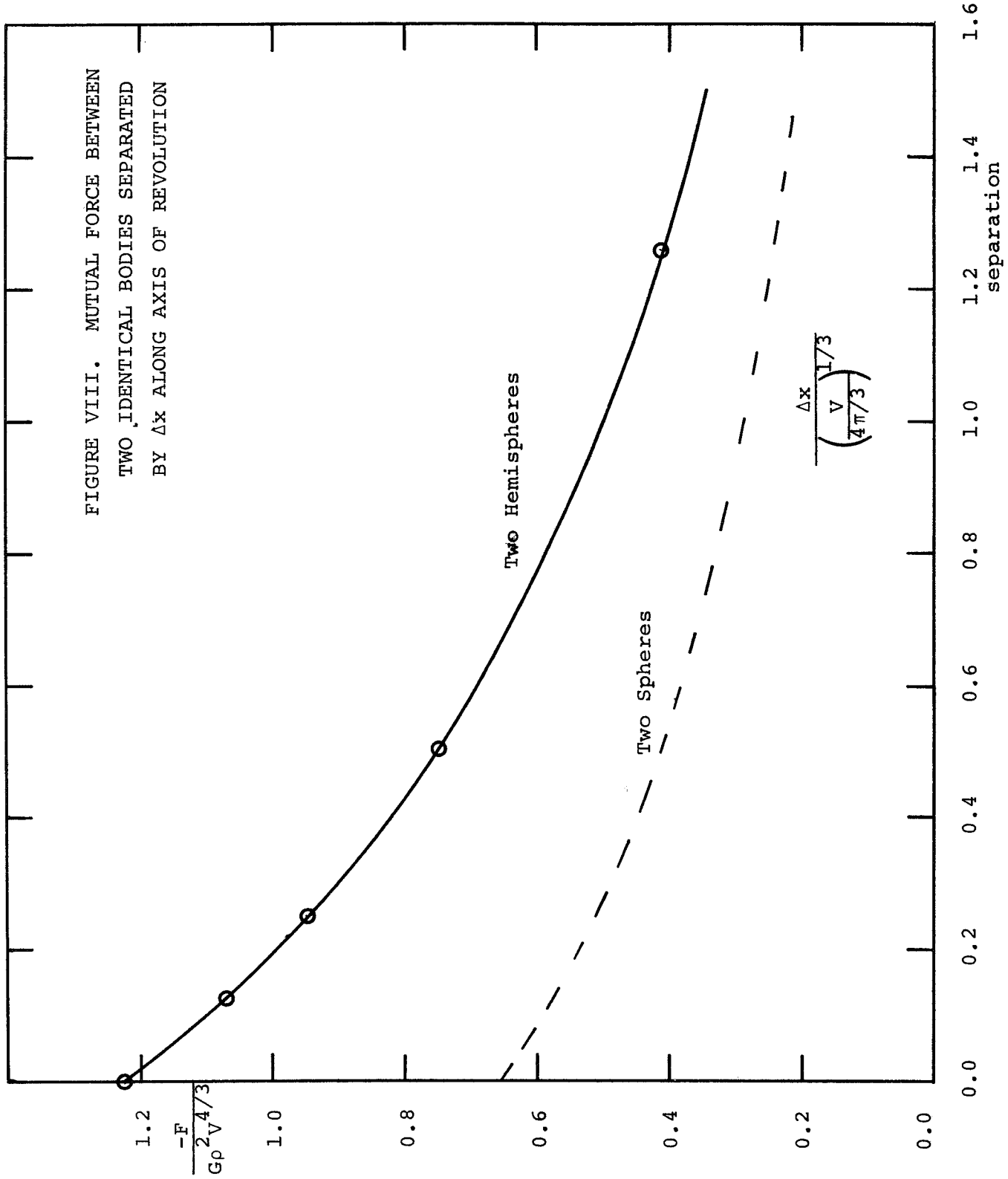
$$\frac{F_x}{G \rho_A \rho_B V_A^{2/3} V_B^{2/3}} = \frac{l_A^3 l_B^3}{V_A^{2/3} V_B^{2/3}} \sum_A \sum_B \frac{d_{ab} \cdot \hat{x}}{d_{ab}^3} \quad (18)$$

where V_A and V_B are the volumes, respectively, of "A" and "B". The double summation in (18) represents six summations for the arrays of cubes and is a task suitable only for a digital computer. The total is adjusted when only a partial summation is performed (for the symmetric case mentioned) and normalized by the factor in front.

With the analytic expression (16) for the two hemispheres face-to-face, the results of using various computer models of hemispheres can be compared. Figure VII indicates the accuracy as a function of the number of cubes per body in the model. Note that the results are consistently below the exact analytic value, but converge to well within 1% for hemisphere models with only six or seven cubes on a radius length. A check of the double precision program indicates no truncation error for the range of calculation shown in Figure VII.

To obtain a feeling for the dependence of the force on separation, the hemispheres are separated by a translation along the x axis, and the results are shown in Figure VIII and Appendix A. For very small separations, models with 1508 cubes per hemisphere are used to approximate the slope of the curve as the begin to separate:

FIGURE VIII. MUTUAL FORCE BETWEEN
TWO IDENTICAL BODIES SEPARATED
BY Δx ALONG AXIS OF REVOLUTION



$$\begin{aligned}
\left. \frac{\frac{\partial F}{\partial x}}{G\rho^2 V} \right|_{\substack{\text{hemispheres} \\ \text{are touching}}} &\cong \left(\frac{4\pi}{3} \right)^{1/3} \left. \text{slope in} \right|_{\Delta x=0} \\
&\quad \left. \text{fig. VIII} \right| \\
&\cong \left(\frac{4\pi}{3} \right)^{1/3} \left(\frac{0.01315}{0.01} \right) \\
&\cong 2.12 \qquad \qquad \qquad (19)
\end{aligned}$$

II.5 Two Blocks

A computer model was also developed for two identical, homogeneous blocks for various width to length ratios. Only blocks with square cross section in the y-z plane are considered, since the primary objective is to maximize the magnitude of the force between them. The results are shown in Figure IX and Appendix B, where the "best" geometry dictates a width to length ratio of about 2.85 with a mutual force of

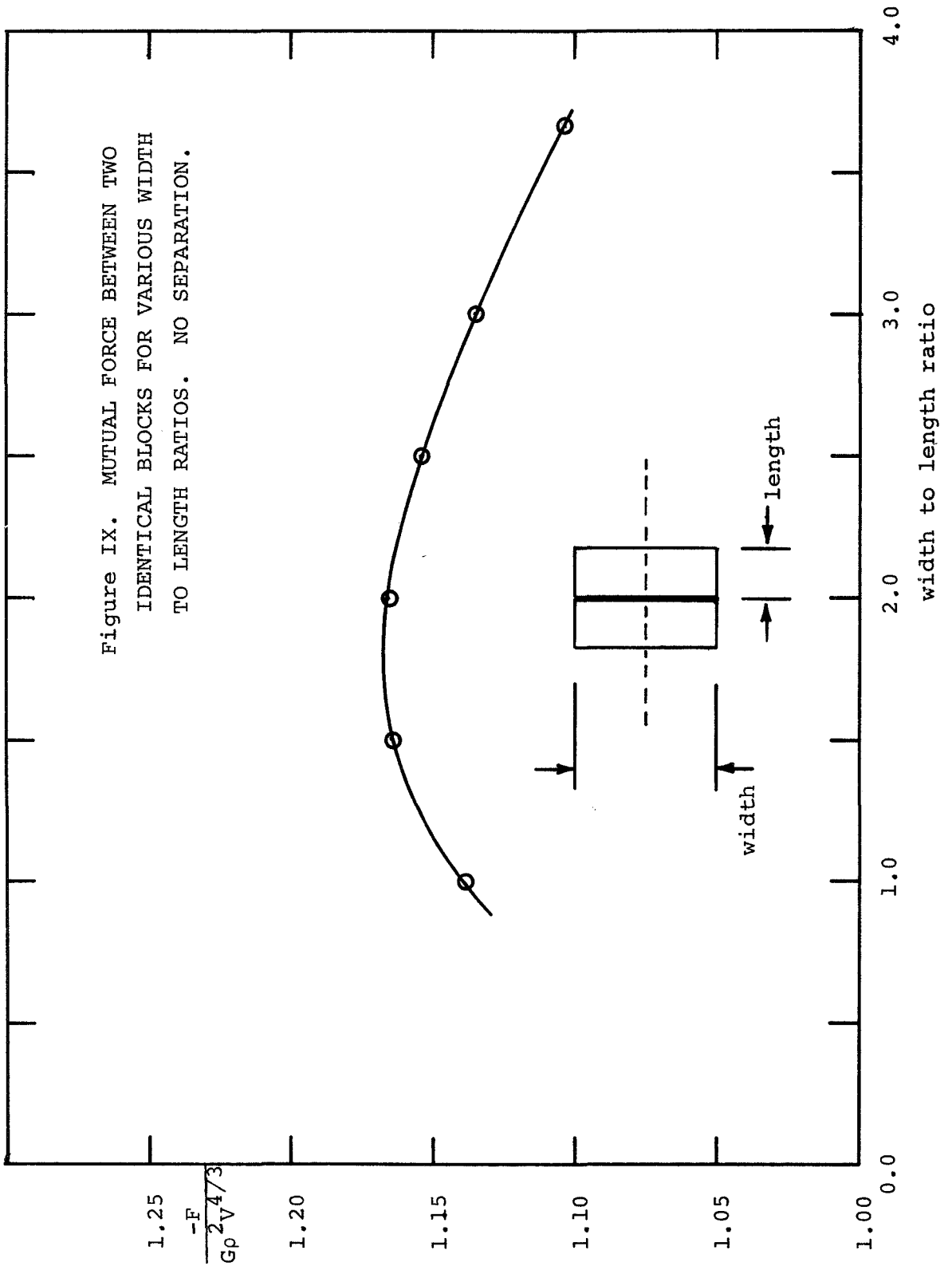
$$\frac{F_x}{G\rho^2 V^{4/3}} \cong -1.166$$

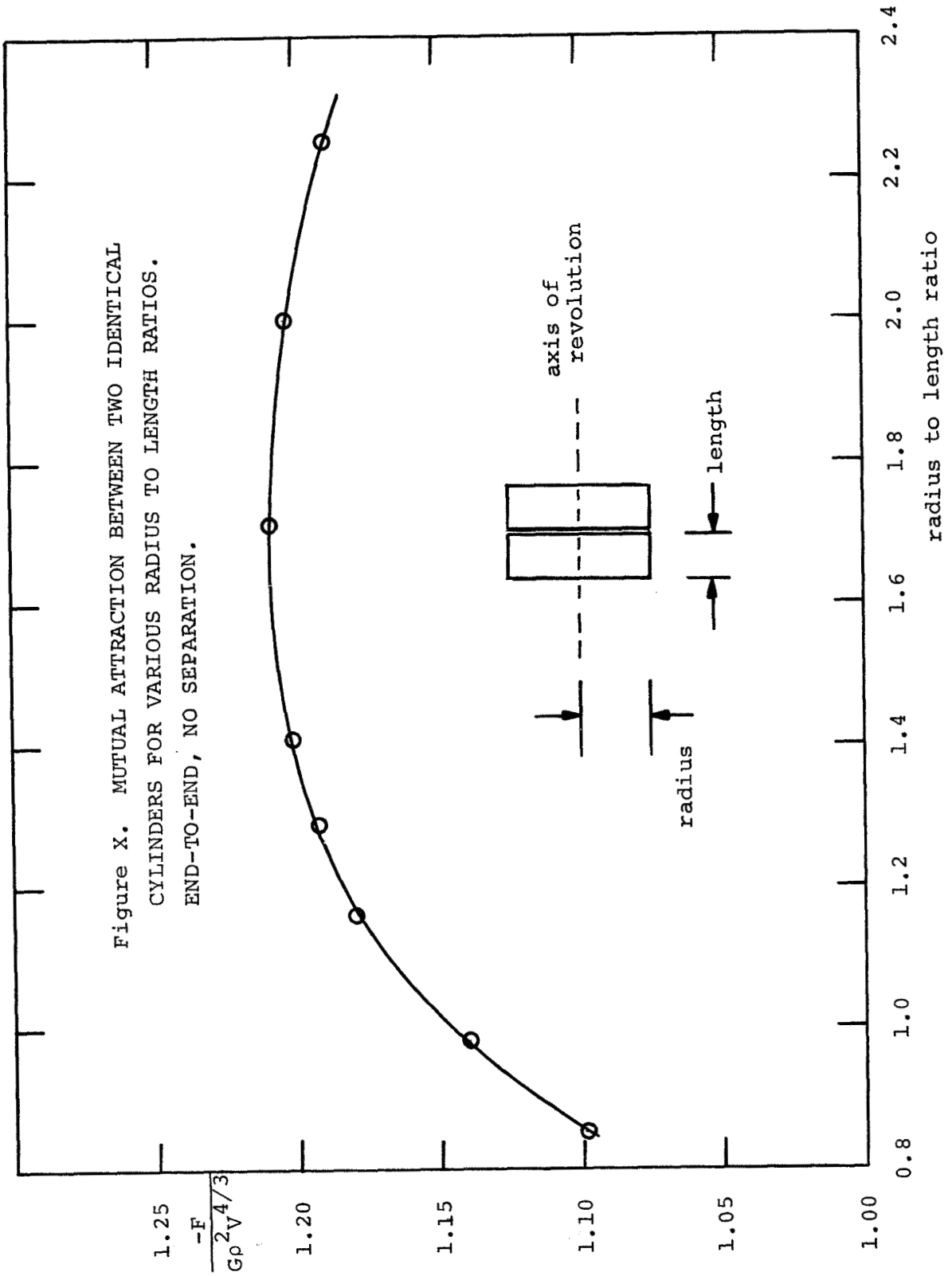
and a first derivative (obtained in the same manner as (19)):

$$\left. \frac{\frac{\partial F}{\partial x}}{G\rho^2 V} \right|_{\substack{\text{blocks are} \\ \text{touching}}} \cong 2.02$$

II.6 Two Right Cylinders

Two identical right cylinders, situated end-to-end, are treated





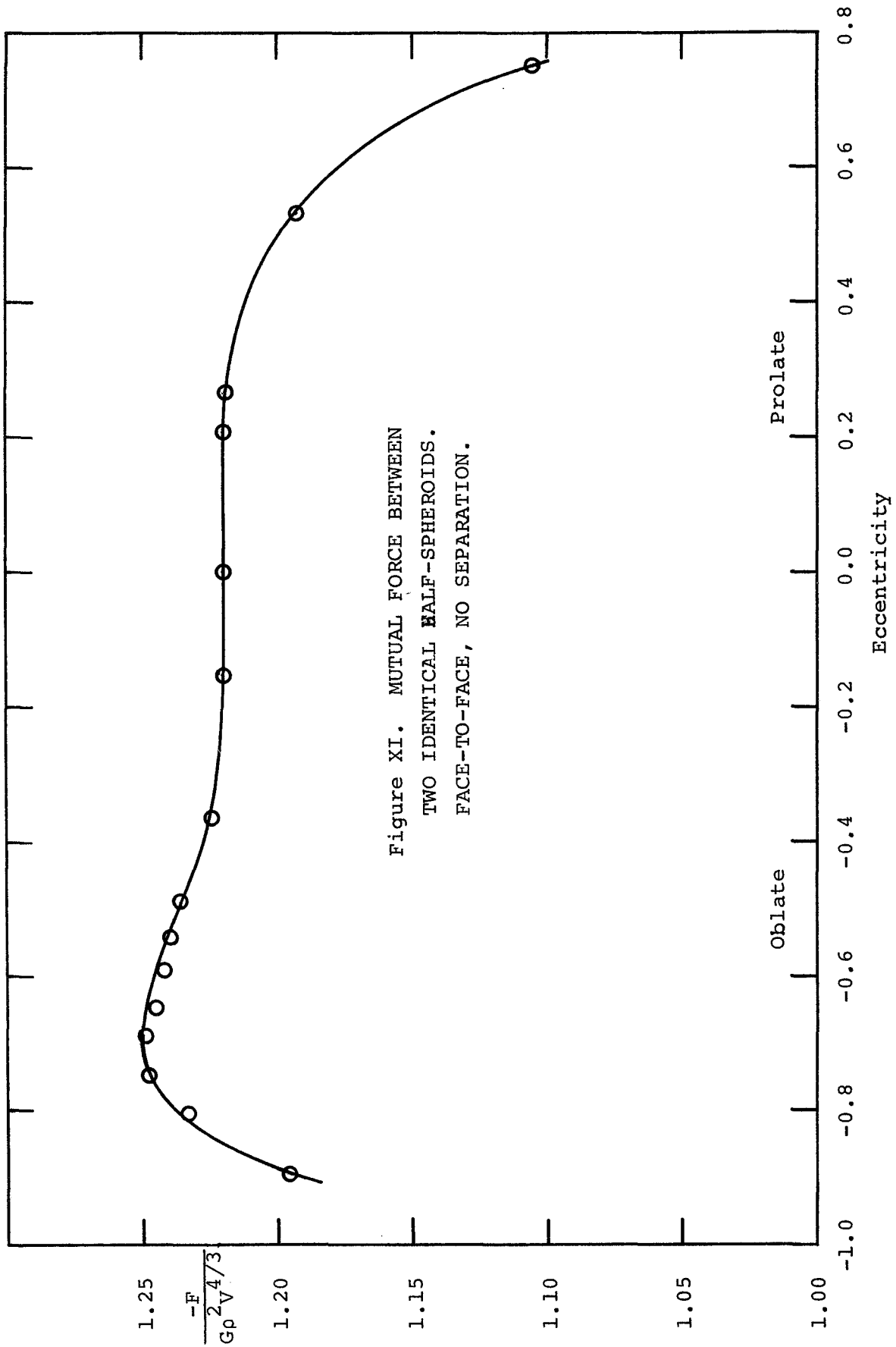


Figure XI. MUTUAL FORCE BETWEEN
TWO IDENTICAL HALF-SPHEROIDS.
FACE-TO-FACE, NO SEPARATION.

analogously for various radius to length ratios. As is the case with the blocks, the optimization of the cylinders yields a gravitational force nearly that of the hemispheres. For a radius to length ratio of 1.72, the force is

$$\frac{F_x}{G\rho^2 V^{4/3}} \cong -1.210$$

and

$$\left. \frac{\frac{\partial F}{\partial x}}{G\rho^2 V} \right|_{\substack{\text{cylinders} \\ \text{are touching}}} \cong 2.08 .$$

All the results are shown in Figure X and Appendix C.

II.7 Two Spheroids

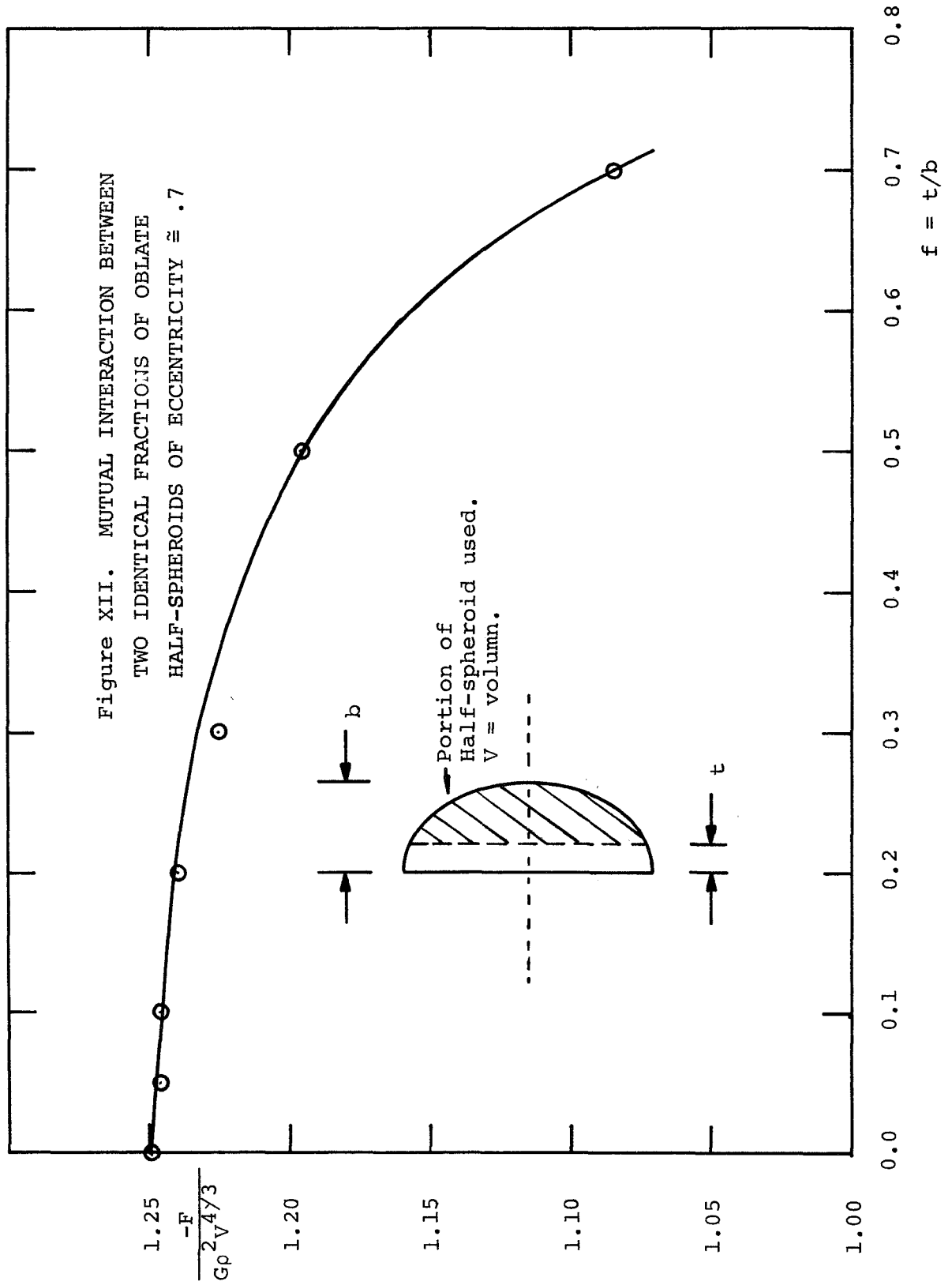
In order to learn how much better one can do in terms of maximizing the level of force between two bodies, a larger class of bodies is examined. The half spheroid, with circular cross section in the y-z plane introduces an extra parameter, its eccentricity. For convenience this was defined as positive for prolate cases (the spheroid is longer in the x direction) and negative for oblate cases.

The results shown in Figure XI and Appendix D, indicate the largest force corresponds to an oblate spheroid of eccentricity = .69. For this case the force is

$$\frac{F}{G\rho^2 V^{4/3}} \cong -1.249$$

and

$$\left. \frac{\frac{\partial F}{\partial x}}{G\rho^2 V} \right|_{\substack{\text{spheroids are} \\ \text{touching}}} \cong 2.09 .$$



Note the very small improvement over the hemisphere (eccentricity = 0) in terms of maximizing the force. Also evident from Figure XIII is the insensitivity of the magnitude of the force to changes in eccentricity near $e = 0$, a significant fact from the standpoint of precision machining.

One additional parameter is introduced in this final case ($e \sim .7$) in an attempt to further increase the force. Only a fraction of the half spheroid is used, and the results normalized to account for the reduction in mass. As indicated in Figure XII and Appendix D, the effect detracts from the total force.

II.8 Summary of Chapter II

It is apparent that one could continue the efforts of Section II.7 in a systematic attempt to determine the "best" shape. But it is also evident from the cases examined in Chapter II (see Figure XIII) that very little additional force can be obtained - probably only one or two per cent.


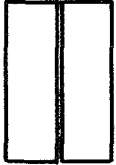

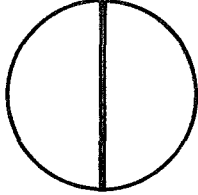

Further, the necessity for precision fabrication of the bodies tends to rule out an irregular shape. This leaves the cylinder, or hemisphere as prime candidates as far as the maximization of the magnitude of the force is concerned.

It should be noted, however, that with increases in the level of force there is also an increasing dependence upon small separations. Presumably this will detract somewhat from the over-all performance of a system composed of "better" shapes when the dependence of the torque upon small separations is required to be small.

III. THE EFFECT OF USING HEMISPHERES INSTEAD OF SPHERES IN A BEAMS - TYPE EXPERIMENT

The results of Chapter II suggest that the use of hemispheres instead of spheres might very well improve the performance of the

Figure XIII. Summary of the Gravitational Interactions between Bodies of Uniform Density, for a Given Amount of Mass.

NO SEPARATION (X) BETWEEN BODIES		best* shape with sphere		best* width/length ratio ≈ 3.0		best* radius/length ratio ≈ 1.72		best* eccentricity ≈ .694	
	two identical spheres	two identical spheres of same mass	two identical blocks	two identical cylinders	two identical cylinders	two identical cylinders	two identical hemispheres	two identical half-spheroids (oblate)	
$\frac{-F}{G\rho^2 V^{4/3}}$.650	.864	1.166 +1% -0%	1.210 +1% -0%	1.228	1.249 +1% -0%			
$\frac{\partial F}{\partial x} \frac{(0)}{G\rho^2 V}$	1.047	1.312	2.02 ±10%	2.08 ±10%	2.12 ±10%	2.09 ±10%			

* Note: The "best" choice implies maximizing the magnitude of the force between the bodies.
 F is the gravitational force.
 ρ is the mass density.
 V is the volume of one body.
 G is the gravitational constant.

Beams-type experiment. In this chapter this possibility is examined by comparing a system involving two identical, uniform hemispheres, a so-called "one-arm device," with a similar system using spheres (Reference 2).

A computer model using 140 cubes per hemisphere is used to treat the hemisphere case. As in Chapter II, the mutual interactions among all the cubes are totaled, only in this case, each force interaction is multiplied by the appropriate moment arm length. Positive torque is taken in the sense that the attraction of body "A" to "B" causes "A" to rotate in a counterclockwise direction. An extension of this analysis to a four-arm device (eight masses) would require approximately four times as much computer time and was not carried out for that reason.

III.1 Criteria for Comparing Performances

Three criteria are used to compare the performances of the two systems. Of prime importance is the level of angular acceleration which can be achieved. The acceleration is a quantity which must be measured experimentally, thus it is desirable to keep it as large as possible. The acceleration is calculated by dividing the total torque generated, by the moment of inertia of the near body (assumed to be free to accelerate) about the pivot. For the spheres, using the parallel axis theorem, this is

$$\begin{aligned}
 I_{\text{pivot}} &= I_{\text{c.m.}} + Ma^2 \\
 &= M\left[\frac{2}{5} \left(\frac{3V}{4\pi}\right)^{2/3} + a^2\right] \\
 &\cong M[.100 V^{2/3} + a^2]
 \end{aligned}
 \tag{20}$$

where M and V are the mass and volume, respectively, of the body and "a" is the distance from the pivot to its center of mass. For the hemispheres:

$$\begin{aligned}
 I_{\text{pivot}} &= I_{\text{c.m.}} + Ma^2 \\
 &= M\left[\frac{2}{5}R^2 - \left(\frac{3}{8}R\right)^2 + a^2\right] \\
 &= M\left[.158V^{2/3} + a^2\right] \quad . \quad (21)
 \end{aligned}$$

The second criteria is a dimensionless torque parameter, normalized in the following manner:

$$\frac{\text{Torque}}{G\rho^2V^{4/3}a} \quad .$$

A large torque is desirable as there will be unknown bias torques in the suspension system. Unlike the acceleration, the torque will increase with increasing the size of the experiment.

However, it is wise to keep the system as compact as possible to reduce the effects of temperature variations and of disturbance torques due to external distributions of mass. Furthermore, it is advantageous to restrict the quantity of mass required when designing an experiment intended for space.

Since the force between two adjacent bodies is proportional to the volume raised to the four-thirds power, division of the torque by that quantity eliminates the effect of increasing the mass of the system. In order to compare systems of comparable size, the torque is further normalized by a characteristic moment arm. The length "a" is used as it seems to be a key parameter.

A second normalization of torque (also dimensionless),

$$\frac{\text{Torque}}{G\rho^2 l^5},$$

reflects the level of torque achievable for a given size of experiment, when the amount of mass is not restricted. The length "l" is the distance from the pivot to the center of mass of the far body.

III.2 Constraints on the Possible Geometrical Configurations

For all cases an important constraint is imposed upon the operation of the system. The requirement is that there be no first order change in torque when the angular separation of the torque arms changes by a small increment $\pm \Delta\theta$. This is necessary because the servo-control system will not be able to maintain a perfectly constant separation θ_0 . This constraint may be expressed as

$$\left. \frac{\partial T}{\partial \theta} \right|_{\theta_0} = 0$$

and the torque is required to be a maximum for a particular θ_0 . For the spheres on a two-arm device this constraint leads to the relation

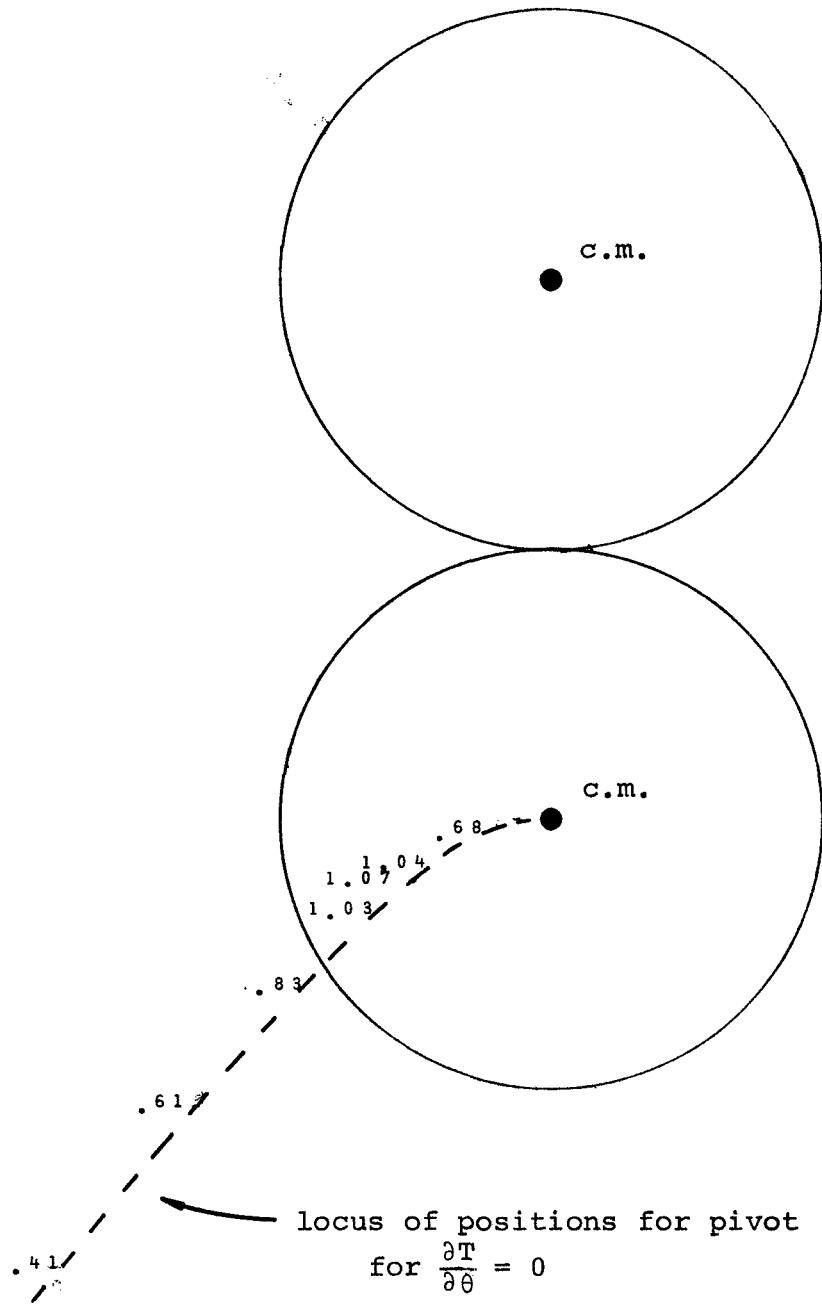
$$\theta_0 = \cos^{-1} \left\{ \frac{1}{2}(q^2+12)^{1/2} - \frac{q}{2} \right\}$$

where

$$q = \frac{(a/l)^2 + 1}{a/l} .$$

This specifies a single parameter family of possible geometrical configurations, as shown in Figure XIV, if the spheres are to remain touching, or very nearly so.

Figure XIV. FOR $\frac{\partial T}{\partial \theta} = 0$ AND USING SPHERES: THE POSSIBLE LOCATIONS OF THE PIVOT RELATIVE TO THE SPHERES AND CORRESPONDING LEVELS OF ANGULAR ACCELERATION ($\text{rad}/\text{sec}^2 \times 10^6$) FOR A ONE ARM DEVICE.



Two hemispheres, however, will remain in close proximity to each other for an unlimited number of orientations. In this analysis the faces of the hemispheres are kept parallel, but in general, this is not necessary. Allowing the faces to shift relative to one another introduces another parameter, and hence, there is a double parameter family of geometric locations for the pivot which satisfy $\partial T / \partial \theta = 0$. Figure XV locates several of the positions with the small numbers, which correspond to the levels of angular acceleration. Each point also corresponds to a particular orientation of hemisphere "B" as shown for three particular cases.

II.3 Comparison of Results of a One-Arm Device Using Either Spheres or Hemispheres

The levels of angular acceleration and torques are indicated in Figures XIV and XV for the spheres and Figures XV, XVI, and Appendix E for the hemispheres. In Figure XVI, the accelerations are plotted against the ratio of torque arms (a/l). The spheres are represented by the solid line and the hemispheres by the dots. Since there is an additional parameter associated with the hemispheres, there are an infinite number of points for each (a/l) ratio. There is an upper limit, however, for each a/l , and even with the few data points collected, one can get a good idea of the maximum acceleration for each a/l .

It appears as if the angular acceleration can be increased by only a few per cent with the use of hemispheres for the one arm case. Note, however, that the larger accelerations occur in situations where the pivot is very close to the center of mass of hemisphere "A". An examination of the expressions for the moments of inertia (20 and 21) reveals that for small "a", the first term dominates in each of these expressions. This means that the moment of inertia for the hemispheres is about 60% greater than that of spheres in this case, and hence, the angular acceleration is diminished by that amount. In order to get

Figure XV. FOR $\frac{\partial T}{\partial \theta} = 0$ AND USING HEMISPHERES: THE POSSIBLE LOCATIONS OF THE PIVOT RELATIVE TO HEMISPHERE A, CORRESPONDING LEVELS OF ANGULAR ACCELERATION (rad/sec² X 10⁶), AND THREE CORRESPONDING POSITIONS OF HEMISPHERE B FOR A ONE ARM DEVICE.

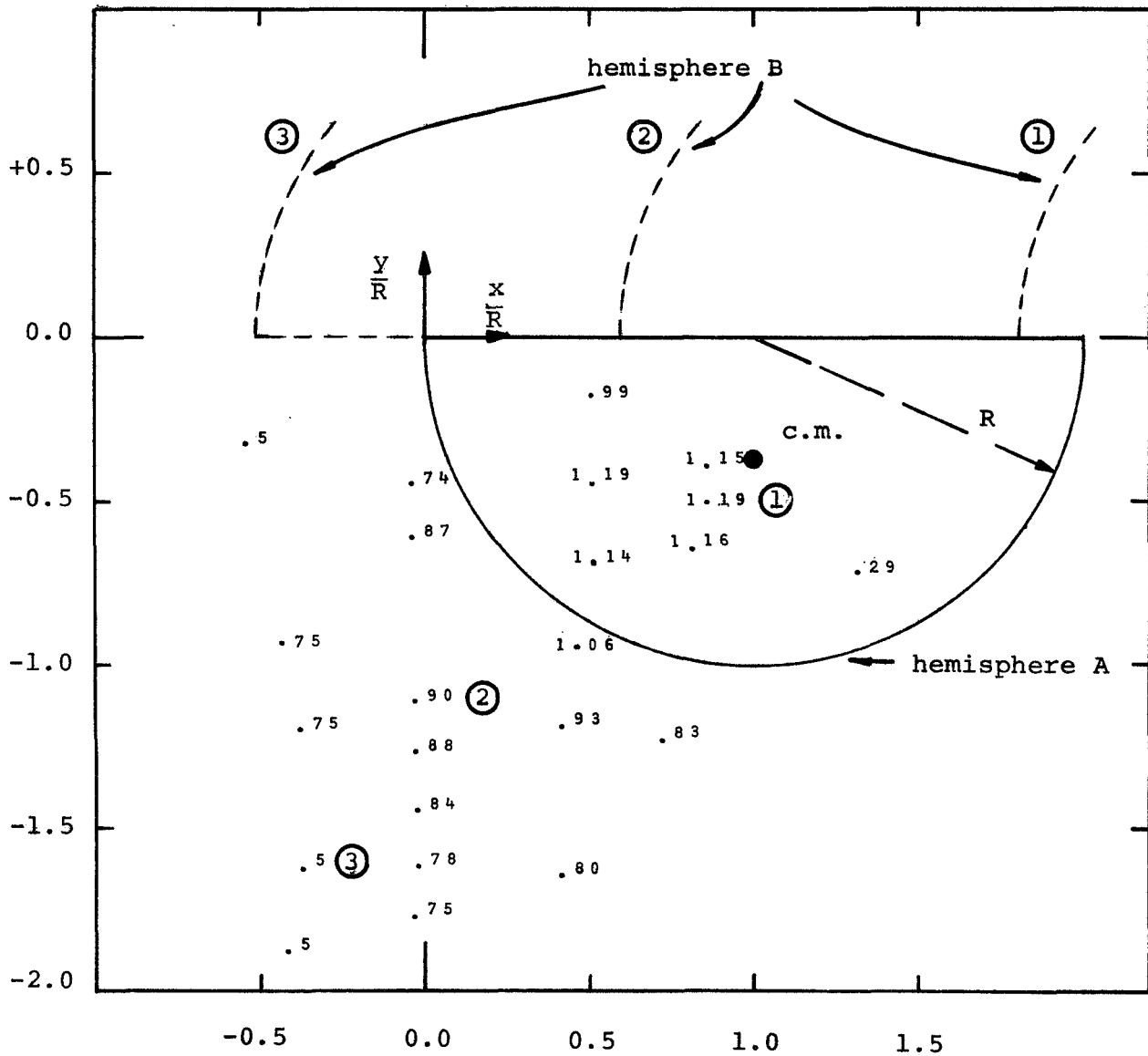


Figure XVI. FOR $\frac{\partial T}{\partial \theta} = 0$. COMPARISON OF ANGULAR ACCELERATIONS AND NON-DIMENSIONALIZED TORQUES FOR SPHERES AND HEMISPHERES FOR A ONE ARM DEVICE.

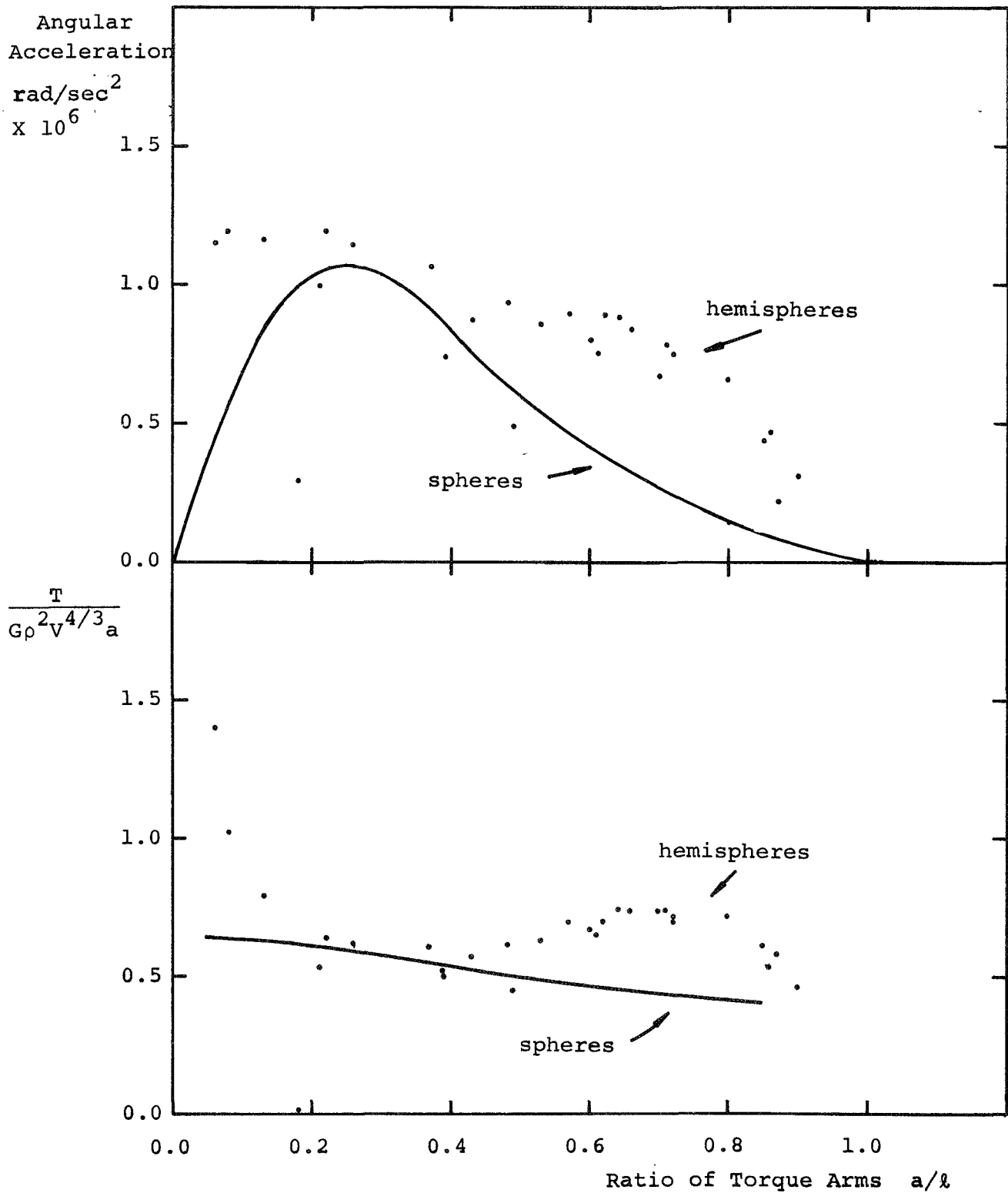
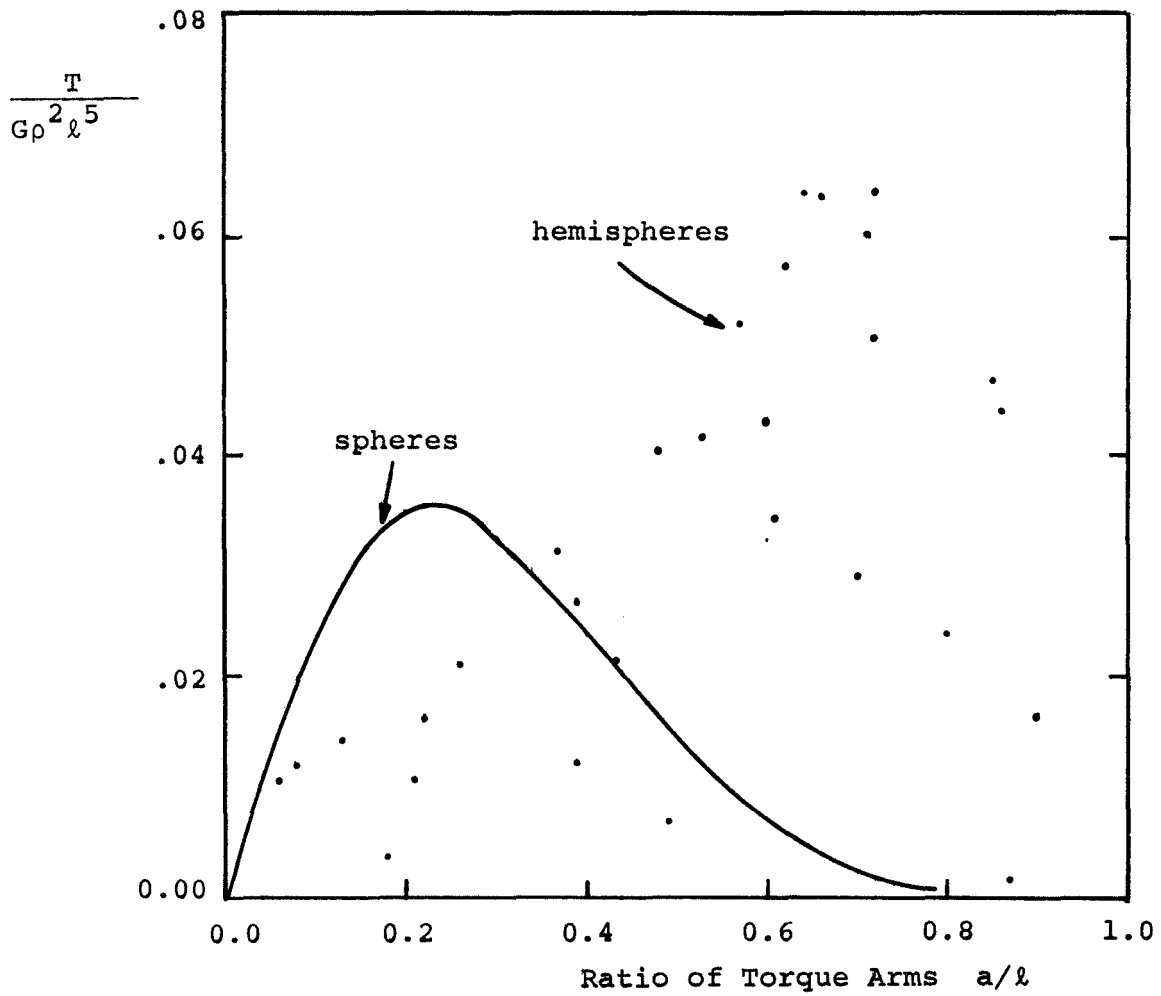


Figure XVII. FOR $\frac{\partial T}{\partial \theta} = 0$. COMPARISON OF TORQUES
 NORMALIZED TO $G\rho^2 l^5$ FOR SPHERES AND
 HEMISPHERES FOR A ONE ARM DEVICE.



a net increase in the acceleration, as is the case, the torque generated must overcome this "handicap".

As Blood (Reference 2) has shown, optimum operation of a four-arm sphere device dictates higher a/l 's and the pivot moves away from the center of mass of "A". This greatly reduces the weighting of the first term in moment of inertia, and there is a good chance the relative performance of the hemispheres will improve significantly.

Examination of the levels of torque normalized to $G\rho^2V^{4/3}a$ indicates some improvement, especially for small "a" again. In the bottom half of Figure XVI one can again visualize an upper bound on the envelope of possible torques with the use of hemispheres. This torque parameter reflects the torque achievable for a given amount of mass and a given size of experiment.

The peak at very small "a" might very well shift to larger "a" for a four-arm device. It is not clear at this point just how large the peak is, but it appears to be well over twice as large (maybe significantly larger) as the corresponding curve for the spheres.

Note that for every a/l one can find a configuration involving hemispheres which will increase both the angular acceleration and $T/G\rho^2V^{4/3}a$.

Finally, if one is not particularly concerned about the amount of mass incorporated into the experiment, but only on the size, Figure XVII compares the torques of the two systems. There is a marked improvement for some ratios of a/l , but not for the smaller ratios. This means that the previous optimizations conflict with this one. Whether or not they will merge for a four-arm device is unknown.

IV. SUMMARY AND CONCLUSIONS

With the 89% increase in force between two identical hemispheres over spheres of the same mass, the fundamental question is whether or

not this would carry over to the problem of generating torque and angular acceleration in a Beam's-type experimental set up.

As shown by Blood, the optimum arrangement calls for a four-arm device. Analysis of a one-arm device indicates that the performance can indeed be improved, but not by a straight factor of two. There is evidence, however, that more improvement, particularly in the levels of angular acceleration, may well show up in a four-arm device. Hopefully, this can be investigated with the use of a more analytic, more efficient method currently being developed by the author.

Finally, it should be kept in mind that the analysis of the hemisphere device was based on approximate methods, and also, restricted the orientations of the hemispheres relative to one another. Both of these simplifications would tend to diminish the true optimum performance levels of the device.

Appendix A

Computer Results for the Calculation of the Force Between Two Hemispheres

Normalized Separation	Normalized Force	Number of Cubes per Hemisphere in Model
$\frac{\Delta x}{\left(\frac{3V}{4\pi}\right)^{\frac{1}{3}}}$	$\frac{-F}{G\rho^2 V^{\frac{4}{3}}}$	
0.0	1.17541	44
0.0	1.21212	140
0.0	1.21405	240
0.0	1.21797	420
0.0	1.22058	736
0.0	1.22117	1004
0.0	1.22425	1508
0.0	1.22422	2112
0.01	1.21110	1508
0.02	1.19816	1508
0.03	1.18543	1508
0.038	1.172	736
0.063	1.141	736
0.126	1.070	736
0.252	0.944	736
0.505	0.748	736
1.26	0.411	736
2.52	0.193	736

Appendix B

Computer Results for the Calculation of the Force Between Two Blocks

Normalized Separation	Width/Length Ratio	Normalized Force	Number of Cubes per Block
$\frac{\Delta x}{\left(\frac{3V}{4\pi}\right)^{\frac{1}{3}}}$		$\frac{-F}{G\rho^2V^{\frac{4}{3}}}$	
0.0	2.0	1.1395	600
0.0	2.5	1.1645	400
0.0	3.0	1.1657	576
0.0	3.5	1.1539	784
0.0	4.0	1.1349	124
0.0	4.667	1.1040	588
0.01	3.0	1.1545	576
0.02	3.0	1.1433	576
0.03	3.0	1.1323	576
0.10	3.0	1.0592	576
0.20	3.0	0.9651	576

Appendix C

Computer Results for the Calculation of the Force Between Two Right Cylinders

Normalized Separation	Radius/Length Ratio	Normalized Force	Number of Cubes per Cylinder
$\frac{\Delta x}{\left(\frac{3V}{4\pi}\right)^{\frac{1}{3}}}$		$\frac{-F}{G\rho^2 V^{\frac{4}{3}}}$	
0.0	0.407	0.7829	520
0.0	0.691	1.0184	768
0.0	0.853	1.0989	784
0.0	0.981	1.1405	1040
0.0	1.162	1.1804	1456
0.0	1.289	1.1930	1128
0.0	1.409	1.2035	780
0.0	1.716	1.2095	592
0.0	1.719	1.2097	1160
0.0	2.006	1.2033	1580
0.0	2.257	1.1894	1024
0.0	2.570	1.1675	1328
0.0	3.009	1.1320	768
0.01	1.716	1.1970	592
0.02	1.716	1.1846	592
0.03	1.716	1.1725	592
0.10	1.716	1.0926	592
0.20	1.716	0.9916	592

$\frac{\Delta x}{\left(\frac{3V}{4\pi}\right)^{\frac{1}{3}}}$	Radius/Length Ratio	$\frac{-F}{G\rho^2 V^{\frac{4}{3}}}$	Number of Cubes per Cylinder
0.40	1.716	0.8257	592
1.00	1.716	0.5085	592
2.00	1.716	0.2649	592

Appendix D

Computer Results for the Calculation of the Force
Between Two Half-Spheroids

Normalized Separation	Eccentricity (pos. if pro- late; neg. if oblate)	Normalized Force	Number of Cubes per half spher- oid
$\frac{\Delta x}{\left(\frac{3V}{4\pi}\right)^{\frac{1}{3}}}$		$\frac{-F}{G\rho^2 V^{\frac{4}{3}}}$	
0.0	-.898	1.1955	380
0.0	-.805	1.2335	696
0.0	-.747	1.2478	1024
0.0	-.694	1.2493	1284
0.0	-.694	1.2481	872
0.0	-.646	1.2452	776
0.0	-.593	1.2420	404
0.0	-.541	1.2403	640
0.0	-.491	1.2357	556
0.0	-.361	1.2245	520
0.0	-.155	1.2206	736
0.0	+.206	1.2206	688
0.0	+.265	1.2191	668
0.0	+.536	1.1933	800
0.0	+.753	1.1064	464
0.0	-.699	1.2318	512

$\frac{\Delta x}{\left(\frac{3V}{4\pi}\right)^{\frac{1}{3}}}$	Eccentricity	$\frac{-F}{G\rho^2 V^{\frac{4}{3}}}$	Number of Cubes per half-spher- oid
0.02	-.699	1.2191	512
0.03	-.699	1.2066	512
0.10	-.699	1.1239	512
0.20	-.699	1.1019	512

Normalized Separation	Eccentricity	Fraction of Spheroid	Normalized Force	Number of Cubes per Body
$\frac{\Delta x}{\left(\frac{3V}{4\pi}\right)^{\frac{1}{3}}}$		f	$\frac{-F}{G\rho^2 V^{\frac{4}{3}}}$	
0.0	-.693	.05	1.2459	544
0.0	-.695	.10	1.2465	1020
0.0	-.694	.20	1.2390	1200
0.0	-.700	.30	1.2248	844
0.0	-.697	.50	1.1961	1272
0.0	-.694	.70	1.0852	492

Appendix E

Computer Results for the Calculation of the Torque

Generated by Two Hemispheres when $\frac{\delta T}{\delta \theta} = 0$

Position of Pivot		Position of near edge of B	Ratio of Torque Arms	Normalized Torque	Ang. Acc.
$\frac{x_p}{R}$	$\frac{y_p}{R}$	$\frac{x}{R}$	a/l	$\frac{T}{G\rho^2V^{4/3}a}$	$\times 10^6 \frac{\text{rad}}{\text{sec}^2}$
- .50	-2.50	-1.17	.90	.47	.31
- .50	- .31	+1.48	.49	.45	.49
- .38	-1.85	- .57	.86	.53	.47
- .38	- .86	+ .68	.61	.65	.75
- .33	-1.59	- .51	.85	.61	.43
- .33	-1.18	+ .18	.72	.70	.75
0.0	- .59	+1.18	.43	.57	.87
0.0	-5.00	- .83	.87	.58	.22
0.0	- .43	+1.47	.39	.51	.74
0.0	-4.88	- .48	.80	.72	.66
0.0	-1.74	- .02	.72	.72	.75
0.0	-1.02	+ .72	.53	.65	.86
0.0	-1.60	.04	.71	.74	.78
0.0	-1.10	.59	.57	.70	.90
0.0	-1.42	.24	.66	.73	.84
0.0	-1.26	.40	.62	.72	.88
0.0	-1.31	.31	.64	.74	.87
+ .57	- .15	1.85	.21	.53	.99
.53	- .43	1.59	.22	.64	1.19
.50	-2.20	.17	.70	.74	.67
.50	- .65	1.41	.26	.62	1.14
.47	- .90	1.14	.37	.61	1.06
.45	-1.62	.51	.60	.66	.80
.45	-1.18	.88	.48	.61	.93
.88	- .36	1.91	.06	1.40	1.15
.86	- .49	1.81	.08	1.02	1.19
.75	-1.19	1.20	.39	.50	.83
.83	- .60	1.71	.13	.79	1.16
1.34	- .69	2.25	.18	.01	.29

REFERENCES

1. Beams, J.W., Rose, R.D., Parker, H.M., Lowry, R.A., Kuhlthau, A.R., "Determination of the Gravitational Constant G", Physical Review Letters, 23, 12, Sept. 22, 1969, pp. 655-658.
2. Blood, B.E., "An Elementary Analysis of the Adaptation of the Beams' Experimental Concept to a $\Delta G/G$ Detector to be Used in Space", M.I.T. Measurement Systems Laboratory Report, RN-60, June 1970.
3. Hildebrand, F.B., Methods of Applied Mathematics, second edition, Prentice-Hall, Inc., Englewood Cliffs, N.J., 1965, pp. 123-125.
4. Madden, S.J., private communication.
5. MacMillan, W.D., The Theory of the Potential, Dover Publications, Inc., N.Y., N.Y., 1958, pp. 360-362.

APPENDIX E

ANALYSIS OF AN EXPERIMENT TO DETERMINE
THE GRAVITATIONAL CONSTANT IN AN ORBITING
SPACE LABORATORY

ANALYSIS OF AN EXPERIMENT TO DETERMINE
THE GRAVITATIONAL CONSTANT IN AN
ORBITING SPACE LABORATORY

by

John P. Vinti

September, 1970

APPROVED:

J. Markey

Director
Measurement Systems Laboratory

Measurement Systems Laboratory
Massachusetts Institute of Technology
Cambridge, Massachusetts 02139

ANALYSIS OF AN EXPERIMENT TO DETERMINE THE GRAVITATIONAL CONSTANT IN AN
ORBITING SPACE LABORATORY

by

John P. Vinti

M.I.T. Measurement Systems Laboratory

Cambridge, Massachusetts 02139

Abstract

The paper begins with the idea that the gravitational constant G and its possible variation ΔG with gravitational potential could be determined, in principle at least, from the orbit of an artificial satellite of an artificial planet, both of known mass and both in a gravitationless environment. Such an experiment could be conducted only in a zero-g laboratory, approximated by a space-craft in orbit about the earth. As an alternative to a circumferential orbit, the small satellite might be replaced by a small test object which moves back and forth in a cylindrical tunnel through a large sphere (the "planet").

Both of these arrangements would be disturbed by the gravity-gradient force produced by the earth, this disturbing force being of the same order of magnitude as the main force of the sphere on the test object.

The paper then goes on to describe Wilk's three-tunnel method. This would involve drilling three tunnels, along perpendicular diameters of a tungsten sphere, either translationally constrained or unconstrained, but free to rotate inside a space-craft in orbit about the earth. A test object would be placed in each tunnel and constrained to remain on its axis by means of an electrostatic suspension. Inertia reaction wheels, governed by servomechanisms, would then slowly rotate the sphere so as to keep each test object at rest. Measurements of the components of angular velocity would then result in a value for G , provided that a number of corrections are made, plus some other measurements. In the

case of the unconstrained sphere, the three-tunnel feature would almost entirely eliminate the effects of the earth's gravity-gradient.

The paper considers the effects of earth gravity-gradient, aerodynamic drag, and gravitational forces produced by the space-craft itself. (The force corrections for a given test-object, produced by the finite diameter of its own tunnel and by the other two tunnels, are deferred to a subsequent paper.) There is then a presentation and discussion of the equations required to reduce the observations to obtain G. Finally there follow the extra equations, not needed in the reduction, that are required for a computer simulation. The latter would serve to find out under what conditions the experiment would be made invalid by extraction of any test object from a tunnel and to check and aid the design of the servomechanisms.

Acknowledgements

This report was sponsored by the National Aeronautics and Space Administration under NASA Contract No. 9-8328.

The publication of this report does not constitute approval by the National Aeronautics and Space Administration of the findings or the conclusions contained therein. It is published only for the exchange and stimulation of ideas.

Table of Contents

1.	Introduction	1
2.	A Drag-Free Spherical Laboratory in Orbit	2
3.	The Gravity-Gradient Term	3
4.	The Three-Tunnel Method of Wilk	4
5.	Rotation of the Sphere: Wilk's Null Method	6
6.	Wilk's Experiment in an Orbiting Laboratory	8
7.	Reference Systems	10
	a. The Equatorial System (Inertially Oriented)	10
	b. A System Almost Fixed in the Space-Craft	10
	c. The Tunnel System, Fixed in the Sphere	12
	d. Transformations Among the Above Systems	12
8.	Equations of Motion of the Space-Craft and of the Test Objects	15
9.	The Unconstrained Sphere: Case α	18
10.	The Constrained Sphere: Case β	20
11.	Force on a Test Object from the Earth's Gravity Gradient	21
12.	Higher Harmonic Terms in the Gravity-Gradient Field	29
13.	Quadratic Terms in the Gravity-Gradient Field	31
14.	Summary of Earth Gravity-Gradient Effects on a Test Object	32
15.	Gravitational Effects of the Space-Craft itself.	33
16.	The Effects of Drag on a Test Object	37
17.	Reduction of the Observations: Unconstrained Sphere	40
18.	Reduction of the Observations: Constrained Sphere	42
19.	The Computer Simulation	44
	References	47
	List of Principal Symbols.	48

1. Introduction

Experiments to yield the gravitational constant G can also yield variations ΔG , arising say from variations in gravitational potential, if the experiments are performed accurately enough. The three-tunnel rotating sphere (of Section 4) is intended to be an example of such an experiment. Although ΔG is of prime interest in the studies sponsored by NASA, it is helpful to regard the experiment as though a measurement of G were the desired result.

Of all the fundamental constants of physics, G is the only one which is not known with an accuracy better than one part in a thousand. Recent theories of gravitation now make it desirable to know it much more accurately.

The lack of such an accurate value has never produced inaccuracy in dynamical astronomy, since G always appears as a factor of a mass M and the product $\mu \equiv GM$ can usually be determined accurately. E.g., for a planet moving around the sun

$$G(M_1+M_2) = (2\pi/P)^2 a_s^3, \quad (1)$$

where M_1 , M_2 , P , and a_s are respectively the masses of the sun and of the planet, the period, and the semi-major axis. But one does not know M_1 and M_2 accurately.

Suppose one could construct an isolated system consisting of an artificial satellite of mass M_2 moving around an artificial planet of mass M_1 , with no perturbing forces from other sources. Measurement of the masses and of P and a_s would then lead to a value for G . Before the modern space program such an experiment could not be imagined, because of the pervasive presence of unwanted gravitational fields. With the advent of artificial satellites and space laboratories, however, the situation has changed.

2. A Drag-Free Spherical Laboratory in Orbit.

Consider a spherical laboratory, having a spherically symmetric interior, traveling in an orbit around the earth that is made drag-free by means of external jets. Imagine it kept inertially oriented, relative to the fixed stars, also by means of external jets.

A massive true sphere would then remain floating at the center of the laboratory. (It could be used to monitor the jets that keep the space-craft drag-free.) A small test object in orbit about this sphere would then be in effect an artificial satellite of an artificial planet.

Let $\underline{\underline{R}}$ be the position vector of the center of mass of the sphere of mass M_s , in some large-scale astronomer's inertial system, and let $\underline{\underline{f}}(\underline{\underline{R}})$ be the total gravitational field at $\underline{\underline{R}}$ produced by all mass outside the space craft. Also let $\underline{\underline{s}}$ be the position vector of a small test-object, of mass m , relative to the center of mass of the sphere. Let it be in close orbit about M_s . Then

$$\ddot{\underline{\underline{R}}} = \underline{\underline{f}}(\underline{\underline{R}}) + \frac{Gm}{s^3} \underline{\underline{s}} \quad (2)$$

$$\ddot{\underline{\underline{R}}} + \ddot{\underline{\underline{s}}} = \underline{\underline{f}}(\underline{\underline{R}} + \underline{\underline{s}}) - \frac{GM_s}{s^3} \underline{\underline{s}} \quad (3)$$

Subtraction of (2) from (3) gives

$$\ddot{\underline{\underline{s}}} = - \frac{G(M_s + m)}{s^3} \underline{\underline{s}} + \underline{\underline{f}}(\underline{\underline{R}} + \underline{\underline{s}}) - \underline{\underline{f}}(\underline{\underline{R}}) \quad (4.1)$$

$$= - \frac{G(M_s + m)}{s^3} \underline{\underline{s}} + \underline{\underline{s}} \cdot [\nabla \underline{\underline{f}}(\underline{\underline{R}})]_C + \dots \quad (4.2)$$

Eq. (4.2) is obtained from (4.1) by expanding $\underline{\underline{f}}(\underline{\underline{R}} + \underline{\underline{s}})$ in a Taylor's series in the neighborhood of $\underline{\underline{s}} = 0$ and using only the first two terms. The expression $\underline{\underline{s}} \cdot [\nabla \underline{\underline{f}}(\underline{\underline{R}})]_C$, the first-order gravity gradient term, causes trouble. If this term were absent, we should have an example of the simplest two-body problem, with an inverse-square force. The orbit would be an ellipse, so that by measuring the masses M_s and m ,

the period P , and the semi-major axis a_s we could use Eq. (1) to obtain G .

Instead of letting m move in an orbit about M_s , we could drill a narrow cylindrical hole along a diameter of M_s and let m vibrate back and forth.* In this case the force produced on m by M_s would be

$$\underline{f}(M_s, m) = -\left(\frac{4\pi}{3} G\rho s\right)m, \quad (5)$$

where ρ is the uniform density of the sphere. Then

$$\ddot{\underline{s}} = -\frac{4\pi}{3} G\rho\left(1+\frac{m}{M_s}\right)\underline{s} + \underline{f}(\underline{R}+\underline{s}) - \underline{f}(\underline{R}) \quad (6)$$

If a_o is the radius of the sphere

$$\frac{4\pi}{3}G\rho = GM_s/a_o^3 \quad (7)$$

and

$$\ddot{\underline{s}} = -\frac{G(M_s+m)}{a_o^3}\underline{s} + \underline{s}\cdot[\nabla\underline{f}(\underline{R})]_{\underline{c}} + \dots \quad (8)$$

If the gravity-gradient term were negligible, the test object would move in simple-harmonic motion, with the same period as that of a circular close orbit.

3. The Gravity-Gradient Term

In either of the above cases the gravity-gradient term causes difficulties. We may approximate a true inertial system by taking an inertially oriented system, with origin at the center of mass of the earth. This procedure involves neglecting the lunar-solar perturbation, but the latter will not affect appreciably the values of $\underline{s}\cdot[\nabla\underline{f}(\underline{R})]_{\underline{c}}$. If μ is the product of G and the mass of the earth, then

* See for example Forward and Berman 1968.

$$\underline{f}(\underline{R}) = -\mu \underline{R}/R^3, \quad (9)$$

closely enough for present purposes. Then

$$\underline{s} \cdot \nabla \underline{f}(\underline{R}) = \frac{\mu \underline{s}}{R^3} [-\underline{I}_s + 3\underline{I}_R (\underline{I}_R \cdot \underline{I}_s)] , \quad (10)$$

where \underline{I}_R and \underline{I}_s are unit vectors along \underline{R} and \underline{s} , respectively. The maximum value of the bracket is 2, so that the maximum value of the gravity gradient field is

$$\text{max. grav. grad.} = \frac{2\mu \underline{s}}{R^3} \quad (11)$$

For a fairly close orbit about the earth, $R \approx$ radius of the earth. Also

$$\mu \approx G \frac{4\pi}{3} \rho_e R_e^3 \quad (12)$$

where R_e and ρ_e are respectively the radius and the mean density of the earth. Thus

$$\text{max. grav. grad.} \approx \frac{8\pi}{3} G \rho_e \underline{s} \quad (13)$$

In either of the two cases, the field produced by the sphere is

$$f(\text{sphere}) \approx \frac{4\pi}{3} G \rho \underline{s}, \quad (14)$$

where ρ is the density of the sphere. The ratio of the maximum gravity-gradient field to this is $2\rho_e/\rho \approx 11/19$, if the sphere is made of tungsten.

The gravity-gradient effect is thus very serious and either of the above methods would require important corrections. We thus turn to another method, due to Wilk (1970).

4. The Three-Tunnel Method of Wilk.

In its simplest form, Wilk's method would involve the use of a drag-free spherical laboratory, with a spherically symmetric interior, in orbit about the earth, and inertially oriented relative to the fixed stars. The sphere would float at the center of mass of the space-

craft and have three tunnels along mutually perpendicular diameters. Since the three tunnels would produce a slight departure from spherical symmetry, both external and internal gravitational fields would produce a small torque on it, so that some means would have to be found to keep it inertially oriented. (Such trouble will actually be avoided in the later forms.)

With a small test object in each tunnel, their equations of motion would be

$$\ddot{x} = -\frac{4\pi}{3} G\rho x + (\underline{s} \cdot \nabla \underline{f}')_x \quad (\text{x-tunnel}) \quad (15.1)$$

$$\ddot{y} = -\frac{4\pi}{3} G\rho y + (\underline{s} \cdot \nabla \underline{f}')_y \quad (\text{y-tunnel}) \quad (15.2)$$

$$\ddot{z} = -\frac{4\pi}{3} G\rho z + (\underline{s} \cdot \nabla \underline{f}')_z \quad (\text{z-tunnel}) \quad (15.3)$$

In Eqs. (15) \underline{f}' is the gravitational field produced by all matter outside the sphere. The equations would ultimately require corrections for the effects of the tunnels on the main field terms involving ρ and also for the higher-order gravity gradient terms.

If V' is the potential corresponding to \underline{f}' , these equations reduce to

$$\frac{\ddot{x}}{x} = -\frac{4\pi}{3} G\rho - \left(\frac{\partial^2 V'}{\partial x^2} \right)_0 \quad (16.1)$$

$$\frac{\ddot{y}}{y} = -\frac{4\pi}{3} G\rho - \left(\frac{\partial^2 V'}{\partial y^2} \right)_0 \quad (16.2)$$

$$\frac{\ddot{z}}{z} = -\frac{4\pi}{3} G\rho - \left(\frac{\partial^2 V'}{\partial z^2} \right)_0 \quad (16.3)$$

the second derivatives of V' being evaluated at the center of the sphere, since they come from a Taylor expansion in the neighborhood

of $\underline{s} = 0$. Addition then gives

$$\frac{\ddot{x}}{x} + \frac{\ddot{y}}{y} + \frac{\ddot{z}}{z} = -4\pi G\rho - (\nabla^2 V')_0 \quad (17)$$

Since V' corresponds to f' , the field external to the sphere, we then have

$$(\nabla^2 V')_0 = 0, \quad (18)$$

whether or not the tunnels go all the way through the sphere. Then

$$-4\pi G\rho = \frac{\ddot{x}}{x} + \frac{\ddot{y}}{y} + \frac{\ddot{z}}{z} \quad (19)$$

The method as described would thus eliminate the main difficulty about the gravity gradient terms. It is clear, however, that the accelerations \ddot{x} , \ddot{y} , \ddot{z} could not be measured accurately enough to improve present values of G , even if one could produce the requisite spherical symmetry and inertial orientation. Wilk has therefore turned to another procedure, although he still retains the important feature of the three tunnels.

5. Rotation of the Sphere: Wilk's Null Method

Suppose one rotates the sphere, by means of inertia wheels, about each of the three perpendicular axes defined by the tunnels. Let ω_1 , ω_2 , and ω_3 be the corresponding components of the angular velocity of the sphere, in that inertial system with which the tunnels momentarily coincide. In a coordinate system in which the sphere is at rest there then appear centrifugal forces $x(\omega^2 - \omega_1^2)$, $y(\omega^2 - \omega_2^2)$, $z(\omega^2 - \omega_3^2)$ along the x , y , z tunnels respectively. Here

$$\omega^2 = \omega_1^2 + \omega_2^2 + \omega_3^2 \quad (20)$$

On such rotation there also appear other inertial forces, viz Coriolis forces and $\dot{\omega}$ forces, but they are perpendicular to the tunnels.

The equations for motion along the tunnels now become

$$\ddot{x} = -\frac{4\pi}{3} G\rho + \omega^2 - \omega_1^2 - \left(\frac{\partial^2 V'}{\partial x^2} \right)_0 \quad (21.1)$$

$$\ddot{y} = -\frac{4\pi}{3} G\rho + \omega^2 - \omega_2^2 - \left(\frac{\partial^2 V'}{\partial y^2} \right)_0 \quad (21.2)$$

$$\ddot{z} = -\frac{4\pi}{3} G\rho + \omega^2 - \omega_3^2 - \left(\frac{\partial^2 V'}{\partial z^2} \right)_0 \quad (21.3)$$

Addition then gives

$$4\pi G\rho = 2\omega^2 - \frac{\ddot{x}}{x} - \frac{\ddot{y}}{y} - \frac{\ddot{z}}{z} \quad (22)$$

To achieve the validity of (21) and (22), one has to avoid friction of the test objects with the walls of the tunnels. This requires the use of a suspension system, perhaps electrostatic, to balance out the perpendicular Coriolis and $\dot{\omega}$ forces.

To get rid of the acceleration difficulties, i.e., the troubles produced by the terms in \ddot{x} , \ddot{y} , and \ddot{z} , Wilk then proposes to use servomechanisms that will keep the inertia wheels turning at such rates that the centrifugal forces just balance the gravitational forces.

Eq. (22) would then become

$$2\pi G\rho = \omega^2 \quad (23)$$

Measurements of ω_1 , ω_2 , and ω_3 over an appreciable time interval would then give a value for $G\rho$ and thus for G . The servomechanisms will so govern the actions of the inertia reaction wheels as to produce known torques on the sphere. On the simplest assumption, which I shall write down as an example, for concreteness, they will have the

mathematical form:

$$L_1 = k_{11}\dot{x} + k_{12}\ddot{x} \quad (\text{x-tunnel}) \quad (23.1)$$

$$L_2 = k_{21}\dot{y} + k_{22}\ddot{y} \quad (\text{y-tunnel}) \quad (23.2)$$

$$L_3 = k_{31}\dot{z} + k_{32}\ddot{z} \quad (\text{z-tunnel}) \quad (23.3)$$

The problem of design of the servos consists in achieving suitable values for the constants $k_{\mu\nu}$.

Even if the servos are not perfect, the term $\ddot{x}/x + \ddot{y}/y + \ddot{z}/z$ will now be much smaller, so that it need not be measured with as much accuracy as if it were the main term in (22).

6. Wilk's Experiment in an Orbiting Laboratory

Within the next few years it is likely that there will be a manned space station in orbit about the earth, called a "Skylab." Let us assume that it will have a mass of about 10^5 lb., and that it will have an approximately circular orbit at an altitude of about 500 kilometers. Let us also assume it to be a cylinder, of length about 40 feet and diameter about 20 feet, so oriented by the earth's gravity-gradient that its axis will always point approximately towards the center of mass of the earth, and let it be free of spin about its axis.

The purpose of the rest of this paper is to develop the theory of Wilk's experiment as it might be carried out aboard the Skylab. I shall consider various possibilities, as follows.

(a) The sphere may or may not be placed at the center of mass of the space craft.

(b) It may be held in place as regards translation, being allowed to rotate freely by means of a system of gimbals. Or, it may be allowed to drift in translation, with some method of moving it back after a certain amount of drift.

(c) The space-craft, besides being equipped with external jets to regulate its orientation, may or may not be equipped with external

jets to make it drag-free. If so equipped, some freely drifting test body, perhaps the sphere, would have to be kept in place by sensors and servomechanisms that could turn the drag-removing jets on or off, as the test body moves respectively away from or toward its position of equilibrium.

The theory will first involve a treatment of three reference systems, with the direction cosines to go from one to another. Then it will have to account for various corrections to be applied to Eqs. (21) for the motions of the three test objects in the tunnels.

For the reduction of the data to obtain a number for G , these corrections will arise from the gravity gradient of the earth, the non-spherical gravitational environment in the space-craft packed full with equipment and astronauts, non-gravitational forces on the space-craft, particularly drag, and the effects on a given test object of the finite diameter of its own tunnel and the effects of the other two tunnels.

For a computer simulation of the experiment one will also have to assume an orbit and a distribution of mass in the space-craft. There will then be nine unknowns, viz $x, y, z, \omega_1, \omega_2, \omega_3$, and three Eulerian angles or independent direction cosines that describe the orientation of the sphere relative to the inertial system. The necessary nine equations will be Eqs. (21), as above corrected, Eqs. (23) with assumed values for the constants $k_{\mu\nu}$, and three more equations describing the changing orientation of the sphere. The purpose of the computer simulation is in general to test out the feasibility of the whole experiment and in particular to find whether any of the test objects is likely to be extracted from its tunnel. It should also help to decide on numerical values for the $k_{\mu\nu}$, in the servo equations (23).

7. Reference Systems

a. The Equatorial System (Inertially-Oriented)

This is a system with origin E at the center of mass of the earth, Z-axis pointing towards the earth's north pole, and X-axis pointing towards the vernal equinox. (I leave the matter undecided whether corrections should be made for variations in the directions of E Z and E X, i.e., for the earth's precession and nutation.) Then with $\underline{\underline{I}}$ a unit vector along the X-axis, $\underline{\underline{K}}$ a unit vector along the Z-axis, and $\underline{\underline{J}} = \underline{\underline{K}} \times \underline{\underline{I}}$, the position vectors are as follows for

$$C = \text{C.M. of Skylab: } \underline{\underline{r}}_C = \underline{\underline{I}} X_C + \underline{\underline{J}} Y_C + \underline{\underline{K}} Z_C \quad (24.1)$$

$$O = \text{C.M. of Sphere: } \underline{\underline{r}}_O = \underline{\underline{I}} X_O + \underline{\underline{J}} Y_O + \underline{\underline{K}} Z_O \quad (24.2)$$

$$\text{C.M. of a Test Object: } \underline{\underline{r}} = \underline{\underline{I}} X + \underline{\underline{J}} Y + \underline{\underline{K}} Z \quad (24.3)$$

b. A System Almost Fixed in the Space Craft

I shall assume that $X_C, Y_C, Z_C, \dot{X}_C, \dot{Y}_C, \dot{Z}_C$ are all given to us as functions of time during the experiment, by the orbit trackers. Then, with

$$r_C \equiv (X_C^2 + Y_C^2 + Z_C^2)^{\frac{1}{2}} \quad (25.1)$$

$$p \equiv | \underline{\underline{r}}_C \times \dot{\underline{\underline{r}}}_C |, \quad (25.2)$$

I define the unit vectors

$$\underline{\underline{k}}_O \equiv \frac{\underline{\underline{r}}_C}{r_C} = \frac{1}{r_C} (\underline{\underline{I}} X_C + \underline{\underline{J}} Y_C + \underline{\underline{K}} Z_C) \quad (26.1)$$

$$\underline{\underline{j}}_O \equiv p^{-1} \underline{\underline{r}}_C \times \dot{\underline{\underline{r}}}_C \quad (26.2)$$

$$\underline{\underline{i}}_O \equiv \underline{\underline{j}}_O \times \underline{\underline{k}}_O = \frac{1}{r_C p} [r_C^2 \dot{\underline{\underline{r}}}_C - \underline{\underline{r}}_C (\underline{\underline{r}}_C \cdot \dot{\underline{\underline{r}}}_C)] \quad (26.3)$$

In this system we take the center of mass of the Skylab as origin. Also \underline{k}_O is a unit vector pointing from the center of mass of the earth toward the center of mass of the Skylab, \underline{j}_O is a unit vector pointing along the instantaneous orbital angular momentum of the Skylab, and \underline{i}_O is then given by the right-hand rule.

If the axis of the Skylab points toward the earth's center of mass, then $-\underline{k}_O$ points along this direction. If the orbit is circular, $\underline{r}_C \cdot \dot{\underline{r}}_C$ vanishes, $p = r_C |\dot{\underline{r}}_C|$, and $\underline{i}_O = \dot{\underline{r}}_C / |\dot{\underline{r}}_C|$, a unit vector in the direction of the Skylab's orbital velocity.

There are other expressions for these unit vectors. If δ and α are respectively the declination and right ascension of the Skylab and I and Ω the osculating inclination and the osculating right ascension of the orbital node, then

$$\underline{k}_O = \underline{I} \cos \delta \cos \alpha + \underline{J} \cos \delta \sin \alpha + \underline{K} \sin \delta \quad (27.1)$$

$$\underline{j}_O = \underline{I} \sin I \sin \Omega - \underline{J} \sin I \cos \Omega + \underline{K} \cos I \quad (27.2)$$

Also

$$\underline{i}_O = -\underline{I}_A \sin f + \underline{I}_B \cos f, \quad (27.3)$$

where f is the osculating true anomaly and \underline{I}_A and \underline{I}_B are unit vectors along the major and minor axes of the osculating ellipse.

Here

$$\begin{aligned} \underline{I}_A = & \underline{I} (\cos \Omega \cos \omega - \sin \Omega \cos I \sin \omega) \\ & + \underline{J} (\sin \Omega \cos \omega + \cos \Omega \cos I \sin \omega) \\ & + \underline{K} \sin I \sin \omega \end{aligned} \quad (27.4)$$

$$\begin{aligned} \underline{I}_B = & \underline{I} (-\cos \Omega \sin \omega - \sin \Omega \cos I \cos \omega) \\ & + \underline{J} (-\sin \Omega \sin \omega + \cos \Omega \cos I \cos \omega) \\ & + \underline{K} \sin I \cos \omega, \end{aligned} \quad (27.5)$$

where ω is the osculating argument of perigee, not to be confused with the angular velocity in Eq. (20).

c. The Tunnel System, Fixed in the Sphere

Let \underline{i} , \underline{j} , \underline{k} be unit vectors along the tunnels. Then, for a test object

$$\underline{r} - \underline{r}_0 \equiv \underline{s} = \underline{i}x + \underline{j}y + \underline{k}z, \quad (28.1)$$

where y and z will vanish along the axis of the x -tunnel, z and x along that of the y -tunnel, and x and y along that of the z -tunnel.

With respect to the system (a):

$$\underline{s} = \underline{I}(X-X_0) + \underline{J}(Y-Y_0) + \underline{K}(Z-Z_0) \quad (28.2)$$

and with respect to the system (b):

$$\underline{s} = \underline{i}_0 \xi_1 + \underline{j}_0 \xi_2 + \underline{k}_0 \xi_3 \quad (28.3)$$

d. Transformations among the Above Systems

Let us denote the unit vectors \underline{I} , \underline{J} , \underline{K} in the equatorial system by \underline{I}_μ ($\mu = 1, 2, 3$) and the unit vectors \underline{i}_0 , \underline{j}_0 , \underline{k}_0 in the "space-craft system" by $\underline{i}_{0\mu}$ ($\mu = 1, 2, 3$). Also let β be the rotation matrix that carries the space-craft system into the equatorial system. Then

$$\underline{I}_\nu = \sum_\mu \beta_{\nu\mu} \underline{i}_{0\mu} \quad (29.1)$$

$$\underline{i}_{0\nu} = \sum_\mu \tilde{\beta}_{\nu\mu} \underline{I}_\mu = \sum_\mu \underline{I}_\mu \beta_{\mu\nu}, \quad (29.1)$$

where

$$\beta_{\nu\mu} = \underline{I}_\nu \cdot \underline{i}_{0\mu} \quad (29.3)$$

$$\tilde{\beta}_{\nu\mu} = \beta_{\mu\nu} = \underline{i}_{0\nu} \cdot \underline{I}_\mu \quad (29.4)$$

The direction cosines $\tilde{\beta}_{\nu\mu}$ can be read directly from Eqs. (26), so that they will be known in terms of $X_C, Y_C, Z_C, \dot{X}_C, \dot{Y}_C, \dot{Z}_C$, to be furnished by the orbit trackers. Then, for a given test object, with its position vector \underline{s} relative to the center of mass of the sphere having components ξ_μ relative to the space-craft system, we can dot (28.3), viz

$$\underline{s} = \sum_{\mu} \underline{i}_{\nu O\mu} \xi_{\mu} \quad (28.3)$$

with \underline{I}_{ν} , to obtain

$$X_{\nu} - X_{O\nu} = \sum_{\mu} \underline{I}_{\nu} \cdot \underline{i}_{\nu O\mu} \xi_{\mu} = \sum_{\mu} \beta_{\nu\mu} \xi_{\mu} , \quad (29.5)$$

the components of \underline{s} in the equatorial system.

Next let α be the rotation matrix that carries the tunnel system into the space-craft system. Then

$$\underline{i}_{\nu O\nu} = \sum_{\mu} \alpha_{\nu\mu} \underline{i}_{\nu O\mu} \quad (30.1)$$

$$\underline{i}_{\nu} = \sum_{\mu} \alpha_{\mu\nu} \underline{i}_{\nu O\mu} \quad (30.2)$$

$$\alpha_{\nu\mu} = \underline{i}_{\nu O\nu} \cdot \underline{i}_{\nu O\mu} \quad (30.3)$$

$$\xi_{\nu} = \sum_{\mu} \alpha_{\nu\mu} x_{\mu} \quad (30.4)$$

$$x_{\nu} = \sum_{\mu} \alpha_{\mu\nu} \xi_{\mu} \quad (30.5)$$

Finally, let γ be the rotation matrix that carries the tunnel system into the equatorial system. Then

$$\underline{\underline{I}}_v = \sum_{\mu} \gamma_{v\mu} \underline{\underline{i}}_{\mu} \quad (31.1)$$

$$\underline{\underline{i}}_v = \sum_{\mu} \gamma_{\mu v} \underline{\underline{I}}_{\mu} \quad (31.2)$$

$$\gamma_{\mu v} = \underline{\underline{i}}_v \cdot \underline{\underline{I}}_{\mu} \quad (31.3)$$

The components $X_v - X_{Ov}$ of $\underline{\underline{s}}$ in the equatorial system then follow from the x_{μ} in the tunnel system by dotting (28.1), viz

$$\underline{\underline{s}} = \sum_{\mu} \underline{\underline{i}}_{\mu} x_{\mu} \quad (28.1)$$

with $\underline{\underline{I}}_v$ and using (31.3). We obtain

$$X_v - X_{Ov} = \sum_{\mu} \gamma_{v\mu} x_{\mu} \quad (31.4)$$

Now we have seen how to obtain the $\beta_{\mu v}$ and it is planned to measure the inertial orientation of each tunnel, so that we shall thereby obtain the $\gamma_{\mu v}$.

From the β 's and γ 's we can then obtain the α 's, since the α , β , and γ matrices are connected by the equation

$$\gamma = \beta \alpha \quad (32)$$

To prove (32), use (29.1), (30.1), and (31.3). Adopting the summation convention, we find from (29.1) and (30.1)

$$\underline{\underline{I}}_v = \beta_{v\mu} \underline{\underline{i}}_{O\mu} = \beta_{v\mu} \alpha_{\mu\sigma} \underline{\underline{i}}_{\sigma} = (\beta\alpha)_{v\sigma} \underline{\underline{i}}_{\sigma} \quad (33)$$

On comparing (33) with (31.1), we find

$$\gamma_{\nu\mu} = (\beta\alpha)_{\nu\mu}, \quad (34)$$

so that (32) is proved. Then, from (32),

$$\alpha = \beta^{-1}\gamma = \tilde{\beta}\gamma, \quad (35)$$

since β is a rotation matrix. Then

$$\alpha_{\mu\nu} = \sum_{\sigma} \tilde{\beta}_{\mu\sigma} \gamma_{\sigma\nu} = \sum_{\sigma} \beta_{\sigma\mu} \gamma_{\sigma\nu} \quad (36)$$

Eq. (36) then permits evaluation of the α 's from the β 's and γ 's.

8. Equations of Motion of the Space-craft and of the Test Objects

Let \underline{r}_C be the position vector of the center of mass C of the Skylab relative to that of the earth. $\underline{f}_E(\underline{r}_C)$ be the earth's gravitational field at C, and M be the total mass of the Skylab. If we consider the extreme case in which we represent it by two masses, each M/2 at a separation equal to its length, we find that the total earth gravitational force on the Skylab is given by

$$\underline{F}(\text{total}) = M \underline{f}_E(\underline{r}_C) + \underline{F}', \quad (37.1)$$

where

$$|\underline{F}'| \approx 10^{-12} M |\underline{f}_E(\underline{r}_C)| \quad (37.2)$$

We may henceforth write (37.1) without the \underline{F}' , for the total gravitational force of the earth on the Skylab. Its equation of motion is then

$$\ddot{\underline{r}}_C = \underline{f}_E(\underline{r}_C) + \underline{D}/M + \underline{J}/M + \underline{f}_{Ls} \quad (38)$$

Here \underline{J} is the force on the space-craft produced by any external jets that we may use, \underline{D} is the total non-gravitational force, mostly aerodynamic drag, and \underline{f}_{LS} is the lunar-solar perturbation, which we shall ordinarily neglect.

Now let O be the center of the sphere, $\underline{b} \equiv \vec{CO}$, and \underline{s} be the position vector of a test object relative to O . Its position vector \underline{r} , relative to the center of mass E of the earth, is then given by

$$\underline{r} = \underline{r}_C + \underline{b} + \underline{s} = \underline{r}_O + \underline{s} , \quad (39)$$

where

$$\underline{r}_O \equiv \underline{r}_C + \underline{b} , \quad (40)$$

the position vector of O relative to E .

When the electrostatic suspension is so adjusted that a test object in a tunnel does not touch its walls, the motion of the test object satisfies

$$\ddot{\underline{r}} = \ddot{\underline{r}}_C + \ddot{\underline{b}} + \ddot{\underline{s}} = \underline{f}_E(\underline{r}) + \underline{f}_L(\underline{r}) + \underline{f}_S(\underline{r}) + \underline{f}_\perp , \quad (41)$$

where $\underline{f}_L(\underline{r})$ is the gravitational field at the test object produced by the laboratory, $\underline{f}_S(\underline{r})$ is the gravitational field produced by the sphere, and \underline{f}_\perp is the perpendicular force produced by the suspension and the instrumentation. It is here assumed that the suspension and the instrumentation in the Skylab produce zero longitudinal force.

Suppose the sphere is fixed, translationally, on the axis of the space-craft, which in turn has its axis pointing approximately toward the center of mass of the earth. Then

$$\ddot{b} = b \frac{\ddot{r}_C}{r_C} \quad (42)$$

If the orbit is approximately circular, with mean motion n , then

$$\ddot{b} \approx -bn^2 r_C / r_C \quad (43)$$

so that

$$|\ddot{b}| \approx bn^2 \quad (44)$$

Now

$$|f_{\sim s}(\tilde{r})| \approx \frac{4\pi}{3} G \rho s, \quad (45)$$

where $\rho \approx 19 \text{ gm/cm}^3$ for tungsten. From the Keplerian law $\mu = n^2 R_e^3$, we find that

$$G \frac{4\pi}{3} \rho_e \approx n^2, \quad (46)$$

where ρ_e is the earth's mean density. Then

$$|f_{\sim s}(\tilde{r})| \approx \frac{\rho}{\rho_e} n^2 s \quad (47)$$

and

$$\left| \frac{\ddot{b}}{f_{\sim s}(\tilde{r})} \right| \approx \frac{\rho_e}{\rho} \frac{b}{s} \approx \frac{5.5}{19} \frac{b}{s} \quad (48)$$

With $b = 20 \text{ feet} \approx 600 \text{ cm}$ and $s = 10 \text{ cm}$, the ratio amounts to about 17.

Thus \ddot{b} is much larger than $f_{\sim s}(\tilde{r})$, which is supposed to be the main force in the experiment.

Now if the axis really pointed accurately toward E, we could evaluate $\ddot{\underline{b}}$ accurately from (42), with sufficiently accurate values of $X_C, Y_C, Z_C, \dot{X}_C, \dot{Y}_C,$ and $\dot{Z}_C,$ and the drag. But the most one can do in orienting the space-craft is to point its axis, as closely as possible, along the perpendicular to the plane of the horizon. There would thus arise an error, which although small as a fraction, would undoubtedly produce too large an error in $\ddot{\underline{b}},$ which already swamps $\underline{f}_S.$ It thus appears that translational restraint of the sphere would destroy the experiment, unless one placed the sphere very close to the center of mass C of the space-craft.

I shall therefore consider only two possibilities:

α) The sphere is not at C and is not constrained to the space craft by any tethers or rods, but its center actually remains at a point O fixed relative to the space-craft by virtue of external jets. An astronaut could bring this about, watching the sphere and turning the external jets on or off to keep O fixed. That is, he could act both as sensor and servomechanism.

β) The center O of the sphere is tied to the center of mass C of the spacecraft.

9. The Unconstrained Sphere: Case α

In this case the sphere is in free fall, so that

$$\ddot{\underline{r}}_O = \underline{f}_E(\underline{r}_O) + \underline{f}_L(\underline{r}_O) \quad (49)$$

Eq. (41) becomes

$$\ddot{\underline{r}}_O + \ddot{\underline{s}} = \underline{f}_E(\underline{r}_O + \underline{s}) + \underline{f}_L(\underline{r}_O + \underline{s}) + \underline{f}_S(\underline{r}_O + \underline{s}) + \underline{f}_\perp \quad (50)$$

Subtraction of (49) from (50) then yields

$$\ddot{\underline{s}} = \underline{f}_{\underline{E}}(\underline{r}_{\underline{O}} + \underline{s}) - \underline{f}_{\underline{E}}(\underline{r}_{\underline{O}}) + \underline{f}_{\underline{L}}(\underline{r}_{\underline{O}} + \underline{s}) - \underline{f}_{\underline{L}}(\underline{r}_{\underline{O}}) + \underline{f}_{\underline{S}}(\underline{r}_{\underline{O}} + \underline{s}) + \underline{f}_{\underline{J}} \quad (51)$$

Now, by (28.1)

$$\underline{s} = \sum_{\mu} \underline{i}_{\mu} \underline{x}_{\mu} \quad (52)$$

If $\underline{\omega}$ denotes the angular velocity of the sphere relative to the fixed-star inertial system, we have

$$\dot{\underline{i}}_{\mu} = \underline{\omega} \times \underline{i}_{\mu} \quad (53)$$

Let

$$\sum_{\mu} \underline{i}_{\mu} \dot{\underline{x}}_{\mu} = \underline{v} \quad (54)$$

the velocity of the test object relative to the tunnel system. Two differentiations of (52) then give

$$\ddot{\underline{s}} = \sum_{\mu} \underline{i}_{\mu} \ddot{\underline{x}}_{\mu} + \dot{\underline{\omega}} \times \underline{s} + 2\underline{\omega} \times \underline{v} + \underline{\omega} \times (\underline{\omega} \times \underline{s}) \quad (55)$$

Here

$$\underline{\omega} \times (\underline{\omega} \times \underline{s}) = \underline{\omega} (\underline{\omega} \cdot \underline{s}) - \omega^2 \underline{s} \quad (56)$$

so that

$$[\underline{\omega} \times (\underline{\omega} \times \underline{s})]_{\mu} = \omega_{\mu} (\underline{\omega} \cdot \underline{s}) - \omega^2 \underline{x}_{\mu} \quad (57)$$

In a given tunnel μ , the forces $\dot{\underline{\omega}} \times \underline{s}$ and $2\underline{\omega} \times \underline{v}$ are perpendicular to the axis, and thus neutralized by the $\underline{f}_{\underline{J}}$ in (50). The suspension is designed to do this. Also, in the μ -tunnel

$$\underline{s}_\mu = \underline{x}_\mu, \quad (58)$$

so that (57) becomes

$$[\underline{\omega} \times (\underline{\omega} \times \underline{s})]_\mu = \underline{x}_\mu (\omega_\mu^2 - \omega^2) \quad (59)$$

Eqs. (51), (55), and (59) thus give

$$\ddot{\underline{x}}_\mu = (\omega^2 - \omega_\mu^2) \underline{x}_\mu + \underline{i}_\mu \cdot [f_{\underline{E}}(\underline{r}_{\underline{O}+\underline{s}}) - f_{\underline{E}}(\underline{r}_{\underline{O}})] + \underline{i}_\mu \cdot [f_{\underline{L}}(\underline{r}_{\underline{O}+\underline{s}}) - f_{\underline{L}}(\underline{r}_{\underline{O}})] + f_{\underline{S}\mu}(\underline{r}_{\underline{O}+\underline{s}}) \quad (\mu = 1, 2, 3) \quad (60)$$

Eq. (60) is notable for its lack of any drag term. The sphere force $f_{\underline{S}\mu}$ is approximately $4\pi G\rho x_\mu/3$. The term $(\omega^2 - \omega_\mu^2) \underline{x}_\mu$ is the centrifugal force and the other two terms are the gravity-gradient terms arising respectively from the earth and the space laboratory itself. Before we evaluate the various terms in (60) it is best to derive the corresponding equation for Case β , where the sphere is tethered to remain at the center of mass C of the space-craft.

10. The Constrained Sphere: Case β

Here $\vec{CO} = 0$, by hypothesis. Eq. (50) remains unchanged, but may now be written

$$\ddot{\underline{r}}_{\underline{C}} + \ddot{\underline{s}} = f_{\underline{E}}(\underline{r}_{\underline{C}+\underline{s}}) + f_{\underline{L}}(\underline{r}_{\underline{C}+\underline{s}}) + f_{\underline{S}}(\underline{r}_{\underline{C}+\underline{s}}) + \underline{f}_{\underline{J}} \quad (61)$$

In this case we assume no jets, so that \underline{J} vanishes in (38). But now we do have drag \underline{D} . With neglect of \underline{f} (lunar-solar), we obtain

$$\ddot{\underline{r}}_{\underline{C}} = f_{\underline{E}}(\underline{r}_{\underline{C}}) + \underline{D}/M \quad (62)$$

Subtraction of (62) from (61) yields

$$\ddot{\tilde{s}} = \tilde{f}_E(\tilde{r}_C + \tilde{s}) - \tilde{f}_E(\tilde{r}_C) + \tilde{f}_L(\tilde{r}_C + \tilde{s}) + \tilde{f}_S(\tilde{r}_C + \tilde{s}) + \tilde{f}_\perp - D/M \quad (63)$$

The equation for a test object in the μ 'th tunnel now becomes

$$\begin{aligned} \ddot{x}_\mu = & (\omega^2 - \omega_\mu^2)x_\mu + i_\mu \cdot [\tilde{f}_E(\tilde{r}_C + \tilde{s}) - \tilde{f}_E(\tilde{r}_C)] \\ & + i_\mu \cdot \tilde{f}_L(\tilde{r}_C + \tilde{s}) + f_{S\mu}(\tilde{r}_C + \tilde{s}) - i_\mu \cdot D/M \quad (\mu=1,2,3) \end{aligned} \quad (64)$$

Comparison of (60) and (64) shows that, in the case of tethered constraint of 0 at C, the gravitational force of the laboratory enters as a direct force and not just as the gravity-gradient force of the unconstrained case. If the laboratory is symmetric with respect to its mid-section, however, this direct force will be zero. If it is almost symmetric, it may still not exceed the gravity-gradient force in the unconstrained case. Finally, there is a drag term in the constrained case and none in the unconstrained case.

By evaluating $\tilde{f}_E(\tilde{r}_O + \tilde{s})$, $\tilde{f}_L(\tilde{r}_O + \tilde{s})$, and $f_{S\mu}(\tilde{r}_O + \tilde{s})$, we can obtain all the gravitational terms in both equations. There will then remain only the drag term in (64) to be considered.

11. Field at Test Object from the Earth's Gravity Gradient

The field at the test object, arising from the earth's gravity gradient, is

$$\tilde{f}_{EG}(s) = \tilde{f}_E(\tilde{r}_O + \tilde{s}) - \tilde{f}_E(\tilde{r}_O), \quad (65)$$

where $\tilde{r}_O = \tilde{r}_C + \tilde{b}$, $\tilde{b} \neq 0$ for Case α , and $\tilde{b} = 0$ for Case β . The earth's gravitational potential V is given by

$$V = -\frac{\mu}{r} + \frac{\mu J_2 R_e^2}{r^3} P_2\left(\frac{z}{r}\right) + \dots \quad (66)$$

where $J_2 = (1.08)10^{-3}$ and

$$z = z_0 + k \cdot s \quad (67)$$

Then

$$\underline{f}_E(\underline{r}_0 + \underline{s}) = -\nabla_s V \quad (68)$$

Since

$$P_2\left(\frac{z}{r}\right) = \frac{3}{2} \frac{z^2}{r^2} - \frac{1}{2}, \quad (69)$$

we have

$$V = -\frac{\mu}{r} - \frac{\mu J_2 R_e^2}{2r^3} + \frac{3}{2} \frac{\mu J_2 R_e^2 z^2}{r^5} + \dots \quad (70)$$

Thus we need expressions for r^{-1} , r^{-3} , and $z^2 r^{-5}$ as functions of the tunnel coordinates x , y , z of a test object. By (39)

$$r^2 = r_0^2 + 2\underline{r}_0 \cdot \underline{s} + s^2 \quad (71)$$

Also, by (40)

$$\underline{r}_0 = \sum_{v=1}^3 I_{cv} X_{cv} + \sum_{v=1}^3 i_{ov} b_v \quad (72)$$

Here the b_v 's are the components of \underline{b} in the space-craft system and thus approximately constant. The X_{cv} are the components of \underline{r}_c in the equatorial system and thus known from the specification of the orbit. We need, however, to express \underline{r}_0 in the tunnel system. To do so,

apply (30.1) and (31.1) to (72). Then

$$\underline{r}_0 = \sum_{\sigma} \underline{i}_{\sigma} Q_{\sigma} \quad (73.1)$$

$$Q_{\sigma} \equiv \sum_{\nu} (X_{\nu\sigma} \gamma_{\nu\sigma} + b_{\nu} \alpha_{\nu\sigma}) \quad (73.2)$$

Here α is the matrix that rotates the tunnel system into the space-craft system and γ the matrix that rotates the tunnel system into the equatorial system. Also

$$l_{\sigma} = Q_{\sigma}/r_0 \quad (\sigma = 1, 2, 3) \quad (74)$$

are the direction cosines of \underline{r}_0 , the position vector of the center of the sphere, in the tunnel system.

Inserting

$$r_0^2 = \sum_{\sigma} Q_{\sigma}^2 \quad (75)$$

$$\underline{s} = \sum_{\sigma} \underline{i}_{\sigma} x_{\sigma} \quad (76)$$

into (71), we find

$$\frac{r^2}{r_0^2} = 1 + \frac{2}{r_0} \sum_{\sigma} Q_{\sigma} x_{\sigma} + \frac{s^2}{r_0^2} \quad (77)$$

so that

$$\frac{r}{r_0} = (1 - 2\lambda h + h^2)^{-\frac{1}{2}} = \sum_{n=0}^{\infty} h^n P_n(\lambda) \quad (78)$$

where

where

$$h \equiv -\frac{s}{r_0} \quad (79.1)$$

$$\lambda \equiv \frac{1}{r_0 s} \sum_{\sigma} Q_{\sigma} x_{\sigma} \quad (79.2)$$

Here $P_n(\lambda)$ is the Legendre polynomial. We thus obtain

$$\frac{r_0}{r} = 1 - \frac{\lambda s}{r_0} + \frac{s^2}{r_0^2} \left(\frac{3}{2} \lambda^2 - \frac{1}{2} \right) + \dots \quad (80)$$

which results in

$$\frac{\mu}{r} = \frac{\mu}{r_0} - \frac{\mu}{r_0^2} \sum_{\sigma} l_{\sigma} x_{\sigma} - \frac{\mu(x^2+y^2+z^2)}{2r_0^3} + \frac{3\mu}{2r_0^3} (\sum_{\sigma} l_{\sigma} x_{\sigma})^2 + \dots \quad (81)$$

To find r^{-3} , we differentiate (78) with respect to λ . The result is

$$\frac{r_0^3}{r^3} = (1-2\lambda h+h^2)^{-\frac{3}{2}} = \sum_{n=1}^{\infty} h^{n-1} P_n'(\lambda) \quad (82)$$

To find r^{-5} , differentiate (82) with respect to λ , to find

$$\frac{r_0^5}{r^5} = (1-2\lambda h+h^2)^{-\frac{5}{2}} = \frac{1}{3} \sum_{n=2}^{\infty} h^{n-2} P_n''(\lambda) \quad (83)$$

Eqs. (82) and (83) become

$$\frac{r_0^3}{r^3} = 1 - \frac{3}{r_0} \sum_{\sigma} l_{\sigma} x_{\sigma} - \frac{3(x^2+y^2+z^2)}{2r_0^2} + \frac{15}{2r_0^2} (\sum_{\sigma} l_{\sigma} x_{\sigma})^2 + \dots \quad (84)$$

$$\frac{r_o^5}{r^5} = 1 - \frac{5}{r_o} \sum_{\sigma} l_{\sigma} x_{\sigma} - \frac{5(x^2+y^2+z^2)}{2r_o^2} + \frac{35}{2r_o^2} (\sum_{\sigma} l_{\sigma} x_{\sigma})^2 + \dots \quad (85)$$

But we need $z^2 r^{-5}$. Here

$$z = z_o + \tilde{K} \cdot s \quad (85.1)$$

By (31.1)

$$\tilde{K} = \sum_{\mu} \gamma_{3\mu} i_{\mu} \quad (86)$$

Thus

$$z = z_o + \sum_{\mu} \gamma_{3\mu} x_{\mu} \quad (87)$$

and

$$z^2 = z_o^2 + 2z_o \sum_{\mu} \gamma_{3\mu} x_{\mu} + (\sum_{\mu} \gamma_{3\mu} x_{\mu})^2 \quad (88)$$

Multiplication of (85) by (88) then yields

$$\begin{aligned} \frac{r_o^5 z^2}{r^5} &= z_o^2 + 2z_o \sum_{\mu} \gamma_{3\mu} x_{\mu} + (\sum_{\mu} \gamma_{3\mu} x_{\mu})^2 \\ &\quad - \frac{5z_o^2}{r_o} \sum_{\sigma} l_{\sigma} x_{\sigma} - \frac{10z_o}{r_o} (\sum_{\mu} \gamma_{3\mu} x_{\mu}) (\sum_{\sigma} l_{\sigma} x_{\sigma}) - \frac{5z_o^2}{2r_o^2} (x^2+y^2+z^2) \\ &\quad + \frac{35z_o^2}{2r_o^2} (\sum_{\sigma} l_{\sigma} x_{\sigma})^2 + o(s^3) \end{aligned} \quad (89)$$

On inserting (81), (84), and (89) into (70), we find

$$\begin{aligned}
U \equiv -V = & \frac{\mu}{r_0} \left[1 - \frac{1}{r_0} \sum_{\sigma} \ell_{\sigma} x_{\sigma} - \frac{x^2+y^2+z^2}{2r_0^2} + \frac{3}{2r_0^2} (\sum_{\sigma} \ell_{\sigma} x_{\sigma})^2 \right] \\
& + \frac{\mu J_2 R_e^2}{2r_0^3} \left[1 - \frac{3}{r_0} \sum_{\sigma} \ell_{\sigma} x_{\sigma} - \frac{3}{2r_0^2} (x^2+y^2+z^2) + \frac{15}{2r_0^2} (\sum_{\sigma} \ell_{\sigma} x_{\sigma})^2 \right] \\
& - \frac{3}{2} \frac{\mu J_2 R_e^2}{r_0^5} z_0^2 \left[1 + \frac{2}{z_0} \sum_{\mu} \gamma_{3\mu} x_{\mu} + \frac{1}{z_0^2} (\sum_{\mu} \gamma_{3\mu} x_{\mu})^2 \right] \\
& - \frac{5}{r_0} \sum_{\sigma} \ell_{\sigma} x_{\sigma} - \frac{10}{z_0 r_0} (\sum_{\mu} \gamma_{3\mu} x_{\mu}) (\sum_{\sigma} \ell_{\sigma} x_{\sigma}) - \frac{5}{2r_0^2} (x^2+y^2+z^2) \\
& + \frac{35}{2r_0^2} (\sum_{\sigma} \ell_{\sigma} x_{\sigma})^2 + O(s^3) \tag{90}
\end{aligned}$$

Here

$$r_0^2 = (X_c + \sum_{\mu} \beta_{1\mu} b_{\mu})^2 + (Y_c + \sum_{\mu} \beta_{2\mu} b_{\mu})^2 + (Z_c + \sum_{\mu} \beta_{3\mu} b_{\mu})^2 \tag{91.1}$$

$$z_0 = Z_c + \sum_{\mu} \beta_{3\mu} b_{\mu}, \tag{91.2}$$

where the b_{μ} 's are the (almost) constant components of \tilde{b} in the spacecraft system, $\beta_{1\mu}$, $\beta_{2\mu}$, and $\beta_{3\mu}$ are the direction cosines of $\tilde{i}_{0\mu}$ in the equatorial system, and X_c , Y_c , Z_c are the components of \tilde{r}_c in the equatorial system. Also

$$\ell_{\sigma} \equiv \frac{Q_{\sigma}}{r_0} = \frac{1}{r_0} [X_c \gamma_{1\sigma} + Y_c \gamma_{2\sigma} + Z_c \gamma_{3\sigma} + b_1 \alpha_{1\sigma} + b_2 \alpha_{2\sigma} + b_3 \alpha_{3\sigma}], \tag{91.3}$$

$$(\sigma = 1, 2, 3)$$

where the l_σ are the direction cosines of \underline{r}_0 in the tunnel system, $\gamma_{1\sigma}, \gamma_{2\sigma}, \gamma_{3\sigma}$ are the direction cosines in the equatorial system of a unit vector along the σ 'th tunnel, $\alpha_{1\sigma}, \alpha_{2\sigma}, \alpha_{3\sigma}$ are the direction cosines in the space-craft system of a unit vector along the σ 'th tunnel, and the b's are the same as above.

The component along the σ 'th tunnel of $f_{\underline{E}}$ in Eq. (68) is then given by computing $\partial U/\partial x_\sigma$ and putting $x_\mu = 0, \mu \neq \sigma$:

$$\begin{aligned}
 f_{\underline{E}\sigma}(\underline{r}_0 + \underline{s}) = & -\frac{\mu}{r_0^2} l_\sigma - \frac{\mu}{r_0^3} x_\sigma + \frac{3\mu}{r_0^3} l_\sigma^2 x_\sigma \\
 & + \frac{\mu J_2 R_e^2}{2r_0^3} \left[-\frac{3l_\sigma}{r_0} - \frac{3x_\sigma}{r_0^2} + \frac{15}{r_0^2} l_\sigma^2 x_\sigma \right] \\
 & - \frac{3}{2} \frac{\mu J_2 R_e^2 z_0^2}{r_0^5} \left[\frac{2\gamma_{3\sigma}}{z_0} + \frac{2\gamma_{3\sigma}^2}{z_0^2} x_\sigma - \frac{5l_\sigma}{r_0} \right. \\
 & \left. - \frac{20l_\sigma \gamma_{3\sigma} x_\sigma}{z_0 r_0} - \frac{5x_\sigma}{r_0^2} + \frac{35l_\sigma^2 x_\sigma}{r_0^2} \right] + \dots
 \end{aligned} \tag{92}$$

Let $(f_\sigma)_{g.g.}$ be the component along the σ 'th tunnel of the earth gravity gradient force, viz,

$$(f_\sigma)_{g.g.} = f_{\underline{E}\sigma}(\underline{r}_0 + \underline{s}) - f_{\underline{E}\sigma}(\underline{r}_0) \tag{93}$$

It is obtained from (92) by dropping all the terms independent of x_σ :

$$\begin{aligned}
(f_{\sigma})_{g.g.} = & -\frac{\mu x_{\sigma}}{r_o^3} + \frac{3\mu l_{\sigma}^2}{r_o^3} x_{\sigma} + \frac{\mu J_2 R_e^2}{2r_o^3} \left(-\frac{3x_{\sigma}}{r_o^2} + \frac{15l_{\sigma}^2 x_{\sigma}}{r_o^2} \right) \\
& - \frac{3}{2} \frac{\mu J_2 R_e^2}{r_o^5} z_o^2 \left(\frac{2\gamma_{3\sigma}^2 x_{\sigma}}{z_o^2} - \frac{20\gamma_{3\sigma} l_{\sigma} x_{\sigma}}{z_o r_o} - \frac{5x_{\sigma}}{r_o^2} + \frac{35l_{\sigma}^2 x_{\sigma}}{r_o^2} \right) + \dots
\end{aligned}
\tag{94}$$

This corresponds to a Taylor expansion of the earth's potential V , through terms in the second degree, in the neighborhood of $\underline{s} = 0$, so that

$$\sum_{\sigma} \frac{(f_{\sigma})_{g.g.}}{x_{\sigma}} = -(\nabla^2 V)_o, \tag{95}$$

which must vanish, since the earth potential satisfies Laplace's equation (and not Poisson's) anywhere outside the earth. It is a simple matter to verify this. We find immediately

$$\sum_{\sigma} \frac{(f_{\sigma})_{g.g.}}{x_{\sigma}} = \frac{30\mu J_2 R_e^2 z_o}{r_o^7} (r_o \sum_{\sigma} \gamma_{3\sigma} l_{\sigma} - z_o) \tag{96}$$

By (91.3), we then compute

$$\begin{aligned}
r_o \sum_{\sigma} l_{\sigma} \gamma_{3\sigma} = & x_c \sum_{\sigma} \gamma_{3\sigma} \gamma_{1\sigma} + y_c \sum_{\sigma} \gamma_{3\sigma} \gamma_{2\sigma} + z_c \sum_{\sigma} \gamma_{3\sigma}^2 \\
& + b_1 \sum_{\sigma} \alpha_{1\sigma} \gamma_{3\sigma} + b_2 \sum_{\sigma} \alpha_{2\sigma} \gamma_{3\sigma} + b_3 \sum_{\sigma} \alpha_{3\sigma} \gamma_{3\sigma}
\end{aligned}
\tag{97}$$

Here the coefficients of x_c and y_c vanish and that of z_c is unity. To evaluate the coefficients of the b 's, note that, since the matrices α , β , and γ satisfy $\gamma = \beta\alpha$, we have

$$\alpha\gamma^{-1} = \beta^{-1}, \quad (98)$$

from which

$$\sum_{\sigma} \alpha_{\mu\sigma} (\gamma^{-1})_{\sigma\nu} = \sum_{\sigma} \alpha_{\mu\sigma} \gamma_{\nu\sigma} = (\beta^{-1})_{\mu\nu} = \beta_{\nu\mu} \quad (99)$$

Thus the coefficient of b_{μ} is $\beta_{3\mu}$, so that

$$r_{\sigma} \sum_{\sigma} \ell_{\sigma} \gamma_{3\sigma} = z_{\sigma} + \sum_{\mu} \beta_{3\mu} b_{\mu} = z_{\sigma} \quad (100)$$

by (91.2). Insertion of this result into (96) shows that

$$\sum_{\sigma} \frac{(f_{\sigma})_{g \cdot g}}{x_{\sigma}} = 0, \quad (101)$$

to this order, as expected.

12. Higher Harmonic Terms in the Gravity-Gradient Force

To obtain an estimate of the effect of the J_2 term in (94), let us consider the case where the σ 'th tunnel is parallel to \underline{r}_{σ} , so that $\ell_{\sigma} = 1$. The contribution of the J_2 term is then

$$(f_{\sigma})_{gg} (J_2) = N_{\sigma} x_{\sigma}, \quad (102)$$

where

$$N_{\sigma} = \frac{3\mu J_2 R_e^2}{2r_{\sigma}^5} (4 - 2\gamma_{3\sigma}^2 + \frac{20\gamma_{3\sigma} z_{\sigma}}{r_{\sigma}} - \frac{30z_{\sigma}^2}{r_{\sigma}^2}) \quad (103)$$

If the tunnel and \underline{r}_{σ} are also parallel to the earth's polar axis, then $X_{\sigma} = Y_{\sigma} = 0$, $Z_{\sigma} = r_{\sigma}$, and $\gamma_{3\sigma} = 1$, so that

$$N_{\sigma} = \frac{3\mu J_2 R_e^2}{2r_o^5} (-8) = -\frac{12\mu J_2 R_e^2}{r_o^5} \approx -\frac{12\mu J_2}{R_e^3} \quad (104)$$

Let us compare this with the main field on the test object, viz

$$f_{\sigma}(\text{sphere}) \approx \frac{4\pi}{3} G\rho x_{\sigma}, \quad (105)$$

when $\rho \approx 20 \text{ gm/cm}^3$ for tungsten. Then

$$\begin{aligned} \left| \frac{N_{\sigma} x_{\sigma}}{f_{\sigma}(\text{sphere})} \right| &\approx \frac{12J_2}{R_e^3} \frac{4\pi}{3} G\rho_e R_e^3 \left[\frac{4\pi}{3} G\rho \right]^{-1} \\ &= 12J_2 \frac{\rho_e}{\rho}, \end{aligned} \quad (106)$$

where $\rho_e \approx 5.5 \text{ gm/cm}^3$, the mean density of the earth. Then

$$\text{ratio} \approx (12)10^{-3} \frac{5.5}{20} = (3.3)10^{-3} \quad (107)$$

Thus the J_2 gravity-gradient field may amount to 1/300 of the main field. The gravity-gradient fields from the higher harmonics of the earth's potential may be expected to be about 10^{-3} of this or about $(3)10^{-6}$ of the main field.

In the formal reduction of data, however, they will not enter since (101) will still hold, when we take a sum over the three tunnels. In the computer simulation where we are concerned with each tunnel separately -- to make sure that no test object is ejected -- it is only the J_2 among the higher harmonics that may count and its effect is marginal.

13. Quadratic Terms in the Gravity Gradient Force

For the estimate of quadratic terms it will suffice to consider only the monopole part of the earth's potential, viz

$$U = \frac{\mu}{r} = \frac{\mu}{r_0} [1+h\lambda + h^2(\frac{3}{2}\lambda^2 - \frac{1}{2}) + h^3(\frac{5}{2}\lambda^3 - \frac{3}{2}\lambda)+\dots], \quad (108)$$

by (78). Its cubic part is

$$U_3 = \frac{\mu}{r_0} [\frac{5}{2}(\lambda h)^3 - \frac{3}{2}h^2(h\lambda)] \quad (109)$$

With use of (79.1), (79.2), and (74), this becomes

$$U_3 = \frac{\mu}{2r_0^4} [-5(\sum_{\sigma} l_{\sigma} x_{\sigma})^3 + 3(x^2+y^2+z^2)\sum_{\sigma} l_{\sigma} x_{\sigma}] \quad (110)$$

Then

$$\frac{\partial U_3}{\partial x_{\sigma}} = \frac{\mu}{2r_0^4} [-15l_{\sigma}(\sum_{\sigma} l_{\sigma} x_{\sigma})^2 + 6x_{\sigma}\sum_{\sigma} l_{\sigma} x_{\sigma} + 3l_{\sigma}(x^2+y^2+z^2)] \quad (111.1)$$

Thus the quadratic gravity-gradient term in the σ 'th tunnel is given by

$$\delta_3 f_{g.g.\sigma} = \frac{3\mu}{2r_0^4} l_{\sigma}(3-5l_{\sigma}^2)x_{\sigma}^2 \quad (111.2)$$

The quantity $|3l_{\sigma} - 5l_{\sigma}^3|$ has a maximum value 2, occurring for $l_{\sigma} = \pm 1$, so that

$$|\delta_3 f_{g.g.\sigma}|_{\max} = \frac{3\mu x_{\sigma}^2}{r_0^4} \approx 3G \frac{4\pi\rho_e}{3} \frac{x_{\sigma}^2}{R_e}$$

Comparison with the main field

$$f_{\sigma}(\text{sphere}) \approx \frac{4\pi}{3} G\rho x_{\sigma}$$

gives

$$|\text{ratio}| \approx 3 \frac{\rho_e}{\rho} \frac{x_\sigma}{R_e},$$

where $\rho_e \approx 5.5 \text{ gm/cm}^3$, $\rho \approx 19 \text{ gm/cm}^3$, $R_e \approx (6.4)10^8 \text{ cm}$, and $|x_\sigma| < 10 \text{ cm}$. Thus the quadratic gravity gradient term is less than $(1.4)10^{-8}$ of the main force on the test object.

14. Summary of Earth Gravity-Gradient Effects on a Test Object

a. Sphere Unconstrained, but Maintained by Means of External Jets at a Point Fixed in the Space-Craft

In this case the gravity-gradient field $f_{\sigma g.g.}$ at the test object is given by

$$\begin{aligned} \frac{f_{\sigma g.g.}}{x_\sigma} = & -\frac{\mu}{r_o^3} (1-3l_\sigma^2) + \frac{3\mu J_2 R_e^2}{2r_o^5} [-1+5l_\sigma^2 - 2\gamma_{3\sigma}^2 \\ & + \frac{20\gamma_{3\sigma} l_\sigma z_o}{r_o} + \frac{5z_o^2}{r_o^2} (1-7l_\sigma^2)] + O(x_\sigma^2) \end{aligned} \quad (112)$$

Here the position vector of the center of the sphere is $\underline{r}_o = \underline{r}_c + \underline{b}$, where \underline{r}_c is the position vector of the sphere's center of mass relative to that of the earth. If the axis of the space-craft is kept pointing perpendicular to the plane of the horizon, the components b_μ of \underline{b} will be almost constant in the system $\underline{i}_o, \underline{j}_o, \underline{k}_o$, when \underline{k}_o is a unit vector along \underline{r}_c and \underline{j}_o is a unit vector along the osculating orbital angular momentum.

Then

$$r_o^2 = (x_c + \sum_\mu \beta_{1\mu} b_\mu)^2 + (y_c + \sum_\mu \beta_{2\mu} b_\mu)^2 + (z_c + \sum_\mu \beta_{3\mu} b_\mu)^2 \quad (112.1)$$

$$z_o = z_c + \sum_{\mu} \beta_{3\mu} b_{\mu} \quad (112.2)$$

$$r_o \ell_{\sigma} = X_c \gamma_{1\sigma} + Y_c \gamma_{2\sigma} + Z_c \gamma_{3\sigma} + b_1 \alpha_{1\sigma} + b_2 \alpha_{2\sigma} + b_3 \alpha_{3\sigma} \quad (112.3)$$

Here X_c, Y_c, Z_c are the coordinates of the center of mass of the space-craft in the equatorial system, $\gamma_{1\sigma}, \gamma_{2\sigma}, \gamma_{3\sigma}$ are the direction cosines of the σ 'th tunnel in the equatorial system, $\alpha_{1\sigma}, \alpha_{2\sigma}, \alpha_{3\sigma}$ are the direction cosines of the σ 'th tunnel in the space-craft system $\underline{i}_o, \underline{j}_o, \underline{k}_o$, and $\beta_{3\mu}$ ($\mu = 1, 2, 3$) are the direction cosines of the earth's polar axis in the system $\underline{i}_o, \underline{j}_o, \underline{k}_o$. Also ℓ_{σ} ($\sigma = 1, 2, 3$) are the direction cosines of \underline{r}_o in the tunnel system.

b. Center of Sphere Constrained to Remain at the Center of Mass of the Space-Craft

In this case the sphere is constrained relative to translation, but mounted in a system of gimbals so that it can rotate freely. Also $b = 0$.

The above formulas for $f_{\sigma g.g.}$ then get simplified by the omission of the terms in b_1, b_2, b_3 . We may then put $\underline{r}_o = \underline{r}_c$ and $Z_o = Z_c$. The direction cosines ℓ_{σ} are then those of \underline{r}_c in the tunnel system.

15. Gravitational Effects of the Space-craft Itself

Since the Skylab is to be a cylinder, filled with all sorts of equipment and carrying several astronauts, it will produce a gravitational field on a test object. Since the environment will be complex and indeed unpredictable, it will be impossible to calculate this field. Instead, I shall assume that everything is tied down during a run, say for an hour. This means that the astronauts would have to be persuaded to remain as stationary as possible during this time.

To treat the gravitational potential V_L produced by the Skylab itself, let us expand it in a Taylor's series in the neighborhood of the center of the sphere. On carrying terms through the cube of \underline{s} , the position vector of the test object relative to the center of the sphere, we can then specify V_L by means of 18 coefficients. These coefficients will be constant if and only if everything is tied down during the run. If the sphere is constrained, all 18 coefficients will indeed be required to specify the field $f_{L\sigma}$ produced by the space laboratory on the test object in the σ 'th tunnel. If the sphere is unconstrained, only the gravity-gradient part, $f_{L\sigma}'$, of this field remains and $f_{L\sigma}'$ requires only 10 constants for its specification.

The idea behind this kind of treatment of the laboratory field is to treat the above constants, as well as G , as unknowns to be determined from the highly redundant data that will be obtained during a run. A statistical reduction of these data will then give both G and the "constants" and will test their constancy and thus the reliability of the experiment.

Let $U_L = -V_L$. Then the gravitational field produced by the spacecraft itself on the test object in the σ 'th tunnel will be given by

$$f_{L\sigma} = \frac{\partial U_L}{\partial x_\sigma}, \quad (113)$$

where x_σ is the distance from the center of the sphere to the test object in the σ 'th tunnel.

Now let ξ_μ ($\mu=1,2,3$) be the components of \underline{s} in a system fixed in the space-craft. The system $\underline{i}_0, \underline{j}_0, \underline{k}_0$, as mentioned above, is approximately such a system. If we now expand U_L as a Taylor's series in the ξ_μ 's, the coefficients will be constants, if and only if everything is tied down during the run.

Through cubic terms, this Taylor's series takes the form (See

Hildebrand 1964 for the method)

$$\begin{aligned}
 U_L(\underline{r}_0 + \underline{s}) - U_L(\underline{r}_0) &= \sum_{\mu} A_{\mu} \xi_{\mu} \\
 &+ \frac{1}{2} \left[\sum_{\mu} B_{\mu} \xi_{\mu}^2 + \sum_{\mu < \nu} C_{\mu\nu} \xi_{\mu} \xi_{\nu} \right] \\
 &+ \frac{1}{3} \left[\sum_{\mu} D_{\mu} \xi_{\mu}^3 + \sum_{\nu} \xi_{\nu} \sum_{\mu \neq \nu} E_{\mu\nu} \xi_{\nu}^2 + F \xi_1 \xi_2 \xi_3 \right]
 \end{aligned} \tag{114}$$

There are three A's, three B's, three C's, three D's, six E's and one F, or 19 coefficients in all. But

$$B_1 + B_2 + B_3 = (\nabla^2 U_L)_0 = 0, \tag{115}$$

since we are here not including the sphere itself (which does not have to be hollow at its center) as part of the space-craft. Thus there are 18 independent coefficients.

If we let α be the matrix of the rotation that takes one from the tunnel system i_{μ} to the space-craft system $i_{0\mu}$, then

$$i_{0\nu} = \sum_{\mu} \alpha_{\nu\mu} i_{\mu} \tag{30.1}$$

$$\xi_{\nu} = \sum_{\mu} \alpha_{\nu\mu} x_{\mu} \tag{30.4}$$

In the σ 'th tunnel, however,

$$\xi_{\mu} = \alpha_{\mu\sigma} x_{\sigma}, \tag{116}$$

not summed. Insertion of (116) into (114) then yields

$$\begin{aligned}
 U_L - U_L(0) &= x_{\sigma} \sum_{\mu} A_{\mu} \alpha_{\mu\sigma} + \frac{1}{2} x_{\sigma}^2 \left[\sum_{\mu} B_{\mu} \alpha_{\mu\sigma}^2 + \sum_{\mu < \nu} C_{\mu\nu} \alpha_{\mu\sigma} \alpha_{\nu\sigma} \right] \\
 &+ \frac{1}{3} x_{\sigma}^3 \left[\sum_{\mu} D_{\mu} \alpha_{\mu\sigma}^3 + \sum_{\mu} \alpha_{\mu\sigma} \sum_{\nu \neq \mu} E_{\mu\nu} \alpha_{\nu\sigma}^2 + F \alpha_{1\sigma} \alpha_{2\sigma} \alpha_{3\sigma} \right]
 \end{aligned} \tag{117}$$

Then

$$\begin{aligned}
 f_{L\sigma} = \frac{\partial U_L}{\partial x_\sigma} &= \sum_{\mu} A_{\mu} \alpha_{\mu\sigma} + x_{\sigma} \left[\sum_{\mu} B_{\mu} \alpha_{\mu\sigma}^2 + \sum_{\mu < \nu} C_{\mu\nu} \alpha_{\mu\sigma} \alpha_{\nu\sigma} \right] \\
 &+ x_{\sigma}^2 \left[\sum_{\mu} D_{\mu} \alpha_{\mu\sigma}^3 + \sum_{\mu \neq \nu} E_{\mu\nu} \alpha_{\mu\sigma} \alpha_{\nu\sigma}^2 + F \alpha_{1\sigma} \alpha_{2\sigma} \alpha_{3\sigma} \right] \quad (118)
 \end{aligned}$$

If the sphere is constrained (and we have seen that constraining it will completely ruin the experiment unless its center is then fixed at the center of mass of the space-craft), the net gravitational field of the space-craft itself on the test object is given by (118), with 18 independent coefficients. If, however, the space-craft is approximately symmetric with respect to its mid-section, the terms involving the A_{μ} 's will be "small". That is, they will certainly be much smaller than they would be if the center of the sphere were 20 feet from the center of mass of the space-craft.

If the sphere is unconstrained, then the net field on a test object, produced by the space-craft, is given by a gravity-gradient term alone. This is

$$f'_{L\sigma} = f_{L\sigma}(r_0+s) - f_{L\sigma}(r_0), \quad (119)$$

where

$$f_{L\sigma}(r_0) = \sum_{\mu} A_{\mu} \alpha_{\mu\sigma}, \quad (120)$$

Thus

$$\begin{aligned}
 \frac{f'_{L\sigma}}{x_{\sigma}} &= \sum_{\mu} B_{\mu} \alpha_{\mu\sigma}^2 + \sum_{\mu < \nu} C_{\mu\nu} \alpha_{\mu\sigma} \alpha_{\nu\sigma} \\
 &+ x_{\sigma} \left[\sum_{\mu} D_{\mu} \alpha_{\mu\sigma}^3 + \sum_{\mu \neq \nu} E_{\mu\nu} \alpha_{\mu\sigma} \alpha_{\nu\sigma}^2 + F \alpha_{1\sigma} \alpha_{2\sigma} \alpha_{3\sigma} \right] \quad (121)
 \end{aligned}$$

This gives the net field on the test object, when the sphere is unconstrained, but $b \neq 0$. (Of course the constants in (121) will have values differing from those when $b = 0$.) When one sums the equations of motion

over the three tunnels, there is a further simplification, as follows.

$$\begin{aligned} & \sum_{\sigma} \left(\sum_{\mu} B_{\mu} \alpha_{\mu\sigma}^2 + \sum_{\mu < \nu} C_{\mu\nu} \alpha_{\mu\sigma} \alpha_{\nu\sigma} \right) \\ &= \sum_{\mu} B_{\mu} \sum_{\sigma} \alpha_{\mu\sigma}^2 + \sum_{\mu < \nu} \sum_{\sigma} C_{\mu\nu} \alpha_{\mu\sigma} \alpha_{\nu\sigma} \end{aligned} \quad (122.1)$$

$$= \sum_{\mu} B_{\mu}, \quad (122.2)$$

since α is an orthogonal matrix. Also $\sum_{\mu} B_{\mu} = 0$, by (115), so that

$$\sum_{\sigma} \frac{f_{L\sigma}}{x_{\sigma}} = \sum_{\mu} D_{\mu} \sum_{\sigma} x_{\sigma} \alpha_{\mu\sigma}^3 + \sum_{\mu \neq \nu} \sum_{\sigma} E_{\mu\nu} \sum_{\sigma} x_{\sigma} \alpha_{\mu\sigma} \alpha_{\nu\sigma}^2 + F \sum_{\sigma} x_{\sigma} \alpha_{1\sigma} \alpha_{2\sigma} \alpha_{3\sigma} \quad (123)$$

In this case only 10 coefficients remain to be determined, in the reduction of the data. Of course there will still be 18 in the computer simulation, where one must consider each tunnel separately, in searching for possible extraction of a test object.

16. The Effects of Drag on a Test Object

If the sphere is unconstrained, it is in free fall in the gravitational field of the earth and the spacecraft, and the aerodynamic drag on the space-craft has no effect on the test object.

Suppose now that the sphere is constrained, as in Case β , at the center of mass of the space-craft. The effect of space-craft drag on a test object in the σ 'th tunnel then appears as a force per unit mass

$$f_{D\sigma} = -\frac{D}{M} \cdot \underline{i}_{\sigma} \quad (124)$$

Here M is the total mass of the space-craft, of the order 10^5 pounds and \underline{i}_{σ} is a unit vector along the σ 'th tunnel. The vector \underline{D} is the total non-gravitational force acting on the space-craft. If this force is entirely aerodynamic drag, it is given by

$$\underline{D} = -\frac{1}{2} C_D A \rho_a \underline{v}_a \underline{v}_a \quad (125)$$

Here ρ_a is the atmospheric density, \underline{v}_a is the resultant velocity of the space-craft relative to the (rotating) atmosphere, $v_a \equiv |\underline{v}_a|$, A is the projected area of the space-craft perpendicular to \underline{v}_a , and C_D is a dimensionless coefficient ≈ 2.2 . Here A will be of the order $20' \times 40' = 800 \text{ ft}^2$. Even if the axis of the cylinder is perpendicular to the space-craft velocity $\dot{\underline{r}}_C$, this figure is not exact because $\underline{v}_a \neq \dot{\underline{r}}_C$.

Indeed

$$\underline{v}_a = \dot{\underline{r}}_C - \Omega_e \underline{K} \times \underline{r}_C, \quad (126)$$

which says that the net velocity of the space-craft, relative to the atmosphere, is its velocity in the equatorial system minus the velocity in the same system of the atmosphere, considered to be rotating like a rigid body along with the earth. Here Ω_e is the sidereal rate of rotation of the earth and \underline{K} a unit vector along its polar axis.

If \underline{I}_μ ($\mu=1,2,3$) are the unit vectors in the equatorial system, we have

$$\dot{\underline{r}}_C = \sum_{\mu} \underline{I}_\mu \dot{X}_{C\mu} \quad (127)$$

and

$$\underline{K} \times \underline{r}_C = \underline{J} X_C - \underline{I} Y_C \quad (128)$$

Also

$$\underline{I}_\mu \cdot \underline{i}_\sigma = \gamma_{\mu\sigma} \quad (31.3)$$

Then, from Eqs. (124) through (128) and (31.3), we find

$$F_{D\sigma} = \frac{1}{2} C_D \frac{A}{M} \rho_a v_a [(\dot{X}_C + \Omega_e Y_C) \gamma_{1\sigma} + (\dot{Y}_C - \Omega_e X_C) \gamma_{2\sigma} + \dot{Z}_C \gamma_{3\sigma}], \quad (129)$$

where the γ 's are the direction cosines of the σ 'th tunnel in the equatorial system and where

$$v_a^2 = \dot{\underline{r}}_C^2 - 2\Omega_e (X_C \dot{Y}_C - Y_C \dot{X}_C) + \Omega_e^2 (X_C^2 + Y_C^2) \quad (130)$$

Estimates show that the term in Ω_e^2 is about 1/200 of the main term \dot{r}_c^2 and that the term in Ω_e is about 2/15 of it. Since $\Omega_e > 0$ and $X_c \dot{Y}_c - Y_c \dot{X}_c > 0$ for a direct orbit, as the Skylab will have, the rotation of the atmosphere diminishes the effect of drag, as expected.

To estimate the ratio of $f_{D\sigma}$ to the main field $\frac{4\pi}{3} G \rho x_\sigma$, we consider the case where the given tunnel is parallel to \underline{v}_a . Then by (124) and (125)

$$f_{D\sigma} = \frac{1}{2} \frac{C_D^A}{M} \rho_a v_a^2 \quad (131)$$

Here $v_a^2 \sim \dot{r}_c^2 \sim \mu/r_c$, for an orbit with small eccentricity. Approximating r_c by R_e and writing

$$\mu \sim G \frac{4\pi}{3} \rho_e R_e^3, \quad (132)$$

where ρ_e is the earth's mean density, we then obtain

$$f_{D\sigma} \sim \frac{C_D^A}{2M} \rho_a G \frac{4\pi}{3} \rho_e R_e^2 \quad (133)$$

But

$$f_{\text{main}} \sim G \frac{4\pi}{3} \rho x_\sigma, \quad (134)$$

where ρ is the density of tungsten. Then

$$\frac{f_{D\sigma}}{f_{\text{main}}} \sim \frac{C_D^A}{2M} \frac{\rho_a \rho_e}{\rho} \frac{R_e^2}{x_\sigma} \quad (135)$$

With $C_D = 2.2$, $A = 800 \text{ ft}^2 = 743,200 \text{ cm}^2$, $\rho_e = 5.5 \text{ gm/cm}^3$, $\rho = 19 \text{ gm/cm}^3$, $R_e = (6.4)10^8 \text{ cm}$, $M = 10^5 \text{ lb} = (4.54)10^7 \text{ gm}$, we find

$$\frac{f_{D\sigma}}{f_{\text{main}}} = (2.14)10^{14} \rho_a \quad (136)$$

if $x_\sigma = 10$ cm and ρ_a is in gm/cm^3 .

We consider an orbit at an altitude of 500 km. The atmospheric density ρ_a is a highly variable quantity. According to Jacchia (1969), at 500 kilometers the exospheric temperature T_{ex} can vary from about 700°K at sunspot minimum to 1900°K at sunspot maximum. There is also a variation of a few hundred degrees between day and night. Reference to the U.S. Standard Atmosphere Supplements, 1966 furnishes the following data (which at 500 km do not depend on which seasonal model is used)

T_{ex}	ρ_a (in gm/cm^3)	$f_{D\sigma}/f_{\text{main}}$ at $x = 10$ cm
800° K	1.54×10^{-16}	0.033
1900°K	5.74×10^{-15}	1.23

At $x_\sigma = 2$ cm, these values of the ratio would be five times larger. Thus at certain phases of the sun spot cycle, the effect of drag can be very serious. At 400 km, the ratio is about twice that at 500 km for $T_{\text{ex}} = 1900^\circ\text{K}$. and about eight times that at 500 km for $T_{\text{ex}} = 800^\circ\text{K}$.

If the sphere is kept constrained, so that drag enters the picture, its effects can thus be very important and highly variable, depending strongly on the phase of the sunspot cycle, time of day, and altitude.

17. Reduction of the Observations: Unconstrained Sphere

To reduce the observations when the sphere is not constrained, we may use Eqs. (60), (94), and (121). In so doing, we write

$$f_{s\sigma}(r_{\sim 0} + s) = -\frac{4\pi}{3} G \rho x_\sigma - f_{G\sigma}^T \quad (137)$$

where $f_{G\sigma}^T$ is the attractive correction to the gravitational field of the sphere, produced by the finite diameter of the σ 'th tunnel and the presence of the two other tunnels. I defer the evaluation of $f_{G\sigma}^T$ to another report. Then

$$\begin{aligned}
\ddot{x}_\sigma = & -\frac{4\pi}{3} G\rho x_\sigma - f_{G\sigma}^T + (\omega^2 - \omega_\sigma^2) x_\sigma \\
& + x_\sigma \left[-\frac{\mu}{r_o^3} (1-3\ell_\sigma^2) + \frac{3\mu_J 2R_e^2}{2r_o^5} \left\{ -1+5\ell_\sigma^2 - 2\gamma_{3\sigma}^2 \right. \right. \\
& \left. \left. + \frac{20\gamma_{3\sigma} \ell_\sigma z_o}{r_o} + 5 \frac{z_o^2}{r_o^2} (1-7\ell_\sigma^2) \right\} \right] \\
& + x_\sigma \left[\sum_\mu B_{\mu\sigma} \alpha_{\mu\sigma}^2 + \sum_{\mu < \nu} C_{\mu\nu} \alpha_{\mu\sigma} \alpha_{\nu\sigma} \right] \\
& + x_J^2 \left[\sum_\mu D_{\mu\sigma} \alpha_{\mu\sigma}^3 + \sum_{\mu \neq \nu} E_{\mu\nu} \alpha_{\mu\sigma} \alpha_{\nu\sigma}^2 + F \alpha_{1\sigma} \alpha_{2\sigma} \alpha_{3\sigma} \right] \quad (138)
\end{aligned}$$

On forming $\Sigma_\sigma \ddot{x}_\sigma / x_\sigma$, the whole gravity-gradient term drops out (including the effects of the higher harmonics that are not indicated in (138)), as does part of the term arising from the gravitational effects of the space-craft itself. We shall then be neglecting only the truly negligible quadratic gravity gradient terms and the quartic terms of the space-craft potential. We obtain

$$\begin{aligned}
\Sigma_\sigma \ddot{x}_\sigma / x_\sigma = & -4\pi G\rho - \Sigma_\sigma f_{G\sigma}^T / x_\sigma + 2\omega^2 \\
& + \Sigma_\sigma x_\sigma \left[\sum_\mu D_{\mu\sigma} \alpha_{\mu\sigma}^3 + \sum_{\mu \neq \nu} E_{\mu\nu} \alpha_{\mu\sigma} \alpha_{\nu\sigma}^2 + F \alpha_{1\sigma} \alpha_{2\sigma} \alpha_{3\sigma} \right] \quad (139)
\end{aligned}$$

Now suppose that the design has been such that no test object is

extracted during a run and that the servomechanisms work well, so that each \ddot{x}_σ remains small. Let us also suppose that at times $t_1, t_2, t_3, \dots, t_N$ we observe ω^2 , each x_σ , and the orientation of the tunnel system relative to the inertial system, so that we know all the γ 's at each instant. If the orbit trackers give us the $X_{c\mu}$'s and $\dot{X}_{c\mu}$'s at each instant, we can then determine the β 's, to a certain approximation, if the cylinder is kept properly oriented. We can then determine the α 's from $\alpha = \beta^{-1}\gamma$. Numerical differentiation can furnish the small terms \ddot{x}_σ .

In Eq. (139) there are then the unknowns $G\rho$, three D's, six E's, and F, or 11 unknowns in all, and all presumably constant, if everything in the space-craft has been tied down during the run, and if the space-craft has been kept properly oriented. We then have N equations to determine the 11 unknowns. By taking $N \gg 11$, we can increase the accuracy of determination of $G\rho$, with use of statistical methods for reducing the highly redundant set of data.

18. Reduction of the Observations: Constrained Sphere

To reduce the observations when the sphere is constrained, we may use Eqs. (64), (112) with the b_μ 's zero, (118), (129), and (137). We obtain

$$\begin{aligned} \ddot{x}_\sigma/x_\sigma = & -\frac{4\pi}{3} G\rho - f_{G\sigma}^T/x_\sigma + (\omega^2 - \omega_\sigma^2)x_\sigma \\ & - \frac{\mu}{r_c^3} (1-3\ell_\sigma^2) + \frac{3\mu J_2 R_e^2}{2r_c^5} [-1+5\ell_\sigma^2 - 2\gamma_{3\sigma}^2 + \frac{20\gamma_{3\sigma}\ell_\sigma z_c}{r_c} \\ & + \frac{5z_c^2}{r_c^2} (1-7\ell_\sigma^2)] \\ & + x_\sigma^{-1} \left[\sum_\sigma A_\mu \alpha_{\mu\sigma} + \sum_\mu B_\mu \alpha_{\mu\sigma}^2 + \sum_{\mu < \nu} \sum C_{\mu\nu} \alpha_{\mu\sigma} \alpha_{\nu\sigma} \right] \end{aligned}$$

$$\begin{aligned}
& + x_\sigma [\sum_\mu D_\mu \alpha_{\mu\sigma}^3 + \sum_{\mu \neq \nu} E_{\mu\nu} \alpha_{\mu\sigma} \alpha_{\nu\sigma}^2 + F \alpha_{1\sigma} \alpha_{2\sigma} \alpha_{3\sigma}] \\
& + \frac{\psi(t)}{x_\sigma} [(\dot{X}_c + \Omega_e Y_c) \gamma_{1\sigma} + (\dot{Y}_c - \Omega_e X_c) \gamma_{2\sigma} + \dot{Z}_c \gamma_{3\sigma}] \quad (\sigma = 1, 2, 3)
\end{aligned} \tag{140}$$

Here l_σ is given by (91.3), with the b_μ 's placed equal to zero. The quantity $\psi(t)$, defined by

$$\psi(t) = \frac{C_D A}{2M} \rho_a v_a, \tag{141}$$

is a highly variable and largely unknown quantity, because of the atmospheric density ρ_a .

Assume that the $X_{c\mu}$, $\dot{X}_{c\mu}$, x_σ , ω_σ , γ 's, and α 's are given, as before, at each time of measurement. With N times, Eq. (140) then furnishes $3N$ equations for $19+N$ unknowns. These include G_0 , three A's, three B's, three C's, three D's, six E's, and one F, which add to 20, minus one equation of condition, viz $\sum_\mu B_\mu = 0$. They also include the N values of $\psi(t)$. If we choose N so large that

$$3N > N+19, \text{ i.e., } N \geq 10 \tag{142}$$

we shall have enough data to do the reduction and thus find G_0 .

We could not do the summing over σ in this case, because of the need to determine the values of the unknown $\psi(t)$. Larger values of N should give more accuracy, through greater redundancy, up to the point where the time becomes so large that things cannot be kept tied down in the space-craft.

In this scheme, harmonics of the earth's potential higher than J_2 are not included in the earth gravity-gradient field. They may give a field of the order $(3)10^{-6}$ of the main field $4\pi G_0 x_\sigma/3$. In the other method, with the sphere unconstrained, they did not enter the picture

at all, since they disappeared on summing over σ .

19. The Computer Simulation

The above equations for the \ddot{x}_σ 's are sufficient for the reduction of the data. In this reduction we have given to us the x_σ , the $X_{C\mu}$, $\dot{X}_{C\mu}$, the γ 's, and the ω 's.

The purpose of a computer simulation is to find out whether any test object will be extracted from one of the tunnels and to check or aid the design of the servomechanisms. Now an experimental run is not expected to last longer than one orbital revolution, else we could not hope to keep things tied down in the space-craft. For the rather qualitative purpose of computer simulation, it should thus suffice to use an elliptic (or circular) orbit as input for the $X_{C\mu}$, $\dot{X}_{C\mu}$. It would also be reasonable to omit the J_2 part of the earth gravity gradient field in (140), since it does not amount to more than about 1/300 of the main field $4\pi G\rho x_\sigma/3$.

The simulation begins with Eqs. (138) for the unconstrained sphere or Eqs. (140) for the constrained sphere. The other necessary equations will be those that tell us how the ω 's and the $\gamma_{\mu\nu}$ vary with time. (This is on the assumption that the space-craft maintains the orientation that has been described, so that the direction cosines $\beta_{\mu\nu}$ and $\alpha_{\mu\nu}$ can then be found from the $\gamma_{\mu\nu}$ and the $X_{C\mu}$ and $\dot{X}_{C\mu}$.)

I shall assume that the principal moments of inertia of the sphere, viz A, B, and C, are those about the axes of the tunnels and that they have been measured. If \underline{S} is the total spin angular momentum of the sphere, relative to its center of mass, then

$$\underline{S} = \underline{i} A\omega_1 + \underline{j} B\omega_2 + \underline{k} C\omega_3 \quad (143)$$

The variation of the ω 's is then given by

$$\dot{\underline{S}} = \underline{L} , \quad (144)$$

where the dependence of the torque \underline{L} will be expressible by means of Eqs.(23) or something similar. Since $\dot{\underline{i}} = \underline{\omega} \times \underline{i}$, etc, Eqs. (144) and (23) result in

$$A\dot{\omega}_1 - (B-C)\omega_2\omega_3 = k_{11}\dot{x} + k_{12}\dot{y} \quad (145.1)$$

$$B\dot{\omega}_2 - (C-A)\omega_3\omega_1 = k_{21}\dot{y} + k_{22}\dot{z} \quad (145.2)$$

$$C\dot{\omega}_3 - (A-B)\omega_1\omega_2 = k_{31}\dot{z} + k_{32}\dot{x} \quad (145.3)$$

for the variation of the ω 's.

To describe the orientation of the sphere we need either three differential equations for Eulerian angles or nine differential equations for the direction cosines $\gamma_{\mu\nu}$. Of these six will be redundant, since the $\gamma_{\mu\nu}$ obey six orthonormal relations. It appears simpler to use the direction cosines. The computer simulation will then involve integrating fifteen differential equations, with six equations of constraint on the $\gamma_{\mu\nu}$ that will serve as checks.

From

$$\underline{\omega} = \underline{i}\omega_1 + \underline{j}\omega_2 + \underline{k}\omega_3 \quad (146)$$

$$\dot{\underline{i}} = \underline{\omega} \times \underline{i}, \quad \dot{\underline{j}} = \underline{\omega} \times \underline{j}, \quad \dot{\underline{k}} = \underline{\omega} \times \underline{k} \quad (147)$$

$$\dot{\underline{i}}_\nu = \sum_{\mu} \underline{i}_\mu \dot{\gamma}_{\mu\nu}, \quad (148)$$

we readily deduce

$$\begin{aligned}
 \dot{\gamma}_{11} &= -\gamma_{13}\omega_2 + \gamma_{12}\omega_3 & \dot{\gamma}_{12} &= \gamma_{13}\omega_1 - \gamma_{11}\omega_3 & \dot{\gamma}_{13} &= -\gamma_{12}\omega_1 + \gamma_{11}\omega_2 \\
 \dot{\gamma}_{21} &= -\gamma_{23}\omega_2 + \gamma_{22}\omega_3 & \dot{\gamma}_{22} &= \gamma_{23}\omega_1 - \gamma_{21}\omega_3 & \dot{\gamma}_{23} &= -\gamma_{22}\omega_1 + \gamma_{21}\omega_2 \\
 \dot{\gamma}_{31} &= -\gamma_{33}\omega_2 + \gamma_{32}\omega_3 & \dot{\gamma}_{32} &= \gamma_{33}\omega_1 - \gamma_{31}\omega_3 & \dot{\gamma}_{33} &= -\gamma_{32}\omega_1 + \gamma_{31}\omega_2
 \end{aligned}
 \tag{149}$$

Since γ is an orthogonal matrix, satisfying $\gamma\tilde{\gamma} = 1$, Eqs. (149) are subject to the six orthonormal relations

$$\sum_{\nu} \gamma_{\mu\nu} \gamma_{\sigma\nu} = \delta_{\mu\sigma} \quad (\mu, \sigma = 1, 2, 3)
 \tag{150}$$

as conditions of constraint.

In doing the computer simulation, one will have to guess various possible distributions of mass in the space-craft, in order to estimate the coefficients in the Taylor's series (114). One will also have to guess various values for the $k_{\mu\nu}$ in (145) that describe the servos. Numerical integration of the system of 15 differential equations can be checked by seeing if Eqs. (150) are satisfied. The results can then be used to find the values of the $k_{\mu\nu}$ that are required to keep the \ddot{x}_{σ} small (ideally, zero) and to prevent extraction of any test object from a tunnel.

REFERENCES

Forward, R.L., Berman, D., "Free-Fall Experiments to Determine the Newtonian Gravitational Constant G", Exploitation of Space for Experimental Research, Vol. 24, Science and Technology, Series - Amer. Astronautical Soc. 1968.

Hildebrand, F.B., 1964, "Advanced Calculus for Applications", Prentice-Hall, Inc., Englewood Cliffs, N.J., p. 348.

Jacchia, L.G., 1969, "Atmospheric Density Variations during Solar Maximum and Minimum", in Annals of the IQSY, Vol. 5, Solar-Terrestrial Physics: Terrestrial Aspects, M.I.T. Press, pp. 323-339.

United States Standard Atmosphere Supplements 1966, Sponsored by ESSA, NASA, and the U.S. Air Force, pp. 220-289.

Wilk, L., Private Communication

List of Principal Symbols

<u>Symbol</u>	<u>Page of First Appearance</u>
a_o	3 3
A	37,44 (different meanings)
A_μ	35
\tilde{b}	16
B	44
B_μ	35
C	10,44 (different meanings)
C_D	37
$C_{\mu\nu}$	35
\tilde{D}	35
E	10
$E_{\mu\nu}$	35
$\tilde{f}(R)$	2
\tilde{f}'	5
f (sphere)	4
$\tilde{f}_E(r)$	16
\tilde{f}_{LS}	15
$\tilde{f}_L(\tilde{x})$	16
$\tilde{f}_S(\tilde{x})$	16
\tilde{f}_\perp	16
$(f_o)_{gg}$	27
F	35
G	1
h	24
$\tilde{i}, \tilde{j}, \tilde{k}$	12
$\tilde{i}_o, \tilde{j}_o, \tilde{k}_o$	10

<u>Symbol</u>	<u>Page of First Appearance</u>
$i_{\sim\sigma}$	13
I, J, K_{\sim}	10
J_2	22
J_{\sim}	15
$k_{\mu\nu}$	8
l_{σ}	23
L_1, L_2, L_3	8
L_{\sim}	45
M	15
N_{σ}	29
O	10
p	10
P_2	22
Q_{σ}	23
r_{\sim}	10
r_c	10
r_o	10
s_{\sim}	13
T_{ex}	40
U	26
v_a	37
V	21
x, y, z	5
x_{μ}	19
X, Y, Z	10
X_c, Y_c, Z_c	10

<u>Symbol</u>	<u>Page of First Appearance</u>
X_0, Y_0, Z_0	10
$\alpha_{\mu\nu}$	13
$\beta_{\mu\nu}$	12
$\gamma_{\mu\nu}$	14
ξ_1, ξ_2, ξ_3	13
λ	23
ρ'	3
ρ_e	5
ρ_a	37
ω	6
$\omega_1, \omega_2, \omega_3$	6

APPENDIX F

ANALYSIS OF THE GRAVITATIONAL FIELD IN
WILK'S SPHERE WITH THREE TUNNELS

ANALYSIS OF THE GRAVITATIONAL FIELD
IN WILK'S SPHERE WITH THREE TUNNELS

by

John P. Vinti

September, 1970

APPROVED:

W. Markey

Director
Measurement Systems Laboratory

Measurement Systems Laboratory
Massachusetts Institute of Technology
Cambridge, Massachusetts 02139

Acknowledgements

Mr. Leonard Wilk devised the three-tunnel method and made many valuable suggestions. Mr. W. E. Lee carried out an independent derivation of Eq. (10) for a single tunnel.

This report was sponsored by the National Aeronautics and Space Administration under NASA Contract No. 9-8328.

The publication of this report does not constitute approval by the National Aeronautics and Space Administration of the findings or the conclusions contained therein. It is published only for the exchange and stimulation of ideas.

Table of Contents

Acknowledgements	ii
Abstract	1
1. Introduction	1
2. The Main Gravitational Field	2
3. The Intersection of the Tunnels	3
4. Effects of the Tunnel σ on f_{σ}	4
5. Effects of the Perpendicular Tunnels on f_{σ}	8
6. The Field of a Disk	9
7. Corrections from the Empty Cylinders	11
8. Corrections from the Empty Spherical Segments	15
9. The Total Gravitational Field from the Sphere	17
10. Summary of the Notation	22
References	22
Appendix: Vestigial Tunnels	23
Figures	27

ANALYSIS OF THE GRAVITATIONAL FIELD
IN WILK'S SPHERE WITH THREE TUNNELS

by

John P. Vinti

M.I.T. Measurement Systems Laboratory
Cambridge, Massachusetts 02139

ABSTRACT

In Wilk's three-tunnel method for the determination of the gravitational constant G , the main gravitational field acting on a test object in a tunnel is given by $4\pi G\rho s/3$, where ρ is the density of the sphere and s the distance from the center of the sphere to the test object.

The present paper derives that correction $f_{G\sigma}^T$ to this expression which is produced by the finite diameters of the three tunnels. The difficulties arising from the complicated intersection, a dodecahedron with curved faces, are first pointed out. They are then eliminated by letting each tunnel have a flat end, at a distance from the center not less than the radius of the sphere circumscribing the dodecahedron.

Section (4) derives the correction produced on a given test object by the finite diameter of its own tunnel. Sections (5) through (8) derive the correction produced by the two perpendicular tunnels. The final result for $f_{G\sigma}^T$ is given in Section (9).

The paper is intended to supplement the main report on this method, listed in the references.

1. Introduction

A previous report by the author (Vinti 1970) dealt with the determination of the gravitational constant G in an orbiting space laboratory. The method investigated is due essentially to Wilk (1970), who proposed

the use of a tungsten sphere with tunnels along three mutually perpendicular diameters. Inertia reaction wheels, governed by servomechanisms, would keep the sphere slowly turning in such a way as to maintain a small test object motionless on the axis of each tunnel. From this balance of gravitational field against centrifugal force, a measurement of the components of angular velocity of the sphere would lead to a value of G. The method would of course involve many other measurements and corrections. The purpose of the three tunnels, rather than one, is to eliminate, to a large extent, the effects of the earth's gravity-gradient, in those cases where it is possible to do a summation over the three tunnels.

2. The Main Gravitational Field

Inside a uniform rigid sphere, of density ρ and radius R, the gravitational field strength \underline{f} is inward radial, of magnitude

$$f = 4\pi G\rho s/3, \quad (1)$$

where $f = |\underline{f}|$ and s is the distance of a field point from the center of the sphere. Eq. (1) follows readily from Gauss's theorem. Inside a single cylindrical tunnel, of negligible radius, drilled along a diameter of the sphere, the field would have the same value. If there are three tunnels, each of negligible radius, the attractive field f_σ on a small test particle in the σ 'th tunnel would then be given by

$$f_\sigma = 4\pi G\rho s_\sigma/3, \quad (2)$$

where s_σ is the distance of the test particle from the center of the sphere.

3. The Intersection of the Tunnels

As soon as one takes into account the finite radius of each tunnel there appear corrections to (2). For a test object in a given tunnel σ these are the effects of the finite radius of the σ -tunnel and the effects of the other two finite tunnels. If the tunnels are drilled all the way through, there is then a complicated intersection at the center, which would get counted three times, unless one takes special precautions. This intersection is a polyhedron with 12 curved faces. If the radius of a tunnel is a , the radius of a sphere inscribed in this polyhedron is \underline{a} and the radius of a sphere circumscribed about it is $a\sqrt{3/2}$.

For a model with $2a = 1.875$ inches, the volume of the inscribed sphere is 56.5 cm^3 and that of the circumscribed sphere 103.8 cm^3 , by calculation. A laboratory-drilled model was found to have a volume of $(62 \pm 2) \text{ cm}^3$, so that the polyhedron is closer to the inscribed than to the circumscribed sphere.

If instead of drilling the tunnels all the way through the sphere, one uses a drill with a flat end and stops drilling at a distance b from the center in each case, there is no intersection of the tunnels if $b \geq a(3/2)^{1/2}$. If $b = a(3/2)^{1/2}$, the flat end of each tunnel is tangent to the above "circumscribed sphere".

It appears unlikely that one can find a complete analytical solution for the gravitational field in a tunnel, when the actual intersection is permitted. In any special case, it is possible that one could then do a numerical integration to find the field. In what follows, however, I shall assume that each tunnel consists of two parts, each running from $r = b$ to $r = R$. If $b = a(3/2)^{1/2}$, there is still no intersection. Unless there turns out to be an experimental reason for being able to see through a tunnel, such a configuration of partial tunnels should be as good as that of the complete tunnels. It would

be better in one way, since it would give a larger field for small values of x_σ .

4. Effects of the Tunnel σ on f_σ

Figure 1 shows the arrangement, the cylinders ABCD and EFGH being hollowed out of the sphere of density ρ and radius R . Here Q is a source point and P a field point on the axis. Region (1) is intact and regions (2) and (3) have cavities (the tunnel). (Of course the figure is not drawn to scale.) It is sufficient to consider a field point P in the upper cavity alone, but source-points will have to cover all three regions (1), (2), and (3).

Let f be the axial component of the field strength at P , taken positive towards O . Then

$$f = f_1 + f_2 + f_3, \quad (3)$$

where f_i is the contribution of region i .

With cylindrical coordinates z, r, ϕ , the rectangular coordinates of a source point Q are $r \cos \phi, r \sin \phi$, and z and those of the field point P are $0, 0, s$. Then

$$QP^2 = r^2 \cos^2 \phi + r^2 \sin^2 \phi + (z-s)^2 = r^2 + (z-s)^2, \quad (4)$$

r being the distance from Q to the axis. Then

$$df_i = \frac{G\rho r dr d\phi dz}{QP^2} \cos \psi \quad (5)$$

For f_1 , r goes from 0 to $(R^2 - z^2)^{1/2}$, z from $-b$ to b , and ϕ from 0 to 2π . Also

$$\cos \psi = \frac{s-z}{QP} \quad (6)$$

From Eqs. (5) and (6) and these limits, we then obtain

$$f_1 = 2\pi G\rho \int_{-b}^b (s-z) dz \int_0^{\sqrt{R^2-z^2}} [r^2+(s-z)^2]^{-\frac{3}{2}} r dr \quad (7)$$

After integration with respect to r, (7) becomes

$$\frac{f_1}{2\pi G\rho} = 2b - \int_{-b}^b [R^2+s^2-2sz]^{-\frac{1}{2}} (s-z) dz \quad (8)$$

The substitution

$$u \equiv R^2 + s^2 - 2sz \quad (9)$$

then results in

$$\frac{f_1}{2\pi G\rho} = 2b - (2s^2)^{-1} [(R^2-s^2)(u_2^{\frac{1}{2}}-u_1^{\frac{1}{2}}) - \frac{1}{3}(u_2^{\frac{3}{2}}-u_1^{\frac{3}{2}})], \quad (10)$$

where

$$u_1 \equiv R^2+s^2+2bs \quad (10.1)$$

$$u_2 \equiv R^2+s^2-2bs \quad (10.2)$$

Eq. (10) agrees with the result of a calculation by W. E. Lee (unpublished).

To evaluate f_2 , note that in (5) the limits become ϕ from 0 to 2π as before, r from a to $\sqrt{R^2-z^2}$, and z from b to $\ell = \sqrt{R^2-a^2} - b$.

Then

$$\frac{f_2}{2\pi G\rho} = \int_b^{\ell} (s-z) dz \int_a^{\sqrt{R^2-z^2}} [r^2+(s-z)^2]^{-\frac{3}{2}} r dr \quad (11)$$

The substitution

$$v \equiv r^2+(s-z)^2 \quad (12)$$

leads to

$$\int_0^{\sqrt{R^2-z^2}} [r^2+(s-z)^2]^{-\frac{3}{2}} r dr = [a^2+(s-z)^2]^{-\frac{1}{2}} - [R^2+s^2-2sz]^{-\frac{1}{2}}, \quad (13)$$

so that

$$\frac{f_2}{2\pi G\rho} = \int_b^{\ell} (s-z) dz \left\{ [a^2+(s-z)^2]^{-\frac{1}{2}} - [R^2+s^2-2sz]^{-\frac{1}{2}} \right\} \quad (14)$$

It is convenient to leave f_2 in this form until we find f_3 .

To find f_3 , use as limits in (5): ϕ from 0 to 2π , r from a to $\sqrt{R^2-z^2}$, and z from $-\ell$ to $-b$. Then

$$\frac{f_3}{2\pi G\rho} = \int_{-\ell}^{-b} (s-z) dz \int_a^{\sqrt{R^2-z^2}} [r^2+(s-z)^2]^{-\frac{3}{2}} r dr \quad (15)$$

Application of (13) to (15), with replacing of z by z' , then shows that

$$\frac{f_3}{2\pi G\rho} = \int_{-\ell}^{-b} (s-z') dz' \left\{ [a^2+(s-z')^2]^{-\frac{1}{2}} - [R^2+s^2-2sz']^{-\frac{1}{2}} \right\} \quad (16)$$

On putting $z' = -z$, this becomes

$$\frac{f_3}{2\pi G\rho} = \int_b^{\ell} (s+z) dz \left\{ [a^2+(s+z)^2]^{-\frac{1}{2}} - [R^2+s^2+2sz]^{-\frac{1}{2}} \right\} \quad (17)$$

Addition of (14) and (17) now gives

$$\frac{f_2+f_3}{2\pi G\rho} = \int_b^{\ell} \left[\frac{s-z}{\sqrt{a^2+(s-z)^2}} + \frac{s+z}{\sqrt{a^2+(s+z)^2}} - \frac{s-z}{\sqrt{R^2+s^2-2sz}} - \frac{s+z}{\sqrt{R^2+s^2+2sz}} \right] dz \quad (18)$$

To combine (18) with (8), first rewrite the latter by decomposing the integral into one from 0 to b and one from -b to 0. In the latter rewrite the dummy variable z as z' and then put z' = -z. Eq. (8) then becomes

$$\frac{f_1}{2\pi G\rho} = 2b \int_0^b \frac{(s-z)dz}{\sqrt{R^2+s^2-2sz}} + \int_0^b \frac{(s+z)dz}{\sqrt{R^2+s^2+2sz}} \quad (19)$$

The sum of (18) and (19) takes the form

$$\begin{aligned} \frac{f_1+f_2+f_3}{2\pi G\rho} = 2b + \int_b^{\ell} \left[\frac{s-z}{\sqrt{a^2+(s-z)^2}} + \frac{s+z}{\sqrt{a^2+(s+z)^2}} \right] dz \\ - \int_0^{\ell} \left[\frac{s-z}{\sqrt{R^2+s^2-2sz}} + \frac{s+z}{\sqrt{R^2+s^2+2sz}} \right] dz \end{aligned} \quad (20)$$

To evaluate these integrals, make the substitutions

$$u_1 \equiv a^2+(s-z)^2 \quad (21.1)$$

$$u_2 \equiv a^2+(s+z)^2 \quad (21.2)$$

$$v_1 \equiv R^2+s^2-2sz \quad (21.3)$$

$$v_2 \equiv R^2+s^2+2sz \quad (21.4)$$

With use of (3), the result is then

$$\begin{aligned}
 \frac{f}{2\pi G\rho} = & 2b + \sqrt{a^2 + (s-b)^2} - \sqrt{a^2 + (s+b)^2} \\
 & - \frac{R^2 + s^2}{2s^2} \left[\sqrt{a^2 + (\ell-s)^2} - \sqrt{a^2 + (\ell+s)^2} \right] \\
 & - \frac{1}{6s^2} \left\{ [a^2 + (\ell+s)^2]^{\frac{3}{2}} - [a^2 + (\ell-s)^2]^{\frac{3}{2}} \right\} \quad (22)
 \end{aligned}$$

As a check on (22), note that for $a = b = 0$, in which case $\ell = R$, this reduces to Eq. (1), as it should.

5. Effects of the Perpendicular Tunnels on f_σ

Figure 2 shows a tunnel T_1 perpendicular to the tunnel σ , the axis of σ being along GP, with P a field point on its axis, at distance s from O, the center of the sphere. The perpendicular tunnel T_1 consists of the empty cylinders ABCD and A'B'C'D' and of the empty spherical segments CDE and C'D'E'. There is no need to draw the other perpendicular tunnel T_2 .

The axial field correction at P, produced by the perpendicular tunnels T_1 and T_2 , is then four times the sum of the axial fields produced at P by the cylinder ABCD and the spherical segment CDE, both of density $-\rho$.

A straightforward attempt to evaluate the field produced at P, either by the cylinder ABCD or by the spherical segment CDE, would involve the calculation of a triple integral over three cylindrical coordinates. One finds at once that the integration over the angular coordinate yields an elliptic integral, of large modulus, which would then have to be integrated twice more. Such a straightforward attack is therefore to be shunned.

6. The Field of a Disk

To avoid the above difficulty, I shall regard both the cylinder ABCD and the spherical segment CED in Figure 2 as composed of elementary disks. The procedure will then be to calculate the potential produced by each disk at P, take its directional derivative along the axis of the σ tunnel to find the field produced by each disk, and then integrate over all the disks to find the field corrections produced by ABCD and CED.

Since the center of each disk is farther from the field point P than from any source point, the potential at P can be expressed by means of a converging series of zonal harmonics, similar to that for an axially symmetric planet. In ABCD the disks all have the same radius a, but in CED the radius varies.

Let dz be the thickness of such a disk, r_d its radius, r_p the distance from its center O_d to the field point P in Figure 2, and θ the angle from O_dE to $r_p \equiv \overline{O_dP}$. If

$$\mu_d = -G\pi r_d^2 \rho dz, \quad (23)$$

the zonal expansion for the potential V_d produced by the disk at P takes the form

$$V_d = -\frac{\mu_d}{r_p} \left[1 - \sum_{k=1}^{\infty} \left(\frac{r_d}{r_p} \right)^{2k} J_{2k} P_{2k}(\cos \theta) \right] \quad (24)$$

The odd zonals drop out, because of the symmetry with respect to the plane of the disk. If the mass of the disk is

$$M_d = -\pi r_d^2 \rho dz, \quad (25)$$

the J's are given by

$$M_d J_{2k} = - \int (r/r_d)^{2k} P_{2k}(\cos \theta') \sigma dS, \quad (26)$$

integrated over the disk. Here $\theta' = \frac{\pi}{2}$, $\sigma = -\rho dz$, and $dS = r^2 dr d\phi$.

The result is

$$J_{2k} = - \frac{P_{2k}(0)}{k+1}, \quad (26.1)$$

where

$$P_{2k}(0) = \frac{(-1)^k (2k)!}{2^{2k} (k!)^2} \quad (26.2)$$

From (26.1) and (26.2), the first few J_{2k} 's are $J_2 = 1/4$, $J_4 = 1/8$, $J_6 = 5/64$, and $J_8 = -7/128$.

With $00_d = z$, we now have in (24)

$$r_p^2 = z^2 + s^2 \quad (27.1)$$

$$\cos \theta = -z/r_p, \quad (27.2)$$

so that

$$V_d = - \frac{\mu_d}{r_p} + \mu_d \sum_{k=1}^{\infty} \frac{r_d^{2k}}{r_p^{2k+1}} J_{2k} P_{2k}(z/r_p), \quad (28)$$

since $P_{2k}(-\xi) = P_{2k}(\xi)$. The attractive field produced by the disk along the σ tunnel is given by

$$f_d = \frac{\partial V_d}{\partial s} = \frac{\mu_d s}{r_p^3} + \mu_d \sum_{k=1}^{\infty} J_{2k} r_d^{2k} \frac{\partial}{\partial s} [\tilde{r}_p^{2k-1} P_{2k}(z/r_p)] \quad (29)$$

or

$$f_d = \frac{\mu_d s}{r_p^3} - \frac{\mu_d s}{r_p^3} \sum_{k=1}^{\infty} J_{2k} \left(\frac{r_d}{r_p} \right)^{2k} \left[(2k+1) P_{2k} \left(\frac{z}{r_p} \right) + \frac{z}{r_p} P'_{2k} \left(\frac{z}{r_p} \right) \right] \quad (30)$$

7. Corrections from the Empty Cylinders

The attractive field f_{ABCD} produced by the cylinder ABCD is then given by placing $r_d = a$ and $\mu_d = -G\pi a^2 \rho dz$ in (30) and integrating it from $z = b$ to $z = R_1 = \sqrt{R^2 - a^2}$. On using (27.1) and placing

$$\lambda \equiv z/r_p = z(z^2 + s^2)^{-\frac{1}{2}} \quad (31)$$

we thus find

$$f_{ABCD} = -G\pi a^2 \rho s \int_b^{R_1} (z^2 + s^2)^{-\frac{3}{2}} dz + G\pi a^2 \rho s \sum_{k=1}^{\infty} J_{2k} a^{2k} \int_b^{R_1} (z^2 + s^2)^{-k-\frac{3}{2}} Q_k(\lambda) dz, \quad (32.1)$$

where

$$Q_k(\lambda) \equiv (2k+1) P_{2k}(\lambda) + \lambda P'_{2k}(\lambda) \quad (32.2)$$

With use of the identities

$$P_{2k}(\lambda) \equiv \frac{1}{4k+1} [P'_{2k+1}(\lambda) - P'_{2k-1}(\lambda)] \quad (33)$$

and

$$\lambda P_{2k}(\lambda) = \frac{2k+1}{4k+1} P_{2k+1}(\lambda) + \frac{2k}{4k+1} P_{2k-1}(\lambda), \quad (34)$$

we then find

$$Q_k(\lambda) \equiv P'_{2k+1}(\lambda) \quad (35)$$

On placing $z = s \tan \alpha$ in (32.1), we find

$$(z^2+s^2)^{-\frac{3}{2}} dz = s^{-2} \cos \alpha d\alpha = s^{-2} d \sin \alpha = s^{-2} d\lambda \quad (36)$$

and

$$(z^2+s^2)^{-k-\frac{3}{2}} dz = s^{-2k-2} (1-\lambda^2)^k d\lambda \quad (37)$$

Insertion of (35) and (37) into (32.1) then yields

$$\frac{(f_{ABCD})_s}{G\pi a^2 \rho} = \lambda_1^{-\lambda_2} + \sum_{k=1}^{\infty} J_{2k} \left(\frac{a}{s} \right)^{2k} \int_{\lambda_1}^{\lambda_2} (1-\lambda^2)^k P'_{2k+1}(\lambda) d\lambda, \quad (38)$$

where

$$\lambda_1 \equiv b(b^2+s^2)^{-\frac{1}{2}} \quad (38.1)$$

$$\lambda_2 \equiv R_1(R_1^2+s^2)^{-\frac{1}{2}} \quad (38.2)$$

Before we proceed further, it is interesting to check (38). If we put $b = 0$ and $R_1 = \infty$, the field f_{ABCD} should be half that produced at a distance s from its axis by an infinite cylinder of radius a and density $-\rho$. In such a case $\lambda_1 = 0$ and $\lambda_2 = 1$. The integrals in (38) then take the form

$$\begin{aligned}
\int_0^1 (1-\lambda^2)^k P'_{2k+1}(\lambda) d\lambda &= \frac{1}{2} \int_{-1}^1 (1-\lambda^2)^k P'_{2k+1}(\lambda) d\lambda \\
&= \frac{1}{2} (1-\lambda^2)^k P_{2k+1}(\lambda) \Big|_{\lambda=-1}^1 + k \int_{-1}^1 \lambda (1-\lambda^2)^{k-1} P_{2k+1}(\lambda) d\lambda,
\end{aligned} \tag{39}$$

on integration by parts. The first term vanishes and so does the second, since $\lambda(1-\lambda^2)^{k-1}$ is a polynomial in λ of degree $2k-1$. Its expansion in Legendre polynomials does not include $P_{2k+1}(\lambda)$, so that orthogonality proves the vanishing.

Thus (38) reduces to

$$2f_{ABCD} = - \frac{2G\pi a^2 \rho}{s} \tag{40}$$

Suppose one places a pill box of radius s around an infinite cylinder of radius a and density $-\rho$ and applies Gauss's theorem to it. The latter states that the attractive flux (inward) through it is equal to the product of $4\pi G$ and the mass in the pill box. The result is (40). Thus Eq. (38) survives this check.

The correction from the four empty cylinders is thus

$$4f_{ABCD} = \frac{4G\pi a^2 \rho}{s} \left[\lambda_1 - \lambda_2 + \sum_{k=1}^{\infty} J_{2k} \left(\frac{a}{s} \right)^{2k} I_k \right], \tag{41}$$

where λ_1 and λ_2 are given by (38.1) and (38.2), the J_{2k} by (26.1), and

$$I_k \equiv \int_{\lambda_1}^{\lambda_2} (1-\lambda^2)^k P'_{2k+1}(\lambda) d\lambda \tag{42}$$

It is simple to work out the I_k . We find

$$\begin{aligned}
I_1 &= \frac{3}{2} \int_{\lambda_1}^{\lambda_2} (1-\lambda^2)(5\lambda^2-1)d\lambda \\
&= \frac{3}{2} [\lambda_1 - \lambda_2 + 2(\lambda_2 - \lambda_1)^3 - (\lambda_2 - \lambda_1)^5] \quad (43.1)
\end{aligned}$$

$$\begin{aligned}
I_2 &= \frac{1}{8} \int_{\lambda_1}^{\lambda_2} (1-\lambda^2)(315\lambda^4 - 70\lambda^3 + 15\lambda)d\lambda \\
&= \frac{1}{8} [35(\lambda_2 - \lambda_1)^9 - 120(\lambda_2 - \lambda_1)^7 + 150(\lambda_2 - \lambda_1)^5 - 80(\lambda_2 - \lambda_1)^3 + 15(\lambda_2 - \lambda_1)] \quad (43.2)
\end{aligned}$$

$$\begin{aligned}
I_3 &= \frac{1}{16} \int_{\lambda_1}^{\lambda_2} (1-\lambda^2)^3(3003\lambda^6 - 3465\lambda^4 + 945\lambda^2 - 35)d\lambda \\
&= \frac{1}{16} [-231(\lambda_2 - \lambda_1)^{13} + 1134(\lambda_2 - \lambda_1)^{11} - 2261(\lambda_2 - \lambda_1)^9 + 2324(\lambda_2 - \lambda_1)^7 \\
&\quad - 1281(\lambda_2 - \lambda_1)^5 + 350(\lambda_2 - \lambda_1)^3 - 35(\lambda_2 - \lambda_1)] \quad (43.3)
\end{aligned}$$

By means of an integration by parts, like that of (39), it is easy to show that $|I_k| < 2k+2$. Also, by (26.1) and (26.2)

$$|J_{2k}| = (k+1)^{-1} \frac{1 \cdot 3 \cdot 5 \dots (2k-1)}{2 \cdot 4 \cdot 6 \dots 2k}, \quad (43.4)$$

so that

$$|J_{2k} I_k| < \frac{3 \cdot 5 \dots 2k-1}{4 \cdot 6 \dots 2k} < \frac{35}{64} \text{ if } k \geq 4 \quad (43.5)$$

The ratio of the k'th term in (41) to the main term $4\pi G \rho s/3$ is thus less than $\frac{105}{64} \left(\frac{a}{s}\right)^{10} < 2(10^{-10})$ for $a = 0.5$ cm and $s = 5$ cm. It

thus appears reasonable to stop at $k = 3$.

8. Corrections from the Empty Spherical Segments

The corrective field f_{CED} produced by a spherical segment is to be obtained by considering a disk in it of variable radius $r_d = \xi$, thickness dz , and

$$\mu_d = -G\pi\xi^2\rho dz \quad (44)$$

We make these substitutions in (30) and integrate the latter over z from $z = R_1$ to $z = R$, where R is the radius of the sphere and $R_1 = \sqrt{R^2 - a^2}$. The result is then

$$f_{CED} = \int_{R_1}^R f_d dz \quad (45)$$

Here, however

$$\xi^2 = R^2 - z^2, \quad (46)$$

so that the integration is more difficult. We have for the attractive field produced by the disk on the test object

$$f_d = -\frac{G\pi\rho(R^2 - z^2)sdz}{r_p^3} + G\pi\rho s(R^2 - z^2)dz \sum_{k=1}^{\infty} J_{2k} \frac{(R^2 - z^2)^k}{r_p^{2k+3}} Q_k(\lambda) \quad (47)$$

This follows from (30), (44), (46), and (32.2), where $Q_k(\lambda)$ is given by (35) and $\lambda \equiv z/r_p$. The J_{2k} are still given by (26.1).

Then

$$\begin{aligned}
4f_{\text{CED}} &= -4G\pi\rho s \int_{R_1}^R \frac{R^2 - z^2}{r_p^3} dz \\
&\quad + 4G\pi\rho s \sum_{k=1}^{\infty} J_{2k} \int_{R_1}^R \frac{(R^2 - z^2)^{k+1}}{r_p^{2k+3}} Q_k(\lambda) dz
\end{aligned} \tag{48}$$

From (27.1) and (46), we now have

$$r_p^2 = R^2 + s^2 - \xi^2 = h_0^2 - \xi^2 \tag{49.1}$$

$$h_0^2 \equiv R^2 + s^2 \tag{49.2}$$

Consider the first integral in (48). If we change to ξ as independent variable, it becomes

$$\int_{R_1}^R \frac{R^2 - z^2}{r_p^3} dz = \int_0^a \xi^3 (R^2 - \xi^2)^{-\frac{1}{2}} (h_0^2 - \xi^2)^{-\frac{3}{2}} d\xi \tag{50}$$

$$= \frac{1}{Rh_0^3} \int_0^a \xi^3 \left(1 + \frac{1}{2} \frac{\xi^2}{R^2} + \dots\right) \left(1 + \frac{3}{2} \frac{\xi^2}{h_0^2} + \dots\right) d\xi \tag{50.1}$$

$$= \frac{1}{Rh_0^3} \left[\frac{a^4}{4} + \frac{1}{6} \left(\frac{1}{2R^2} + \frac{3}{2h_0^2} \right) a^6 + \dots \right] \tag{50.2}$$

Next consider the integral multiplying J_2 . It is

$$N_1 = \int_{R_1}^R \frac{(R^2 - z^2)^2}{r_p^5} Q_1(\lambda) dz = \int_{R_1}^R \frac{(R^2 - z^2)^2}{r_p^5} \left(\frac{15}{2} \frac{z^2}{r_p^2} - \frac{3}{2} \right) dz \quad (51)$$

$$= \int_0^a \frac{\xi^5 d\xi}{\sqrt{R^2 - \xi^2} (h_0^2 - \xi^2)^{5/2}} \left[\frac{15}{2} \frac{(R^2 - \xi^2)}{h_0^2 - \xi^2} - \frac{3}{2} \right] \quad (51.1)$$

To obtain the term in a^6 , we may drop ξ in this integral everywhere except in the main ξ^5 factor. Then

$$N_1 \approx \frac{1}{Rh_0^5} \left(\frac{15}{2} \frac{R^2}{h_0^2} - \frac{3}{2} \right) \frac{a^6}{6} \quad (51.2)$$

$$\approx \frac{a^6}{4} \left[\frac{5R}{(R^2 + s^2)^{7/2}} - \frac{1}{R(R^2 + s^2)^{5/2}} \right] < \left(\frac{a}{R} \right)^6 \quad (51.3)$$

Here $R \approx 10$ cm, so that if the tunnel diameter is less than 1 cm, $\left(\frac{a}{R}\right)^6 < \frac{1}{64} 10^{-6}$. Also, since $J_2 = \frac{1}{4}$, the factor $4\pi G \rho s J_2$ is $3/4$ of the main field $4\pi G \rho s / 3$ on the test object. It appears that all the terms containing the J_{2k} 's can be neglected. Also, in (50.2), the term in a^6 is less than $\frac{1}{3} (a/R)^6$, so that we can neglect it also.

Thus, closely enough

$$4f_{CED} = - \frac{G\pi\rho a^4}{R(R^2 + s^2)^{3/2}} s \quad (52)$$

9. The Total Gravitational Field from the Sphere

On adding (22), (41), and (52), we find the total gravitational field produced on a test object by the sphere containing tunnels.

It is

$$\begin{aligned}
f_{\sigma} = & 2\pi G\rho \left[2b + \sqrt{a^2 + (s-b)^2} - \sqrt{a^2 + (s+b)^2} \right. \\
& - \frac{R^2 + s^2}{2s^2} \left\{ \sqrt{a^2 + (\ell-s)^2} - \sqrt{a^2 + (\ell+s)^2} \right\} \\
& - \frac{1}{6s^2} \left\{ [a^2 + (\ell+s)^2]^{3/2} - [a^2 + (\ell-s)^2]^{3/2} \right\} \\
& + \frac{4G\pi a^2 \rho}{s} \left[\lambda_1^{-\lambda_2} + \sum_{k=1}^{\infty} J_{2k} \left(\frac{a}{s} \right)^{2k} I_k \right] \\
& - \frac{G\pi \rho a^4}{R(R^2 + s^2)^{3/2}} s + \pi G\rho s^0 \left\{ \left(\frac{a}{R} \right)^6 \right\} \tag{53}
\end{aligned}$$

Here the first three lines represent the field that would be produced on the axis of a single tunnel in the sphere. The fourth line gives a diminution of the attractive field, produced by the four empty cylinders in the other two tunnels. The last line gives the diminution of the attractive field that is produced by the four empty spherical segments in the other two tunnels. It is assumed that each tunnel has a flat end, at a distance b from the center of the sphere.

If the tunnels are drilled all the way through, we can proceed as follows. First put $b = 0$ in Eq. (53). The dodecahedral intersection is then counted three times as a cavity. To correct this error, we need to add to (53) twice the field produced by the solid dodecahedron, of density $+\rho$. If we now expand the potential of this dodecahedron in spherical harmonics, only the zonal harmonics enter on the axis of a tunnel, since the tesserals and sectorials contain a term $\sin^m \theta$, ($m \geq 1$) and $\sin \theta$ vanishes on the axis.

The dipole term vanishes, since the center of mass of the dodecahedron is at the center of the sphere. By the construction we see also that the principal axes are along the tunnels and by symmetry the principal moments of inertia are all equal. This fact makes the quadrupole moment vanish. Also the dodecahedron is symmetric with respect to the plane $x_{\sigma} = 0$, so that the zonal part of the third harmonic (or octupole moment) vanishes. The first non-vanishing term after the monopole moment is thus the zonal fourth harmonic (16-pole moment), producing a field that goes like s^{-6} .

We may express the volume of the dodecahedron as

$$\Omega = k \frac{4\pi}{3} a^3, \quad (53.1)$$

where k is a universal constant, on dimensional grounds. We can thus determine k experimentally, by making a model of the dodecahedron and determining its volume. In the example in Section 3, the volume was 62 cm^3 and $4\pi a^3/3$ was 56 cm^3 . Thus, approximately, $k = 62/56 = 1.094$.

The mass of the dodecahedron is then

$$M_d = \Omega \rho \quad (53.2)$$

By the theory of potential, the zonal part of the potential, V_d , at a field point outside it is then

$$V_d = - \frac{\mu}{r} \left[1 - \frac{C_4}{r^4} P_4\left(\frac{z}{r}\right) + \dots \right] \quad (53.3)$$

Here

$$\mu = GM_d = G\rho k \frac{4\pi a^3}{3} \quad (53.4)$$

and

$$r = (x^2 + y^2 + z^2)^{1/2}, \quad (53.5)$$

where x, y, z are the coordinates of the field point. Also P_4 is the Legendre polynomial of degree 4 and

$$M_d C_4 = - \int r^4 \rho P_4\left(\frac{z}{r}\right) d\tau, \quad (53.6)$$

integrated over the dodecahedron.

To find the attractive field f_{dod} along a tunnel, we differentiate V_d with respect to z and put $z = r = s$ in the result, which is

$$f_{\text{dod}} = \frac{\mu}{s^2} \left(1 - 5 \frac{C_4}{s^4} + \dots\right) \quad (53.7)$$

To put an upper limit on $|C_4|$, we may use (53.6). Since $|P_4(\frac{z}{r})| \leq 1$ and since the dodecahedron is contained within its circumscribed sphere of radius

$$R = a(3/2)^{1/2}, \quad (53.8)$$

we obtain

$$M_d |C_4| < 4\pi\rho \int_0^R r^6 dr, \quad (53.9)$$

so that

$$\mu |C_4| < \frac{4\pi G}{7} \rho R^7 \quad (53.10)$$

With use of (53.4), (53.7), (53.8), and (53.10), we find that the fourth harmonic part of f_{dod} is bounded by

$$\frac{5\mu|C_4|}{s^6} < \frac{135\sqrt{1.5}}{14} \pi G\rho \frac{a^7}{s^6} \quad (53.11)$$

The main field is $4\pi G\rho s/3$. Since the dodecahedron has to be counted twice in this calculation, the fractional correction produced by the fourth harmonic is bounded by

$$\frac{270\sqrt{1.5}}{14} \pi \frac{G\rho a^7}{s^6} \frac{3}{4\pi G\rho s} = \frac{405\sqrt{1.5}}{28} \left(\frac{a}{s}\right)^7 \approx (17.7) \left(\frac{a}{s}\right)^7 \quad (53.12)$$

For $a = 0.5$ cm and $s = 5$ cm, this would amount to 2 parts in a million. We may thus safely neglect the fourth harmonic, since the above upper limit on $|C_4|$ is probably a large overestimate.

Thus

$$f_{\text{dod}} = k \frac{G4\pi a^3 \rho}{3s^2}, \quad (53.13)$$

to sufficient accuracy. Here $k \approx 1.094$, but may be determined more accurately by a better experiment.

To summarize: when the tunnels are drilled all the way through, f_σ is given by (53), with $b = 0$, plus the correction

$$\delta f_\sigma(\text{intersection error}) = 2k \left(\frac{4\pi G a^3 \rho}{3s^2} \right) + \text{negligible terms} \quad (53.14)$$

The correction $f_{G\sigma}^T$ of Vinti (1970) is then

$$f_{G\sigma}^T = f_\sigma - \frac{4\pi}{3} G\rho s \quad (54)$$

10. Summary of the Notation

R = radius of the sphere

a = radius of a tunnel

b = distance of flat end of a tunnel from the center of the sphere

$$R_1 = \sqrt{R^2 - a^2}$$

$$l = R_1 - b$$

s = distance of a test object from the center of the sphere

$$\lambda_1 = b(b^2 + s^2)^{-1/2}$$

$$\lambda_2 = R_1(R_1^2 + s^2)^{-1/2}$$

$$J_{2k} = -P_{2k}(0)/(k+1)$$

$$P_{2k}(0) = \frac{(-1)^k (2k)!}{2^{2k} (k!)^2}$$

$$I_k = \int_{\lambda_1}^{\lambda_2} (1-\lambda^2)^k P_{2k+1}(\lambda) d\lambda, \text{ with examples for } I_1, I_2, I_3 \text{ in Eqs. (43)}$$

$P_n(x)$ = Legendre polynomial of x, of degree n

ρ = density of the sphere

G = gravitational constant

References:

Lee, W.E. 1969, Private communication

Vinti, J.P. 1970, "Analysis of an Experiment to Determine the Gravitational Constant in an Orbiting Space Laboratory", Measurement Systems Laboratory Report RE-72, 1970.

Wilk, L., 1970, Private Communication

Appendix : Vestigial Tunnels

This is an afterthought about both the present report and Vinti 1970.

Instead of drilling three perpendicular tunnels in the sphere, one might proceed as follows in achieving the balance of gravitational force against centrifugal force that has been described for measuring G.

Suppose we are given the completed sphere, accurately machined to be a good geometrical sphere. Since there will be some inhomogeneities, its center of mass will not quite coincide with its geometrical center. Determine the position of its center of mass, perhaps by means of physical pendulum experiments, and indicate this position with reference to some fiducial marks on the sphere.

Since the sphere will not be dynamically perfect, it will have unique principal axes. Determine these principal axes, perhaps by means of torsion pendulum experiments, and mark the six points at which they intersect the sphere. Also determine the three principal moments of inertia, viz. $A < B < C$. (The center of mass will have to be at the intersection of the principal axes.)

Instead of drilling three tunnels, simply attach six short thin hollow cylinders, each perhaps an inch long, on the outside of the sphere, at the exit points of the principal axes. These cylinders may be of some material much less dense than tungsten; they would contain the suspension systems.

Use the inertia reaction wheels, servomechanisms, and suspension systems, so that on rotation of the sphere, test objects in three of these "vestigial" tunnels will remain fixed (or almost so) on the axes. The servos will now not only have to prevent extraction but also to prevent collision of the test objects with the sphere. Since the "tunnels" are now much more accessible, however, it may be easier to design the necessary suspension systems.

The expression for the gravitational field f_g on a test particle is now much simpler. With origin at the center of mass and x, y, z taken along the principal axes, let s be the distance from the center of mass and θ and λ be the corresponding colatitude and longitude. Then

$$x = s \sin\theta \cos\lambda \quad (54.1)$$

$$y = s \sin\theta \sin\lambda \quad (54.2)$$

$$z = s \cos\theta \quad (54.3)$$

If M is the mass of the sphere and R its radius, the gravitational potential V outside the sphere is given by

$$V = -\frac{GM}{s} \left[1 - \sum_{n=1}^{\infty} \left(\frac{R}{s}\right)^n J_n P_n(\cos\theta) + \sum_{n=1}^{\infty} \left(\frac{R}{s}\right)^n P_n^m(\cos\theta) (C_{n,m} \cos m \lambda + S_{n,m} \sin m \lambda) \right] \quad (55)$$

Suppose we truncate this series at $n = 2$. With the origin at the center of mass, we have

$$J_1 = C_{1,1} = S_{1,1} = 0 \quad (56)$$

Since the axes are principal axes, we also have

$$C_{2,1} = S_{2,1} = S_{2,2} = 0 \quad (57)$$

We then obtain

$$V = -\frac{GM}{s} \left[1 - \frac{R^2}{s^2} J_2 \left(\frac{3}{2} \frac{z^2}{s^2} - \frac{1}{2} \right) + \frac{3R^2}{s^2} \sin^2 \theta C_{2,2} \cos 2\lambda + \dots \right] \quad (58)$$

Using

$$\sin^2 \theta \cos 2\lambda = \frac{x^2 - y^2}{s^2}, \quad (59)$$

we find

$$V = -\frac{GM}{s} - \frac{GMR^2 J_2}{2s^3} + \frac{3}{2} \frac{GMR^2 J_2 z^2}{s^5} - \frac{3GMR^2 C_{2,2}}{s^5} (x^2 - y^2) + \dots \quad (60)$$

In the x-tunnel the attractive field $f_x = \partial V / \partial x$ with $y = z = 0$; in the y tunnel $f_y = \partial V / \partial y$ with $z = x = 0$; in the z-tunnel $f_z = \partial V / \partial z$ with $x = y = 0$.

On carrying out this procedure and using

$$J_2 = \frac{C - \frac{1}{2}(A+B)}{MR^2} \quad (61)$$

$$C_{2,2} = \frac{B-A}{4MR^2}, \quad (62)$$

we find

$$f_x = \frac{GM}{x^2} + \frac{3}{2} \frac{G(B+C-2A)}{x^4} + \dots \quad (63.1)$$

$$f_y = \frac{GM}{y^2} + \frac{3}{2} \frac{G(C+A-2B)}{y^4} + \dots \quad (63.2)$$

$$f_z = \frac{GM}{z^2} + \frac{3}{2} \frac{G(A+B-2C)}{z^4} + \dots, \quad (63.3)$$

there being a cyclic symmetry, as expected.

For a perfectly homogeneous sphere, of course, $A = B = C$, so that the above quadrupole terms, which can be measured, would give some correction for inhomogeneities. However, a good-sized hole near the surface and near a tunnel would cause trouble. Eqs. (63) are about as far as one can go and still determine coefficients in (55) experimentally.

There should also be a small correction for the gravitational field of the thin external cylinders that constitute the vestigial tunnels.

This should be easy to calculate.

This method of "vestigial tunnels" would appear to be much simpler than the method first considered, both in construction of the equipment and in reduction of the data. It also preserves the advantage of Wilk's original proposal in those cases where it pays to sum over the tunnels, i.e., when the sphere is in free fall. This follows because summing over the three tunnels always eliminates most of the gravity-gradient effects. On summation over the tunnels, these depend, to a high accuracy, only on the Laplacian of the gravitational potential of matter external to the sphere, which always vanishes at the sphere's center of mass.

Finally, the field given by (63) is independent of thermal expansion and contraction of the sphere. This statement does not hold for Eq.(53) for the field inside an interior tunnel, unless one knows how much to correct the density ρ in that expression. Another way of saying the same thing is that, except for the weak dependence of the moment of inertia differences in (63) on the temperature, the fundamental unknown to be determined in this method of vestigial tunnels is G and not $G\rho$.

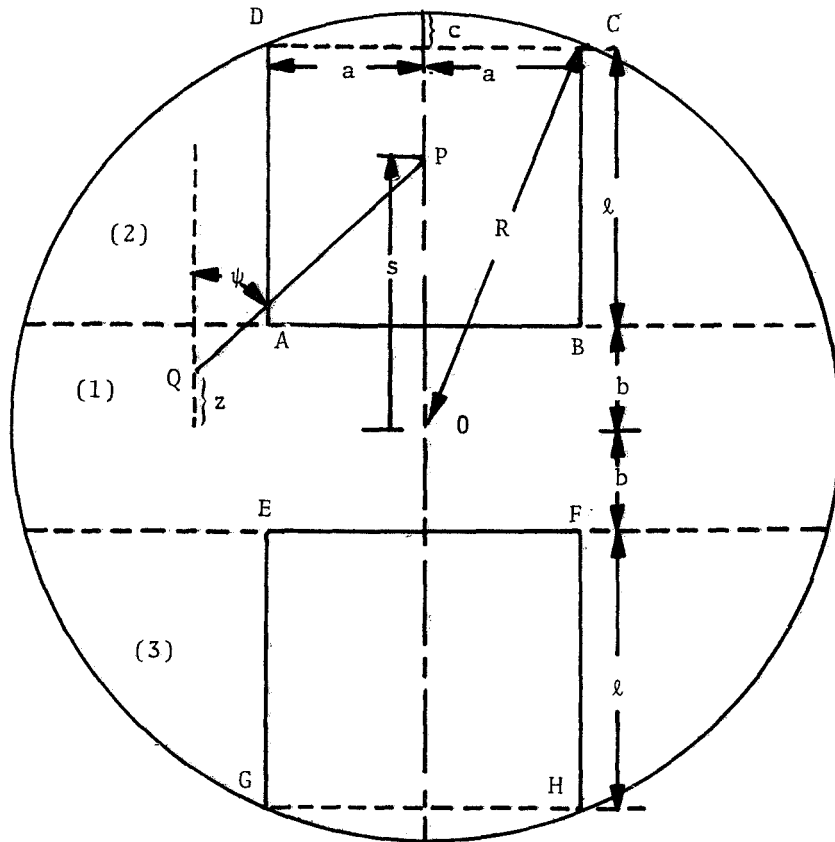


FIGURE 1.

$$R^2 = (\ell + b)^2 + a^2$$

$$c = R - \ell - b$$

$$OP = s$$

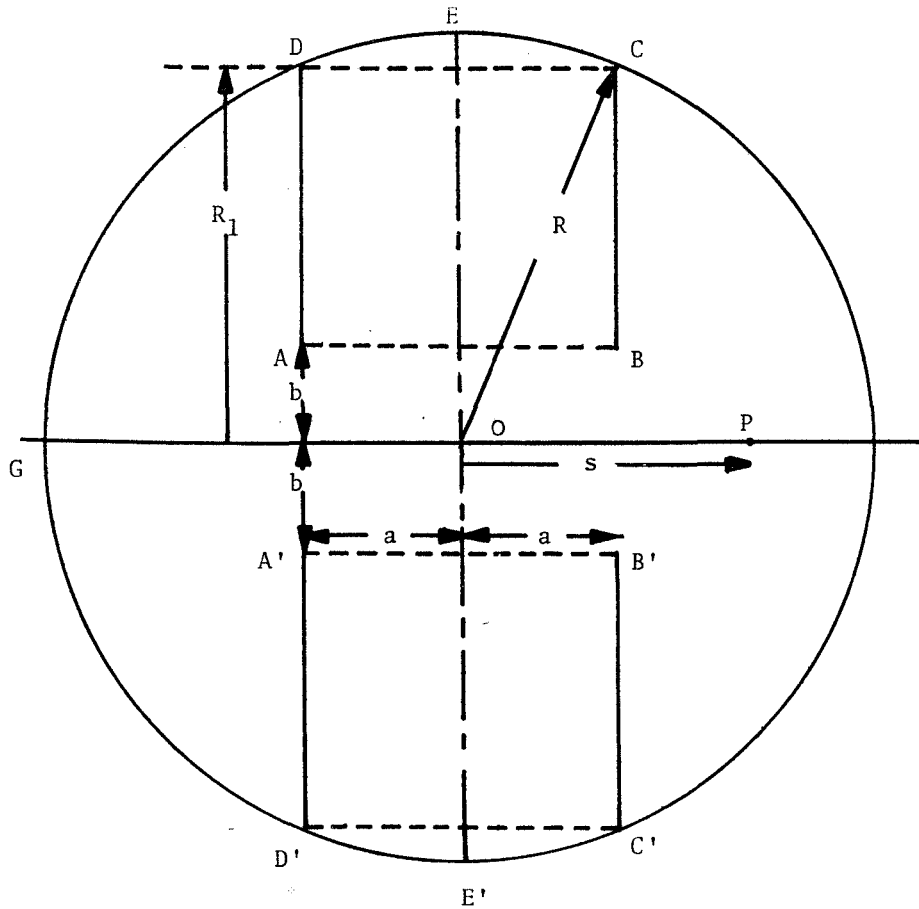


FIGURE 2. A Perpendicular Tunnel, T_1

Cylinders ABCD, A'B'C'D' empty

Spherical Segments CDE, C'D'E' empty

GP = axis of tunnel σ

$$R_1^2 = R^2 - a^2$$

APPENDIX G

A STUDY OF PRIMARY MASSES FOR
GRAVITATIONAL EXPERIMENTS

A STUDY OF PRIMARY MASSES
FOR GRAVITATIONAL EXPERIMENTS

Report to

Measurement Systems Laboratory
Massachusetts Institute of Technology

October 1970

72609

Arthur D. Little, Inc.

TABLE OF CONTENTS

	<u>Page</u>
Foreword	v
Summary	vii
I. INTRODUCTION	1
II. GRAVITATIONAL FIELD UNCERTAINTIES	3
A. BACKGROUND	3
B. PERTURBATION OF THE FIELD BY THE TUNNEL	4
C. PERTURBATION OF THE FIELD BY THE MASS OF THE SUPPORT SYSTEM	10
D. EFFECT OF SPHERICITY ERROR	12
E. EFFECT OF SPATIAL VARIATIONS OF DENSITY	15
F. EFFECTS OF TEMPERATURE	20
III. SUSPENSION SYSTEMS FOR SECONDARY TEST MASSES	25
A. BACKGROUND	25
B. DIAMAGNETIC SUPPORT SYSTEM	26
C. PERMANENT MAGNET--SUPERCONDUCTOR SUPPORT SYSTEM	29
D. DISTURBING FIELDS ORIGINATING IN THE SUSPENSION SYSTEM	30
IV. MATERIALS AND FABRICATION OF THE PRIMARY MASS	35
A. BACKGROUND	35
B. GENERAL CHARACTERISTICS OF CANDIDATE MATERIALS	35
C. MATERIALS PREPARATION TECHNIQUES	38
D. MACHINING AND HANDLING OF MATERIALS	40
E. DETERMINATION OF THE QUALITY OF FINISHED SPHERES	40
F. POTENTIAL SUPPLIERS AND PROCESSORS	41

	<u>Page</u>
V. EXPERIMENT COOLING CONSIDERATIONS	43
A. BACKGROUND	43
B. EXPERIMENT COOLING REQUIREMENTS	44
C. CRYOGENIC COOLING TECHNIQUES	45
REFERENCES	49

FOREWORD

A study of dense primary masses for use in gravitational experiments was performed by Arthur D. Little, Inc., Cambridge, Massachusetts, for the Measurement Systems Laboratory, Department of Aeronautics and Astronautics, Massachusetts Institute of Technology, under account number DSR 71390 in support of National Aeronautics and Space Administration, Manned Spacecraft Center, Contract NAS9-8328. The authors acknowledge the assistance and cooperation of Mr. Leonard S. Wilk, the Project Monitor, Dr. Bernard E. Blood, and Professor Winston R. Markey, Director, of the Measurement Systems Laboratory. The principal Arthur D. Little, Inc., personnel contributing to the program included: Dr. Alfred E. Wechsler, Technical Review of the project; Dr. Alfred G. Emslie and Peter F. Strong, gravitational field uncertainties; Dr. A. G. Emslie and Dr. Ivan Simon, suspension systems for secondary test masses; Philip C. Johnson and Dr. Alfred E. Wechsler, materials for the primary mass; and Arthur A. Fowle, experiment cooling considerations. The program at Arthur D. Little, Inc. was under the overall direction of David L. Richardson.

SUMMARY

PURPOSE AND SCOPE

The purpose of this program was to study and recommend the material and fabrication techniques for laboratory size primary masses whose physical and geometrical characteristics are very accurately known. In addition, studies were made of suspension systems for a test mass within the primary masses and techniques for cooling experiments to cryogenic temperatures.

The program included investigation of materials suitable for fabricating the primary masses by considering gravitational field uncertainties due to density, density inhomogeneity, temperature, strain, geometry, the presence of suspension systems and other sources of uncertainty. The suitability of elemental materials whose density is greater than 15 grams per cubic centimeter are discussed from the point of view of density, homogeneity, strength, fabricability, costs, availability, and the associated contribution to gravitational uncertainties. These materials are categorized according to their state of technology for fabrication, developments required to achieve a uniform mass, and the probability of success of achieving a primary mass of known uniform density. The general applicability of diamagnetic suspension systems to space gravity experiments is discussed. The applicability of a quadropole and sextipole system for suspension of a test mass in a tunnel within the primary mass of the proposed experiment are discussed. Experiment cooling requirements are estimated and both open-cycle and closed-cycle cryogenic refrigeration techniques are examined.

CONCLUSIONS AND RECOMMENDATIONS

1. The $\Delta G/G$ experiment to test the Brans-Dicke theory is impossible if carried out at 300°K but has a reasonable chance of success at liquid helium temperature. The measurement of the absolute value

of G to a much higher accuracy is feasible at either temperature. The proposed earth-orbital mission is to measure both G and to test the suitability of the apparatus for later experiments in highly elliptical solar orbit to measure $\Delta G/G$. To accomplish the latter missions in a meaningful way, it is essential that the earth-orbital experiments be performed at cryogenic temperatures.

2. The primary sphere should be rotated in such a way that the test particle always stays in the same longitudinal position in the tunnel within a very close tolerance. This is necessary because of considerable non-linearity in the longitudinal force due to the tunnel itself and to possible defects in fabrication of the sphere.
3. The support system must be capable of holding the test particle at all times within 1 micron of the tunnel axis. This is necessary because of significant variation of the longitudinal force with distance from the tunnel axis.
4. The primary sphere should be round to 10^{-5} cm.
5. Gross density variation across the sphere should be less than 1 part in 10^{-6} .
6. Fine scale density variations of 2% on a scale of 10^{-4} cm are tolerable.
7. The test mass should be made from a diamagnetic material and should be supported in a quadropole superconducting magnetic field which has superconducting current elements to avoid dissipation within the sphere.
8. Tungsten is the primary candidate for fabrication of the principal mass. Fabrication techniques have been demonstrated for achieving spheres of 99% theoretical density. Uranium is unsuitable because

of non-crystallographic phase changes below 43°K, it's non-cubic structure (causing an isotropy in its properties), and poor oxidation resistance. Tantalum will be a good candidate if its lower density is acceptable in the experiment.

9. An excessively long time may be required to achieve equilibrium cryogenic temperatures if the experiment is cooled radiatively.
10. Open-cycle helium refrigeration systems in zero gravity require an as yet unproven liquid-vapor separator to ensure the venting overboard of only gaseous phase helium.
11. A mechanical helium refrigeration system with long life and smaller size and weight than an open-cycle system is the best selection for both earth-orbital and solar-orbital gravitational experiments.

I. INTRODUCTION

Albert Einstein's general theory of relativity has been challenged by the Brans-Dicke scalar-interaction theory which predicts that the value for the Newtonian gravitational constant (G) will decrease under the influence of increasing gravitational potential.⁽¹⁾ This dependence on potential is predicted to be very weak. Within the earth's field the maximum effect,⁽²⁾ measured as $\Delta G/G$, for an initially remote observer approaching the earth is estimated to be approximately 7×10^{-11} . For a highly elliptical orbit of the sun (1.0 to 0.1 astronomical units), the maximum $\Delta G/G$ effect⁽²⁾ could be as large as 9×10^{-9} .

Recent advances in space exploration present opportunities for experiments for testing the Brans-Dicke theory. To make measurements of $\Delta G/G$ to the desired degree of accuracy will require instrumentation of unprecedented sensitivity. The Measurement Systems Laboratory of MIT has been investigating experiments for earth and solar orbit whose primary objective is the detection and measurement of non-Newtonian effects. A secondary objective of the proposed experiments is to provide a more accurate measure of G than is now available. One experiment configuration consists of a dense homogeneous sphere with a diametral tunnel. An unrestrained test mass is placed in the tunnel and caused to orbit about the center of the sphere. The rotation of the sphere is controlled so that the test mass does not touch the sides of the tunnel. In the absence of disturbing forces the test mass will orbit in an ellipse whose center is at the center of the sphere and hence the rotational rate of the sphere will be independent of the parameters of the ellipse, the radius of the sphere, and the size of the test mass. The proposed experiment relies on the measurement of gravitational forces associated with a laboratory-sized primary mass whose physical and geometrical characteristics must be accurately known.

This report summarizes analyses of gravitational field uncertainties in the primary mass, material and fabrication techniques, suspension systems for test masses, and cryogenic refrigeration techniques for cooling the proposed experiment.

II. GRAVITATIONAL FIELD UNCERTAINTIES

A. BACKGROUND

In analyzing the errors in the proposed G-experiment we have to distinguish between two quite different objectives for which the experiment is being designed. The first objective is the measurement of the absolute value of G to a much higher accuracy than the figure of 1 part in 300 that has been achieved up to now in earth-based experiments. This part of the experiment, which we will refer to as the G-experiment, is to be performed in earth orbit and the goal is an accuracy of 1 part in 10^5 . It is therefore required that the gravitational field of the primary sphere be known to an accuracy of 10^{-6} . This imposes stringent requirements on the geometrical accuracy of the sphere and on the uniformity and stability of its density.

The second part of the experiment, which we will refer to as the ΔG experiment, is to test the Brans-Dicke theory which predicts that G is not a constant but depends on the gravitational potential at the measurement location. The test of the theory therefore requires detection of very small changes in G, of the order of 1 part in 10^{11} , in an eccentric earth orbit or preferably in an eccentric solar orbit. For this purpose, therefore, the parameters that affect the measured value of G do not need to be known to high accuracy but must be stable to 1 part in 10^{11} for the duration of the experiment, which may be about a year.

We will consider the perturbation of the field by each of the following causes:

1. The tunnel
2. The support system
3. Sphericity error
4. Large-scale density gradient

5. Small-scale density variations
6. Secular temperature variation
7. Temperature gradient
8. Dissipation in the support system

B. PERTURBATION OF THE FIELD BY THE TUNNEL

1. Field on the Axis

The field on the axis of the tunnel is the undisturbed field due to the complete sphere less that due to the mass removed from the tunnel. The field of the complete sphere is

$$f_z = -\frac{4\pi G\rho}{3} z \quad (1)$$

where G is the gravitational constant, ρ is the density of the sphere, z is a cylindrical coordinate directed along the axis of the tunnel, and f_z is the force per unit mass.

We consider the mass removed from the tunnel to be approximately a right circular cylinder of length $2R$, where R is the radius of the sphere. The potential of an elementary disk of the cylinder of thickness dz' at a point distant z' from the center of the disk is

$$dV = -2\pi G\rho dz' (\sqrt{z'^2 + a^2} - z') \quad (2)$$

where a is radius of the tunnel. The potential of the whole cylinder at the point z is therefore

$$V = -2\pi G\rho \left\{ \int_0^{R-z} dz' (\sqrt{z'^2 + a^2} - z') + \int_0^{R+z} dz' (\sqrt{z'^2 + a^2} - z') \right\} \quad (3)$$

The field of the cylinder is therefore

$$\begin{aligned} \Delta f_z &= - \frac{\partial V}{\partial z} = - 2\pi G\rho \left[\left\{ \sqrt{(R-z)^2 + a^2} - (R-z) \right\} - \left\{ \sqrt{(R+z)^2 + a^2} - (R+z) \right\} \right] \\ &= - 2\pi G\rho \left[2z + \sqrt{(R-z)^2 + a^2} - \sqrt{(R+z)^2 + a^2} \right] \end{aligned} \quad (4)$$

The resultant field on the axis of the tunnel is the difference of fields (1) and (4):

$$f_z(0,z) = - 2\pi G\rho \left[\sqrt{(R+z)^2 + a^2} - \sqrt{(R-z)^2 + a^2} - \frac{4}{3} z \right] \quad (5)$$

The ratio $\Delta f_z / f_z$ of Equations (4) and (1) gives the relative magnitude of the disturbance in the field due to the tunnel. This ratio is plotted in Figure 1 as a function of z for various values of the tunnel radius a . It is seen that the disturbance reaches a value of about 7% at the end of the tunnel for a 1-cm diameter tunnel.

The departure of the field from the simple linear relation of Eq (1) means that the test particle in the tunnel does not describe an elliptical orbit as in the case of the linear force. Indeed the orbit is no longer a closed curve and the period is no longer isochronous. These uncertainties are minimized if, by suitable rotation of the sphere, the test particle is made to describe a circular orbit of very accurately controlled radius. We will assume henceforth that this mode of operation will be used. The question then is, with what accuracy must the orbital radius of the test particle be measured?

Now G is determined from measurements of the angular velocity ω of the test particle and its orbital radius z by means of the formula

$$\omega^2 = - \frac{f_z}{z} \quad (6)$$

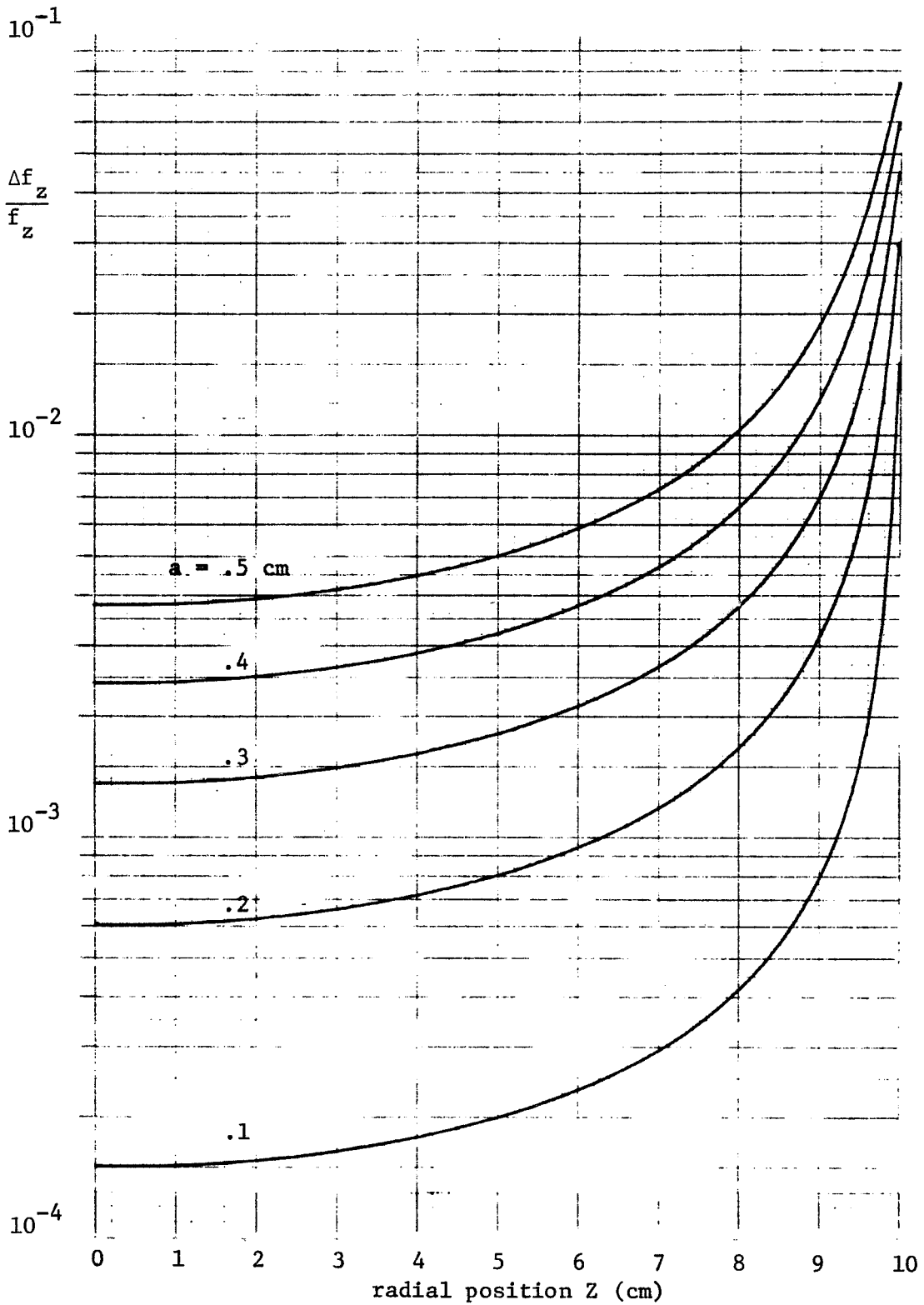


FIGURE 1. DISTURBANCE OF THE FIELD
DUE TO THE TUNNEL

where f_z , in general, is of the form

$$f_z = - G\rho[kz - F(z)] \quad (7)$$

and $F(z)$ is a small nonlinear term. Therefore (6) becomes

$$\omega^2 = G\rho \left[k - \frac{F(z)}{z} \right] \quad (8)$$

The error in G due to an uncertainty Δz in the longitudinal position of the test particle is therefore

$$\frac{\Delta G}{G} = \frac{\frac{\partial}{\partial z} \left\{ \frac{F(z)}{z} \right\} \Delta z}{k - \frac{F(z)}{z}} \approx \frac{1}{k} \frac{\partial}{\partial z} \left\{ \frac{F(z)}{z} \right\} \Delta z \quad (9)$$

This is the desired formula for the necessary positional accuracy Δz . We now apply it to the case of f_z given by Eq (5) which can be written approximately as

$$f_z = - 2\pi G\rho \left(\frac{2}{3} z - \frac{a^2 z^3}{R^4} \right) \quad (10)$$

On comparing this with (7) we get

$$k = \frac{4\pi}{3} \quad (11)$$

$$F(z) = \frac{2\pi a^2 z^3}{R^4} \quad (12)$$

Therefore, from (9)

$$\frac{\Delta G}{G} = \frac{3a^2 z \Delta z}{R^4} \quad (13)$$

For the G-experiment we assume that $\Delta G/G = 10^{-6}$, $a = 0.5$ cm, $z = 5$ cm, and $R = 10$ cm. Then $\Delta z = 2.7 \times 10^{-3}$ cm, which is certainly not an impossible accuracy. The ΔG -experiment is more difficult. To attain $\Delta G/G = 10^{-11}$ requires values such as $a = 0.05$ cm (1 mm tunnel diameter) and $\Delta z = 2.7 \times 10^{-6}$ cm, with z and R the same as before. One can argue, of course, that since Δz is a random error, the figure of 2.7×10^{-6} cm is really the time averaged value of Δz . This means that if N observations of Δz are made during the course of a single ΔG determination, the accuracy requirement can be relaxed to $2.7 \times 10^{-6} \sqrt{N}$ cm. We will not attempt to evaluate N since signal processing is beyond the scope of this report.

2. Off-Axis Field in the Tunnel

By fitting a solution of Laplace's equation to the known field on the tunnel axis we can find the off-axis field. Since the field $f_z(0,z)$ on the axis ($r=0$) varies nearly linearly with z we take for the potential the following sum of solutions of Laplace's equation that are polynomials in the cylindrical coordinates r and z and are symmetrical in z :

$$V = A(r^2 - 2z^2) + B(3r^4 - 24r^2z^2 + 8z^4) \quad (14)$$

The field components are

$$f_r = -\frac{\partial V}{\partial r} = -2Ar - B(12r^3 - 48rz^2) \quad (15)$$

$$f_z = -\frac{\partial V}{\partial z} = 4Az + B(48r^2z - 32z^3) \quad (16)$$

On the axis,

$$f_z(0,z) = 4Az - 32Bz^3 \quad (17)$$

We determine A and B by comparing (17) with the expansion of Eq (5) up to cubic terms in z:

$$f_z(0, z) = -2\pi G\rho \left[\left(\frac{2R}{\sqrt{R^2 + a^2}} - \frac{4}{3} \right) z - \frac{Ra^2 z^3}{(R^2 + a^2)^{5/2}} \right] \quad (18)$$

Therefore

$$A = -\frac{2\pi G\rho}{4} \left(\frac{2R}{\sqrt{R^2 + a^2}} - \frac{4}{3} \right) \quad (19)$$

$$B = -\frac{2\pi G\rho}{32} \cdot \frac{Ra^2}{(R^2 + a^2)^{5/2}} \quad (20)$$

On substituting these values of A and B into (15) and (16) we find for the off-axis field components:

$$f_r = 2\pi G\rho \left[\frac{1}{2} \left(\frac{2R}{\sqrt{R^2 + a^2}} - \frac{4}{3} \right) r + \frac{3}{8} \frac{Ra^2}{(R^2 + a^2)^{5/2}} (r^3 - 4rz^2) \right] \quad (21)$$

$$f_z = -2\pi G\rho \left[\left(\frac{2R}{\sqrt{R^2 + a^2}} - \frac{4}{3} \right) z + \frac{1}{2} \frac{Ra^2}{(R^2 + a^2)^{5/2}} (3r^2 z - 2z^3) \right] \quad (22)$$

From (22) we see that if the test particle is displaced by a distance r from the axis of the tunnel, due to the action of some transverse field, the longitudinal field acting on the particle is changed by an amount δf_z that is given approximately by

$$\frac{\delta f_z}{f_z} = \frac{9}{4} \frac{a^2 r^2}{R^4} \quad (23)$$

This change in f_z , if undetected, produces an error in G of amount

$$\frac{\Delta G}{G} = \frac{9}{4} \frac{a^2 r^2}{R^4} \quad (24)$$

For $a = 0.5$ cm, $R = 10$ cm, $\Delta G/G = 10^{-6}$, 10^{-11} , the maximum allowable undetected values of r are $r = 0.1$ cm and $r = 4 \times 10^{-4}$ cm, respectively. The transverse variation of f_z therefore poses less of a problem than the longitudinal departure from linearity. Monitoring the transverse displacement of the particle can be avoided by means of a support system capable of holding the particle within 4 microns of the tunnel axis.

C. PERTURBATION OF THE FIELD BY THE MASS OF THE SUPPORT SYSTEM

We will consider only the case of a quadrupole diamagnetic support system consisting of a thin walled metal tube divided longitudinally into four sectors and attached to the wall of the tunnel. The potential on the axis of the tunnel is

$$V = - \int_{-L}^L \frac{Gm dz'}{\sqrt{(z' - z)^2 + b^2}} = - Gm \left\{ \sinh^{-1} \left(\frac{L-z}{b} \right) + \sinh^{-1} \left(\frac{L+z}{b} \right) \right\} \quad (25)$$

where m is the mass per unit length and b the mean radius of the tube. $2L$ is the length of the tube which may be greater than the diameter $2R$ of the sphere.

The field on the axis is

$$\Delta f_z = - \frac{\partial V}{\partial z} = - \frac{Gm}{b} \left\{ \frac{1}{\sqrt{1 + \left(\frac{L-z}{b} \right)^2}} - \frac{1}{\sqrt{1 + \left(\frac{L+z}{b} \right)^2}} \right\} \quad (26)$$

The relative perturbation is

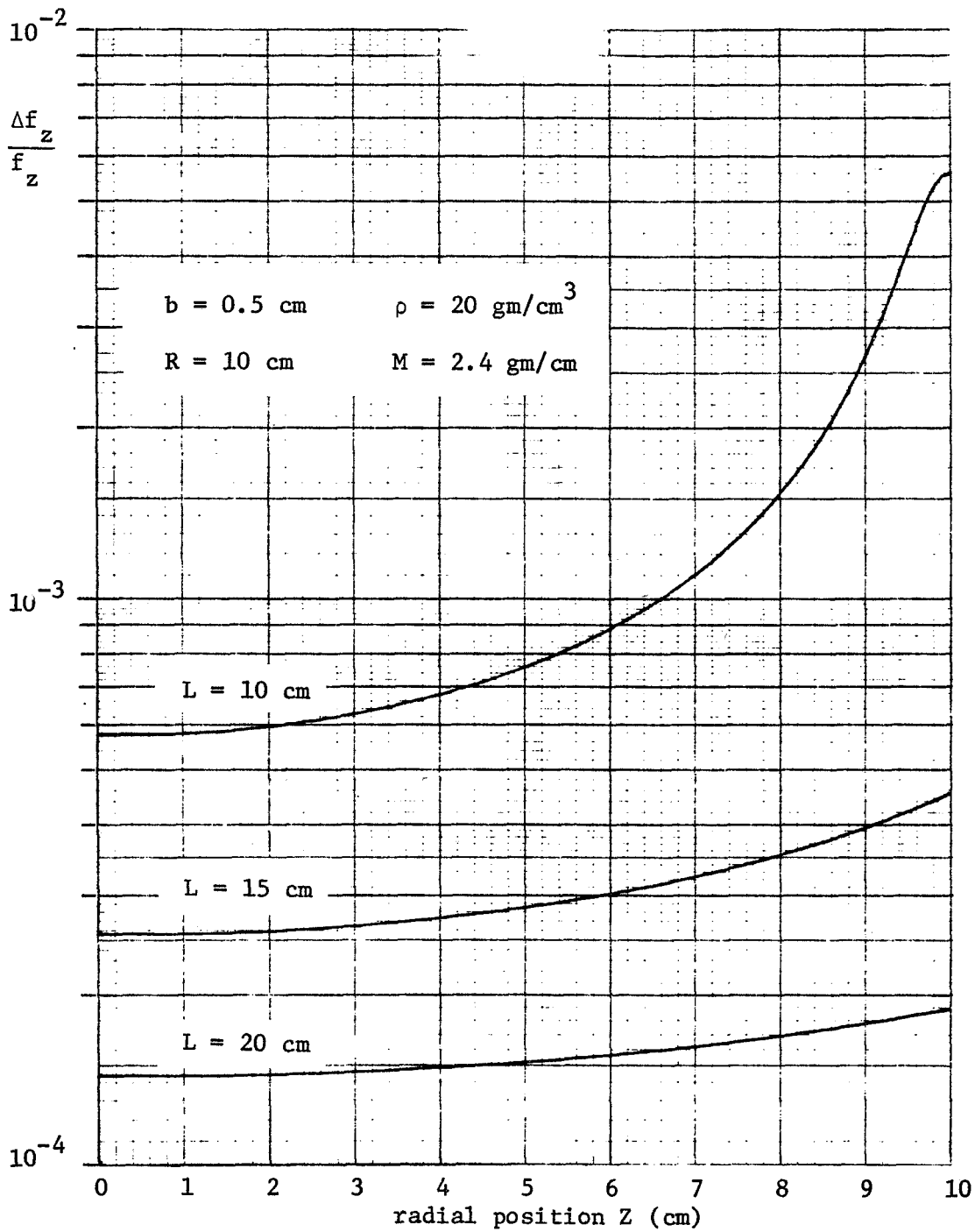


FIGURE 2. DISTURBANCE OF THE FIELD DUE TO A QUADROPOLE DIAMAGNETIC TEST MASS SUPPORT

$$\frac{\Delta f_z}{f_z} = \frac{3m}{4\pi\rho bz} \left\{ \frac{1}{\sqrt{1 + \left(\frac{L-z}{b}\right)^2}} - \frac{1}{\sqrt{1 + \left(\frac{L+z}{b}\right)^2}} \right\} \quad (27)$$

where, as before, ρ is the density of the sphere. The effect of the tunnel itself is not included since this has already been discussed.

Figure 2 shows how $\Delta f_z/f_z$ depends on z for three values of L , for the case of a copper tube of cross section 0.3 cm^2 and density 8 gm/cm^3 , for which $m = 2.4 \text{ gm/cm}$. The figure shows that $\Delta f_z/f_z$ decreases as the length of the tube increases. This is understandable since for an infinite tube the longitudinal field is zero.

On comparing Figure 2 with Figure 1 we see that the effect of the tube is less than that of the tunnel. We therefore do not need to consider the effect on $\Delta G/G$.

D. EFFECT OF SPHERICITY ERROR

The field of an out-of-round sphere is closely equivalent to that of a perfect sphere with a superimposed surface distribution of mass $\sigma(\theta', \phi')$. If $\Delta R(\theta', \phi')$ is the sphericity error as a function of the spherical angles θ' and ϕ' , then

$$\sigma(\theta', \phi') = \rho \Delta R(\theta', \phi') \quad (28)$$

where ρ is the density of the sphere.

We will consider first the case where $\Delta R(\theta', \phi')$ has the form of an axially symmetric second order spherical harmonic:

$$\Delta R = \frac{1}{2} \Delta R_0 (3 \cos^2 \theta' - 1) \quad (29)$$

where ΔR_0 is the maximum departure in shape from the mean spherical

surface. It is to be noted that the first order harmonic $\cos\theta'$ merely corresponds to a displacement of the sphere.

The equivalent surface distribution of mass is

$$\sigma = \frac{\rho\Delta R_o}{2} (3 \cos^2\theta' - 1) \quad (30)$$

The potential due to σ is of the form:

$$v_i = A \frac{r'^2}{R^2} (3 \cos^2\theta' - 1) \quad , \quad r' \leq R \quad (31)$$

$$v_o = A \frac{R^3}{r'^3} (3 \cos^2\theta' - 1) \quad , \quad r' \geq R \quad (32)$$

where r' is the radial spherical coordinate and A is an arbitrary constant. v_i and v_o satisfy Laplace's equation and match over the surface of the sphere. The other boundary condition at $r' = R$ is that

$$\frac{\partial v_i}{\partial r'} - \frac{\partial v_o}{\partial r'} = -4\pi G\sigma \quad (33)$$

This gives, from (30), (31), and (32),

$$A = -\frac{2\pi}{5} G\rho R\Delta R_o \quad (34)$$

Therefore, from (31),

$$v_i = -\frac{2\pi G\rho\Delta R_o r'^2 (3 \cos^2\theta' - 1)}{5R} \quad (35)$$

The force components are

$$\Delta f_{r'} = -\frac{\partial v_i}{\partial r'} = \frac{4\pi G\rho\Delta R_o r' (3 \cos^2\theta' - 1)}{5R} \quad (36)$$

$$\Delta f_{\theta'} = -\frac{1}{r'} \frac{\partial v_i}{\partial \theta'} = \frac{-4\pi G \rho \Delta R_o r' (3 \sin \theta' \cos \theta')}{5R} \quad (37)$$

If the tunnel is drilled at the angle θ' , the longitudinal force in the tunnel is $\Delta f_{r'}$, and the transverse force is $\Delta f_{\theta'}$. It is to be noted that these forces are linear in the tunnel coordinate z , which is equal to r' . Therefore $\Delta f_{r'}$ does not contribute any error in G due to error in measurement of the position of the test particle.

The maximum value of $\Delta f_{r'}$ occurs for $\theta' = 0$ and is given by

$$\Delta f_{r'} = \frac{8\pi G \rho \Delta R_o r'}{5R} = \frac{8\pi G \rho \Delta R_o z}{5R} \quad (38)$$

The transverse force is maximum when the tunnel is drilled at 45° to the polar axis and has the value

$$\Delta f_{\theta'} = \frac{-6\pi G \rho \Delta R_o z}{5R} \quad (39)$$

We have seen earlier that for the ΔG -experiment the test particle must be held at a distance $r_o < 1 \times 10^{-4}$ cm from the axis of the tunnel in order to overcome the transverse variation in the longitudinal force. The support system must therefore supply a restoring force at this distance at least as large as the transverse force given by Eq (39). The required spring constant is therefore

$$K = \frac{6\pi G \rho \Delta R_o z}{5R r_o} \quad (40)$$

For $\Delta R_o = 10^{-5}$ cm, $R = 10$ cm, $G = 6.7 \times 10^{-8}$, $\rho = 20$ gm/cm³, $z = 5$ cm, and $r_o = 1 \times 10^{-4}$ cm, we get $K = 2.5 \times 10^{-7}$ dyne/(cm gm), which indicates that there should be no difficulty in providing the necessary support system to take care of this effect of the sphericity error.

It is worth noting that sphericity errors involving higher order harmonics than the second give nonlinear contributions to the longitudinal force. For example, in the case of the third harmonic $5 \cos^3 \theta - 3 \cos \theta$ we find, by the same method, that

$$\left(\Delta f_r \right)_{\max} = \frac{12\pi G \rho \Delta R_o z^2}{7R^2} \quad (41)$$

On applying Eq (9) we find that

$$\frac{\Delta G}{G} = \frac{9}{7} \frac{\Delta R_o \Delta z}{R^2} \quad (42)$$

For the ΔG -experiment we take $\Delta G/G = 10^{-11}$, $\Delta R_o = 10^{-5}$ cm, $R = 10$ cm and find $\Delta z = 1 \times 10^{-4}$ cm. Therefore the required resolution in the position of the test particle is much less severe than in the case of the tunnel force. This means that a sphericity tolerance of 10^{-5} cm is adequate.

E. EFFECT OF SPATIAL VARIATIONS OF DENSITY

Two kinds of density variation in the metal sphere will be considered--small-scale variations due to the microcrystalline structure of the metal and large-scale variation due perhaps to frozen strains, to change in microstructure across the sphere, or to the presence of a temperature gradient across the sphere.

1. Large-Scale Density Variations

Since the density variation will not in general be related to the position of the tunnel, we use, as before, polar coordinates r', θ', ϕ' to describe the density distribution and the associated gravitational field. For simplicity we restrict the discussion to the case where the density distribution is independent of ϕ' . Then the

perturbation in gravitational potential v is related to the density discrepancy $\Delta\rho$ by Poisson's equation

$$\frac{1}{r'^2} \frac{\partial}{\partial r'} \left(r'^2 \frac{\partial v}{\partial r'} \right) + \frac{1}{r'^2 \sin^2 \theta'} \frac{\partial}{\partial \theta'} \left(\sin \theta' \frac{\partial v}{\partial \theta'} \right) = -4\pi G \Delta\rho \quad (43)$$

To avoid integrating this equation we assume a form for v and calculate $\Delta\rho$ by differentiation. For example, if

$$v = -Ar'^n \cos \theta' \quad (44)$$

then

$$4\pi G \Delta\rho = \{n(n+1) - 2\} Ar'^{n-2} \cos \theta' \quad (45)$$

For $n = 3$ we get the case of a uniform density gradient:

$$4\pi G \Delta\rho = 10 Ar' \cos \theta' = 10 Az' \quad (46)$$

$$v = -Ar'^3 \cos \theta' \quad (47)$$

The constant A , from (46), is related to the density difference $\Delta\rho_0$ between the pole and the center of the sphere by the formula

$$A = \frac{4\pi G \Delta\rho_0}{10 R} \quad (48)$$

The field components are then

$$\Delta f_{r'} = \frac{6\pi G \Delta\rho_0 r'^2 \cos \theta'}{5R} \quad (49)$$

$$\Delta f_{\theta'} = -\frac{2\pi G \Delta\rho_0 r'^2 \sin \theta'}{5R} \quad (50)$$

Eq (49) shows that the maximum perturbation in the axial field in the tunnel occurs when the tunnel happens to be aligned with the density gradient and is

$$\Delta f_{r, \max} = \frac{6\pi G \Delta \rho_o z^2}{5R} \quad (51)$$

where z as usual is the axial coordinate.

On applying Eq (9) we find for the error in G

$$\frac{\Delta G}{G} = \frac{9}{5} \frac{\Delta \rho_o}{\rho} \frac{\Delta z}{R} \quad (52)$$

For the ΔG -experiment we assume that $\Delta G/G = 10^{-11}$, $\Delta \rho_o/\rho = 10^{-6}$, $R = 10$ cm and find that the required resolution in test particle position, without including the effect of time averaging, is $\Delta z = 5 \times 10^{-5}$ cm, which is about one wavelength of light.

2. Random Small-Scale Density Variations

A general theory of the effect of a random distribution of density inhomogeneities has been given by S. Madden.⁽³⁾ We will therefore limit our discussion to a very approximate treatment of this problem along somewhat different lines.

Let the density variation $\Delta \rho$ from the mean be represented by a Fourier series

$$\Delta \rho = \sum \Delta \rho(k) e^{i\vec{k} \cdot \vec{r}} \quad (53)$$

where k is the wavenumber $2\pi/\lambda$ of a Fourier component. The summation means that a sufficient number of Fourier components of different k values are added together to give a reasonable approximation of the real density variation. The amplitudes $\Delta \rho(k)$ are complex numbers but

$\Delta\rho$ is taken to be the real part of the right-hand side of (53).

The potential v due to the density fluctuations is given by Poisson's equation

$$\nabla^2 v = -4\pi G \sum A_k e^{i\vec{k}\cdot\vec{r}} \quad (54)$$

The solution (particular integral) is

$$v = 4\pi G \sum \frac{1}{k^2} A_k e^{i\vec{k}\cdot\vec{r}} \quad (55)$$

The z -component of force is therefore

$$\Delta f_z = -\frac{\partial v}{\partial z} = 4\pi i G \sum \frac{k_z}{k^2} A_k e^{i\vec{k}\cdot\vec{r}} \quad (56)$$

The mean square value of f_z is

$$\overline{(\Delta f_z)^2} = 16 \pi^2 G^2 \sum \frac{k_z^2}{k^2} |A_k|^2 \quad (57)$$

Now let $P(k)$ be the power spectral density of $\Delta\rho(k)$, so that

$$|A_k|^2 = P(k) \Delta k_x \Delta k_y \Delta k_z \quad (58)$$

Then (57) becomes, on replacing the sum by an integral,

$$\overline{(\Delta f_z)^2} = 16 \pi^2 G^2 \iiint \frac{P(k) k_z^2 dk_x dk_y dk_z}{k^4} \quad (59)$$

Next we assume that $P(k)$ has a constant value P_0 up to a spatial frequency k_m and is zero for all higher frequencies. Then on setting $k_z = k \cos\theta$, $dk_x dk_y dk_z = 2\pi \sin\theta k^2 dk d\theta$ we get

$$\begin{aligned} \overline{(\Delta f_z)^2} &= 16 \pi^2 G^2 P_0 \int_0^{k_m} \int_0^\pi \frac{2\pi k^4 \cos^2\theta \sin\theta d\theta dk}{k^4} \\ &= \frac{64}{3} \pi^3 G^2 P_0 k_m \end{aligned} \quad (60)$$

From (58), P_0 can be expressed in terms of the mean square density fluctuation $\overline{(\Delta\rho)^2}$ as

$$\overline{(\Delta\rho)^2} = \iiint_{R \leq k_m} P_0 dk_x dk_y dk_z = \frac{4\pi}{3} k_m^3 P_0 \quad (61)$$

Therefore

$$\overline{(\Delta f_z)^2} = \frac{16 \pi^2 G^2 \overline{(\Delta\rho)^2}}{k_m^2} \quad (62)$$

We may express k_m in terms of a characteristic length or grain size L by the formula

$$k_m = \frac{\pi}{L} \quad (63)$$

Therefore

$$(\Delta f_z)_{\text{rms}} = 4G(\Delta\rho)_{\text{rms}} L \quad (65)$$

Relative to the main force $f_z = 4 G z/3$, we can write

$$\frac{(\Delta f_z)_{\text{rms}}}{f_z} = \frac{3(\Delta \rho)_{\text{rms}} L}{\pi \rho z} \quad (66)$$

Let $L = 1 \times 10^{-4}$ cm, $z = 5$ cm, $(\Delta \rho)_{\text{rms}}/\rho = .02$. Then $(\Delta f_z)_{\text{rms}}/f_z = 10^{-6}$. Therefore a sphere made of a metal composed of 1-micron grains with 2% density variation meets the requirement of the G-experiment. Actually, since, in view of our earlier discussion, the test particle must always be kept near the axis of the tunnel at a distance of perhaps 0.5 cm from the tunnel wall, rather than in the sphere itself, the rms force will be considerably less than the value calculated.

F. EFFECTS OF TEMPERATURE

In this section we consider the effects of both time and space variations of the temperature of the sphere due to varying environment, to nonisotropic heat input to the sphere, and to dissipation of energy in the support system.

1. Secular Variation of Temperature

In the ΔG -experiment the heat input from the sun to the space vehicle will change by a considerable factor during the course of the experiment. One may therefore expect that in spite of the best efforts to control the temperature of the sphere, some systematic drift will actually occur.

An increase ΔT in the temperature of the sphere causes the density to decrease according to the formula

$$\frac{\Delta \rho}{\rho} = - 3\alpha \Delta T \quad (67)$$

where α is the coefficient of linear expansion of the material. The angular velocity of the test particle, which is given by the formula

$$\omega = \sqrt{\frac{4\pi G\rho}{3}} \quad (68)$$

will therefore also decrease.

If the temperature change is below the level of detection, the change in ω will be interpreted as a change in G . Since, according to (68), G and ρ affect ω in exactly the same way, the result is that the temperature change ΔT causes an error in G given by

$$\frac{\Delta G}{G} = - 3 \alpha \Delta T \quad (69)$$

Table I gives calculated values of $\Delta G/G$ for tungsten and gold at 300°K with temperature control to 0.001 °C, which is the state-of-the-art limit for long periods of time with varying environment. It is seen that the error in G is well below the goal of 10^{-6} for the G -experiment, but is more than three orders of magnitude above the 10^{-11} error required for the ΔG -experiment. It appears therefore that the ΔG -experiment is impossible at room temperature.

At cryogenic temperatures, however, the situation is completely different. The expansion coefficient falls by several orders of magnitude, and temperature control to 0.0001°C or less becomes quite feasible for indefinite periods of time. We have not been able to obtain data for tungsten and gold at these temperatures, but the general trend is shown in Table I for lead, silver, and copper. We have calculated $\Delta G/G$ for these metals at temperatures of 300 K and 10 K. It is seen that the 10^{-11} goal is approached, particularly for copper. Below 10 K the expansion coefficient falls with temperature with a law that appears to lie between T^2 and T^3 . One would therefore anticipate a further factor of about 1/10 in $\Delta G/G$ if the equipment is operated at the temperature of liquid

TABLE I

ERROR DUE TO TEMPERATURE VARIATION

<u>SPHERE</u>	<u>T</u> (K)	<u>α</u> (°C) ⁻¹	<u>ΔT</u> (°C)	<u>$\frac{\Delta G}{G}$</u>
Tungsten	300	4.4×10^{-6}	.001	1.4×10^{-8}
Gold	300	14.2×10^{-6}	.001	4.3×10^{-8}
Lead	300	29.0×10^{-6}	.001	8.7×10^{-8}
	10	3.2×10^{-6}	.0001	9.6×10^{-10}
Silver	300	19.1×10^{-6}	.001	5.7×10^{-8}
	10	0.1×10^{-6}	.0001	3.0×10^{-11}
Copper	300	16.8×10^{-6}	.001	5.0×10^{-8}
	10	0.04×10^{-6}	.0001	1.2×15^{-11}

helium at 4°K. Silver and copper, for example, would then have $\Delta G/G$ values of about 3×10^{-12} and 1×10^{-12} , respectively.

Although operation at cryogenic temperatures presents some difficulties there are several advantages besides that of temperature stability. For example, creep practically disappears entirely at these temperatures since it proceeds by thermal excitation. Another advantage is that the support system can use persistent currents in superconductors with complete absence of dissipation.

2. Effect of a Temperature Gradient

A temperature gradient in the metal sphere produces a corresponding density gradient. If ΔT is the temperature difference between

the surface and center of the sphere and α is the expansion coefficient, the density difference $\Delta\rho$ between the same two points is given approximately by

$$\frac{\Delta\rho}{\rho} = - 3 \alpha\Delta T \quad (70)$$

This formula does not take thermal stress into account. We have shown earlier that a density gradient produces a nonlinear force in the tunnel (Eq 51) and that this causes an error in the measurement of G of magnitude

$$\frac{\Delta G}{G} = \frac{9}{5} \frac{\Delta\rho}{\rho} \frac{\Delta z}{R} \quad (71)$$

where Δz is the resolution in test particle position. For $\Delta G/G = 10^{-11}$, $\Delta z = 5 \times 10^{-5}$ cm, and $R = 10$ cm, $\Delta\rho/\rho$ is 10^{-6} . Therefore for a tungsten sphere at room temperature, with $\alpha = 4.4 \times 10^{-6} (\text{°C})^{-1}$, we find from (70) that the maximum allowable ΔT is 0.08°C .

To estimate the actual ΔT we assume that the sphere has a coating with an emissivity $\epsilon = 0.02$ and is radiatively coupled to a black spherical enclosure that has a 1°C temperature difference across its diameter. We find that, owing to the relatively high conductivity of tungsten, ΔT is less than 10^{-4}°C . Temperature gradients are therefore not a problem.

3. Dissipation of Energy in the Support System

The heat input to the sphere in the case of a diamagnetic support system operated at room temperature is about 2×10^{-3} watt. Since the sphere is a good thermal conductor and is weakly coupled by radiation to an external shield, the important effect of the heat input is the overall temperature rise rather than the temperature gradient.

The equilibrium temperature T of the sphere is given by the equation

$$4\pi R^2 \epsilon \sigma (T^4 - T_0^4) = Q \quad (72)$$

where Q is the rate of heat input, T_0 is the temperature of the surrounding black shield, ϵ is the emissivity of the sphere, R is the radius of the sphere, and σ is the Stefan-Boltzmann constant. Since T differs very little from T_0 , we can write (72) as

$$16\pi R^2 \epsilon \sigma T_0^3 \Delta T = Q \quad (73)$$

where ΔT is the temperature rise of the sphere relative to the shield.

We take $T_0 = 300$ K, $\epsilon = 0.02$, $R = 10$ cm, and $Q = 2 \times 10^{-3}$ watt. Then $\Delta T = 0.13^\circ\text{C}$. For the case of tungsten with $\alpha = 4.4 \times 10^{-6} (\text{°C})^{-1}$, the nominal fractional error in G is 1.7×10^{-6} . This error can be removed by calibration to within the accuracy of determination of Q . Such calibration will probably reduce $\Delta G/G$ to about 10^{-9} . Therefore the heat dissipation will not affect the G -experiment. As far as the ΔG -experiment is concerned the dissipation merely adds to the impossibility of doing this experiment at room temperature. As mentioned above the dissipation is zero at cryogenic temperatures if superconducting metal is used in the support system.

III. SUSPENSION SYSTEMS FOR SECONDARY TEST MASSES

A. BACKGROUND

We have shown in Section II that for the ΔG experiment one must constrain the test mass to within about 1μ of the tunnel axis in order to avoid uncertainties due to the off-axis variation in the longitudinal component of the gravitational force in the tunnel. The suspension system must be able to maintain this radial tolerance in the presence of transverse forces arising from

1. sphericity error of the primary sphere,
2. electrification of the test particles,
3. gravitational fields of other objects in the space craft,
4. D'Alembert force on the test mass due to acceleration of the primary sphere.

We will here consider only disturbances (1) and (2).

A further important requirement of the suspension system is that it should not exert an appreciable longitudinal force on the test mass.

Several different kinds of suspension systems using electric or magnetic fields have been tried or developed. These include

1. Servo-controlled support of a ferromagnetic body by a magnetic field (J. W. Beams' ultra-centrifuge)⁽⁴⁾
2. Servo-controlled support of a conducting body by an electrostatic field (Nordsieck's electrostatically supported gyro)^(5,6)
3. Passive support of a diamagnetic or superconducting body by a fixed magnetic field (Ivan Simon's ADL tiltmeter or John Harding's superconducting gyro)⁽⁷⁾

4. Passive support of a small magnet by the induced magnetic field of a superconductor (demonstrated many years ago by Ivan Simon).

For the present purpose of suspending a small test mass in a long narrow tunnel, the passive methods (i.e., methods without servo control) have obvious advantages since no monitoring of the particle's transverse position is required. We will therefore confine our discussion to these methods.

B. DIAMAGNETIC SUPPORT SYSTEM

We will first consider the case of room-temperature operation in which the supporting magnetic field is generated by four linear conductors placed in the tunnel with the cross-sectional geometry shown in Figure 3. The currents in all conductors are the same in magnitude but alternate in direction. For ease of calculation we assume that the field is the same as if the currents were concentrated along lines at the points A,B,C,D forming a square of edge $2b$.

The field components are, in electromagnetic units,

$$H_x = - \frac{2I(y - b)}{(x - b)^2 + (y - b)^2} + \frac{2I(y + b)}{(x - b)^2 + (y + b)^2} - \frac{2I(y + b)}{(x + b)^2 + (y + b)^2} + \frac{2I(y - b)}{(x + b)^2 + (y - b)^2} \quad (74)$$

$$H_y = \frac{2I(x - b)}{(x - b)^2 + (y - b)^2} - \frac{2I(x - b)}{(x - b)^2 + (y + b)^2} + \frac{2I(x + b)}{(x + b)^2 + (y + b)^2} - \frac{2I(x + b)}{(x + b)^2 + (y - b)^2} \quad (75)$$

where I is the current in each conductor.

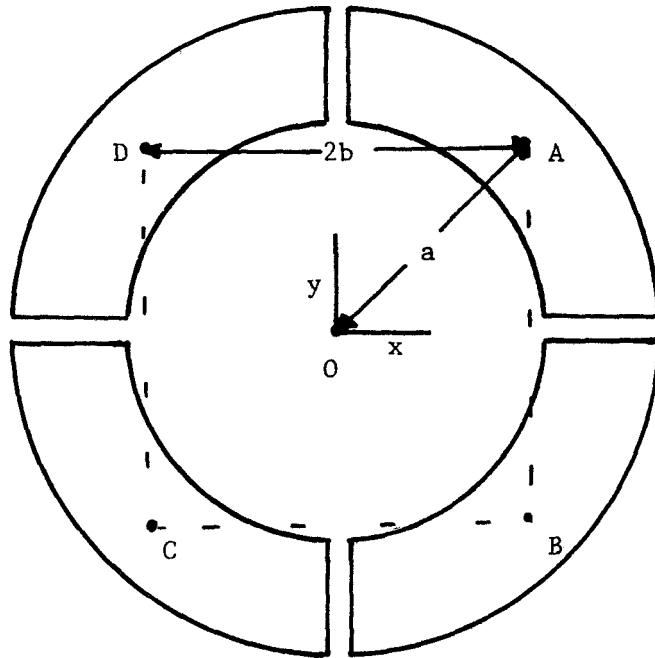


Figure 3. Quadrupole electrodes for diamagnetic support system.

For small values of x and y , (74) and (75) reduce to

$$H_x = \frac{4Ix}{b^2} \quad (76)$$

$$H_y = -\frac{4Iy}{b^2} \quad (77)$$

which is a quadrupole field.

The square of the field magnitude is:

$$H^2 = \frac{16 I^2 r^2}{b^4} \quad (78)$$

The force on a small diamagnetic test body of volume v and diamagnetic susceptibility χ placed in the tunnel at a distance r from the axis is:

$$F_r = \frac{1}{2} \chi v \frac{\partial H^2}{\partial r} = \frac{16 I^2 \chi v r}{b^4} \quad (79)$$

This magnetic force can balance a transverse gravitational or inertial force of magnitude

$$f = \frac{16 I^2 \chi r}{\rho b^4} = \frac{64 I^2 \chi r}{\rho a^4} \quad (80)$$

per unit mass, where ρ is the density of the test body and a is the radius of the circle passing through the points A,B,C,D.

The restoring spring constant of the support system is

$$K = \frac{64 I^2 \chi}{\rho a^4} \quad (81)$$

Let $\chi/\rho = 5 \times 10^{-6} \text{ gm}^{-1} \text{ cm}^3$ (graphite)

$a = 0.5 \text{ cm}$

$I = 0.7 \text{ amp} = 0.07 \text{ abamp}$

Then $K = 2.5 \times 10^{-5} \text{ dyne/cm gm}$.

For a sphericity error of 10^{-5} cm in the primary mass the transverse force in the tunnel, from Eq (39), has a maximum value of $2.5 \times 10^{-11} \text{ dyne/gm}$. The restoring force provided by the suspension system will therefore hold the test mass at a distance of $1.0 \times 10^{-6} \text{ cm}$ from the tunnel axis which is very well within the requirement of 1μ .

The dissipation in the support system is 2 milliwatts if the conductors have a radial thickness of 0.005 cm and are made of copper with a resistivity of $1.7 \times 10^{-6} \text{ ohm cm}$. However, since from our discussion in Section II cryogenic temperatures are essential for the ΔG experiment, the conductors can be made of superconducting material in which case the dissipation becomes zero.

It is worth noting that if more than four conductors are used in the suspension system the power of r in Eq (78) becomes higher than two. This means that the restoring force is no longer linear in r , with the result that the test mass is not held so close to the axis of the tunnel. The quadrupole configuration is therefore optimum for the present application.

C. PERMANENT MAGNET--SUPERCONDUCTOR SUPPORT SYSTEM

In the permanent magnet--superconductor support system the test mass is a small permanent magnet and the supporting magnetic field is produced by currents induced by the magnet in a superconducting tube that lines the wall of the tunnel. The induced currents are in such a direction that the magnet is repelled from the walls of the tube. Evaluation of the radial force on the magnet is a somewhat intractable problem but we have derived

the following approximate formula based on the analogous problem of a magnetic dipole placed between two infinite parallel superconducting planes:

$$F_r \approx -\frac{\mu^2}{5a} r \quad (82)$$

where μ is the dipole moment of the magnet, r is the displacement of centroid of the magnet from the tube axis, and a is the tube radius. This formula is valid only for $r \ll a$.

We will assume at first that the test mass consists of a magnet of volume 1 mm^3 of platinum-cobalt alloy (PLACOVAR) magnetized to its maximum remanent flux of 3000 gauss. Then $\mu = 3/4\pi (\text{dyne})^{1/2} \text{ cm}^2$. Therefore if $a = 0.5 \text{ cm}$, $F_r/r = -1.8 \text{ dyne/cm}$. Since the density of the alloy is 15.7 gm/cm^3 , the mass of the magnet is 0.0157 gm and the spring constant per unit mass is $K = 115 \text{ dyne/cm gm}$. This value is about 7 orders of magnitude larger than that for the diamagnetic system. It appears therefore that the ferromagnetic--superconducting suspension system can be arranged to supply any needed transverse restoring force. It is not advisable, however, to provide much excess magnetization since this merely increases the longitudinal magnetic force due to end effects of the superconducting tube without giving any useful gain in the radial constraint. A further reason for making the magnet as weak as possible is the possibility of local quenching of the superconductivity of the tube if the magnetic field exceeds the critical value of a few hundred gauss.

D. DISTURBING FIELDS ORIGINATING IN THE SUSPENSION SYSTEM

The proper action of the suspension system can be disturbed by fields that originate in the suspension system itself. Such fields include electrostatic fields due to charges on the test mass, magnetic fields due to the end effects in the support system, and magnetic fields due to trapped flux in the superconducting tube.

1. Electrostatic Fields

An electric charge q on the test mass causes a radial force given approximately, for small displacements r from the tunnel axis, by

$$F_r = \frac{q^2 r}{a^3} \quad (83)$$

where a is the radius of the tunnel. For a test mass of 0.0157 gm the (unstable) spring constant is therefore

$$K = - \frac{64 q^2}{3 a} \quad \left(\frac{\text{dyne}}{\text{cm gm}} \right) \quad (84)$$

It is of interest to calculate the charge needed to annul the restoring spring constant of the support system. In the diamagnetic case, for which $K = 2.5 \times 10^{-5}$ dyne/cm gm, and with $a = 0.5$ cm we get $q = 2 \times 10^{-4}$ statcoulomb. The corresponding potential, if the test mass is a sphere of diameter 0.1 cm, is about 1 volt.

For the case of the permanent magnet test mass, where the restoring spring constant can possibly be as large as 115 dyne/cm gm, the necessary charge is 0.5 statcoulomb and the potential is 3000 volts.

These results suggest that some means for removing charge from the test mass, by inclusion of some radioisotope for example, is desirable in the case of the diamagnetic test mass, but not for the permanent magnet test mass.

Charge on the test mass will also produce a longitudinal force due the finite length of the tunnel. If we consider only the effect of one end of the tunnel, the force is of the order of

$$F_z = - \frac{q^2}{a^2} e^{-2kl} \quad (85)$$

where ℓ is the distance of the test mass from the end of the tunnel and ka is the first zero of the Bessel function $J_0(x)$, i.e., $ka = 2.4048$. It is to be noted that the force is in the same direction as the gravitational force of the primary sphere. If the end of the tunnel were closed by a conducting sheet, the force would be reversed in direction but of about the same magnitude.

It is clearly essential that the force F_z given by (85) be kept smaller than the variation in gravitational force due to ΔG . For a test particle of mass .0157 gm located at 5 cm from the center of the primary sphere the change in gravitational force for $\Delta G/G = 10^{-11}$ is 4×10^{-18} dyne. Eq (85) gives the same force, with $a = 0.5$ cm, $\ell = 5$ cm, when $q = 26$ statcoulomb, corresponding to a test mass potential of 160,000 volt. Therefore the end effect appears to be negligible.

2. Magnetic Fields

The end effect produced by the finite length of the superconducting tube gives rise to a longitudinal force on the test mass given approximately by

$$F_r = \frac{\mu}{4a} e^{-2k_1 \ell} \quad (86)$$

where $k_1 a$, the first zero of the Bessel function $J_1(x)$, is 3.8317. This value of $k_1 a$ arises from the boundary condition that the normal component of field at the surface of a superconductor must be zero. On taking $\mu = 3/4\pi$ (dyne)^{1/2} cm², $a = 0.5$ cm, and $\ell = 5$ cm, we find that $F_r = 5 \times 10^{-34}$ dyne, which is to be compared with the force of 4×10^{-18} dyne due to ΔG . The end effect of the superconducting tube is therefore completely negligible.

The effect of trapped flux cannot be dismissed so easily. If in the process of cooling down the tube below the superconducting

transition temperature T_c a small area of the tube wall above T_c is surrounded by metal below T_c , the ambient magnetic flux threading this area is trapped and becomes compressed until the field reaches the critical field B_c , which is of the order of a hundred gauss. Under these conditions the trapped flux in an island of area 1 mm x 1 mm acts like an isolated magnetic pole of strength $p = 1/4\pi$ (dyne)^{1/2} cm. If the test mass magnet of dipole moment $\mu = 3/4\pi$ (dyne)^{1/2} cm² is opposite this pole at a separation $a = 0.5$ cm, the test mass experiences a longitudinal force $F = p\mu/a^3 = 0.15$ dyne which is enormous compared with the force of 4×10^{-18} dyne due to ΔG . It is clear therefore that the greatest of care must be taken to cool the superconducting tube from one end in such a way that no islands of normal material are formed.

Alternatively, it may well be argued that the risk of trapped flux is too great and that a diamagnetic test mass supported by currents in non-superconducting material at low temperature is to be preferred.

IV. MATERIALS AND FABRICATION OF THE PRIMARY MASS

A. BACKGROUND

Information on the suitability and characteristics of the candidate materials for the primary mass has been developed through a brief review of the pertinent literature and discussions with potential suppliers, processors, and fabricators. Discussions were held with personnel at Oak Ridge National Laboratory (ORNL), Y-12 Plant of Union Carbide Corp., Nuclear Metals Division of Whittaker Corporation, and Battelle Memorial Institute.

We examined only materials with a density greater than that of tantalum, 16.6 gm/cc. With the exception of uranium, alloys were not considered because of potential problems of density variation due to alloy macro-segregation. Although we believe that there are no particular advantages to be gained by alloying the noble metals, tungsten, or tantalum, alloys of uranium provide some advantages in terms of isotropic properties and oxidation resistance, and are therefore worth consideration.

B. GENERAL CHARACTERISTICS OF CANDIDATE MATERIALS

Pertinent properties of candidate materials are summarized in Table II. Osmium, irridium, and rhenium are not desirable for the primary mass because of cost and difficulty of fabrication. Gold and platinum are less expensive, but they have marginal strength. To be dimensionally stable, they would have to be used in the soft, annealed condition and almost certainly would creep under their own weight. The remaining materials deserve more careful consideration.

1. Tungsten

Tungsten is a strong candidate because of its availability, density, strength and crystal structure. However, fabrication difficulties

TABLE II. PROPERTIES OF MATERIALS

Material	Density (g/cc)	Melting Point (°C)	Crystal Structure	Yield Strength ^a (10 ³ psi)	Tensile ^a Strength (10 ³ psi)	Elonga- tion ^a (%)	Elastic Modulus (10 ⁶ psi)	Workability	Machin- ability	Oxidation Resistance	Availability (100 Kg)	Mat. Costs (\$/Kg)
Osmium	22.57	3000	Hexagonal close packed	---	---	---	80	not possible	---	Good	Twice U.S. annual consump- tion	6500-7300
Iridium	22.42	2410	Face centered cubic	---	80-290	---	74	hot, very difficult	---	Excellent	Approx. 1/4 US annual consumption	5000-5200
Platinum	21.45	1769	Face centered cubic	5-27	18-30	3-40	25	Excellent	Fair	Excellent	Readily	4700-4800
Rhenium	21.02	3180	Hexagonal Close Packed	---	164-322	---	67	Fair	---	Good	Marginal	1200-1300
Gold	19.32	1063	Face centered cubic	0-70	19-32	4-45	12	Excellent	Fair	Excellent	Yes, on US loan	1100
Tungsten	19.3	3370	Body centered cubic	60 ^b	70 ^b	0 ^b	59	Hot, difficult	Diffi- cult	Good	Readily	10-13
Uranium	19.07	~1150	Orthorhombic <660°C Tetragonal 660-775°C Body Centered Cubic <775°C	30-100	60-170	5-20	26-29	Hot, good	Good	Poor	Readily, controlled	7-9
Uranium- 8% Mo	~17.5	1130-1200	Body centered cubic	122 ^c	127 ^c	16 ^c	---	Hot, good	---	Good	Readily, controlled	22-25
Tantalum	16.6	2996	Body centered cubic	26-95	30-100	3-36	27	Good	Good	Good	Readily	65-77

^a Annealed and hardened conditions

^b Pressed and sintered

^c Cast

primarily associated with densification and machining are likely to occur. These are discussed in greater detail below.

2. Uranium and Uranium-Molybdenum Alloys

Despite its good availability, and adequate mechanical and fabricability qualities, uranium may be unsuitable because of its phase changes, its non-cubic structure (causing anisotropy in its properties) and poor oxidation resistance.

a. Phase Changes and Anisotropy

In addition to the phases listed in Table II, uranium undergoes a non-crystallographic phase change to an anti-ferromagnetic state at 43°K.^(8,9) Below this temperature the coefficient of thermal expansion in the a and b crystal directions is large and negative while that in the c direction is large and positive. The anisotropy can probably be minimized by one or more of the following approaches: 1) consolidation by powder metallurgy; 2) repeated thermal cycling to wash out preferred orientation; and 3) use of a uranium alloy such as uranium-10Mo, which is cubic at least down to room temperature.^(10,11)

b. Oxidation Resistance

A highly polished uranium surface will tarnish over a period of time. Thus the finished spheres may require electro or ion plating with oxidation resistant materials such as nickel, gold or aluminum. Plating of uranium is difficult, but techniques have been developed.⁽¹²⁻¹⁴⁾

An alternate solution to the oxidation problem involves the use of a uranium-molybdenum alloy. These are the so-called "stainless" uranium alloys.

3. Tantalum

Tantalum presents no particular difficulties in terms of properties or fabricability. Its principal drawback is its relatively low density.

C. MATERIALS PREPARATION TECHNIQUES

Cast materials are not suitable for the primary mass because of the un-homogeneous macro and micro porosity which will generally be present. Cast raw material would be suitable only if the ingot can be subsequently hot or cold worked, and this only for cubic materials such as tantalum. Hot isostatic pressing of powders is the most attractive route to follow for the other candidate materials. This method can be used to achieve full density with isotropic properties.

1. Tungsten

Tungsten can be vacuum arc cast then hot extruded or forged. We do not believe that available press capacity is sufficient to work a billet from which a 20 cm diameter sphere could be machined. A survey undertaken by the Nuclear Division of Union Carbide indicated that forging would be marginal even for 4" diameter spheres.⁽¹⁵⁾ Union Carbide did prepare 4" diameter spheres consolidated from Allied Chemical Corporation tungsten powder by hot isostatic pressing. This seems to be the most promising technique for 20 cm spheres. The Union Carbide personnel believe that the type of powder produced by Allied Chemical is required to get full densification. Unfortunately, the Allied Chemical facility is no longer operating. Recently, Nuclear Metals has developed a powder manufacture process by a rotating electrode process. An arc is struck between a stationary nonconsumable electrode and a rotating bar of the material to be atomized. The arc melts the bar, and molten droplets are spun off of it. Atomization takes place in vacuum; and the resultant particles are spherical and have extremely low impurity content. Tungsten powder prepared in this manner may be suitable for the proposed application.

However, an evaluation program would be required to determine whether full density can be achieved on small parts under the temperature and pressure conditions attainable with present large chamber hot isostatic equipment.

Machining of tungsten is difficult but not impossible. Conventional machining can be done with carbide tools. Electrical discharge machining would be the most logical choice for drilling the diametrical tunnels. Tungsten grinds and laps well because the surface finish depends largely on the residual porosity of the material.

2. Uranium and Uranium Alloys

Uranium and its alloys can be vacuum arc cast and then hot worked to eliminate porosity. However, the working will create preferred orientation and therefore anisotropy. While the extent of anisotropy of properties may be minimized by cycling through the phase transitions or by alloying, a more likely approach would again involve hot isostatic pressing of powders. In the case of the alloys, segregation would be on a microscopic scale and the sphere as a whole would be isotropic both in chemistry and crystal orientation. Again an evaluation program would be required to determine if small parts can be prepared adequately.

Union Carbide has had a great deal of experience in machining and finishing of uranium and tungsten.

3. Tantalum

Vacuum arc cast tantalum has excellent forging characteristics. However, the maximum ingot diameter is normally 8 inches so that a special mold might have to be constructed. Alternatively, sufficient hot work may be attainable by upset forging of an 8-inch ingot.

The machining characteristics of tantalum are much like those of stainless steel, i.e., there is a tendency to gall. ORNL has had little

experience with this material, and while they felt it could be done, it may require considerable development.

D. MACHINING AND HANDLING OF MATERIALS

Machining and finishing are by far the most difficult problems. One reason is simply the size and weight of the spheres; handling 20 cm spheres will be much more difficult than for the 10 cm spheres Union Carbide made for the University of Virginia.⁽¹⁵⁾ As far as finishing is concerned, the problems are not felt to be insurmountable. The best sphericity that can be expected is approximately 20-25 microinches.

The most critical step will be forming the tunnels or holes. These most likely will be drilled by electrical discharge machining, honed, and lapped. It may not be possible to meet required tolerances for hole dimensions, orthogonality of the three holes, and displacement of the hole axes at the nominal point of intersection.

E. DETERMINATION OF THE QUALITY OF FINISHED SPHERES

1. Gross Density

The gross density can be computed fairly accurately from the geometry and weight of the sphere before the holes are drilled. An alternative approach would be to use the pycnometer, this would be particularly useful after the holes have been drilled.

2. Geometry

Measurement of the diameter is fairly straightforward using interferometry. Interferometry would offer the most promising possibility for measurement of the hole geometry, but techniques would have to be developed.

3. Local Density

There are no known techniques for non-destructively measuring the local density to the accuracies required. One can hope to minimize the problem by consolidating the sphere to virtual theoretical density. The local density can be evaluated destructively by sampling of sections cut from a prototype sphere.

Union Carbide feels that measurement of the mass and geometrical center displacement by the techniques they developed for the 4 inch spheres is a very powerful tool for determining the overall quality of the spheres. This would also be true for spheres with holes.

F. POTENTIAL SUPPLIERS AND PROCESSORS

1. Tungsten Powder

The most promising source of high purity spherical tungsten powder is Nuclear Metals Division of Whittaker Corporation. They have available several local sources of hot isostatic press services for smaller parts which could be used to evaluate this powder's densification characteristics.

2. Uranium and Uranium Alloys

Union Carbide is the best source for cast and forged uranium and uranium alloys. Again, Nuclear Metals would be the logical source for powders. Nuclear Metals have a good deal of experience with these materials, and have approximately 50 pounds each of natural and depleted uranium already on hand.

3. Tantalum

The prime sources for tantalum ingot and forms are: Fanstel Inc., General Electric Co., Norton Co., Reactive Metals, Inc., Stellite Div. Cabot Corp., Wah Chang Corp., Westinghouse Electric Corp. The prime

independent forgers who do not melt are Ladish Co. and Wyman-Gordon.

4. Powder Consolidation

Consolidation of either the tungsten or uranium powders into a preform for a 20 cm diameter sphere should be done by hot isostatic pressing. Large size equipment, capable of reaching the temperature and pressures required, is available both at Union Carbide and at Battelle Memorial Institute.

5. Machining and Finishing

Because of their extensive background in this type of fabrication, Union Carbide is the best possibility.

6. Quality Determination

Again Union Carbide has a good deal of past experience. The National Bureau of Standards represents another valuable resource, particularly in development of gaging techniques for the holes.

7. Costs

All aspects of the sphere fabrication are developmental in nature. An estimate for the sphere blank consolidation is \$50-100,000 and \$150-250,000 for fabrication and machining of the sphere. Formal proposals were not requested from any of the potential suppliers or processors.

V. EXPERIMENT COOLING CONSIDERATIONS

A. BACKGROUND

For the $\Delta G/G$ experiment it is necessary to maintain the primary mass at cryogenic temperatures if we are to keep within the error budget for this experiment. Furthermore, it is desirable that the experiment be operated at temperatures at liquid helium or lower.

The experiment system designer is confronted with a number of choices in selecting a cryogenic refrigeration system. This selection must be made within the constraints of the available space, weight, and power; the required reliabilities; and the development funds available.

There are three basic cooling techniques which are available for space application. They include:

- a) Passive radiators which cool components to cryogenic temperature levels by radiation to the low-temperature, deep-space environment;
- b) Open-cycle systems of two types. One uses stored high-pressure gas and a Joule-Thomson expansion, and the other uses stored cryogens in either liquid or solid form; and
- c) Closed-cycle systems which utilize mechanical refrigerators to provide cooling at low temperatures and reject heat at high-temperature levels.

Passive radiators are not applicable to the experiments in question because such radiative systems are limited to temperatures above 60°K by imperfect shielding and parasitic heat leaks. The open cycle of the Joule-Thomson type is applicable in spaceborne systems only where the duty cycle is very short and the heat load very low. This is because the Joule-Thomson system requires a high-pressure gas supply that is too heavy for long-term operations.

Thus, there are two cooling techniques which are applicable to cooling the proposed experiments: (a) open-cycle refrigeration systems which use stored liquid or solid cryogens, and (b) closed-cycle systems which utilize a mechanical refrigerator.

A fundamental problem associated with operating such an experiment at cryogenic temperatures is cooling the thermal mass (in this case a dense primary mass) to the desired temperature level of 4.2°K or lower.

In this section, we will discuss in general terms the estimated cooling requirements, suggest techniques for achieving these temperatures, estimate the cool-down time for the experiment, and estimate the weight, power requirements, radiator area (wherever necessary), and development costs for cryogenic refrigeration systems.

B. EXPERIMENT COOLING REQUIREMENTS

We assume that the experiment could be contained within a sphere of radius 10 cm and that the primary mass of the sphere was a tungsten sphere of radius 5 cm. By enclosing the primary mass within an evacuated vessel with multilayer insulation, it is possible to achieve an insulation shielding factor of approximately 100. This is a conservative figure; it is possible to achieve shielding factors of 1000 if there are a minimum of electric leads and heat loss penetration. With the experiment maintained at 4.2°K in an ambient environment of 300°K (normal spacecraft habitable environment), we calculate that the steady-state heat load will be between 0.06 and 0.6 watts. For design purposes, we assume that the refrigeration system should have a capacity of 1 watt.

Another fundamental problem in cryogenically cooling an experiment at extremely low temperatures (less than 4.2°K) is that it may take an extremely long time to achieve equilibrium temperature. This is particularly true if the experiment is cooled radiatively as is the case in the proposed experiment. We estimate that the rate of temperature change near an equilibrium temperature of 4.2°K is approximately

$4.5 \times 10^{-3} \text{ }^\circ\text{K/hr}$ if radiation is the only mode of heat transfer. A detailed analysis of the complete experiment might reveal a more rapid cool-down under the same conditions; however, it will take a long time to achieve radiative equilibrium and other means will be required to establish the desired temperature level. The most obvious means would be to precool the experiment prior to launch and it would appear that precooling is absolutely necessary. Back-filling the experiment with dry helium during the cool-down to take advantage of the heat transfer afforded by gas conduction would aid the cool-down process. Subsequent evacuation of the experiment in orbit is relatively simple.

C. CRYOGENIC COOLING TECHNIQUES

The cryogenic cooling techniques which we believe are applicable to the proposed gravitational experiments are summarized in Table III. For comparison purposes, we have assumed that each system is capable of providing 1 watt of refrigeration at the temperature capability of the system. In each system, we consider the temperature range, the size, system weight, power requirements and radiator area (if any), safety, problem areas, state of development and estimates of the development costs for finished flight hardware.

It must be appreciated that the data on Table III is arrived at by "rule-of-thumb" estimates based, not on preliminary design, but on extrapolation of the characteristics of similar designs. Therefore, they must be regarded as being accurate within a factor of something like 1.5.

The cryogenic cooling systems listed in Table III are very sophisticated. The state of the art of cryogenic technology goes a long way to making such systems possible but advances in the art are needed.

The open-cycle helium system requires the invention of a workable liquid vapor separator to insure the venting overboard of the gaseous phase only. This need has been with us for a long time. In addition, the system is relatively heavy and bulky.

TABLE III. COMPARISON OF 1.0 WATT CRYOGENIC REFRIGERANT SYSTEMS FOR SPACE GRAVITATIONAL EXPERIMENTS

DESCRIPTION OF SYSTEM	Temp (°K)	Experiment Duration (days)	Size		Weight		Power Required (Kw)	Radiation Area (sq meters)	Safety	Problem Areas	State of Development	Development Costs (10 ⁶ \$)
			Primary Cryogen (liters)	Total System (cu meters)	Primary Cryogen (kg)	Total System (kg)						
<u>OPEN CYCLE</u>												
Liquid helium	2-4.2	10 100	330 3300	1.17 11.7	41 413	250 2500	negligible	none	low pressure	Requires elaborate system for venting pressure in zero gravity; temperature control systems are within the state of the art.	All components except venting and temperature control systems are within the state of the art.	0.7
Solid neon with NH ₃ or CO ₂ shield	16-24	10 100	5.9 59	.07 0.7	8.3 83	40 400	negligible	none	low pressure NH ₃ and CO ₂ may be toxic	System activation; temperature control.	No system of this type exists, but should be possible within the state of the art.	1.0
Solid hydrogen with solid NH ₃ or CO ₂ shield	9-13	10 100	18.8 188	0.13 1.3	1.69 16.9	75 750	negligible	none	hydrogen explosion hazard	System activation; temperature control.	No system of this type exists, but should be possible within the state of the art.	1.0
<u>CLOSED CYCLE</u>												
Mechanical helium	4.2	> 100	- (radiator and solar panels not included)	0.2	- (includes solar panels and radiator)	120	1.3 kw	6.5		Development status; temperature control.	Units in exploratory development stage; reliability characteristics need to be proven.	4

The solid CO₂ or NH₃ shielded solid neon or hydrogen open-cycle systems represent an advanced state-of-the-art development. As indicated on the table, no systems of this type exist, but designs based on state-of-the-art should make them possible. These systems are less bulky and of lighter weight than the helium open-cycle system but the lowest achievable temperature is higher. The equipment and procedures needed to charge these systems are complex but are considered practical.

The closed-cycle, mechanical refrigeration systems with helium as the working fluid for spaceborne use do not exist. However, a number of devices of this type are in the exploratory development phase. Some of them are designed to achieve cooling temperatures as low as 3.6°K. The characteristics of the mechanical refrigerator listed in Table III are those of a type we have been developing under Air Force sponsorship. It is designed to be particularly efficient and to have very long life as needed for spaceborne use. It, however, is in a very early stage of development. A complete unit has not been assembled and tested nor, therefore, has its operability or reliability been proven. About the same can be said of competing units. Nevertheless, with sufficient development effort, we believe workable low-temperature mechanical refrigerators will become a reality.

All cooling systems discussed have a common problem of temperature control. Unfortunately, the degree of control necessary is not now known, but it may be orders of magnitude greater than what is now commonly achieved which is the order of $\pm 0.10K$.

The selection of the "best" system for cooling the experiment is not obvious. We feel that the trade-offs favor the selection of the mechanical refrigerator. In this selection we emphasize the relatively low temperatures achievable, the long life, the small size and weight, and the easy integration with the experiment. We accept the need for power and the higher development costs.

REFERENCES

1. C. Brans and R. Dicke, "Mach's Principle and a Relativistic Theory of Gravitation," Physical Review, 124 (3), November, 1961.
2. Michael G. Blicht, "The Feasibility of a Gravitational Clock to Test the General Theory of Relativity," M.I.T. S.M. Physics Thesis, 1969.
3. S. Madden, "Inhomogeneities Treated as a Random Process," M.I.T. Measurement Systems Laboratory Memorandum, Jan. 21, 1970.
4. J. W. Beams, Physics Today, July 1959.
5. T. R. Nordsieck, "Feasibility of a Free Gyro Navigational System," Control Systems Laboratory (U. of Ill.) Internal Report, May 1954, Contract No. DA36-039-SC-56695.
6. H. W. Knoebel, "Electrostatic Vacuum Gyro," presented at the Inst. of Radio Engineers 1961 Winter Convention on Military Electronics, Feb. 1-3, 1961.
7. I. Simon, A. G. Emslie, et al, "Sensitive Tiltmeter Utilizing a Diamagnetic Suspension," Review of Scientific Instruments, Vol 39, No. 11, 1666-1671, Nov. 1968.
8. "Nature of the Low Temperature Phase Transformation in Alpha Uranium," Cryogenics, 8:396-7, Dec. 1968.
9. C. S. Barrett, M. H. Mueller, and R. L. Hilterman, Physical Review, 129, 625, 1963.
10. "Uranium-molybdenum Alloy for Use in a Prompt Burst Reactor," ASME Trans Ser. D., 87, 865-70, Dec. 1965.
11. "Designing with Plutonium and Uranium," Mech. Eng., 88:28-31, June 1966.
12. J. K. Gore and R. Seegmiller, "Surface Treatments and Electroplated Coatings on Uranium," Plating, 50: 215-20, March 1963.
13. R. D. Bland, "Parameter Studies of Ion Plated Aluminum Coatings on Uranium," Electrochem. Tech., 6:272-8, July 1968.
14. J. R. Lundquist, et al, "Nickel Plating of Uranium - Review of Laboratory Studies," Plating, 54:829-37, July 1967.
15. J. H. Nash, A. C. Neeley, and P. S. Steger, "High Density Tungsten Spheres," Union Carbide Corporation Nuclear Division, Rept Y-1654, Nov. 18, 1968.

New Technology Appendix

This report is published in the belief that it constitutes an improvement in the state of the art. The entire report is referenced. See abstracts for more detailed descriptions.